

Isothermal Micro(bio-)calorimetry - Method Optimization and Instrument Development for a Rapid and Reliable Detection of Bacteria

Von der Fakultät für Lebenswissenschaften

der Universität Leipzig

genehmigte

DISSERTATION

zur Erlangung des akademischen Grades

Doctor rerum naturalium

(Dr. rer. nat.)

vorgelegt von

M.Sc. Christian Fricke

geboren am 28.05.1991 in Staßfurt

Dekan: Prof. Dr. Marc Schönwiesner

Gutachter: Prof. Dr. Hauke Harms

Prof. Dr. Lars Wadsö

Tag der Verteidigung: 26. November 2021

Bibliographische Darstellung

Christian Fricke

Isothermal Micro(bio-)calorimetry - Method Optimization and Instrument Development for a Rapid and Reliable Detection of Bacteria

Fakultät für Biowissenschaften, Pharmazie und Psychologie

Universität Leipzig

Dissertation

210 Seiten, 327 Literaturangaben, 50 Abbildungen, 12 Tabellen

Early detection of pathogenic bacteria in food, drinking water and medicine products is one of the essential tasks of routine microbiological analysis. Through analytics, outbreaks can be discovered and consequently, countermeasures can be initiated to minimize health and economic damage. Cultivation of pathogens from contaminated specimens is routinely performed in microbiological laboratories worldwide. The procedure is easy to perform, requires little equipment and provides simple quantitative data in colony-forming units (CFUs) per sample volume. Only the time between preparation and confirmation of a positive (contaminated) sample usually extends over several days. The desired goal should be a technique that can retain the simplicity of cultivation while providing real-time information about the sample under investigation for early detection of potential contamination. Therefore, in the framework of this thesis, systematic heat flow measurements were performed on two model strains, *Lactobacillus plantarum* DSM 20205 and *Pseudomonas putida* mt-2 KT2440. The influence of cultivation techniques (in liquid, on solid and membrane filter placed onto solid medium) in static ampoule systems on calorimetric detection was investigated. In particular, the effect of contamination level (initial bacterial cell number), substrate amount (nutrients and oxygen), and detection limits were systematically evaluated. In addition, microcalorimetric measurements of *Legionella pneumophila* ATCC 33152, a waterborne pathogen, were conducted for the first time. Heat flow profiles demonstrated that high contamination levels (> 1000 CFU) were detected within 24 h. Compared to detection times of up to 10 days by ISO 11731:2017, calorimetric detection can serve as an early warning system. With this knowledge, a uniquely manufactured micro(bio-)calorimetric test system was designed to meet the requirements for detecting bacterial contaminations. In particular, the sample vessel geometry and the operating temperature perfectly matched the microbiological analysis. Within this development work, numerical models were established to investigate the temperature distribution of selected compounds as well as the complete calorimetric system. Based on these models, modifications to the test system were numerically simulated in advance to improve the instrument's performance stepwise. This thesis presents the methodological principles and a calorimetric test system designed as an early warning and detection tool for microbiological samples.

Table of Contents

List of Abbreviations.....	VII
List of Quantities and Units.....	IX
Zusammenfassung.....	1
Summary	7
1. Structure and outline of the thesis.....	15
2. Introduction.....	17
2.1 Detection techniques for bacteria	18
2.1.1 Conventional, culture-based techniques	18
2.1.2 Culture-independent detection techniques.....	22
2.2 Isothermal Micro(bio-)calorimetry.....	24
2.2.1 A brief historical review	25
2.2.2 Micro(bio-)calorimetric principle.....	27
2.2.3 Applications of micro(bio-)calorimetry in the context of bacteria detection	30
2.2.4 Design and construction of isothermal micro(bio-)calorimeters	35
2.2.4.1 General components of an isothermal microcalorimeter.....	35
2.2.4.2 Numerical simulation as a development tool for the construction of microcalorimeters	39
2.2.4.3 Requirements for an isothermal micro(bio-)calorimeter	42
3. Experimental part	45
3.1 Systematic investigation of a culture-based microcalorimetric approach for the detection of bacteria	45
3.1.1 Rapid Calorimetric Detection of Bacterial Contamination: Influence of the Cultivation Technique	45
3.1.2 How to speed up the detection of aerobic microbial contaminations by using isothermal microcalorimetry	59
3.1.3 Rapid culture-based detection of <i>Legionella pneumophila</i> using isothermal microcalorimetry with an improved evaluation method.....	77

3.2	Numerical heat flow and transport simulation as a development tool for the design of isothermal microcalorimeters	89
3.3	Further experiments related to instrument development and selective detection of bacteria.....	109
3.3.1	Development process towards an improved calorimetric test system	109
3.3.2	Detection of bacterial activity using the novel micro(bio-)calorimeter.....	114
3.3.3	Calorimetric measurements on the selectivity of conventional Legionella media for accompanying pathogens.....	116
4.	Discussion.....	119
4.1	Micro(bio-)calorimetry - A culture-based detection technique for bacterial contamination.....	119
4.1.1	Compatibility of cultivation techniques with calorimetric detection - Potential and limitations.....	120
4.1.2	An early warning system for <i>Legionella pneumophila</i> in drinking water based on calorimetry?.....	124
4.2	A novel calorimeter designed for microbiological analysis	126
5.	Conclusion.....	131
6.	Outlook.....	133
7.	References	135
	Declaration of Authorship	149
	Danksagung.....	151
	Curriculum Vitae	153
	List of Publications.....	155
	Appendix	157
A1	Supplementary material for section 3.1.1 (published article 1).....	157
A2	Supplementary material for section 3.1.2 (published article 2).....	165
A3	Supplementary material for section 3.1.3 (published article 3).....	180
A4	Supplementary material for section 3.2 (submitted manuscript).....	184
A5	Author Contributions of Published Articles and Submitted Manuscript.....	197

List of Abbreviations

Abbreviation	Explanation
ABS	acrylonitrile butadiene styrene
A/D converter	analog to digital converter
ATCC	American type culture collection
BAM	bio activity monitor
BCYE	buffered charcoal yeast extract
BHI	brain heart infusion (medium)
BMS	biomagnetic separation
CAD	computer-aided design
CMM	cardiac myocyte medium
CFU	colony-forming unit
CSF	cerebrospinal fluid
DAE	differential-algebraic equation
DNA	deoxyribonucleic acid
DSM-1	Deutsche Sammlung von Mikroorganismen-1 (nutrient agar)
DSMZ	Deutsche Sammlung von Mikroorganismen und Zellkulturen
ELISA	enzyme-linked immunosorbent assay
FEM	finite element method
FTM	fluid thioglycollat (medium)
GF	growth on membrane filter
GIA	growth in agar
GL = LC	growth in liquid corresponds to liquid cultivation
GOA = SC	growth on agar corresponds to solid cultivation
GU	genome units
GVPC	glycine, vancomycin, polymyxin B, cycloheximide
HFS	heat flow sensor
IMC	isothermal microcalorimetry
ISO	International organization for standardization
KBE	koloniebildende Einheit
LB	lysogen broth
LOD	limit of detection
MALDI-TOF	matrix-assisted laser desorption/ionisation - time of flight
MF	membrane filtration
MIC	minimal inhibitory concentration
MMKT2440	minimal medium for <i>P. putida</i> mt-2 KT2440

MRS	De Man, Rogosa, Sharpe medium
MRSA	methicillin-resistant <i>Staphylococcus aureus</i>
MSSA	methicillin-susceptible <i>Staphylococcus aureus</i>
MWY	modified Wadowsky Yee
NTC	negative temperature coefficient
OD	optical density
ODE	ordinary differential equation
PA	polyamide
PCR	polymerase chain reaction
PDB	potato dextrose broth
PDE	partial differential equation
PID controller	proportional-integral-derivative controller
PLT	platelet
RNA	ribonucleic acid
RT	real-time
SD	standard deviation
SPR	surface plasmon resonance
TAM	thermal activity monitor
TEC	thermoelectric cooler
TEG	thermoelectric generator
TSB	tryptic soy broth
VISA	vancomycin-intermediate <i>Staphylococcus aureus</i>
VRSA	vancomycin-resistant <i>Staphylococcus aureus</i>
VSSA	vancomycin-susceptible <i>Staphylococcus aureus</i>
WHO	World health organization

List of Quantities and Units

Symbol	Name	Unit
A	area	m^2
a_w	water activity	
$c_0, c(\text{bacteria}), c_0(\text{bacteria})$	initial concentration of bacteria	CFU mL^{-1}
C_c	mean carbon content of a single bacterium	fg C cell^{-1}
c_{O_2}	concentration of dissolved oxygen in the liquid	mg L^{-1}
C_p	specific heat capacity	$\text{J kg}^{-1} \text{K}^{-1}$
d	diameter	m
dP/dt	time derivative of the thermal power	W s^{-1}
F	volume force	N
g	gravitational acceleration constant	9.81 m s^{-2}
h	heat transfer coefficient	$\text{W m}^{-2} \text{K}^{-1}$
K_p	proportional gain	
K_i	integral gain	
K_d	derivative gain	
K_u	ultimate gain	
m	mass	kg
N_0	initial number of cells	
$N(t)$	number of cells at time t	
n	number of replicates	
n_{TEG}	number of thermocouples	
P	thermal power	W
p	pressure	Pa
Q	total heat	J
q	heat flux	W m^{-2}
r_{ij}	reaction rate of species i in the j -th reaction	$\text{mol L}^{-1} \text{s}^{-1}$
R_{th}	thermal resistance	K W^{-1}
S	sensitivity	V W^{-1}
T	temperature	K
t	time	s
U	electrical potential	V
u	fluid velocity vector	m s^{-1}
V	volume	L
v	velocity magnitude	m s^{-1}
v_{ij}	stoichiometric coefficient of species i in the j -th	

	reaction	
w	mass fraction	%
Y	yield coefficient	

Greek Symbols

α	Seebeck coefficient	$V K^{-1}$
β	mass concentration	$g L^{-1}$
γ	lag time	s
$\Delta_k H_{O_2}$	oxycaloric equivalent	$-455 kJ mol^{-1}$
$\Delta_R H_x$	reaction enthalpy	$J mol^{-1}$
ΔT	temperature difference calibration	K
ε	constant	$W V^{-1}$
κ	thermal conductivity	$W m^{-1} K^{-1}$
μ	dynamic viscosity	Pa s
μ	growth rate	s^{-1}
ξ_j	rate of j -the reaction	$mol L^{-1} s^{-1}$
Π	osmotic pressure	Pa
ρ	density	$kg m^{-3}$
σ	electrical conductivity	$S m^{-1}$
τ	time constant	s
Φ	heat flow	W
φ, Φ_0	cell-specific heat production rate	W

Indices and Subscripts

c	Corrected
dect	Detection / detectable
exp	Experimental
ext	Extern
g	Gaseous
i	Inoculum
l	Liquid
max	Maximum
op	Operating
samp	Sample
th	Thermal
theo	Theoretical

Zusammenfassung

Die mikrobiologische Überwachung unserer alltäglichen Konsumgüter wie Lebensmittel, Trinkwasser und Medizin stellt eines der wichtigsten Instrumente im Kampf gegen bakterielle Verunreinigung dar. Während der Produktion, des Transports oder der Lagerung dieser Güter können pathogene Bakterien durch einen Mangel an Hygiene und/oder fehlender Wartung von Anlagen als Kontaminationen in diese gelangen. Oftmals bildet das Produkt ideale Nährstoffvoraussetzungen, für eine Vermehrung pathogener Bakterienarten. Während des Wachstums sorgen die Krankheitserreger also nicht nur für eine Verminderung der Produktqualität, sondern können auch eine lebensbedrohliche Gefahr für den Menschen darstellen und ernstzunehmende Erkrankungen bei den betroffenen Individuen hervorrufen. Oberste Priorität der mikrobiologischen Analytik ist daher die frühzeitige Erkennung solcher Kontaminationen, um die Produktqualität und dessen Sicherheit zu garantieren sowie gesundheitlichen Schäden bei den Konsumenten vorzubeugen.

Interessanterweise beruht die konventionelle mikrobiologische Analytik auf einer vor über 100 Jahren durch Robert Koch und dessen Mitarbeitern etablierten Kultivierungsmethode. Grundlage der Methode bildet die Anzucht von Bakterien auf festem Nährmedium, auf dem die zu untersuchende Probe ausgestrichen wird. In speziellen Kulturgefäßen, sogenannten Petrischalen, stehen den Bakterien ausreichend Nährstoffe zur Verfügung. Um ideale Kultivierungsbedingungen zu erzielen, werden die Petrischalen in Inkubatoren platziert, welche die richtige Temperatur und ggf. Gaszusammensetzung kontrollieren. Die Detektion der Bakterien ist abhängig von der Stamm-spezifischen Wachstumsgeschwindigkeit. Detektionszeiten von bakteriellen Kontaminationen können bei der konventionellen Analytik von wenigen Tagen bis hin zu mehreren Wochen reichen. Hierbei handelt es sich um eine rein optische Endpunktdetektion und die detektierbare Größe bildet die so genannte koloniebildende Einheit (KbE). Letztere, so die Annahme, hat sich aus einem einzigen teilungsfähigen Bakterium gebildet. Dieses hat sich so häufig repliziert, dass es eine mit dem sichtbaren Auge erkennbare Zellanhäufung (Kolonie) geformt hat. Der Grad der Verunreinigung wird in KbE pro mL oder g Probenmaterial angegeben.

Den vielen Vorteilen dieser Methode, wie z.B. einer einfachen Handhabung der Prozedur, den vergleichsweise geringen Materialkosten und der einfachen Auswertung der Ergebnisse, steht vor allem der hohe Zeitbedarf gegenüber, der zur Abwehr einer Gesundheitsgefährdung ein wesentliches Kriterium darstellt. Wünschenswert wäre eine äquivalente schnellere Methode, die darüber hinaus Echtzeitinformationen über die zu untersuchende Probe während der Kultivierung liefern kann, sodass bakterielle Kontaminationen schneller erkannt und folglich frühzeitig Gegenmaßnahmen ergriffen werden können.

Eine dieser Methoden ist die isotherme Mikrokalorimetrie, bei der die metabolische Wärme, die die Bakterien während des Wachstums an die Umgebung abgeben, in Echtzeit detektiert wird. Sehr sensitive Wärmeflussensoren registrieren dabei den Temperaturanstieg (Bruchteil eines Millikelvins) in der Probe, sodass sich durch annähernd isotherme Bedingungen im Kalorimeter ein Temperaturgradient über den Sensor formt. Dieser Gradient erzeugt wiederum eine Spannung am Sensor (Seebeck-Effekt), die letztendlich als Messsignal aufgezeichnet wird und proportional zum Temperaturgradienten ist. Die bisherigen kalorimetrischen Untersuchungen zur Detektion von Bakterien endeten häufig bei einem *proof of concept* mit Schwerpunkt in der medizinischen Diagnostik. Die Kultivierungsbedingungen weichen erheblich von denen der konventionellen Detektionsmethode in der mikrobiologischen Überwachung ab, da überwiegend 4-mL statische Ampullen verwendet werden, die luftdicht verschlossen im Kalorimeter positioniert werden. Interessanterweise haben sich hier Messungen in flüssigem Medium durchgesetzt. Nur wenige Anwendungen auf festem Medium sind in der Literatur beschrieben.

Der erste Abschnitt dieser Arbeit befasst sich mit experimentellen Studien zum 4-mL statischen Ampullen-System in Bezug auf die kalorimetrische Detektionszeit. Im Rahmen von zwei Modellsystemen *Lactobacillus plantarum* DSM 20205 (**Abschnitt 3.1.1**) und *Pseudomonas putida* mt-2 KT2440 (**Abschnitt 3.1.2**) wurden erstmalig klassische Kultivierungstechniken, wie Wachstum in flüssigem Medium, Wachstum auf/in festem Medium und Voranreicherung über Membranfiltration (spezielle Adapter wurden gefertigt, sodass Membranfilter ($d = 10$ mm) für die 4-mL Ampullen verwendet werden konnten) mit anschließendem Wachstum auf/in festem/flüssigem Medium in kalorimetrischen Messungen systematisch untersucht. Die kalorimetrischen Experimente wurden in zwei kommerziellen Mikrokalorimetern, TAM III und MC-Cal/100 P, durchgeführt. Im Vordergrund dieser Studien stand der Einfluss der Art der Kultivierung auf die Detektionszeit. Neben der Untersuchung von methodischen Aspekten wie der Menge an Inokula, das Füllvolumen der Ampullen sowie das ausgewählte Medium, wurden auch technische Abhängigkeiten wie das Detektionslimit betrachtet und diskutiert. Zur Einordnung der kalorimetrischen Detektionszeiten wurden Referenzmessungen im Rahmen der optischen Inspektion der Bildung von KbE durchgeführt.

Die erzielten Ergebnisse zeigen für beide Bakterien, dass eine kulturbasierte, kalorimetrische Detektion wesentlich früher bakterielle Aktivität, vor allem bei einer hohen anfänglichen Zellzahl, registrieren kann als die rein optische Endpunktdetektion mit dem bloßen Auge. Die Konzentrationsabhängigkeit der kalorimetrischen Messungen ist vor allem vorteilhaft wenn eine Voranreicherung durch Membranfiltration erfolgt, da hierdurch größere Volumina (als das Fassungsvermögen der Ampullen) realisierbar sind. Die Ergebnisse dieser Studien demonstrieren auch, dass die Verwendung von festem Medium zu ähnlichen Detektionszeiten führt und somit eine bessere Vergleichbarkeit mit standardisierten Verfahren bieten kann. Weiter zeigen die Daten, dass das Füllvolumen vor allem bei aerob wachsenden Bakterien in 4-mL statischen Ampullen berücksichtigt werden muss, da hierdurch die Menge an vorhandenem Sauerstoff stark limitiert werden kann. Auswirkungen auf die Detektionszeit werden

relevant, wenn unempfindlichere Kalorimeter (Detektionslimit $> 10 \mu\text{W}$) eingesetzt werden. Zu einer verzögerten Detektion in 4-mL statischen Ampullen kann es ebenfalls kommen, wenn die Probe nur wenige Zellen umfasst und auf festem Medium heranwächst. Hier verdeutlichen die Ergebnisse der Studien, dass der exponentielle Anstieg im Wärmefluss in einen flacheren, linearen Verlauf übergeht, der bestimmt ist durch Diffusion von Nährstoffen.

Aufbauend auf den Studien im ersten Abschnitt dieser Arbeit wurden erstmalig kalorimetrische Messungen mit *Legionella pneumophila* ATCC 33152, einem im Trinkwasser vorkommenden opportunistischen Krankheitserreger durchgeführt (**Abschnitt 3.1.3**). Immer wieder kommt es zu größeren Ausbrüchen weltweit, da sich durch Biofilmaablagerung schlecht gewarteter Trinkwasserleitungssysteme, wo das Wasser oft stagniert, ideale Wachstumsbedingungen für *L. pneumophila* ergeben. Das Bakterium stellt eine direkte Gefahr für immungeschwächte und ältere Menschen dar. Die Übertragung von *L. pneumophila* erfolgt überwiegend durch Bioaerosole, die über den Respirationstrakt aufgenommen werden können. Neben dem Pontiac-Fieber kann das Bakterium auch die tödlich verlaufende Legionärskrankheit verursachen. Dabei handelt es sich um eine atypische Lungenentzündung.

Der Nachweis und die Zählung von *L. pneumophila* ist durch die ISO 11731:2017 vorgeschrieben. Hierbei handelt es sich um einen kulturbasierten Ansatz. Die Wasserprobe wird dabei auf nicht-selektivem gepufferten Holzkohle-Hefeextrakt (engl. *buffered charcoal yeast extract*, BCYE) Agar sowie weiteren selektiven Medien wie z.B. Glycin Vancomycin Polymyxin Cycloheximid (GVPC) Agar ausplattiert (Direktansatz). Antibiotika werden dem Medium zugesetzt, um das Wachstum der im zu untersuchenden Wasser enthaltenen Begleitflora zu hemmen. Die Anreicherung mittels Membranfiltration stellt einen weiteren (indirekten) Ansatz dar. Daneben schreibt die ISO-Norm auch in weiteren Ansätzen eine Hitzebehandlung (Wasserbad bei $50 \text{ }^\circ\text{C}$ für 30 min) der Proben und eine chemische Behandlung bei Verwendung von Membranfiltern (30 mL HCl/KCl- Puffer, pH = 2,2, Einwirkzeit: 5 min) vor, um eine Selektivität innerhalb der Detektion für *L. pneumophila* zu erhalten. Aufgrund des vergleichsweise langsamen Wachstums des Bakteriums, kann die Detektion bis zu zehn Tagen dauern. Die im Rahmen dieser Arbeit durchgeführten kalorimetrischen Messungen von *L. pneumophila* ATCC 33152 auf 1 mL BCYE Agar in 4-mL statischen Ampullen zeigen, dass die metabolische Aktivität der Bakterien in Echtzeit registriert werden kann. In Abhängigkeit der anfänglichen Zellzahl in den Ampullen konnten Detektionszeiten zwischen 24 h (1000 kbE) und 45 h (4 kbE) bestimmt werden. Kalorimetrische Detektionen sind somit innerhalb von ein bis zwei Tagen möglich. Der maximale Wärmefluss bei diesen Experimenten liegt bei etwa $180 \mu\text{W}$ und ist somit ausreichend, um auch von weniger leistungsstarken Kalorimetern (Detektionslimit $> 100 \mu\text{W}$) detektiert werden zu können. Darüber hinaus wird auch eine alternative Auswertung der Detektionszeit präsentiert. Durch Verwendung der ersten Ableitung der Wärmeflusskurven ist es möglich vor allem Störungen, welche durch das thermische Einschwingen der Probe auftreten können, zu reduzieren. Anhand erster, weiterführender Wärmeflussmessungen von häufig vorkommenden Begleitkeimen wie *Pseudomonas aeruginosa* ATCC 27853, *Escherichia coli* ATCC 8739 und *Enterococcus faecalis* ATCC 19433 auf kommerziel-

len Legionellen-Medien wird der Aspekt Selektivität untersucht (**Abschnitt 3.3.3**). Diese vorläufigen Daten zeigen, dass eine vollständige Hemmung bei zwei von drei Begleitkeimen (Ausnahme bei *E. coli*) eintritt, wenn GVPC Agar verwendet wird. Dies wäre eine der Grundvoraussetzungen für eine selektive kalorimetrische Detektion von *L. pneumophila* im Trinkwasser, da jegliche Begleitflora zum netto Wärmefluss signal beitragen würde.

Zusammen mit den Ergebnissen der beiden Modellsysteme *L. plantarum* DSM 20205 und *P. putida* mt-2 KT2440 zeigt diese Arbeit, dass die konventionelle mikrobiologische Analytik kompatibel mit der isothermen Mikrokalorimetrie ist. Zugleich demonstrieren die Wärmeflussdaten, dass vor allem die frühzeitige Detektion bakterieller Kontaminationen mittels Kalorimetrie gelingt. Lediglich ein speziell auf die mikrobiologische Analytik abgestimmtes Kalorimeter fehlt, um mikro(bio)-kalorimetrische Messungen, d.h. kulturbasierte Detektionen von Bakterien mittels Mikrokalorimetrie, durchführen zu können.

Kommerzielle isotherme Mikrokalorimeter verfügen häufig über ein breites Temperaturspektrum (ca. 10 - 100 °C), um neben biologischen Anwendungen auch solche aus den Disziplinen der Physik und Chemie abzudecken. Eine Vielfalt an Probengefäßen in unterschiedlichsten Formen und Füllvolumina steht zur Verfügung, wobei nur ein geringer Teil die passenden Maße für die mikrobiologische Kultivierung auf festem Medium besitzt. Häufig ist die vorhandene Bodenfläche unzureichend, um separate, auszählbare Kolonien zu erhalten. Letzteres hätte den Vorteil, dass neben der schnelleren kalorimetrischen Detektion auch eine Quantifizierung der Kontamination, in Form von KbE, vorgenommen werden kann. Um standardisierte Membranfilter ($d = 47$ mm) in kommerziellen Kalorimetern zu verwenden, stehen zurzeit nur sehr große Probengefäßen (> 100 mL) zur Verfügung. Solche Kalorimeter verfügen häufig über eine geringe Anzahl an Messkanälen. Hochdurchsatz-Mikrokalorimeter können zurzeit etwa 48 Proben simultan messen, jedoch verwenden diese Geräte meistens nur kleine Probengefäße (≤ 4 mL). Auf die Probleme im Rahmen kalorimetrischer Detektion in 4-mL statischen Ampullen System wird bereits im ersten Abschnitt der Arbeit hingewiesen.

Ausgehend von den experimentellen Ergebnissen aus **Abschnitt 3.1** sowie den Anforderungen für die Kultivierung in der konventionellen Mikrobiologie befasst sich der zweite Teil der Arbeit mit dem Design, der Konstruktion und der numerischen Entwicklungsarbeit eines neuen isothermen Mikro(bio)-kalorimeters (**Abschnitt 3.2**). Das Prinzip basiert auf der Messung von Wärmeströmen durch Wärmeflussensoren, so genannten thermoelektrische Generatoren (TEGs). Im Rahmen dieser Arbeit wurde zunächst ein Testsystem entwickelt. Dieses ist in zwei Zonen unterteilt: (i) die äußere Zone wird durch einen Heizlüfter temperiert, (ii) die innere Zone setzt sich aus den Unterteilen der Messkanäle zusammen, in denen sich jeweils die TEGs befinden. Das Probengefäß steht dabei in direktem Kontakt mit dem TEG. Das Unterteil des Sensors befindet sich auf einer Wärmesenke, dessen Temperatur durch zwei Peltier-Module präzise reguliert wird ($T_{\text{Wärmesenke}} = (37.072 \pm 0.001) \text{ °C}$). In der Aufheizphase des Systems unterstützen zwei Heizfolien den Temperaturanstieg auf der Wärmesenke. Das Testsystem verfügt insgesamt über drei Kanäle (zwei Mess- und ein Referenzkanal). Die Betriebs-

temperatur ist auf 37 °C eingestellt und somit ideal geeignet für die Detektion von *L. pneumophila* und anderen mesophilen Krankheitserregern. Es handelt sich hierbei um ein lufttemperiertes Mikrokalorimeter ($T_{\text{Luft}} = (37.0 \pm 0.1) \text{ °C}$). Die Maße ($d = 51 \text{ mm}$, $h = 19 \text{ mm}$) der verwendeten Probengefäße (bestehend aus einem Aluminiumkörper und einem Deckel aus Polyetheretherketon) entsprechen denen handelsüblicher, kleinerer Petrischalen ($d = 50 \text{ mm}$). Das Gesamtvolumen beträgt 35 mL. Die Form der ausgewählten Probengefäße sorgt für einen geringen Platzbedarf (Anordnung mehrerer Messkanäle ist möglich). Zudem können aufgrund der großen Bodenfläche Diffusionsprobleme der Substrate und des Sauerstoffs minimiert werden.

Parallel zu Experimenten des Testsystems unter Laborbedingungen erfolgen numerische Wärmetransport- und -fluss Simulationen anhand einer 3D-Rekonstruktion des Geräts, um die Temperaturverteilung einzelner Komponenten bzw. des gesamten Geräts zu untersuchen. Die Computersimulationen basieren auf der Finite-Elemente-Methode (FEM) und werden in der Simulationssoftware COMSOL Multiphysics[®] ausgeführt. Die experimentellen Daten ergeben einerseits einen groben Überblick über die Leistungen (Temperaturstabilität, Verhalten der TEGs), die das Kalorimeter unter Laborbedingungen erzielen kann und dienen andererseits als Validierung der FEM Ergebnisse. Gleichzeitig enthüllen die numerischen Simulationen Inhomogenitäten in der Temperaturverteilung des Testsystems, die unter experimentellen Bedingungen nicht zugänglich sind. Vor allem räumliche Temperaturgradienten können mit Hilfe der FEM abgebildet werden. Darüber hinaus, können experimentell beobachtete Effekte wie z.B. unterschiedliches Verhalten unter den TEGs durch die Modellberechnungen plausibel erklärt werden.

Mit dem numerischen 3D-Modell steht jetzt ein Tool zur Verfügung mit dessen Hilfe Optimierungen simuliert werden können. Die erhaltenen Temperaturverteilungen zu diesen Modifikationen erlauben es dann, Aussagen zu treffen, um mögliche Verbesserungen für die Fertigung eines Prototyps mit mehr Messkanälen zu berücksichtigen. In **Abschnitt 3.3.1** dieser Arbeit werden erste Ergebnisse zu Änderungen an dem Testsystem präsentiert. Dabei fließen auch erste Erkenntnisse aus experimentellen Messungen mit ein. Außerdem wird anhand erster mikrobiologischer Messungen (*P. putida* mt-2 KT2440 in Flüssigmedium und einer realen Kühlturmprobe auf GVPC Agar) die Anwendbarkeit des Mikro(bio-)kalorimeters für die erfolgreiche Detektion von Bakterien vorgestellt (**Abschnitt 3.3.2**).

Zusammenfassend wurden in dieser Arbeit methodische Optimierungen für eine kalorimetrische Detektion von Bakterien systematisch untersucht. Wärmeflussmessungen weisen eine hohe Kompatibilität zur konventionellen mikrobiologischen Analytik auf, mit dem Vorteil, dass kürzere Detektionszeiten erzielt werden können. Die Ergebnisse dieser Studien heben auch die limitierenden Faktoren in statischen 4-mL Ampullen Systemen hervor, welche bisher überwiegend für die kalorimetrische Detektion von Bakterien verwendet werden. Mit der Entwicklung eines neuen Mikro(bio-)kalorimeters wird in dieser Arbeit ein System präsentiert, welches gezielt für die mikrobiologische Analytik entwickelt wurde und als Frühwarnsystem im Rahmen konventioneller Kultivierung Echtzeitinformationen über den Zustand der Probe liefern kann.

Summary

Microbiological monitoring of our daily consumables such as food, drinking water and drugs represents one of the most critical tools in controlling bacterial contaminations. During production, transport or storage, pathogenic bacteria can contaminate these consumables due to poor hygiene and lack of maintenance of facilities. Often the product provides ideal nutrient conditions for the bacteria to multiply. During bacterial growth, the pathogens not only cause a decline in product quality but can also pose a life-threatening risk to humans and cause serious illness in affected individuals. Therefore, the highest priority of microbiological analysis is the early detection of such contaminations to guarantee the product quality and safety and prevent damage to consumers' health.

Interestingly, the conventional microbiological analysis is based on a cultivation method established over 100 years ago by Robert Koch and co-workers. The principle of the method is the cultivation of bacteria on a solid nutrient medium in which the sample is spread out. In unique culture vessels, so-called Petri dishes, nutrients are available to the bacteria in excess. In order to create ideal cultivation conditions, the Petri dishes are placed in incubators that were adjusted to the optimal temperature and, if necessary, the appropriate gaseous composition. The detection of bacteria depends on the strain-specific growth rate. Detection times of bacterial contamination can range from a few days to several weeks in conventional microbiology. This analysis is a visual endpoint detection, and the detectable quantity is the so-called colony-forming unit (CFU). The latter, it is assumed, has formed from an initial bacterium. This bacterium has replicated so frequently that a cell cluster (colony) is formed, which can finally be counted by the naked eye. The degree of contamination is expressed in CFU per mL or g of sample.

Apart from the many advantages of this method, such as simple handling of the procedure, comparatively low material costs, and the trivial evaluation of the results, the main drawback is the long time required, which is a major criterion for preventing health risks. It would be desirable to have an equivalent faster method to provide real-time information about the sample under investigation during cultivation. Thus bacterial contaminations can be detected at an early stage, and consequentially, countermeasures can be taken in good time.

One of these methods is isothermal microcalorimetry (IMC). Here, the metabolic heat released by bacteria to the environment during growth is detected in real-time. Susceptible heat flow sensors register the temperature increase (a fraction of a millikelvin) in the sample so that a temperature gradient forms across the sensor due to approximately isothermal conditions in the calorimeter. This gradient generates a voltage at the sensor (Seebeck effect), which is ultimately recorded as the measurement signal and proportional to the temperature gradient. The microcalorimetric investigations performed so far in bacterial detection often resulted in proof of concept studies with the main focus on medical

diagnostics. The cultivation conditions differ considerably from conventional detection methods in microbiological monitoring since 4-mL static ampoules are predominantly used. The ampoules are positioned airtight in the calorimeter. Interestingly, measurements in liquid medium have prevailed here. Only a few applications on solid medium are described in the literature.

The first section of this thesis deals with experimental studies on the 4-mL static ampoule system in terms of calorimetric detection time. Two model systems, *Lactobacillus plantarum* DSM 20205 (**section 3.1.1**) and *Pseudomonas putida* mt-2 KT2440 (**section 3.1.2**) are applied to conventional cultivation techniques. Growth in liquid medium, growth on/in solid medium and pre-enrichment via membrane filtration (special adapters were made so that membrane filters ($d = 10$ mm) could be used for the 4-mL ampoules) with subsequent growth on/in solid/liquid medium are systematically investigated in calorimetric measurements for the first time. The experiments are performed in two commercial microcalorimeters, TAM III and MC-Cal/100P. The emphasis of these experiments is on the influence of the type of cultivation on the detection time. Besides investigating methodical aspects like the number of inocula, filling volume of the ampoules, and selected medium, technical dependencies such as the detection limit are discussed and considered in these studies. Visual inspection of CFU formation is conducted as reference measurements to compare detection times with those obtained from calorimetric experiments.

The results show for both bacteria that culture-based calorimetric detection could recognize bacterial activity much earlier than visual endpoint detection with the naked eye, especially at high initial cell numbers. The cell number dependence of calorimetric measurements is particularly advantageous when using pre-enrichment by membrane filtration, as this allows the applicability of larger sample volumes (compared to the capacity of the ampoules). These studies also demonstrate that solid medium leads to similar detection times and can offer better compatibility with standardized procedures. Further, the data show that the filling volume must be considered, especially for aerobically growing bacteria in 4-mL static ampoules, as this can severely limit the amount of oxygen present. Effects on detection time become relevant when less sensitive calorimeters (detection limit > 10 μ W) are used. Delayed detection in 4-mL static ampoules may also occur if the sample contains only a few cells and is incubated on solid medium. The studies suggest that the exponential increase in the heat flow changes into a flatter, linear course governed by substrate diffusion.

Based on the studies in the first section of this thesis, calorimetric measurements were conducted for the first time with *Legionella pneumophila* ATCC 33152, an opportunistic waterborne pathogen (**section 3.1.3**). Major outbreaks repeatedly occur worldwide because biofilm deposition in stagnant and poorly maintained drinking water piping systems provides ideal growth conditions for *L. pneumophila*. The bacterium poses an immediate threat to immunocompromised and older people. Transmission of *L. pneumophila* occurs predominantly through bioaerosols that can be ingested through the respiratory tract. In addition to Pontiac fever, the bacterium can also cause fatal Legionnaires' disease. This disease is an atypical form of pneumonia.

The detection and enumeration of *L. pneumophila* are specified in the ISO 11731:2017. It is a culture-based approach. The water sample is plated onto non-selective buffered charcoal yeast extract (BCYE) agar and other selective media such as glycine vancomycin polymyxin B cycloheximide (GVPC) agar (direct approach). Antibiotics are added to the medium to inhibit the growth of accompanying flora in the water sample. Enrichment via membrane filtrations is another (indirect) approach. In addition, the ISO standard also prescribes a heat treatment (water bath at 50 °C for 30 min) of the samples and a chemical treatment using membrane filters (30 mL, HCl/KCl-buffer, pH = 2.2, exposure time: 5 min) in order to obtain selectivity within the detection for *L. pneumophila*. Due to the comparatively slow growth of *L. pneumophila*, detection can take up to ten days.

The calorimetric measurements of *L. pneumophila* ATCC 33152 on 1 mL BCYE agar in 4-mL static ampoules performed in this work show that the metabolic activity of the bacteria could be detected in real-time. Depending on the initial number of cells present in the ampoule, detection times ranging from 24 h (1000 CFU) and 45 h (4 CFU) could be determined. The maximum heat flow measured in this experiment is approx. 180 μ W, which is sufficient to be detected by less sensitive calorimeters (detection limit > 100 μ W). In addition, an alternative evaluation of the detection time is also presented. By using the first derivative of the heat flow curves, it is possible to reduce the disturbances that can occur due to the thermal transient of the sample. On the basis of further heat flow measurements of common accompanied bacteria, such as *Pseudomonas aeruginosa* ATCC 27853, *E. coli* ATCC 8739, and *Enterococcus faecalis* ATCC 19433, on commercial Legionella media, the aspects of selectivity are addressed (**section 3.3.3**). These preliminary data show that complete inhibition occurred for two of the three bacteria (exception for *E. coli*) when GVPC agar is used. This kind of inhibition would be one of the prerequisites for selective calorimetric detection of *L. pneumophila* in drinking water since any activity of the accompanying flora would contribute to the net heat flow signal.

With the results from the two model systems, *L. plantarum* DSM 20205 and *P. putida* mt-2 KT2440, this thesis shows that conventional microbiological analysis is compatible with isothermal microcalorimetry. At the same time, the heat flow data demonstrate that especially the early detection of bacterial contamination can be achieved using microcalorimetry. The only thing missing is a microcalorimeter specifically designed for microbiological analysis to perform micro(bio-)calorimetric measurements, i.e. culture-based detection of bacteria using IMC.

Commercial isothermal microcalorimeters often have a wide temperature range (approx. 10 - 100 °C) to cover biological applications as well as those in the disciplines of physics and chemistry. Various sample vessels in different shapes and filling volumes are available, although only a small number have the appropriate dimensions for microbiological cultivation on solid media. Often the surface area is insufficient to obtain separate, countable colonies. The latter would benefit that besides the faster calorimetric detection, quantification of contaminations can also be performed in terms of CFU. In order to use standardized membrane filters ($d = 47$ mm) in commercial calorimeters, only massive sample vessels (> 100 mL) are currently available. Such calorimeters often have a limited number of

measuring channels. High-throughput microcalorimeters can measure about 48 samples simultaneously, but these devices usually use only small sample vessels (≤ 4 mL). The issues associated with calorimetric detection in a 4-mL static ampoule system are already pointed out in the first section of this thesis.

Based on the experimental results from **section 3.1** and the requirements for cultivation in conventional microbiology, the second part of the thesis deals with the design, construction and numerical development work of a new isothermal micro(bio-)calorimeter (**section 3.2**). The principle is based on heat flow measurements using heat flow sensors called thermoelectric generators (TEGs). Within the scope of this work, a test system has been developed first. This is divided into two zones: (i) the outer zone is air thermostated by a fan heater, (ii) the inner zone is composed of the lower part of the measurement channels. Each channel contains a TEG. The sample vessel is in direct contact with the TEG. The lower part of the sensor is located on a heat sink. Two Peltier modules precisely regulate the temperature on the heat sink ($T_{\text{heat sink}} = (37.072 \pm 0.001) \text{ }^\circ\text{C}$). During the heating phase of the calorimeter, two foil heaters support the temperature rise on the heat sink. The test system has three channels (two measuring channels and one reference channel). The operating temperature is set at $37 \text{ }^\circ\text{C}$, making it ideal for detecting *L. pneumophila* and other mesophilic pathogens. The microcalorimeter is air-temperature controlled, and the accuracy of the air temperature measured by a temperature probe in the outer zone is $T_{\text{air}} = (37.0 \pm 0.1) \text{ }^\circ\text{C}$.

The dimensions ($d = 51$ mm, $h = 19$ mm) of the sample vessels used (consisting of aluminium bodies and a top made out of polyether ether ketone) correspond to small-size commercial Petri dishes ($d = 50$ mm). The total volume is 35 mL. The shape of the selected sample vessels ensures a low space requirement (arrangement of several measuring channels is thus possible). In addition, diffusion issues of the substrates and oxygen are minimized due to the large surface area.

In parallel to experiments of the test system under laboratory conditions, numerical heat transport and flow simulations are conducted using a 3D reconstruction of the device to investigate the temperature distribution of individual components or the entire instrument. The computer simulations are based on the finite element method (FEM) and are performed in the simulation software COMSOL Multiphysics[®]. On the one hand, experimental data provided a rough overview of the performance (temperature stability, behavior of the TEGs) that the calorimeter can achieve under laboratory conditions and, on the other hand, served as a validation of the FEM results. Likewise, the numerical results reveal inhomogeneities in the temperature distribution of the test system that are not accessible under experimental conditions. In particular, spatial temperature gradients can be visualized with the help of the FEM. In addition, the computer simulations can plausibly explain experimentally observed effects, such as different behavior among the TEGs.

Now, the numerical 3D model serves as a development tool in which optimizations can be simulated in advance. The temperature distributions obtained for these modifications then allow predictions of improvements toward producing a multichannel prototype. Thus, in **section 3.3.1** of this thesis, initial

results on modifications to the test system are shown. Initial findings from experimental measurements are also included. In addition, the applicability of the micro(bio-)calorimeter for the successful detection of bacteria is demonstrated based on preliminary microbiological measurements (including *P. putida* mt-2 KT2440 in liquid medium and a real cooling tower sample on GVPC agar, **section 3.3.2**). In summary, the methodological optimizations for calorimetric detection of bacteria are systematically investigated in this work. Heat flow measurements are highly compatible with conventional microbiological analysis, benefiting that shorter detection times can be achieved. The results of these studies also highlight the limiting factors in static 4-mL ampoule systems, which are predominantly used for calorimetric detection of bacteria. With the development of a new micro(bio-)calorimeter, this work presents an instrument designed explicitly for microbiological analysis. It can provide real-time information about the condition of the sample and, therefore, serving as an early warning system in the context of conventional cultivation.

1. Structure and outline of the thesis

The number of detection and identification methods published in the last decade (on average 1360 peer-reviewed papers annually) ¹ dealing with bacterial contaminations is almost equal to the number of known human pathogens (1400) ². The reason for this extensive and intensive research is easily inferred from the enormous impact on applied sectors, e.g. agriculture ³⁻⁴, medicine ^{1, 5-6}, drinking water ⁷⁻¹¹ and food industry ¹²⁻¹⁵. Common detection methods can be roughly categorized into two different classes: (i) conventional, culture-based (**section 2.1.1**) and culture-independent techniques (**section 2.1.2**). The latter group contains advanced procedures such as molecular biological, immunological, and biosensorical techniques. Microcalorimetry as a detection technique comprises essential features of both classes.

Historically, the first microcalorimetric contributions to investigating bacterial contamination focused on identifying microbial species (**section 2.2.1**) based on their characteristic heat flow pattern in complex medium ¹⁶. This focus is likely because, during this period, variations in the heat flow curves of different bacteria were the preferred subjects of study to investigate the overall metabolism of bacteria ¹⁷. The underlying measurement principle is based on detecting minute traces of heat caused by bacterial activity and measured via susceptible heat flow sensors (**section 2.2.2**). Nowadays, one research focus of microcalorimetric measurements, in the context of microbiological issues, is the detection of bacterial contaminations ¹⁸. However, most applications found in literature are related to medical diagnostics and presenting only a proof of concept (**section 2.2.3**).

The rapid development of instruments and equipment over the last decades has been a significant contribution to this field ¹⁹. Microcalorimetric detection of bacterial contamination became attractive since highly sensitive and easy-to-use isothermal microcalorimeters are commercially available (**section 2.2.4**) ²⁰. These high-performance microcalorimeters allow detection limits in the range of nanowatt (nW) so that metabolic activity of growing bacteria can be discovered much earlier.

Unfortunately, this technique has not yet found its way into the daily routine of a microbiological analytical laboratory. From an instrument perspective, this is mainly attributable to a non-specific instrument development in microcalorimeters. In addition, systematic studies addressing the interplay between cultivation conditions, technical limitations of calorimeters and the biological nature of contamination on the detection of bacteria are still lacking. Based on the aspects above, the main objectives of this thesis are:

- i. Systematic investigations to demonstrate the applicability of conventional cultivation techniques on calorimetric detection of bacteria. Cultivation of *Lactobacillus plantarum* DSM 20205 (representative for an anaerobic system) in and on selective medium for *Lactobacilli* (De Man, Rogosa and Sharpe, MRS) is used as model (**section 3.1.1**).

- ii. Technical and methodical aspects influencing the detection of aerobic contaminations are investigated in a further study. Here, monitoring the growth of *Pseudomonas putida* mt-2 KT2440 was chosen as the studied object (**section 3.1.2**).
- iii. Heat flow measurements of *Legionella pneumophila* ATCC 33152 on BCYE medium are conducted to demonstrate the microcalorimetric applicability of detecting pathogens in drinking water. Additionally, an improved data evaluation using the first derivative of the heat flow curves is presented (**section 3.1.3**).
- iv. Combining numerical simulations and laboratory experiments, a micro(bio-)calorimetric test system was developed and designed explicitly for routine microbiological testing (**section 3.2**).
- v. Further experiments related to the instrument development and selective detection of bacteria are demonstrated (**section 3.3**). Improvements to the test system are supported by experimental data (**section 3.3.1**), and the first applications of microbiological measurements by the micro(bio-)calorimeter (**section 3.3.2**) are given. Complementary heat flow measurements of frequent accompanying pathogens in drinking water such as *Pseudomonas aeruginosa* ATCC 27853, *Escherichia coli* ATCC 8739, and *Enterococcus faecalis* ATCC 19433 on various Legionella media are shown (**section 3.3.3**).

Based on the main findings, the results are summarized and discussed within the scope of this thesis (**section 4.1**). In particular, an evaluation of the microcalorimetric detection of bacteria is addressed, pointing out the superiority and drawbacks of this method relative to the commonly used visual inspection (**section 4.1.1**). Comparisons extend the discussion to culture-independent detection techniques (primarily PCR). Additionally, the limitations of commonly used 4-mL static ampoule systems are highlighted. In **section 4.1.2**, calorimetric detection is discussed in the context of drinking water analysis, focusing on *L. pneumophila*. Detection times, among other techniques, are compared to IMC, and the selectivity issue of culture-based approaches is raised.

Besides the microbiological aspects, the relationship between method optimization and instrument development is also highlighted (**section 4.2**). A summary of the development process, specifications, and features of a modified version of the test system is also provided. **Section 4.2** debates the differences between the micro(bio-)calorimeter designed in this thesis and commercial calorimeters.

Chapter 5 concludes the new findings of this thesis, and **chapter 6** provides an outlook on further possibilities for instrument and method development.

2. Introduction

In our daily life, essential products like drinking water, food, cosmetics, or pharmaceuticals are produced, transported, provided, and stored. At any stage of these processes, unwanted bacteria can invade such consumables due to a lack of hygiene or mismanagement during maintenance^{15, 21}. It is important to note that a distinction must be made between harmless non-pathogens and harmful pathogens. The latter threaten the safety and quality of said products and can cause life-threatening diseases²². For instance, in the food industry, the WHO estimated in 2017: around 600 million people became sick, and 420,000 died after consuming contaminated food (also included chemical contaminations)²³. The treatment costs just caused by foodborne illnesses are 15 billion US dollars per year²³.

Another example is water. The WHO assumed in 2015: 2.2 million global deaths per year are caused by waterborne disease (more than half of the dead are children), and the economic loss is around 12 billion US dollars per year²⁴. Therefore, one of the top priorities of today's microbiological analysis is to ensure reliable detection of microbial contaminations to prevent outbreaks associated with pathogens.

Customers, producers, and suppliers are expecting a cost-effective and fast detection technique. At the same time, microbiological laboratories are seeking a method that: i) is easy to perform (preferably according to standardized protocol), ii) requires little laboratory effort together with cheap equipment, iii) provides reliable as well as reproducible data, and iv) ensures rapid detection²². At the moment, there exists no microbiological method that sufficiently fulfils all the above criteria²². Moreover, the biological properties of the products mentioned above have a substantial impact on the detection of specific pathogens²⁵. Depending on the origin of the sample being analyzed, the state (liquid, solid), interfering product matrices²⁶, and accompanying bacterial flora²⁷ may impede the detection of particular pathogens.

Historically, a conventional bacteriological method, i.e. culturing bacteria in liquid and solid medium with a final enumeration of grown colonies, is the method of choice for microbiological laboratories^{22, 28}. This approach has persisted until today, so that many ISO standards still rely on conventional cultivation techniques and subsequent enumeration¹. Currently, this method most effectively combines the requirements of the microbiological laboratory and the customer's wishes, although the speed of detection is a limiting factor²⁹⁻³⁰. Various other detection methods, such as molecular biological techniques, immunological approaches and biosensors, are superior, as they provide evidence of bacterial contaminations within a few minutes or hours²⁹⁻³¹.

In this connection, the combination of cultivation techniques with microcalorimetric analysis has already shown that a faster detection of bacterial contaminations is achievable in different fields, e.g. water³², food³³ and medicine³⁴. However, the main focus of published applications is in clinical diagnostics^{20, 35-36}. This underappreciated method could be a powerful complement to conventional bac-

teriological methods for detecting bacteria in many other fields due to its real-time monitoring potential. However, apart from inadequate method development and optimization, there is a lack of an instrument that specifically meets the requirements for detecting microorganisms in the context of conventional microbiological analysis.

Before introducing the field of isothermal micro(bio-)calorimetry, a brief overview of common detection techniques for bacteria is presented in the following sections.

2.1 Detection techniques for bacteria

In the beginning, it is important to mention that the two terms “identification” and “detection” must be clearly distinguished from each other. A method addressing bacterial identification is interested in recognizing a particular organism, species or strain within a consortium of other bacteria by its characteristics (e.g. a specific gene sequence)³⁷. The central aspect is to prove the organism's identity by comparing it with well-known organisms through their characteristics³⁸. Regarding bacterial identification, one would like to know the species in a drinking water sample, e.g. *Legionella pneumophila* and *Escherichia coli*. The term limit of identification is uncommon in microbiological analysis. However, it is possible to quantify the percentage match of 16S rDNA gene sequences between two strains³⁹.

In contrast, the goal of a detection method is more general, and the discovery is central. Consequently, there is a strict distinction between “there is something” or “there is nothing” (qualitative approach). Additionally, a kind of quantification is somehow also related to the term detection. Depending on the applied method, different limits of detection (LOD) are possible. The LOD indicates the amount/number/concentration of the quantity to be investigated that can be determined with statistical confidence (quantitative approach)⁴⁰. According to these definitions, detection is a qualitative and quantitative screening method, e.g. a positive sample (there is something above the LOD) can be distinguished from a negative sample (there might be something, but it is below LOD and the applied method detected nothing).

Furthermore, a positive sample allows additional quantification of a target variable. Unfortunately, in microbiological analysis, there is no clear definition for both terms. Thus in this thesis, emphasis is only put on the aspect of bacterial detection as defined above.

2.1.1 Conventional, culture-based techniques

One of the most outstanding achievements in microbiology was the isolation and cultivation of pathogenic bacteria from different sources like liquors (blood, urine, drinking water) and solids (tissue, food, drugs)⁴¹⁻⁴². Starting from a small piece or volume of contaminated material transferred onto a

semi-solid nutrient medium (gelled by agar-agar⁴³), the pathogens can grow to build more or less single bacterial colonies. Alternatively, enrichment cultures of the samples are prepared in nutrient-rich and complex broth media to recover pathogens⁴⁴. Then, a part of this enrichment culture is likewise transferred onto the agar medium. In order to achieve the formation of single colonies, serial dilutions from the original sample or the enrichment cultures are primarily performed⁴⁵. Here, the assumption is that a single colony arose from an initial single bacterial cell. Within a certain incubation period, the initial mother cell and the resulting daughter cells have multiplied so often that enough cells have been formed to make the bacteria pile (colony) visible for the naked eye. For instance, a colony of *E. coli* contains approx. 10^7 to 10^8 cells after 12 h of incubation⁴⁶. From the number of obtained colonies, the initial degree of contamination in the sample can be deduced. The growth process of bacterial cultures is strictly regulated by the cultivation conditions such as temperature, substrate selection and concentration, pH level, oxygenated or anoxic environment.

Based on the origin of the sample and the target microorganism under investigation, standard protocols (ISO norms), which detail the performance of the microbiological analysis and the subsequent evaluation of obtained results, were established. Nowadays, this process is routinely employed in the quality control of our daily consumables. **Figure 1** summarizes some general procedures of conventional bacteriological detection. Depending on the sample's origin, the direct approach is possible, e.g. water from cooling towers and milk. Otherwise, a pre-enrichment by nutrient broth such as peptone water is necessary to increase the concentration of potential pathogens in the sample⁴⁷. The majority of norms are still based on the enrichment and cultivation of the target microorganism on semi-solid agar gel. For instance, according to ISO 11731:2017 (Water quality - Enumeration of *Legionella*), optimized culture media and physical or chemical treatments of the sample should enable selective detection of *Legionella pneumophila*⁴⁸. Further, samples containing low numbers of pathogens (mainly drinking water samples) can also be pre-enriched by membrane filtration⁴⁹.

Besides the qualitative character of the method, a quantitative result is obtained by enumeration of the colonies formed. The evaluation of cultures in conventional microbiology is carried out exclusively visually by well-trained laboratory staff⁵⁰. Thus, the human eye does the most straightforward and most applied inspection. However, this is also the weak spot of the conventional method. The following calculation demonstrates this: Starting from a single pathogenic bacterium ($N_0 = 1$ cell) that grows under optimal conditions with a specific growth rate of $\mu_{\max} = 1.39 \text{ h}^{-1}$ (doubling time for *E. coli* is $t_d = 0.5 \text{ h}$)⁴⁶. Here, the number of cells that form a colony visible represents the detectable quantity. The LOD is approximately 10^7 to 10^8 cells⁴⁶. As a result, a detection time of approx. 11.6 to 13.3 h is expected. Consequentially, visual inspection becomes a time-consuming process, especially for slow-growing pathogens⁵¹. Even a tenfold increase in the doubling time ($t_d = 5 \text{ h}$, not uncommon for *L. pneumophila*⁵²⁻⁵³) with the same LOD leads to a detection time of approx. 116 to 133 h. Thus, the conventional microbiological analysis might lead to delays in countermeasures.

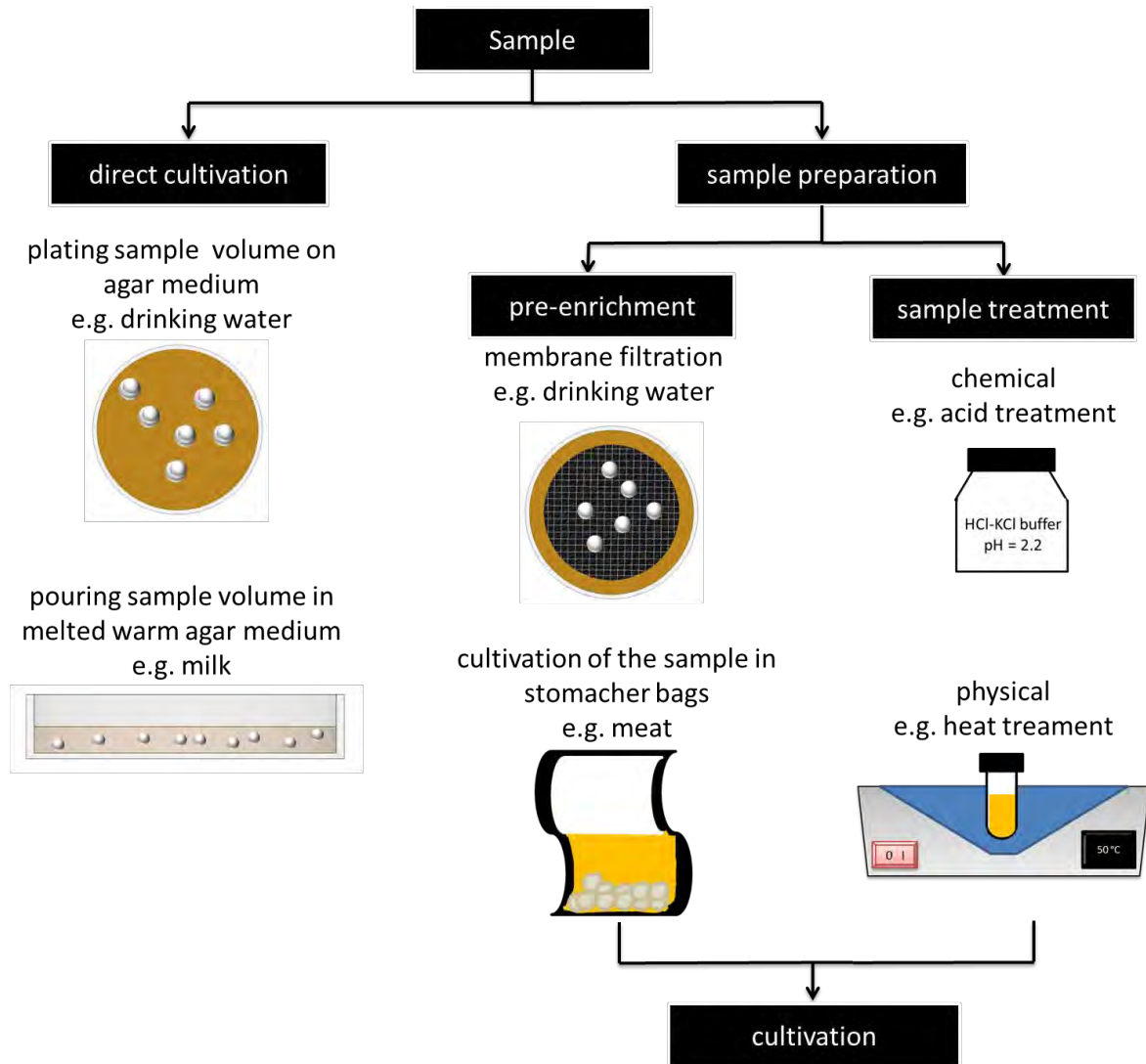


Figure 1: The essential procedures used in the conventional microbiological analysis for the detection of bacterial contaminations.

Additionally, the counting process is prone to error because it is based on subjective decisions⁵⁴⁻⁵⁶. In order to overcome these issues, advanced optical technologies were developed to allow an earlier and more reliable detection. For example, expensive cameras and scanners are involved in so-called automated colony counters capturing images of incubated Petri dishes and visible colonies at an earlier stage of colony formation^{54, 57-58}. For this purpose, image processing algorithms are applied to define and count colonies⁵⁹. However, these automatic counting techniques also have drawbacks, as expensive software tools⁵⁵ and instruments⁶⁰ are required. Further, even dust particles and scratches can lead to erroneous measurements^{50, 54}.

Another optical method approach is the use of microscopy to detect microcolonies^{51, 61}. Likewise, the aim is to minimize the LOD (microcolonies consist of 10^2 to 10^3 cells⁶²), but the quality of the agar can already lead to errors in detection⁶³. However, among optical detection techniques, naked-eye

colony counting on agar is still the dominant approach for the detection of bacterial contamination in conventional microbiological analysis.

The optical inspection techniques mentioned so far have one common feature since they provide quantitative results expressed in colony-forming units (CFU) per milliliter or gram sample²⁸. This metric is straightforward and can quantitatively indicate the degree of bacterial contamination. For instance, 100 CFU / 100 mL for *L. pneumophila* or 0 CFU / 100 mL for *E. coli* in drinking water samples represent a technical threshold value according to the German Drinking Water Ordinance (Trinkwasserverordnung, TrinkwV2001). If the threshold value is exceeded, technical measures must be initiated to protect the health of affected consumers. **Table 1** summarizes some examples of legal and technical threshold values for pathogenic bacteria from different sources.

However, despite the ease of quantification, three significant problems arise with conventional microbiological analysis. First, the clear discrimination of different species is often impossible due to the similar look of colonies on the same culture medium. Therefore, the actual count of a species might be overestimated or underestimated. In order to overcome this issue, chromogenic media are available for certain species to facilitate selective enumeration of species⁶⁴. Second, underestimating cell numbers can occur on plate counts due to cell aggregation⁶⁵.

Table 1: Legal and technical threshold values of selected pathogens from different sources

Source	Species/ bacterial group	Threshold	Reference
drinking water	<i>Escherichia coli</i>	0 CFU/100 mL	TrinkwV 2001 ^[1]
	<i>Pseudomonas aeruginosa</i>	0 CFU/250 mL	TrinkwV 2001
	<i>Legionella</i> spp.	100 CFU/100 mL	TrinkwV 2001 ^[2]
egg products	<i>Salmonella</i> spp.	0 CFU/25 g	EC 2073/2005 ^[3]
	<i>Enterobacteriaceae</i>	10 ^a - 100 ^b CFU/g or mL	EC 2073/2005
minced meat	<i>Escherichia coli</i>	50 ^a - 500 ^b CFU/g	EC 2073/2005
cheeses made from raw milk	Coagulase-positive staphylococci	10 ^{4(a)} - 10 ^{5(b)} CFU/g	EC 2073/2005

^a “m”-value, represents guidance level

^b “M”-value, represents warning value

Third, not all bacteria can be cultured under laboratory conditions. Some pathogens can also enter a so-called viable but nonculturable (VBNC) state⁶⁶.

^[1] Verordnung über die Qualität von Wasser für den menschlichen Grbrauch 1, 2 (Trinkwasserverordnung - TrinkwV Anlage 1 (zu §5 Absatz 2 und 3) Mikrobiologische Parameter

^[2] Verordnung über die Qualität von Wasser für den menschlichen Grbrauch 1, 2 (Trinkwasserverordnung - TrinkwV Anlage 3 (zu § 7 und § 14 Absatz 3) Indikatorparameter

^[3] Commission Regulation (EC) No 2073/2005 of 15 November 2005 on microbiological criteria for foodstuffs

More sophisticated and culture-independent detection methods are available to detect these bacteria as well, which are briefly presented in the following section. Furthermore, advantages and drawbacks are discussed.

2.1.2 Culture-independent detection techniques

Culture-independent techniques form a very heterogeneous group of different approaches addressing the detection of bacterial contaminations. In general, this group can be classified into three subdivisions: (i) molecular-biological, (ii) immunological and (iii) biosensorical.

One of the most popular techniques is the polymerase chain reaction (PCR) ⁶⁷. PCR is assigned to molecular detection methods, which target specific regions in the genome of the pathogens (more precisely, short nucleic acid sequences of the DNA) rather than the entire microorganism ²². These DNA sequences are amplified through several PCR cycles. In order to increase the concentration, further reagents are required, such as template DNA, primers, nucleotides and DNA polymerase ⁶⁸. Finally, in conventional PCR, the amplified target DNA is detected using gel electrophoresis ²⁹. Single-step detection of different bacteria in one sample can be realized by multiplex-PCR (mPCR) ²⁴. Therefore, additional primers are added to detect specific DNA sequences of different bacteria ²². A more sophisticated approach is real-time PCR (RT-PCR), where a fluorescence signal is detected as the target DNA sequence is labeled during the PCR cycles by probes that emit fluorescence ²². The concentration of amplified DNA is proportional to the emitted fluorescence signal. Thus real-time information is provided ²². However, this additional information is also accompanied by extra and more expensive instrumentation since a spectrofluorometer is required to detect the fluorescence signal.

Nowadays, the classical PCR method can also be further enhanced for obtaining quantitative data, which are realized in different forms such as qPCR and digital PCR (dPCR). These quantitative data can be expressed, for instance, in genome units (GUs) per liter determined by standard curves ⁶⁹. The main advantage of PCR techniques is indubitable the fast detection time ⁷⁰⁻⁷¹. All developments indeed render the PCR method more selective and sensitive, but at the same time, the costs for equipment, its maintenance and the use of special chemicals also increase ²². Besides, obtained results are not trivial to interpret, and trained staff is necessary for correct data evaluation ²². However, the main limitation of PCR methods in the context of bacterial detection is the lack of discrimination between living and dead cells since even DNA residues from damaged cells in the sample are amplified and consequently detected ^{27, 29, 32, 72}.

Immunological methods form the second important class. Here, the most frequently applied technique is ELISA (enzyme-linked immunosorbent assay) ⁷³. In general, specific antibodies are used to detect antigens on the pathogen's surface or their produced toxins ¹. These antibodies are coupled with enzymes (e.g. horseradish peroxidase, HPR) ²⁹. A color response caused by an enzymatic reaction between HPR and a chromogenic compound provides the detectable quantity, which in turn is detected

by an ELISA reader⁷⁴. Different ELISA approaches are used such as (i) direct: the enzyme is coupled with primary antibody conjugate, (ii) indirect: the enzyme is coupled with a secondary antibody conjugate, which is linked to a primary antibody conjugate, and (iii) sandwich: the antigen is interconnected between two antibodies (direct and indirect approach is possible)⁷⁴. ELISA allows high sensitivity as well as high specificity for the detection of bacteria. Depending on the chosen approach, different limitations can occur: primary antibody labelling is tedious and expensive (direct ELISA), a secondary antibody can cause cross-reactions (indirect ELISA), and due to the sandwich structure, only antigens with two antigenic sites are measurable (sandwich ELISA)⁷⁴.

The term biosensors summarize the last large class of detection techniques. In general, a biosensor is composed of the following components: (i) the probe, i.e. bio-receptor that recognize a biochemical signal, (ii) the transducer, which translates the biochemical signal into an electrochemical, optical, mass, or thermal signal that can be measured and (iii) an amplifier⁷⁵⁻⁷⁶. The biochemical signal is generated by a reaction between the analyte and the bio-receptor (e.g. enzymes, antibodies or bacteria)^{75, 77}. Among the different kinds of biosensors, optical and electrochemical techniques are frequently used to detect bacteria⁷⁸. The advantages of biosensors are the high specificity as well as sensitivity^{75, 79}. Further, miniaturization is in principle possible and easy to use in different application areas^{75, 78}.

Due to the diversity of biosensors used, it is challenging to generalize limitations and drawbacks in bacterial detection. However, the sample matrix can be limiting the sensitivity and selectivity of the sensor⁷⁸. In particular, when only subcellular structures such as enzymes, DNA or RNA are detected, additional steps for sample preparation and extracting reagents are necessary⁸⁰. Specific biosensors like Surface Plasmon Resonance (SPR) are highly sensitive, but due to the complexity of the measurement, well-trained staff and expensive equipment are required⁸¹.

In summary, there is a wide variety of alternative detection methods that differ from the conventional microbiological analysis. These methods often do not require artificially induced cultivation of the pathogen. Instead, specific components or excreted substrates of the pathogen such as genes, proteins, enzymes, toxins or antibodies are selected for the detection. The superiority in detection time becomes clear when one realizes that these components or substrates are detected very specifically by one or a few chemical reactions. By comparison, forming a new cell (during cultivation) involves a tremendous number of chemical reactions.

Now that a selection of common detection methods has been presented, the focus of the following sections will be on isothermal micro(bio-)calorimetry. First, there is a short introduction to the topic, then a historical review followed by presenting the measurement principle and a summary of applications known from the literature. Finally, the chapter closes with the design and construction process of isothermal microcalorimeters. Included are two brief sections on FEM as a development tool for calorimeters and requirements imposed on an isothermal micro(bio-)calorimeter.

2.2 Isothermal Micro(bio-)calorimetry

There is no precise classification of isothermal microcalorimetric measurements in the context of bacterial detection. The technique is in between conventional methods and biosensors. In this thesis, the term micro(bio-)calorimetry is designated for this purpose. The corresponding instruments are called micro(bio-)calorimeters. Micro(bio-)calorimetry is an interdisciplinary research field composed of two subjects, microbiology and microcalorimetry. A similar term, “*Microbiological calorimetry*”, was introduced by Gustafsson in 1991⁸². The terms bio- (or biological) calorimetry⁸³⁻⁸⁵ or biochemical calorimetry⁸⁶ are used across the board, which are not only aimed at microbiological systems.

Briefly, the metabolic activity of bacteria in culture media is monitored via heat flow sensors under almost isothermal conditions. **Figure 2** illustrates the principle of measurement.

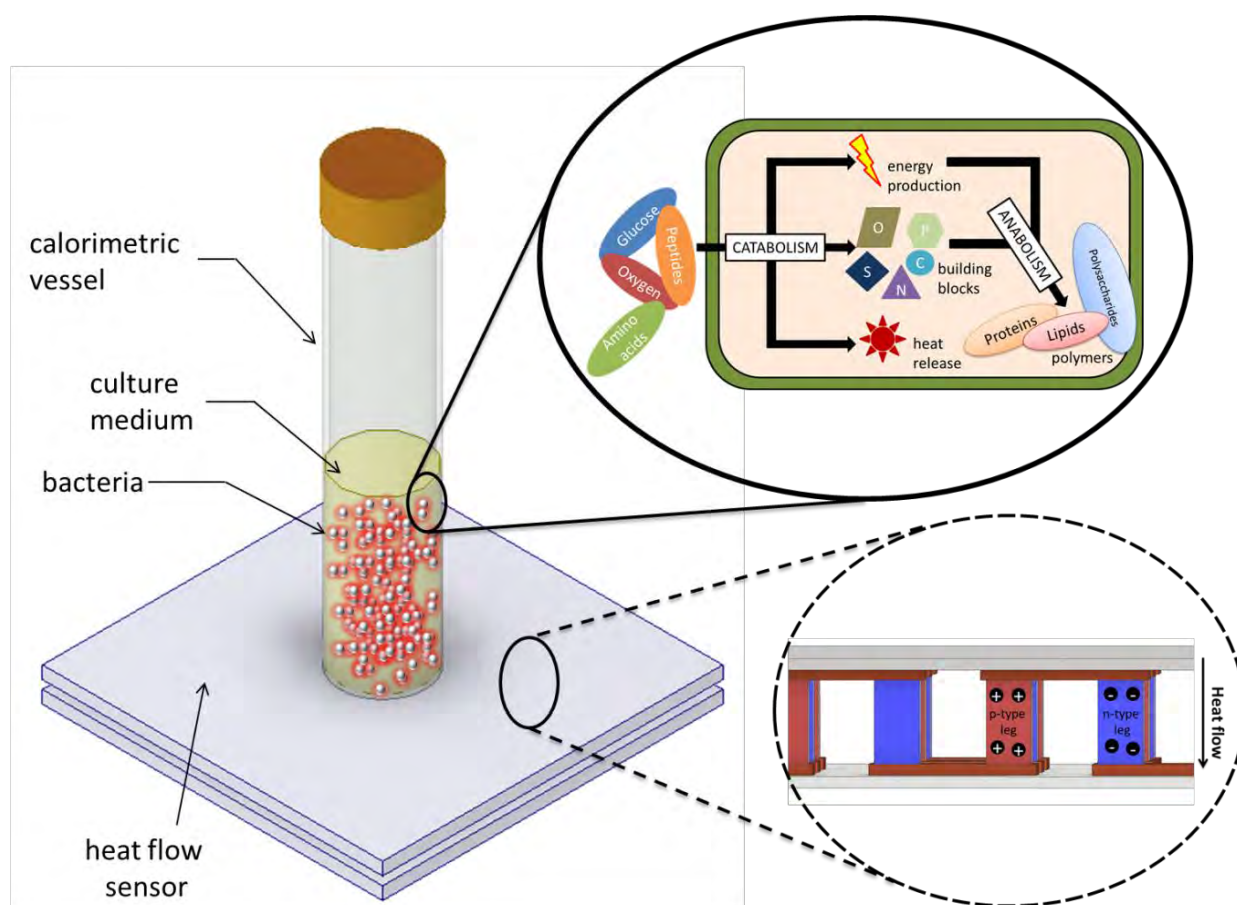


Figure 2: Principle of the micro(bio-)calorimetric measurement for the detection of bacteria. Due to the metabolic activity of growing bacterial cells, the temperature increase in the calorimetric ampoule leads to a heat flow across the heat flow sensor. Parts of the figure are adapted from⁸⁷ and⁸⁸.

The growth of bacteria is mainly an exothermic process (exceptions are known⁸⁹), i.e. heat is produced and caused an increase in temperature in the sample. As a result, a temperature gradient is

formed across the heat flow sensor. Due to the small heat production rate of a single growing bacterial cell (1-4 pW)³², the increase in temperature is relatively small (a fraction of a mK). Therefore, a precise temperature control unit and sensitive heat flow sensors are required to detect microbial heat traces. A detailed description of the measurement principle is given in **section 2.2.2**.

In the following section, the historical development of micro(bio-)calorimetry as an analytical tool for detecting microbial activity is reviewed.

2.2.1 A brief historical review

The first applications of calorimetric experiments on living systems were independently conducted by Crawford in Scotland and Lavoisier and Laplace in France at the end of the 18th century^{86,90}. The ice fusion calorimeter developed by Lavoisier was not scaled for microbiological systems but rather for minor mammalian (**Figure 3**).

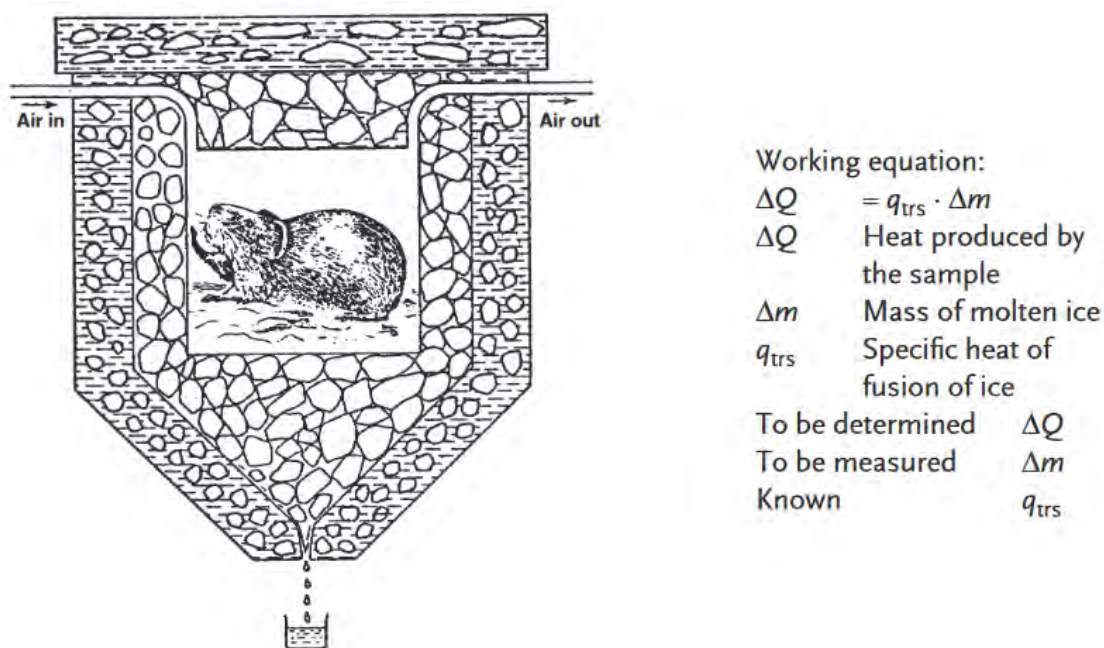


Figure 3: Determining the metabolic activity of guinea pig by an ice fusion calorimeter conducted by Lavoisier and Laplace. The equation shows the relationship between the determined heat ΔQ and the measured mass Δm of melted ice. Reprinted from⁹¹ with permission from © (2014) Wiley-VCH Verlag GmbH & Co. KGaA.

In the middle of the 19th century, the first calorimetric experiments involving microorganisms can be attributed to Dubrunfaut⁹². With his macrocalorimeter, he determined the heat production during the alcoholic fermentation process catalyzed by yeast. At the beginning of the 20th century, the first studies were explicitly conducted addressing the heat production of bacteria⁹³. Tangl and Rubner used

combustion calorimeters to measure the heat of combustion of the nutrient bouillon before cultivation and after cultivation (with bacteria)⁹⁴. From the difference, the energy converted could be determined. Rubner realized that the calorimeters, which were in use at that time, were inadequate and not sensitive enough for directly measuring the heat production of bacteria⁹³. Consequently, he developed a microcalorimeter to investigate various microbial processes, such as the souring of milk⁹³.

Later, Hill independently developed an improved version of the calorimeter designed by Rubner and used it to measure the heat production of microbial processes⁹⁵. Based on the work of Hill, Shearer investigated the heat production of growing *Bacillus coli* (later renamed as *E. coli*⁹⁶) in different culture media and was able to show that the medium composition affects the amount of heat released⁹⁷. In the late 1920s, Bayne-Jones and Rhees combined bacterial counts with the time-dependent heat production and found different growth phases of the bacteria during their calorimetric experiments⁹⁸. They linked for the first time growth phase changes to a switch in the metabolism of the bacteria and determined a cellular heat production rate of a growing bacterium to 10^{-9} cal (4.2 nJ)⁹⁹.

Considerable progress in the study of bacterial metabolism was made in the middle of the 20th century. This progress can be essentially attributed to the advancement of calorimeters. The construction of a new type of calorimeter, developed by Tian and later optimized by Calvet, made a particular contribution⁹⁹. These Tian-Calvet heat conduction type calorimeters represent the foundation of modern microcalorimeters¹⁹. Continuing this work, Wadsö and co-workers developed more sensitive and powerful isothermal microcalorimeters based on the heat conduction type¹⁰⁰. Microcalorimetry became more and more an analytical tool for biological issues during this period, as the design was aimed at biological and biochemical work¹⁰¹⁻¹⁰².

Due to progress, microcalorimetry became interesting in the field of clinical diagnostics⁹⁹. Boling et al. showed that characteristic heat flow patterns could be obtained for bacteria of the family *Enterobacteriaceae*, and thus identification is possible¹⁶. Russel et al. investigated the heat flow pattern of more than 200 clinically relevant strains and claimed that bacterial identification is possible in less than 24 hours¹⁰³. The use of microcalorimetry as a detection tool was made in the 1970s and 1980s mainly to estimate microorganisms in food. In 1974, Berridge et al. detected bacteria in milk and found that 10^5 CFU/mL bacterial concentrations resulted in a detectable heat flow¹⁰⁴. Lampi et al. (1974) examined vacuum-packed food⁹⁹, and soon after, Ripa et al. (1977) detected bacterial growth in contaminated blood culture¹⁰⁵, and Gram et al. (1985) monitored the quality of meat and fish by microcalorimetry^{33, 106}.

During this time, isothermal microcalorimeters were mainly constructed by academia as individual devices. Later, manufacturers like LKB Instruments in Sweden began with serial production of isothermal microcalorimeters and commercialized the multichannel (four-channel) Bio Activity Monitor (BAM), later renamed as Thermal Activity Monitor (TAM)¹⁰⁰, enabling greater sample throughput¹⁰⁷. Nowadays, TA instruments (a successor of LKB), Calimetrix, Symcel and Setaram provide a diverse

portfolio of different microcalorimeters (more information in **section 2.2.4**). However, even today, there are some examples of uniquely constructed calorimeters, e.g. ¹⁰⁸⁻¹¹⁰.

Interestingly, almost 20 years have passed before applications of microcalorimetric detection for bacterial contamination have been recognized again. The focus of recently published microcalorimetric investigations was on clinical diagnostics. In 2007, Trampuz et al. detected pathogenic microorganisms in platelets products ²⁰ and used microcalorimetry to detect bacterial meningitis in cerebrospinal fluid ¹¹¹. Braissant and co-workers extensively investigated a microcalorimetric approach to detect tuberculosis agents ¹¹²⁻¹¹⁴. More details on this topic are given in **section 2.2.3**.

Before addressing some applications in isothermal micro(bio-)calorimetry, the underlying measurement principle of a micro(bio-)calorimetric detection of bacteria is introduced.

2.2.2 Micro(bio-)calorimetric principle

The principle of detecting bacterial contaminations by micro(bio-)calorimetry is based on heat flow measurements. The heat flow Φ (in W) originates from the metabolic activity of bacteria in the sample. In general, the sample contains an initial number of bacteria, N_0 (pure or mixed cultures), substrates such as carbon (primary energy source) and nitrogen. Supplements, e.g. vitamins, trace elements, and buffer, are added to support bacterial growth. Additionally, the sample can contain part of the sample matrix (liquids and solids). If we consider the cellular level, the simplified scheme of an open system, e.g. metabolizing glucose shown in **Figure 4** is obtained.

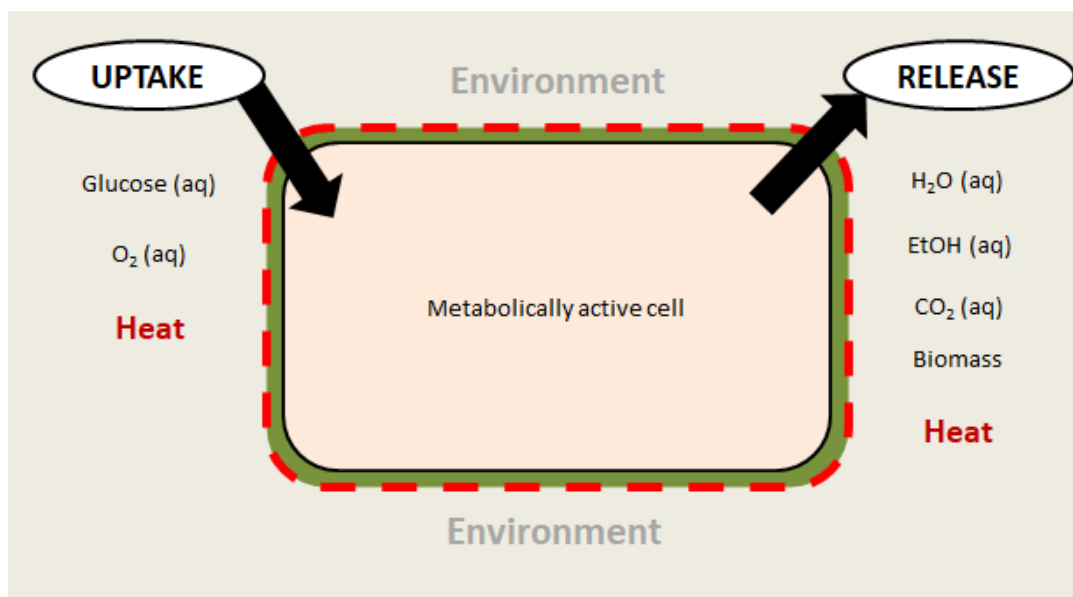
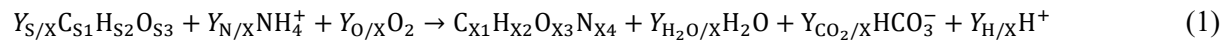


Figure 4: Biothermodynamic view of a metabolically active cell as an open system. The cell membrane represents the system boundary and is indicated by red lines, at which substrates like glucose and oxygen can be taken up by the cell and products like carbon dioxide, water and ethanol are released into the environment. Heat is released (exo-) into or consumed (endothermic) from the environment. The figure is adapted from ¹¹⁵.

However, on a smaller scale, many enzyme-catalyzed reactions taking place to disassemble the glucose molecule (catabolism) and transform the substrates into products such as ethanol, water, carbon dioxide, and new biomass (anabolism) ¹¹⁶⁻¹¹⁷. From a kinetic point of view, the latter does not contribute significantly or only slightly to the overall metabolism ^{82, 118}. Each reaction step is accompanied by heat release (negative reaction enthalpy, exothermic) or heat consumption (positive reaction enthalpy, endothermic) that is determined by the stoichiometry of both processes: product formation and microbial growth ¹¹⁹. Eq. 1 reflects the stoichiometry of the product formation on the example of aerobic microbial growth ¹¹⁹:



Where $C_{S1}H_{S2}O_{S3}$, NH_4^+ and O_2 represent the carbon, nitrogen source, and terminal electron acceptor. $C_{X1}H_{X2}O_{X3}N_{X4}$ stands for the formed biomass and H_2O , HCO_3^- and H^+ for the products formed during the growth process. $Y_{S/X}$, $Y_{N/X}$, $Y_{O/X}$, $Y_{H_2O/X}$, $Y_{CO_2/X}$, $Y_{H/X}$ express the yield coefficient of each reactant consumed and product formed (except for biomass) ¹¹⁹. Despite the stoichiometry, the net reaction heat production rate (i.e. heat flow) reflects the kinetics of the microbial growth process and is detected in real-time by microcalorimetry ^{115, 119-120}. The heat flow is expressed by eq. 2:

$$\Phi = \sum_j \Delta_R H_j \dot{\xi}_j \quad \text{with} \quad \dot{\xi}_j = r_{ij} \cdot \nu_{ij} \quad (2)$$

Where $\Delta_R H_j$ (in kJ mol^{-1}) is the enthalpy of each reaction j taking place in the metabolically active cell, $\dot{\xi}_j$ (in $\text{mol L}^{-1} \text{s}^{-1}$) is the product of the reaction rate r_{ij} (in $\text{mol L}^{-1} \text{s}^{-1}$) and the stoichiometric coefficient ν_{ij} of the species i in the reaction j ¹¹⁹. The proportionality between the reaction enthalpy and the heat flow is only valid for an open system under constant pressure ¹²⁰.

In order to break it down to a simple mathematical relationship (eq. 3), this means that at a present time t , the metabolic caused heat flow $\Phi(t)$ (in W) is determined by the actual number of bacteria $N(t)$ and their specific cellular heat production φ (in W) ¹²¹:

$$\Phi(t) = \varphi \cdot N(t) \quad (3)$$

The specific cellular heat production term reflects the total energy balance of metabolism (growth stoichiometry and formation of products ¹¹⁹) in a single cell and can be viewed in an elementary form as the power output of an engine. For the specific cellular heat production, only a few data of selected cells are reported ¹²²⁻¹²³ since experiments cannot directly determine this quantity due to the small values for bacterial cells (in the range of a few pW) ²⁰. Further, this value may depend strongly on the available energy source and cultivation conditions ¹²³. Thus, it is closely associated with the bacteria's growth rate μ (in h^{-1}) ³².

The heat flow caused by bacterial activity in a contaminated sample can only be detected if the signal exceeds a threshold that is significantly above the baseline noise of the microcalorimeter employed. Unfortunately, empirical threshold values are used for different calorimeters based on a manifold of the sensitivity of the respective calorimeter¹²⁴. The corresponding time is determined as the detection time t_{dect} . Currently, there is no statistical model to assess the earliest metabolic activity that the calorimeter can detect. **Figure 5** reflects the process of determining the detection time for an exemplary heat flow measurement. All studies from the literature dealing with the calorimetric detection of bacterial contaminations recorded the complete heat flow curves reflecting the bacteria growth under batch cultivation conditions (see, e.g. in^{111-112, 125}). However, the yellow-marked area in **Figure 5** is not necessary for the detection. Only the increase of the heat flow signal caused by a contaminated sample has to be recorded.

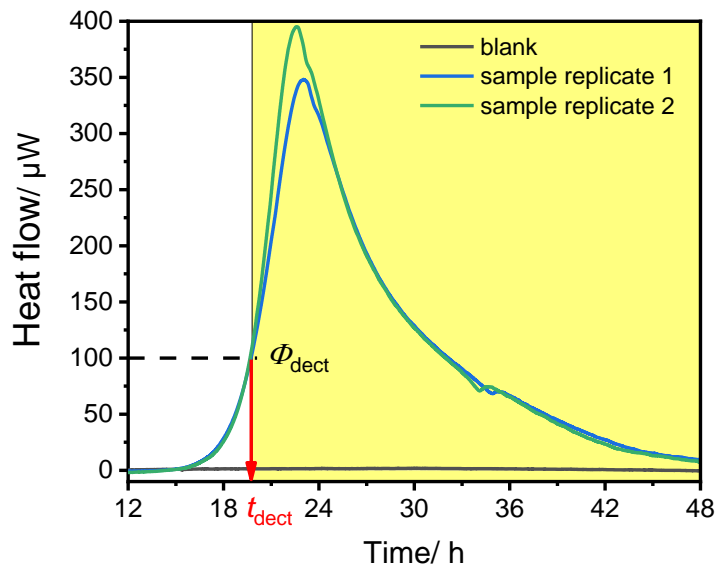


Figure 5: Determining the detection time t_{dect} of a micro(bio-)calorimetric measurement at a predefined detection threshold of $100 \mu\text{W}$. The yellow area displayed the part of the heat flow curve which is not of interest for the detection.

10^4 to 10^5 CFUs are necessary to monitor a detectable heat flow using very sensitive microcalorimeters (detection limits $< 1 \mu\text{W}$)^{18, 32}. If the initial number of bacteria is $N_0 < 10^4$, a growth medium must be added to the sample to initiate bacterial growth. Consequentially, the growth behavior follows an exponential function (eq. 4):

$$N(t) = N_0 \cdot \exp(\mu \cdot t) \quad (4)$$

Finally, eq. 3 and 4 can be coupled through the number of bacteria present in the calorimetric experiment at time t . The resulting equation is (eq. 5):

$$\Phi(t) = \varphi \cdot N_0 \cdot \exp(\mu \cdot t) \quad (5)$$

Rearranging of eq. 5 leads to eq. 6 that shows the proportionality between the detectable heat flow Φ_{dect} (in W) and the detection time t_{dect} (in h) ¹²⁴:

$$t_{\text{dect}} = \frac{\ln\left(\frac{\Phi_{\text{dect}}}{\varphi}\right) - \ln(N_0)}{\mu} \quad (6)$$

In order to obtain the lowest detection time, all parameters related to the bacteria under study (φ , N_0 , μ) should be maximized for their calorimetric detection. It is essential to note that eq. 5 is only valid if enough nutrients are available ¹²⁴.

In the next section, the total records for micro(bio-)calorimetric detection of bacteria are reviewed. Further, the advantages and limitations of this detection method are summarized.

2.2.3 Applications of micro(bio-)calorimetry in the context of bacteria detection

Micro(bio-)calorimetry, like any analytical tool, has advantages and limitations. Regarding bacterial detection, the real-time monitoring potential is a plus since any changes in the measured heat flow can immediately be registered by the operator. For instance, if a sample already contained enough metabolically active bacteria, the produced heat flow can directly be discriminated from the noise of the baseline. The state of the sample (liquid or solid) and its optical properties (transparent or opaque) are theoretically unimportant ¹⁰⁰. However, due to the unspecific nature, any physical, biological, or chemical reaction is accompanied by heat production or consumption and consequentially affects the overall heat flow ¹²⁶. Hence, abiotic side reactions within the sample, such as pH shifts, evaporation, condensation, and degradation processes, must be known or at least considered ^{83, 126}. A further benefit is that the measurements do not require expensive reagents for labelling or initiation ³⁴. In most cases, a cheap and simple culture medium (sometimes supplemented with selective marker) already provides an ideal nutrient supply for the micro(bio-)calorimetric detection of bacteria.

This detection method has already been applied to examine bacterial contaminations in food ³³, agricultural products ¹²⁷, clinical diagnostics ^{20, 111} and tap water ³². Unfortunately, most studies working with artificial contaminations and thus represent only a proof of concept. In the following, a systematic review of micro(bio-)calorimetric applications in the context of bacterial detection is presented. **Table 2** includes the sample material to be tested, the calorimeter used for the investigations and the associated measurement conditions such as temperature, sample volume, and culture medium. In addition, the bacteria examined are listed (if known), and a summary of the most important results is given.

Table 2: Summary of micro(bio-)calorimetric studies addressing the detection of bacteria in different sample materials

Sample material	Calorimeter	$T / ^\circ\text{C}$	$V_{\text{sample}} / \text{mL}$	Culture medium	Investigated microorganisms	Main findings	Ref.
milk	microcalorimeter, continuous flow version (LKB Instruments)	30	1.0	sterile milk (l)	<i>C. lacticum</i> , <i>S. cremoris</i> , <i>E. coli</i> , <i>K. aerogenes</i> , <i>Micrococcus</i> sp. <i>Pseudomonas</i> sp.	The species and age of culture showed a dependence on the heat produced per CFU. The detection limit of $< 5 \cdot 10^5$ CFU mL ⁻¹ was characteristic for calorimetric measurements.	104
blood culture	microcalorimeter, modified version (LKB Instruments)	37	4	TSB (l)	<i>E. coli</i> , <i>S. aureus</i> , <i>N. meningitidis</i>	Optimal blood culture medium composition was microcalorimetrically determined. The effects of different supplements on heat production by the three species were investigated.	105
ground meat and fish	LKB 2277 BioActivity Monitor	21, 30	1	nutrient broth (l)	unkown	Bacterial concentrations from 10^4 to 10^8 cells g ⁻¹ were detectable within 24 h by microcalorimetry. Correlation between the peak of heat production rate and colony counts were established.	33
ac ^a platelets (PLTs)	TAM III, equipped with 48 channels	37	3	TSB (l)	<i>S. sanguinis</i> , <i>E. coli</i> , <i>S. aureus</i> , <i>S. epidermidis</i> , <i>P. ances</i> , <i>C. albicans</i>	The calorimetric detection limit was 1 to 10 CFUs per mL PLTs. Detection times were highly dependent on initial bacterial concentration, e.g. 3.2 h (10^5 CFU mL ⁻¹) and 7.5 h (10^1 CFU mL ⁻¹) for <i>E. coli</i> . Characteristic heat flow patterns of each species were observed and almost independent of the initial concentration.	20
ac cerebrospinal fluid (CSF)			3.1	TSB, BHI (l)	<i>S. pneumoniae</i> , <i>N. meningitidis</i> , <i>L. monocytogenes</i>	A strong correlation between the bacterial titer (CFU mL ⁻¹) and time to calorimetric detection was observed. Detectable heat flows from small sample volumes of CSF were obtained in a few hours, e.g. 3.9 h (10 μ L) and 5.5 h (1 μ L) for <i>N. meningitidis</i> ($c_0 = 1.3 \cdot 10^6$ CFU mL ⁻¹). TSB showed shorter detection times and higher peak heat flows than BHI.	111

Table 2 - Continued

clinical isolates, pure cultures	TAM III, equipped with 48 channels	37	3	TSB with/without cefoxitin (l)	methicillin-resistant <i>S. aureus</i> (MRSA), methicillin-susceptible <i>S. aureus</i> (MSSA)	The treatment of cefoxitin affected the metabolic activity of MSSA but not of MRSA. 30 clinical isolates, 19/20 (MRSA) and 10/10 (MSSA) were correctly discriminated by microcalorimetry. Detectable heat flows for MRSA were obtained within 5 h.	35
clinical isolates, pure cultures	TAM 48,	37	~ 2.2 ^b	Lowenstein-Jensen (LJ) (s)	<i>M. phlei</i> , <i>M. abscessus</i> , <i>M. Kansasii</i> , <i>M. avium</i> , <i>M. bovis</i> , <i>M. chelonae</i> , <i>M. smegmatis</i> , <i>M. tuberculosis</i>	First-time ampoules were filled with agar slants for microcalorimetric detection of bacteria. Detection times were ranging from 20 to 310 h for different mycobacteria and initial concentrations. The maximum heat flow was related to the initial bacterial concentration.	112
	TAM Air		5-7	LJ, Middlebrook 7H9 (s)	<i>M. tuberculosis</i> , <i>M. smegmatis</i> , <i>M. avium</i>	A proof of concept for a low-cost microcalorimeter on the detection of mycobacteria in liquid and on solid medium was presented. Heat flow curves and metabolic activity determined by triphenyl tetrazolium chloride were in good agreement. The same was true for total heat and produced biomass (determined by OD ₆₀₀).	113
ac urine	TAM 48	37	3	sterilized urine with/without calf serum (l)	<i>M. tuberculosis</i> , <i>M. smegmatis</i> , <i>M. phlei</i> , <i>M. kansasii</i>	Growth parameters of different mycobacteria were determined in sterilized urine. Only <i>M. tuberculosis</i> did not grow in sterilized urine. The addition of 10 % calf serum supported the growth of <i>M. tuberculosis</i> . The modified urine caused biofilm formation in <i>M. kansasii</i> and <i>M. tuberculosis</i> cultures. Approx. 2.5 times greater, and extended activity was calorimetrically detected.	114
				sterilized urine (l)	<i>E. coli</i> , <i>E. faecalis</i> , <i>P. mirabilis</i> , <i>S. aureus</i>	The following detection limits were obtained 1 CFU mL ⁻¹ for <i>E. coli</i> , 10 CFU mL ⁻¹ for <i>P. mirabilis</i> and <i>E. faecalis</i> and 10 ³ CFU mL ⁻¹ for <i>S. aureus</i> . Detectable heat flows for <i>E. coli</i> were reached after 3.9 (10 ⁵ CFU mL ⁻¹) to 17.2 h (1 CFU mL ⁻¹). Each species caused a characteristic heat flow pattern in sterilized urine.	125

Table 2 - Continued

ac tap water	Thermal Activity Monitor 2277, TAM III	37	3, 4	LB (l), mineral medium M9 (l)	<i>E. coli</i> , <i>P. putida</i>	Comparison between calorimetric detection and conventional inspection by count plates were conducted. Calorimetric detection took 5 h (12 cells mL ⁻¹) and was superior to optical inspection 9-10 h. A linear correlation between the degree of contamination (logarithmic cell concentration) with the calorimetric detection time using a simple mathematical model was presented.	32
clinical isolates	TAM III, equipped with 48 channels	37	3	BHI with/without vancomycin (l)	<i>Staphylococcus aureus</i> strains (VSSA, hVISA, VISA, VRSA)	Detection times < 8 h of <i>S. aureus</i> strains with reduced susceptibilities to vancomycin were obtained by microcalorimetry. VSSA, hVISA, and VISA phenotypes were reliably discriminated by their thermal response to concentration-dependent treatment of vancomycin.	128
pure cultures	Calvet microcalorimeter	36	1	enriched with digested soy-casein (l)	<i>E. coli</i> , <i>P. mirabilis</i> , <i>K. pneumoniae</i> , <i>P. aeruginosa</i> , <i>E. faecalis</i>	Detection times obtained for <i>P. aeruginosa</i> were 2.9 h (10 ⁶ CFU mL ⁻¹), 4.3 h (10 CFU mL ⁻¹), for <i>E. coli</i> 1.9 h (10 ⁶ CFU mL ⁻¹), 7.6 h (10 CFU mL ⁻¹), for <i>P. mirabilis</i> 1.7 h (10 ⁶ CFU mL ⁻¹), 6.2 h (10 CFU mL ⁻¹), for <i>K. pneumoniae</i> 1.6 h (10 ⁶ CFU mL ⁻¹), 5.6 h (10 CFU mL ⁻¹), for <i>E. faecalis</i> 2.7 h (10 ⁶ CFU mL ⁻¹), 4.7 h (10 CFU mL ⁻¹).	129-131
pure culture	pre-production model CalScreener	37	0.3	LB (l)	<i>P. mirabilis</i>	The detection limit of 3·10 ⁴ cells per vial was determined for the microcalorimeter employed. Detection times were ranging between 2 (10 ⁶ CFU) and 9 h (1 CFU).	18
ac parental drug products	TAM 48	25	3	TSB (l)	<i>C. albicans</i> , <i>S. aureus</i> , <i>Penicillium</i> sp. <i>B. subtilis</i> , <i>A.s brasiliensis</i> , <i>P. aeruginosa</i>	A comparison between microcalorimetry and visual inspection in sterile assessment was made. The application of membrane filters to liquid cultures in microcalorimetric experiments was presented. Detection times obtained from calorimetric monitoring were always superior to visual detection. Further, smaller volumes can be employed in microcalorimetry.	132
		32.5		FTM (l)	<i>C. sporogenes</i>		
pure cultures, stabilized formulations	TAM Air equipped with 8 channels	25	6	TSB	<i>P. brassicacearum</i>	Thermal viable counts of cells (pure cultures) by IMC were superior in speed, sensitivity, and accuracy than count plates. Additionally, thermal viable counts were applicable when cultures were coated onto wheat seeds, besides the natural microflora of the seeds.	133
				LB	<i>B. amyloloquefaciens subsp. plantarum</i>		
				PDB	<i>C. rosea</i>		

Table 2 - Continued

clinical isolates, pure cultures	TAM III, equipped with 48 channels	37	3, 4	TSB, CMM, H-Medium, enriched thioglycolate medium	<i>C. acnes</i> , <i>F. nucleatum</i> , <i>F. magna</i> , <i>P. micra</i> , <i>B.</i> <i>fragilis</i> , <i>A. odontolyti-</i> <i>cus</i> , <i>C. difficile</i>	Optimal medium composition and available oxygen in the headspace (by varying the fill volume of the ampoules) was investigated by IMC. 4-mL filled ampoules showed better growth for the anaerobes. Detection times for different species ranged from 10 to 72 h.	36
maize seed	TAM III	20	4 g	-	unknown	IMC measured the metabolic activity of microbial communities on maize seed. By using PCR techniques, a relationship between heat flow production, total metabolic heat and the microbial community was established. Heat flow measurements can determine the degree of contaminations of biological material.	127

^a ac = artificial contaminated

^b estimated using the filling volume, total heat and oxycaloric equivalent

Generally, three main features can be deduced from almost all studies: (i) measurements are almost exclusively performed in liquid medium. (ii) small sample volumes (< 5 mL) are predominately used, which can be attributed to the small-size vessels available for powerful microcalorimeters and (iii) less effort was put in the direction of applying real samples to calorimetric detection. Significantly the latter might hinder calorimetry from becoming a routinely used microbiological tool until now.

The following sections deal with the construction, design, and development of isothermal micro(bio-)calorimeters.

2.2.4 Design and construction of isothermal micro(bio-)calorimeters

In general, calorimeters are thermophysical instruments for measuring the heat released or consumed during biological, physical, or chemical reactions¹³⁴. Based on the underlying principle of heat measurement, three different isothermal microcalorimeters are known: i) adiabatic, ii) heat conduction and iii) power consumption^{19, 100}. Additionally, a distinction can be made between flow microcalorimeters and batch-type microcalorimeters. The latter is based on a static vessel system, commonly used for micro(bio-)calorimetric measurements. Therefore, in the present work, emphasis will be laid on the heat conduction batch-type microcalorimeter. The term “micro” implies that heat flows in the micro-watt [μW] range can be resolved¹³⁵.

2.2.4.1 General components of an isothermal microcalorimeter

An isothermal microcalorimeter essentially consists of the following components: heat flow sensor (measuring unit), sample vessel, heat sink, temperature control units, insulations, amplifier, and data recorder. **Figure 6** displays the arrangement of all essential components of such a calorimeter.

Conducting experiments in isothermal microcalorimeters require that the temperature is nearly constant during measurement¹³⁵. In order to achieve high-temperature stability, two essential components are required: the insulation and temperature control units. In addition to the choice of heat flow sensors, both aspects greatly influence the sensitivity of isothermal microcalorimeters.

The primary purpose of proper insulation is to ensure that external temperature fluctuations are effectively buffered and thus do not affect the temperature inside the microcalorimeter^{91, 109}. Styrofoam is often used as an insulation layer^{101, 136}. Alternatively, several layers of different thicknesses and other materials can be employed⁹¹. Besides, the medium (e.g. oil, water, air) selected for temperature control of the calorimetric channels can also significantly influence temperature stability. Two different approaches can be found in literature. Better temperature homogeneity is achieved using oil¹⁰⁷ or water¹³⁷⁻¹³⁸. In contrast, with an air-heated thermostat, the temperature homogeneity might be lower, and thus the temperature stability is not as accurate as in the case of using a liquid coolant.

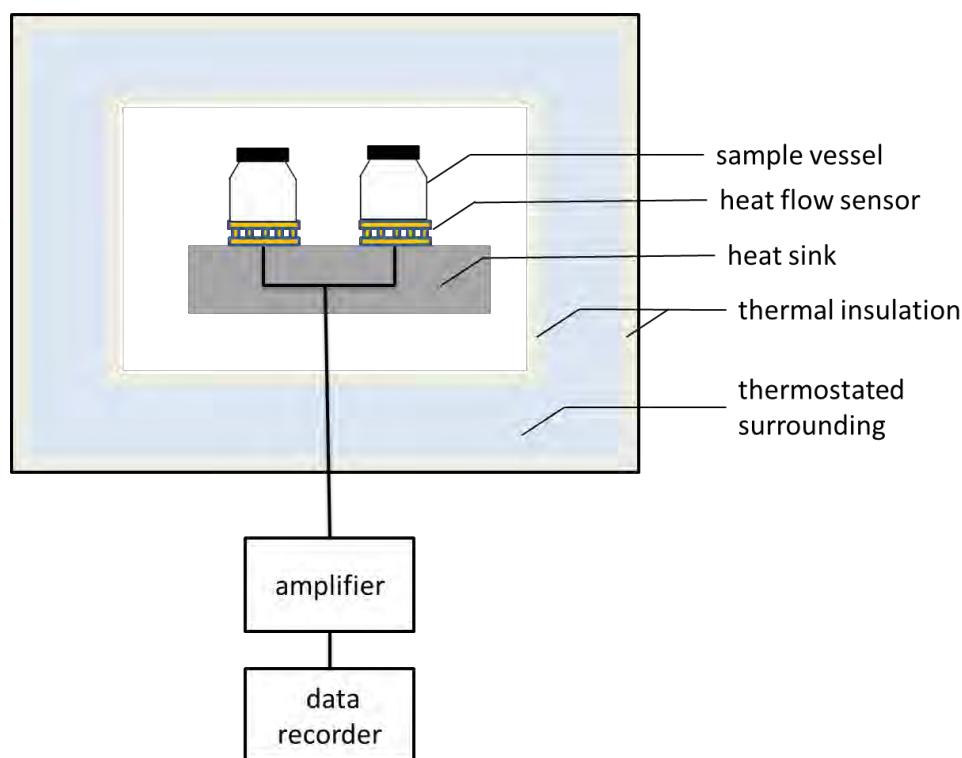


Figure 6: Arrangement of all essential components of a calorimeter. The figure is adapted from ¹³⁹.

Temperature sensors (e.g. Pt100) are primarily used combined with proportional-integral-derivative (PID) controllers to regulate the heat output of heating elements in the calorimeter ¹¹⁰.

The measurement unit in an isothermal microcalorimeter is a heat flow sensor. The heat flow sensor is positioned between the calorimetric vessel, in which the reaction occurs, and a heat sink (**Figure 6**) ^{134, 139}. Thermoelectric generators (TEGs) are widely used as heat flow sensors. TEGs often consist of two ceramic plates, which form the top and bottom sides of the sensor, with an array of interconnected thermocouples in between. For the latter, often, the semiconductor bismuth telluride (Bi_2Te_3) is used. Each thermocouple consists of a p-type ($\text{Bi}_2\text{Te}_3 - \text{Sb}_2\text{Te}_3$ alloy) and n-type ($\text{Bi}_2\text{Te}_3 - \text{Sb}_2\text{Te}_3$ alloy) leg, which is connected via copper plates to another thermocouple ¹⁴⁰. Bismuth telluride is characterized by low thermal conductivity κ and excellent thermoelectric properties (electrical conductivity σ and Seebeck coefficient α) ¹⁴⁰.

Suppose there is a change in heat in the sample vessel due to a reaction, then the local temperature in the sample vessel changes. Typically, the temperature rise is so minimal that it does not significantly affect the isothermal conditions ¹³⁸. However, the temperature of the vessel T_{samp} increases (exothermic reaction) and is thus higher than the operating temperature T_{op} . Consequentially, a temperature gradient ($\Delta T = T_{\text{hot}} - T_{\text{cold}}$) is formed above the TEG ¹⁴¹. **Figure 7** schematically illustrates the underlying physical effects.

The TEG measures the temperature difference between the top and bottom of the sensor. This temperature gradient produces an electrical potential that results from the thermocouple (p- and n-type leg)

due to the Seebeck effect ¹⁴². In short, the p-type leg has a higher number of holes (positive charge carriers, h^+) than the n-type, which has a higher number of electrons (negative charge carriers, e^-) ¹⁴³. Higher thermal energy affects the mobility of the charge carrier in the legs, and the higher temperature on the top (T_{hot}) cause diffusion of h^+ and e^- towards the cold side (bottom) of the sensor (T_{cold}) ⁸⁷.

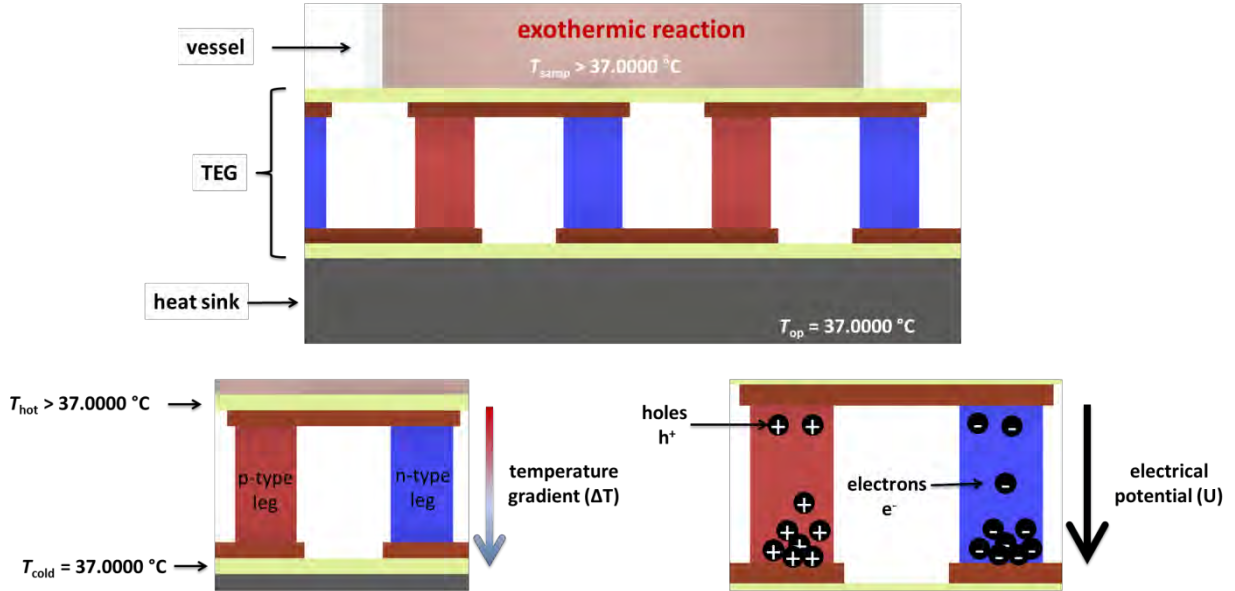


Figure 7: Structure and operation of a TEG with the underlying physical effects using the example of an exothermic reaction in the sample vessel. Due to the exothermic reaction, the top of the sensor is warmer than the bottom, resulting in the formation of a temperature gradient (bottom left). The temperature gradient initiates a net charge in the thermocouple legs to build up an electrical potential (bottom right). The figure is adapted from ⁸⁷.

Consequently, a potential difference (thermovoltage) between the hot and cold sides of the sensor is formed. Hence, the electrical potential can be expressed by eq. 7 ¹³⁶:

$$U = n_{TEG} \cdot (\alpha_{p\text{-type}} - \alpha_{n\text{-type}}) \cdot (T_{hot} - T_{cold}) \quad (7)$$

Where n_{TEG} is the number of thermocouples, $\alpha_{p\text{-type}, n\text{-type}}$ is the Seebeck coefficient (in V K^{-1}) of each leg, T_{hot} and T_{cold} are the temperatures on the hot and cold sides of the TEG (both in K), respectively. The analogously generated thermovoltage is often further amplified and converted into a digital signal employing an A/D converter.

From eq. 7 yields two key parameters that characterize the sensitivity and performance of the TEG. The thermal resistance R_{th} (in K W^{-1} , reciprocal of thermal conductivity k) of the material should be as high as possible since this increases the temperature gradient (ΔT) and subsequently the potential difference (U). The same applies to the Seebeck coefficient α (in mV K^{-1}) ¹⁴⁴. By using these two parameters, the sensitivity S (in V W^{-1}) of the TEG can be calculated as follows (eq. 8) ¹³⁶:

$$S = \alpha \cdot R_{\text{th}} \quad (8)$$

Up to now, an idealized system has always been assumed, i.e. the heat generated in the sample vessel flows completely over the sensor, and parasitic heat flows as well as heat accumulation are neglected¹³⁴. For such an idealized system, the calibration constant ε (in W V^{-1}) is the reciprocal of the sensitivity (eq. 9)¹³⁴:

$$\varepsilon = \frac{1}{S} = \frac{1}{\alpha \cdot R_{\text{th}}} \quad (9)$$

However, such ideal conditions do not prevail in real systems, and the thermal resistance of the TEG alone cannot be used. Instead, the entire measuring unit (TEG + ampoule + possibly other components such as ampoule holder) must be taken into account. In order to determine this thermal resistance, an electrical calibration (mainly done by a resistance heater^{134, 145}) is always necessary. Through this calibration, two crucial pieces of information can be derived: (i) how much heat flows over the TEG and (ii) the thermal resistance of the measuring unit. A fixed or mobile electrical heater can conduct this electrical calibration¹⁴⁵. The mobile heater is inserted in an empty or filled calorimetric vessel, placed in the measurement position and can thus better reproduce the actual heat flow of real measurements¹⁴⁵. Alternatively, chemical reactions such as hydrolysis of triester (e.g. triacetin) can be employed for calibration¹⁴⁶.

So far, the descriptions have been presented from the sensor's point of view. For the following explanation, the perspective is changed to that of the sample. Additionally, physical effects are considered for signal evaluation. In a real system, the calibration constant establishes the relationship between the thermal power P (i.e. heat flow in W) released in the sample and the electrical potential U (in V) generated at the TEG (eq. 10)^{134, 146}.

$$P = \varepsilon \cdot U \quad (10)$$

In order to evaluate the corresponding heat flow signal of an exothermic reaction in the sample, further physical aspects have to be taken into account. Hence, eq. 10 is only valid for reactions where the induced heat flow is comparatively slow¹³⁴⁻¹³⁵, such as bacterial growth¹⁰¹. However, an adequate description for fast kinetic reactions taking place in the sample is not possible using eq. 10 since it does not consider the thermal inertia of the sample vessel and its immediate surroundings. The thermal inertia results from the interaction of heat accumulation with the associated temperature rise and heat run-off. In order to illustrate this situation, the calorimeter equation (eq. 11) is introduced:

$$C_p = \frac{Q}{m \cdot \Delta T} \quad (11)$$

The thermal inertia of the sample vessel and its surrounding is given by their specific heat capacity C_p (in $\text{J kg}^{-1} \text{K}^{-1}$), which is defined as the ratio of the required heat Q (in J) and the product of mass m (in kg) and the temperature change ΔT (in K) undergone by the respective component.

Consequently, the thermal power is corrected for signal evaluation, which can be expressed by the Tian equation (eq. 12) ¹⁰⁹:

$$P_c = P + \tau \cdot \frac{dP}{dt} \quad (12)$$

P_c is the corrected thermal power (in W). The second term contains the time constant τ (in s) and the time derivative of the thermal power dP/dt (in W s^{-1}), reflecting the delay in the recorded voltage signal of the thermal reaction taking place in the sample due to the thermal inertia of the measuring unit ¹⁰⁸.

Concerning the calorimetric vessel, there are no essential requirements for microcalorimetric experiments. However, two aspects have to be considered. First, there must be direct contact between the sample vessel and the heat flow sensor, meaning that almost all heat originating from a temperature change in the vessel flows via the TEG. As mentioned above, the calibration can account for parasitic heat flows in the measurement unit. However, if the thermal resistance of the measuring unit becomes too small, it follows from eq. 7 and 8 that the measured voltage at the sensor will also be minimal, and consequently, problems may arise during detection (signal-to-noise ratio). Alternatively, the vessel must be surrounded by a highly thermally conductive material (e.g. aluminium tubes) that is in contact with the TEG ¹³⁷. Second, the vessel material must be inert against corrosion or, generally, any process producing or consuming heat ^{137, 147}. Different materials such as glass, stainless steel, gold and plastics were successfully applied to microcalorimetric measurements ¹³⁹.

Additionally, different sizes (ranging from 0.4 to 250 mL) and geometries of calorimetric vessels are available ¹⁰⁰. Finally, a large metal body (usually made out of aluminium) is used as a heat sink. Due to the much larger heat capacity of the heat sink compared to the sample, the consumed or released heat in the reaction under investigation can be compensated.

The following section deals with numerical simulations as a particular part of the development process of microcalorimeters.

2.2.4.2 Numerical simulation as a development tool for the construction of microcalorimeters

The design and construction of micro(bio-)calorimeters set high requirements concerning the temperature distribution and stability in the entire system since minor temperature differences caused by bacterial growth have to be detected by the heat flow sensors. The temperature stability in the entire system is affected by time-dependent fluctuations measured by locally placed temperature probes. Thereby, the temperature can only be determined at discrete points within the developed instrument. These usu-

ally include a few selected points in the system, such as local temperatures on the heat sink or in the surrounding medium (air, water or oil). Unfortunately, spatial temperature gradients are not accessible using standard equipment (i.e. temperature probes) under laboratory conditions. From an engineering perspective, it is desirable in the development phase of an instrument to obtain as much as possible information about the system's performance. Therefore, tests under laboratory conditions represent the most important part during this phase for a calorimeter. A valuable criterion here is the performance of the heat flow sensor. In order to understand the produced voltage (or heat flow if sensors are already calibrated), a comprehensive insight into the spatial temperature distribution in the measuring chamber is necessary.

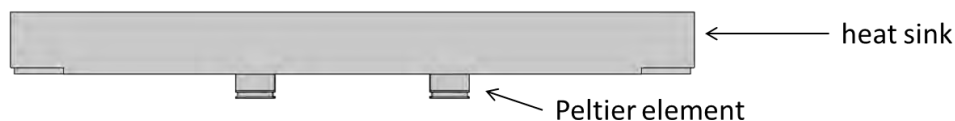
Numerical model simulations can be performed to gain this kind of information. These computer simulations are of great importance in device development and are often part of the entire construction process¹⁴⁸. A popular and widely used approach for solving numerical models is the finite element method (FEM)¹⁴⁹⁻¹⁵¹. In this method, the complex geometry of the model is decomposed into many geometrically simple and finite elements (meshing)¹⁵¹. Depending on the systems' underlying physical effects, partial differential equations (PDE) must be solved numerically¹⁴⁹. For instance, heat transfer and flow phenomena are predominately occurring in a calorimeter. Therefore, the corresponding fundamental equations are solved numerically for each element. In this way, an approximate solution for the complex geometry can be obtained¹⁵⁰.

The general workflow of such a simulation process is shown in **Figure 8**. The first step is to create the geometry of the object to be studied. Thereby dimensions of the object can be taken from measurements under laboratory conditions, or a CAD file is imported into the simulation software to reconstruct the geometry. Depending on the problem to be investigated, the corresponding physics is selected in the second step. In this case, Fourier's law describes the heat transport in solids (**Figure 8**). Further initial and boundary conditions, such as the initial temperature or heat flow boundary conditions, are necessary to obtain a unique solution for the problem under investigation. In the third step, material constants such as thermal conductivity, density, and heat capacity that appear within the PDEs must be assigned to individual domains, faces, edges, or points of the object.

In the penultimate step, the meshing of the object into many small but finite elements takes place. By using selected numerical solvers, a complex system of equations is then solved. In the post-processing step, approximated solutions, e.g., the shown three-dimensional heat sink temperature distribution (**Figure 8**) is visualized and further analyzed.

FEM Workflow

(1) Creating geometry



(2) Selection of physics

heat transfer in solids

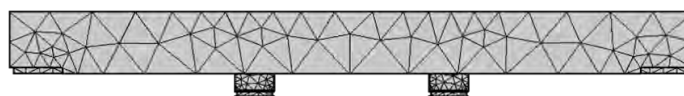
$$q = -k\nabla T \quad \text{Fourier's law} \quad T_0 = 294.15 \text{ K} \quad \text{initial temperature}$$

$$\rho C_p \frac{\partial T}{\partial t} = \nabla \cdot (k\nabla T) + Q \quad \text{heat balance} \quad q_0 = h \cdot (T_{\text{ext}} - T) \quad \text{heat exchange with environment}$$

(3) Assigning materials

component	material	physical properties
heat sink	Al	$C_p = 900 \text{ J}\cdot\text{kg}^{-1}\cdot\text{K}^{-1}, k = 238 \text{ W}\cdot\text{m}^{-1}\cdot\text{K}^{-1}, \rho = 2700 \text{ kg}\cdot\text{m}^{-3}$
top/ bottom Peltier element	$\text{Al}_2\text{O}_3, 96 \%$	$C_p = 900 \text{ J}\cdot\text{kg}^{-1}\cdot\text{K}^{-1}, k = 25 \text{ W}\cdot\text{m}^{-1}\cdot\text{K}^{-1}, \rho = 3800 \text{ kg}\cdot\text{m}^{-3}$
thermocouple Peltier element	Bi_2Te_3	$C_p = 154 \text{ J}\cdot\text{kg}^{-1}\cdot\text{K}^{-1}, k(T), \rho = 7700 \text{ kg}\cdot\text{m}^{-3}$

(4) Meshing



(5 & 6) Solving and post-processing

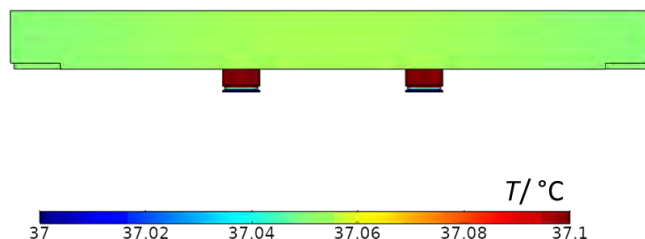


Figure 8: General workflow of numerical simulations based on the FEM.

In the literature, there are already some examples of numerical simulations related to calorimetric issues. In 1982, Davids and Berger have already introduced computational simulations to time-dependent heat conduction processes between the fluid (in which the reaction occurred, heat source) and an aluminium block (heat sink) based on FEM¹⁵². Recently applications of FEM revealed, for instance, dominant heat transfer mechanisms in a Tian-Calvet microcalorimeter during gas dosing experiments¹⁵³ and determination of electronic devices' power dissipation of a proposed non-conventional calorimeter¹⁵⁴. Also, FEM was employed to demonstrate the applicability of computation analysis to heat transport phenomena in large-volume isothermal calorimeters¹⁵⁵ and to visualise the temperature distribution of a 3D model of a micromachined picocalorimeter sensor¹⁵⁶.

Interestingly, all these computational simulations are addressing only specific issues of a calorimeter. Additionally, the complex nature of temperature control systems, a prerequisite for an isothermal microcalorimeter, has so far not been considered. Further, many studies are dealing only with 2D models to reduce computational resources. Thus, three-dimensional spatially resolved temperature distributions cannot be illustrated, which are essential to gain a comprehensive insight into the calorimeter.

Finally, the last section addresses the requirements for an isothermal micro(bio-)calorimeter designed for routine microbiological testing. Further, the advantages and limitations of commercialized biocalorimeters in the context of bacterial detection are presented.

2.2.4.3 Requirements for an isothermal micro(bio-)calorimeter

What are the requirements for a micro(bio-)calorimeter to be explicitly used to detect bacterial contamination in different areas? In order to answer this question, a view to conventional microbiological analysis might be helpful. Here, bacteria grow on solid medium in tiny, flat sample vessels (Petri dishes) made out of glass or plastic. The medium is available in excess (20 - 30 mL), and the large surface area of the Petri dishes ($d = 100$ mm) enables optimal spatial growth of single colonies and gas exchange. Additionally, membrane filters ($d = 47$ mm) can be put onto the medium's surface if prescribed by the ISO norm (**Figure 1**). Temperature control during incubation is not precisely regulated (e.g. 37 ± 1 °C), and the desired temperature range for microbiological analysis is near ambient temperature 20 - 40 °C. Depending on particular needs for certain bacteria, the gaseous environment can be adapted to favorable cultivation conditions.

Concerning micro(bio-)calorimetric measurements, the size and geometry of the sample vessel might be crucial since the amount of available oxygen (for aerobic cultures) and nutrients might be a limiting factor to achieve a detectable heat flow. Here, primarily sealed 4-mL and 20-mL glass ampoules were employed for microcalorimetric detection of bacterial contaminations¹¹³. These ampoules have a too-small surface area to perform conventional microbiological analysis, which may not allow subsequently quantitative enumeration. Besides, a standardized membrane filter cannot be applied.

In contrast to incubators used in conventional microbiology, the temperature is very precisely regulated in micro(bio-)calorimeters. For instance, the 3rd generation TAM III achieves temperature stability of ± 10 μ K over 24 h¹⁰⁷. These stabilities (in the mK range) are necessary since the increase in temperature during bacterial growth and the corresponding heat flows are only a fraction of a few mK and μ W, respectively. Appropriate environmental conditions such as an anoxic gas phase can be created in the closed ampoule system during sample preparation³².

Table 3 compares current commercialised micro(bio-)calorimeters or microcalorimeters (mainly used in the context of bacterial detection) considering all the abovementioned criteria. Additionally, the sensitivity and number of available measuring channels of these calorimeters are also listed.

From this, it is clear that only two quite distinct classes of instruments are currently on the market. On the one hand, calorimeters reflecting the use of small sample volumes (< 20 mL) and many available channels (> 10) at high sensitivity (< 1 μ W) and, on the other hand, devices for high sample volumes (> 20 mL), fewer available channels (< 10) and low sensitivity (> 10 μ W)¹⁰⁰. Consequently, due to the use of smaller sample vessels, an assay arrangement of multiple sample vessels (multichannel microcalorimeter) can be realized in a single instrument¹⁵⁷. However, high sensitivity is required because small sample volumes do not provide excess consumable energy for the microorganisms, converted into new biomass, and released heat during bacterial growth. Less sensitive calorimeters compensate for this with an excess of available energy in larger sample volumes of the medium. In return, less sensitive microcalorimeters are restricted to a few measurement channels.

Table 3: Specifications and features of commercialized micro(bio-)calorimeters adapted from¹⁰⁰

	TAM IV ^{a,[4]}			TAM air ^[5]		CalScreener ^[6]	BioCal 2000 /4000 ^[7]	
Sample vessel								
volume /mL	4	20	125	20	125	0.1 - 0.3	20	125
diameter /mm	10	27	50	27	50	8.5	27	74.1
Temperature								
range /°C	4 - 150			5 - 90		37	5 - 70	
stability /24 h	< \pm 0.1 mK			\pm 1 mK		n. a.	\pm 20 mK	
Sensitivity								
baseline drift μ W /24 h	< 0.04 ^b	< 0.2 ^c	< 6 ^d	< 5	< 55	< 0.2	< 20	< 60
short term noise / μ W	< \pm 0.01	< \pm 0.1	< \pm 0.5	< 1	< \pm 8	< \pm 0.05	n. a.	
limit of detection / μ W	n. a.			2	8	0.1	5	
Number of measuring channels	1 - 48 ^f			8	3	48 (32) ^e	2	4

n. a. = not available

^a includes the TAM IV-48 and TAM IV Micro XL

^b nanocalorimeter

^c 4 mL mini- / multicalorimeter

^d macrocalorimeter

^e using 32 measurement positions and 16 references leads to best stability

^f depending on the selected calorimeter

Interestingly, the CalScreener from Symcel (www.symcel.com/) is the first commercially available micro(bio-)calorimeter focusing on a single, ambient operating temperature of 37 °C. Other micro(bio-

^[4] <https://www.tainstruments.com/wp-content/uploads/BROCH-TAM-IV.pdf>

^[5] <https://www.tainstruments.com/wp-content/uploads/TAM-AIR-brochure.pdf>

^[6] https://issuu.com/symcel/docs/calcreener_-_microbiology_applicat

^[7] <http://downloads.calmetrix.com/Specs/BioCal2Specs.pdf>

)calorimeters cover a more extensive temperature range, which challenges the requirements for the temperature control system and increases production costs. The extensive temperature range offers applications on biological systems and a wide range of applications from chemistry to physics that can also be investigated.

At the moment, the TAM series (TAM III, TAM 48 and TAM Air) from TA instruments (www.tainstruments.com) are the most frequently used microcalorimeters for bacterial detection^{20, 32, 112-113}. The advanced temperature control system significantly facilitates susceptible heat flow measurements, which allow early detection of bacterial contaminations. In addition, the multichannel TAM 48 enables a high throughput of 48 simultaneously measured samples. Unfortunately, only small vessels can be employed (except for the TAM Air), which may not fulfil the criteria for a quantitative enumeration of colonies on solid medium afterwards. Nevertheless, all of these excellent specifications leads to a versatile but quite expensive instrument, which is kind of overqualified for a micro(bio-)calorimeter that is routinely used in the context of microbiological analysis. However, the TAM Air more closely meets the criteria for a micro(bio-)calorimeter, except for the extensive temperature range and the low number of channels in the 125-mL configuration. The same applies to the BioCal 2000/4000 (www.calmetrix.com/).

With the CalScreener, Symcel presents an entirely different approach to tackle issues in micro(bio-)calorimetry. The narrow temperature range and the different sample vessels are a novelty for commercial micro(bio-)calorimeters. A commercially available 48-well microtiter plate can be inserted¹⁵⁷. Experiments with microorganisms can be carried out in sterile, transparent plastic inserts to make microscopic follow-up analysis possible^{18, 157}. However, the equipped 48-well microtiter plates are not suitable for conventional microbiological analysis.

Unfortunately, no existing micro(bio-)calorimeter fulfils the criteria to detect as fast as possible bacterial contaminations, further allows a subsequent enumeration as CFU/mL within the same measurement and has a sufficient number of measuring channels. In order to fill this gap, an early-stage engineered micro(bio-)calorimetric test system was developed in this thesis (**section 3.2**).

3. Experimental part

3.1 Systematic investigation of a culture-based microcalorimetric approach for the detection of bacteria

3.1.1 Rapid Calorimetric Detection of Bacterial Contamination: Influence of the Cultivation Technique

Fricke C, Harms H, Maskow T. (2019):

Rapid Calorimetric Detection of Bacterial Contamination: Influence of the Cultivation Technique
Front. Microbiol. **10** (2530), 1-12.

<https://doi.org/10.3389/fmicb.2019.02530> (published, Methods article)

Significance: Bacterial contamination in various products can always pose a health risk. A prerequisite for early calorimetric detection is to facilitate bacterial growth in static ampoule systems. Therefore, this publication is the first comprehensive and systematic study on conventional microbiological techniques (on solid and in liquid medium) in connection with microcalorimetric detection of bacteria. *Lactobacillus plantarum* DSM 20205 was selected as a model strain to investigate the influence of cultivation techniques (growth in liquid, growth on/in solid, growth on a membrane filter placed on solid medium) on the calorimetric detection time in static ampoule systems. Detection times obtained from visual inspection of colony formation (count plates) and automated turbidity measurements (OD₆₀₀) were compared with those from heat flow measurements. The data demonstrated that all cultivation techniques could be successfully applied to microcalorimetry and showed a substantial reduction in detection time strictly related to the initial concentration of bacteria.

Rapid Calorimetric Detection of Bacterial Contamination: Influence of the Cultivation Technique

Christian Fricke, Hauke Harms and Thomas Maskow*

Department of Environmental Microbiology, Helmholtz Centre for Environmental Research – UFZ, Leipzig, Germany

Modern isothermal microcalorimeters (IMC) are able to detect the metabolic heat of bacteria with an accuracy sufficient to recognize even the smallest traces of bacterial contamination of water, food, and medical samples. The modern IMC techniques are often superior to conventional detection methods in terms of the detection time, reliability, labor, and technical effort. What is missing is a systematic analysis of the influence of the cultivation conditions on calorimetric detection. For the acceptance of IMC techniques, it is advantageous if already standardized cultivation techniques can be combined with calorimetry. Here we performed such a systematic analysis using *Lactobacillus plantarum* as a model bacterium. Independent of the cultivation techniques, IMC detections were much faster for high bacterial concentrations ($> 10^2$ CFU·mL⁻¹) than visual detections. At low bacterial concentrations ($< 10^2$ CFU·mL⁻¹), detection times were approximately the same. Our data demonstrate that all kinds of traditional cultivation techniques like growth on agar (GOA) or in agar (GIA), in liquid media (GL) or on agar after enrichment via membrane filtration (GF) can be combined with IMC. The order of the detection times was GF < GIA \approx GL \approx GOA. The observed linear relationship between the calorimetric detection times and the initial bacterial concentrations can be used to quantify the bacterial contamination. Further investigations regarding the correlation between the filling level (in mm) of the calorimetric vessel and the specific maximum heat flow (in $\mu\text{W}\cdot\text{g}^{-1}$) illustrated two completely different results for liquid and solid media. Due to the better availability of substrates and the homogeneous distribution of bacteria growing in a liquid medium, the volume-related maximum heat flow was independent on the filling level of the calorimetric vessels. However, in a solid medium, the volume-related maximum heat flow approached a threshold and achieved a maximum at low filling levels. This fundamentally different behavior can be explained by the spatial limitation of the growth of bacterial colonies and the reduced substrate supply due to diffusion.

Keywords: bacterial contamination, calorimetric detection, cultivation techniques, isothermal microcalorimetry, *Lactobacillus plantarum*, real-time monitoring

OPEN ACCESS

Edited by:

David Rodriguez-Lazaro,
University of Burgos, Spain

Reviewed by:

Carmen Wachter,
National Autonomous University
of Mexico, Mexico
Olivier Braissant,
University of Basel, Switzerland

*Correspondence:

Thomas Maskow
thomas.maskow@ufz.de

Specialty section:

This article was submitted to
Food Microbiology,
a section of the journal
Frontiers in Microbiology

Received: 24 June 2019

Accepted: 21 October 2019

Published: 01 November 2019

Citation:

Fricke C, Harms H and Maskow T
(2019) Rapid Calorimetric Detection
of Bacterial Contamination: Influence
of the Cultivation Technique.
Front. Microbiol. 10:2530.
doi: 10.3389/fmicb.2019.02530

INTRODUCTION

The fast and reliable detection of microbial contamination in food (Wadsö and Galindo, 2009; Velusamy et al., 2010; Khalef et al., 2016), water (Maskow et al., 2012) and pharmaceuticals (Buckton et al., 1991; Vine and Bishop, 2005) is necessary to prevent disease outbreaks as well as to ensure high quality, safety, and purity of these products. At the moment, the gold

standard for the detection of microbial contaminations is a visual inspection of colony growth in case of solid media or of turbidity in case of liquid media or after standardized cultivation on selective solid media. Colony-forming units (CFU) per mL sample are counted for quantification of the contamination. The basic assumption is that one colony is formed per bacterium in the sample. Since about 10^5 bacteria are necessary to form a colony visible to the human eye (Maskow et al., 2012), extended incubation is required depending on the specific growth rate μ_{\max} of the microorganism. For instance, the standard specification prescribes 48 h incubation for the detection of *Pseudomonas aeruginosa* (ISO 16266:2006): (Jami Al-Ahmadi and Zahmatkesh Roodsari, 2016), 96–120 h for *Salmonella* (ISO 6579-1:2017): (Jay et al., 2005), and 120–144 h for *Listeria* (ISO 11290-1:2017) (Donoso et al., 2017). The great advantage over more sophisticated, molecular biological techniques like quantitative polymerase chain reaction (qPCR) combined with fluorescence detection or microscopic monitoring of selectively labeling probes is the simple handling and interpretation of results (Sieuwert et al., 2008; Hazan et al., 2012). Biosensors represent another large class of detection methods for bacteria (Wang and Salazar, 2016). For instance, conductometric measurements provide rapid and easy handling detection of bacteria (Velusamy et al., 2010). The problem of non-specificity is overcome by selective antibodies but the sample matrix has a more significant influence since interfering quantities can play an important role (Law et al., 2015).

Many detection protocols include the enrichment of the bacteria using membrane filtration processes and subsequent placing the membrane filter onto a selective solid medium (ISO 7704:1985) to ensure that sufficient bacteria form colonies (Taylor et al., 1953; Tsuneishi and Goetz, 1958). Another modification is selective chemical pre-treatment of the sample like, e.g., the acidic treatment for the detection of *Legionella* (Bopp et al., 1981) serving to reduce the growth of unwanted, interfering microorganisms (ISO 11731:2017).

As an alternative to growth on solid media, it is also possible to detect bacterial contamination upon cultivation in (selective) liquid media. Here, mostly optical turbidity measurement is used to quantify the growth of the contaminant (Koch, 1970). Obviously, inherently turbid samples cannot be measured by this method. In addition, turbidity can be affected by dead cells, by-products of microbial activity such as polymers (Clais et al., 2015) or by precipitation.

We propose to monitor growth calorimetrically in order to achieve faster, more reliable, on-line detection that can be combined with different common cultivation techniques. High-performance isothermal microcalorimeters (IMC) are able to quantify tiny amounts of heat in the range from a few nano- to microwatts (Braissant et al., 2010a). IMC can thus be applied as a real-time detector for a variety of microbial contaminants because all living microorganisms dissipate parts of the Gibbs energy of the substrates they assimilated in the form of heat (Gram and Sogaard, 1985; Wadsö, 1995; Von Stockar and Liu, 1999; Trampuz et al., 2007a; Maskow et al., 2012). The application of IMC for the quantification of microbial contamination by various species is already described in the

literature (Levin, 1977; Xie et al., 1995; Trampuz et al., 2007a,b; Braissant et al., 2010b; Bonkat et al., 2011; Ren et al., 2012; Gysin et al., 2018). Interestingly, almost exclusively liquid cultures were used for the quantification of the different bacteria in samples from different origins. The application of calorimetry to bacteria grown on solid agar media was only described by Braissant et al. (2010b) for the bacterial quantification of *Mycobacterium tuberculosis*. The application of membrane filtration for bacterial quantification using IMC has to our knowledge not yet been described. However, qualitative IMC monitoring of the growth of mycobacteria on nylon filters (Solokhina et al., 2017), as well as the qualitative sterility testing of membrane filters (Brueckner et al., 2017) and experiments with three different species on pure titanium disks placed on solid media (Astasov-Frauenhoffer et al., 2012, 2014) could be considered as preparatory work in that direction.

Although IMC is known as a non-specific detection method, an appropriate sample preparation (e.g., chemical treatment) and selective culture media can be used to allow only the growth of microorganisms of concern, whereas accompanying microbial community is suppressed (Bujalance et al., 2006; Veselá et al., 2019).

Our study aims at the systematic investigation of the combination of common cultivation techniques with calorimetric monitoring, using *Lactobacillus plantarum* as a model strain for anaerobic systems, for its potential to identify microbial contaminations faster and more reliably. Emphasis is put on the influence of the cultivation techniques on calorimetric monitoring.

MATERIALS AND METHODS

Bacterial Strain, Medium, and Cultivation

Lactobacillus plantarum DSM 20205 (German Collection of Microorganisms and Cell Cultures, DSMZ, Braunschweig, Germany) was used for the calorimetric investigations. The strain was cultivated on MRS (DE MAN, ROGOSA, SHARPE) medium, which is composed of (in g·L⁻¹): glucose (20), peptone (10), meat extract (10), yeast extract (5), K₂HPO₄ (2), NaCH₃COO·3 H₂O (5), (NH₄)₂HC₃H₅(COO)₃ (2), MgSO₄·7 H₂O (0.2), MnSO₄·4 H₂O (0.05) as well as 1 mL·L⁻¹ Tween 80. Agar (1.5%) was used to solidify the medium. The final pH value was set to 5.7–6.2 by H₂SO₄ ($c = 1 \text{ mol} \cdot \text{L}^{-1}$). One colony of a pre-grown Petri dish was used for the liquid pre-cultures of *L. plantarum*, which were incubated overnight at $30.0 \pm 0.2^\circ\text{C}$ (Unihood 650, UniEquip, Leipzig, Germany). Cells were harvested immediately before the calorimetric experiments. The identity of the species was regularly checked by the morphology of the colonies and once by 16S ribosomal DNA analysis.

IMC Measurement

The calorimetric measurements were performed in 4-mL glass ampoules in a high-performance IMC (Thermal Activity Monitor III, TA Instruments, New Castle, United States). The ampoules and caps were autoclaved at 121°C for 40 min

and then filled with a defined volume of media. In the case of solid media, the ampoules were filled with warm ($\sim 70^\circ\text{C}$), molten MRS-agar medium, closed and stored at 4°C . The prepared glass ampoules containing the solid media were cooled down to room temperature before the bacteria were added. After adding the bacteria, the glass ampoules were set into a pre-heating position (to reach thermal equilibrium) for 15 min. In the last preparation step, the glass ampoules were pushed into the measuring position and after further 45 min (to reach thermal equilibrium), the heat flow signal was recorded.

The calibration of the TAM III was performed by an electric gain calibration (Joule heating) after certain time intervals to ensure precise measurements. The gain calibration consisted of two steps. First, a stable signal in each measuring channel was awaited (slope of the signal $< 250 \text{ nW}\cdot\text{h}^{-1}$). Second, a single pulse of 1 mW was generated for 30 s by an inbuilt electrical calibration heater. The gain and offset were calculated as a result of the instrument response. All measurements were performed at $37.0 \pm 0.0001^\circ\text{C}$. The obtained data were analyzed using *OriginPro* 2018. In all cases, where the high criteria for signal stability could not be met, a linear baseline correction was performed (see **Supplementary Material**).

Sample Preparation

An overnight pre-culture of *L. plantarum* was diluted to an $\text{OD}_{600} \sim 0.15\text{--}0.20$ (U-2900 Spectrophotometer, Hitachi, Tokyo, Japan) and this solution was diluted in series (dilution factors: $f_a = 10^4\text{--}10^8$). Four different test series were performed: (i) GOA, (ii) GL, (iii) GF (**Supplementary Material**) and (iv) GIA. All concentration-dependent experiments were performed in $200 \mu\text{L}$ MRS-medium. As an exception, the GIA experiments were performed in $1000 \mu\text{L}$ MRS-medium. In order to determine the reproducibility of these experiments at varied cell concentrations, triple measurements of the respective test series were conducted.

For GOA, $10 \mu\text{L}$ of each dilution were added onto the agar surface. For GL, also $10 \mu\text{L}$ of each dilution was added to the broth. For GF, 1.8 mL of each dilution was filtrated and the sealed adapters, as well as the membrane filters, were purged with $400 \mu\text{L}$ MRS media. The used sealed adapters were made to measure and fit for a standard membrane filtration system (Sartorius AG, Göttingen, Germany). In these experiments, sterile membrane filters (pore size $0.45 \mu\text{m}$, Cellulose nitrate, Sartorius AG, Göttingen, Germany) were prepared for subsequent membrane filtration under sterile conditions using an autoclaved punch with a diameter of 10 mm (Locheisen-Satz, BGS Technik KG, Wermelskirchen, Germany). For GIA, $10 \mu\text{L}$ of each dilution was added to molten MRS-agar ($45\text{--}50^\circ\text{C}$) and carefully mixed. The homogenization succeeded at these relatively low operating temperatures by using a low agar concentration of 1.5 (w/w)\% . In addition to the concentration-dependent measurements, the dependency on the filling level in the ampoules ($n = 2$) and the reproducibility at a constant concentration ($n = 5$) were investigated. However, sample preparation remained the same in all cases.

Schematically, the individual sample preparation steps, as well as the cultivation, are summarized in **Figure 1**.

In order to quantify the initial concentration of bacteria, the colony-forming units (CFUs) per mL of each dilution step were determined in separate experiments (see **Supplementary Material**). For this purpose, each dilution step was plated in replicates on agar and incubated overnight at $37.0 \pm 0.25^\circ\text{C}$ (New Brunswick Innova 44, Eppendorf, Hamburg, Germany). In addition, the time required for a bacterial cell to form a visible colony was determined. After the first 11 h, the plates were hourly monitored and the colonies were counted after they became visible to the naked eye. To confirm this kind of experiments, a second experiment was performed by a fully automated monitoring process for all dilution stages under the same conditions. Every 10 min the agar plates were scanned and the resulting pictures saved as a jpg file. Subsequently, these files were evaluated. The same procedure was repeated with the growth of colonies on membrane filters. A short summary of these experiments is given in the **Supplementary Material**.

The reference measurements in liquid media ($n = 9$) were performed by monitoring the optical density in a 96-well plate by a photometer (Victor X3, PerkinElmer, Waltham, MA, United States) at 600 nm and $37.0 \pm 0.1^\circ\text{C}$.

RESULTS AND DISCUSSION

Theoretical Background

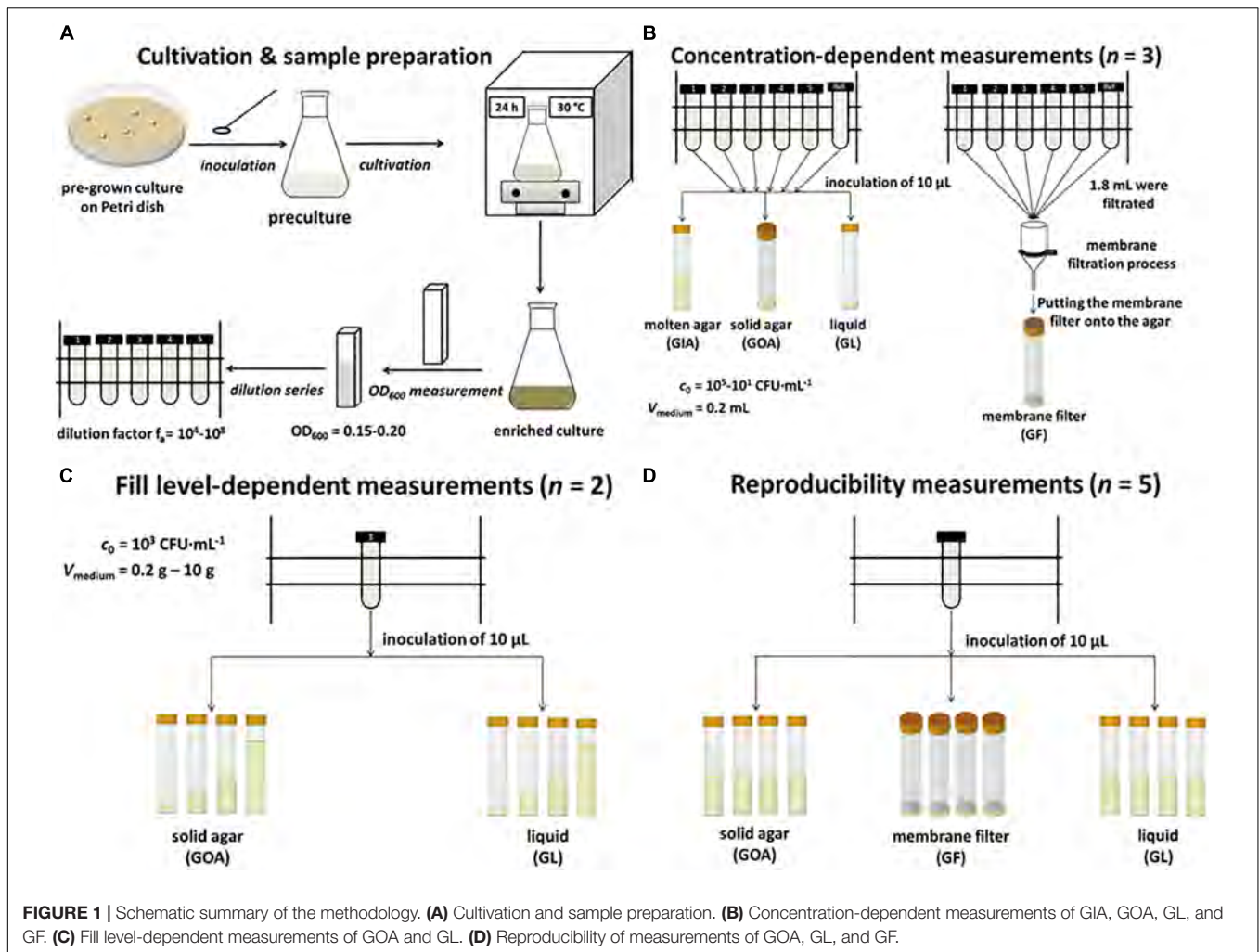
Establishing the relation between the earliest thermal detection time t_{dect} and the concentration of bacteria N_{critical} considered as critical requires a thermokinetic model that is as simple as possible. The simplest assumption is that each bacterium has the same heat production rate (Eq. 1) and that the growth dynamic of the bacterial population can be described by the Malthusian (Eq. 2) (Chang-Li et al., 1988).

$$\phi(t) = N(t) \cdot \phi_0 \quad (1)$$

$$N(t) = N_0 \cdot \exp(\mu_{\text{max}} \cdot t) \quad (2)$$

$\Phi(t)$ (in W) and $N(t)$ (in cells per L) are the heat production rate and the number of bacteria at time t , Φ_0 is the thermal output of a single bacterial cell (in W per Cell). Typical values for bacteria (in the region of a few pW) in their dependency on growth conditions can be found for instance in Maskow et al. (2011), N_0 is the initial concentration of bacteria and μ_{max} (in h^{-1}) is the maximum specific growth rate. The earliest detection time of bacterial contamination obviously depends on the precision of the employed IMC. For instance, a heat flow precision of $\Phi = 2 \cdot 10^{-7} \text{ W}$ is described for the TAM III¹. In reality, however, this thermal detection limit is seldom achieved due to thermal disturbances when the ampoule is inserted, traces of moisture on the outer shell of the glass ampoule, parasitic heat flows, etc. Assuming a detection threshold of $\Phi_{\text{dect}} = 2 \cdot 10^{-6} \text{ W}$, the metabolically caused heat signal can be unambiguously differentiated from the noise of the microcalorimeter (Braissant et al., 2010b). Thus, it is now possible by combining Eqs. 1 and 2 to establish a simple linear

¹www.tainstruments.com



correlation between the detection time $t_{\text{dect.}}$ and the natural logarithm of the initial bacterial concentration N_0 (Eq. 3).

$$\ln N_0 = -\mu_{\text{max}} \cdot t_{\text{dect.}} + \ln \left(\frac{\phi_{\text{dect.}}}{\phi_0} \right) \quad (3)$$

The equation shows the two crucial adjustment screws for reducing the detection time (increasing the initial number of bacteria or reducing the detection limit of the calorimeter used). One might argue that the assumption of a cell-specific heat production rate is too unrealistic. However, if we drop this assumption and postulate more realistic that Φ_0 depends on the growth rate, we come to a very similar correlation as before (Eq. 4) (Maskow et al., 2012).

$$\ln N_0 = -\mu_{\text{max}} \cdot t_{\text{dect.}} + \ln \left(\frac{\Phi_{\text{dect.}}}{\mu_{\text{max}} \cdot \Delta_R H_X \cdot C_C} \right) \quad (4)$$

Here, $\Delta_R H_X$ and C_C stand for the enthalpy change of growth reaction related to the formation of one C-mole biomass and the mean carbon content of a single bacterium, respectively. Independent of the applied equation, a linear relationship between initial concentrations of the bacteria

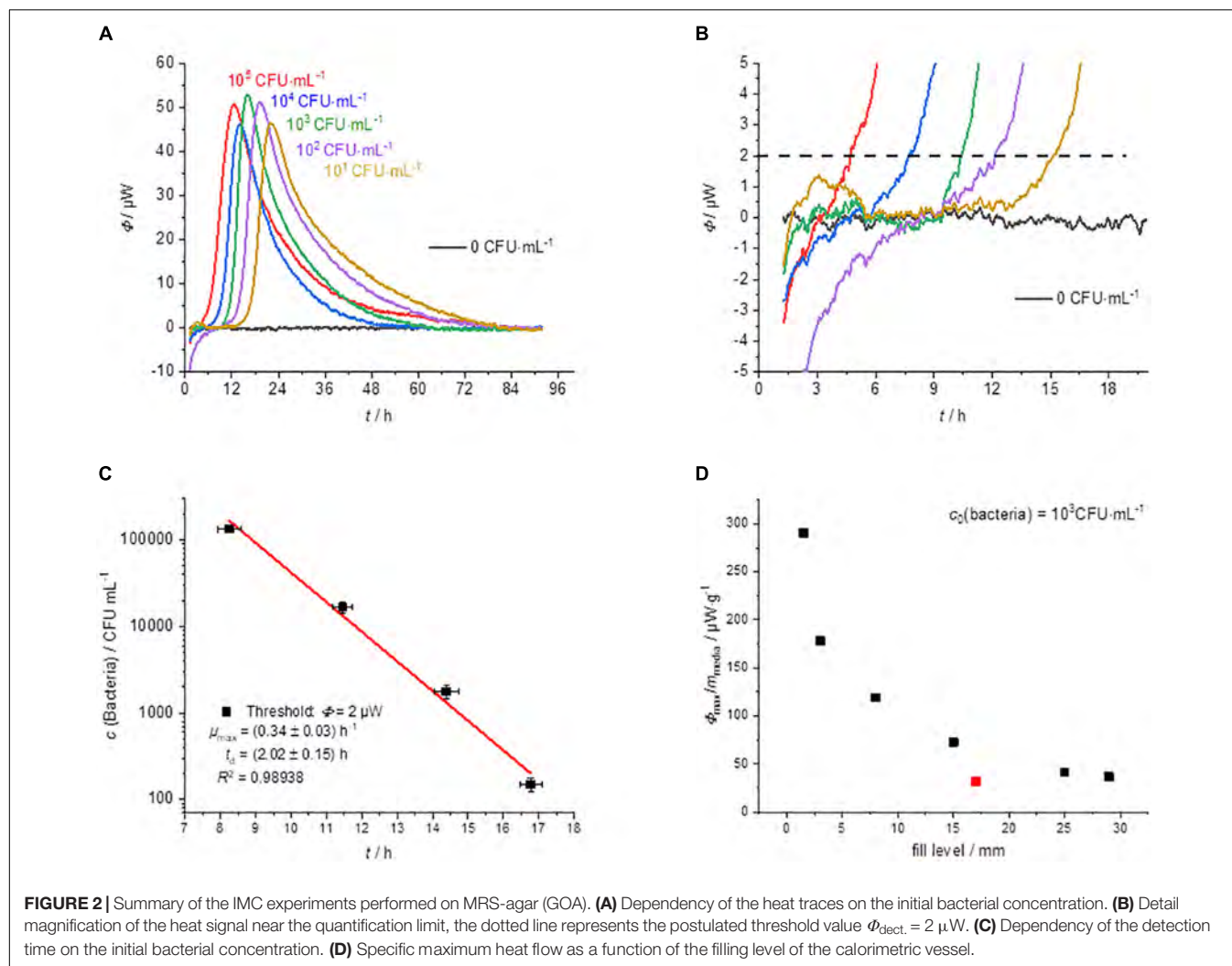
and the detection time $t_{\text{dect.}}$ with μ_{max} as the slope is expected. With the aid of this relation, we can read off the corresponding detection time for any measured heat flow signal of a pure culture of *L. plantarum* and determine the associated initial concentration of bacteria. The final assumption needed for the practical application of this kind of quantification for microbial contamination is a constant specific growth rate μ_{max} during the considered detection times. These conditions are fulfilled when sufficient substrates are available and the bacteria are in the early exponential growth phase.

IMC Measurements of the Different Cultivation Techniques

In the following, the application of the different cultivation techniques to IMC monitoring is described.

Growth on Agar (GOA)

The results of the cultivation of *L. plantarum* on agar are summarized in Figure 2. *L. plantarum* can only ferment the substrate glucose, so we do not expect a complex heat



flow signal as a result. The heat flow signals confirmed this expectation; only a single peak is observed in all measurements. After reaching a maximum the heat flow signal returned to the baseline. With decreasing initial concentration of the bacteria, the heat flow signal shifted as predicted by Eqs. 3 and 4 to later time (Figure 2A). Similar observations were also made by Braissant et al. (2010b) with the detection of mycobacteria. The threshold value for the corresponding detection time was as mentioned set to $\Phi_{\text{dect.}} = 2 \mu\text{W}$ (Figure 2B).

Considering Eqs. 3 and 4 any other threshold value within the exponential growth phase should be resulting in the linearity of the logarithm of the initial bacterial concentration. This was already illustrated using heat flow curves of *Escherichia coli* (Maskow et al., 2012). Also in the present case, we obtained a linear relationship when plotting the detection times against the logarithms of the initial concentrations of bacteria (Figure 2C).

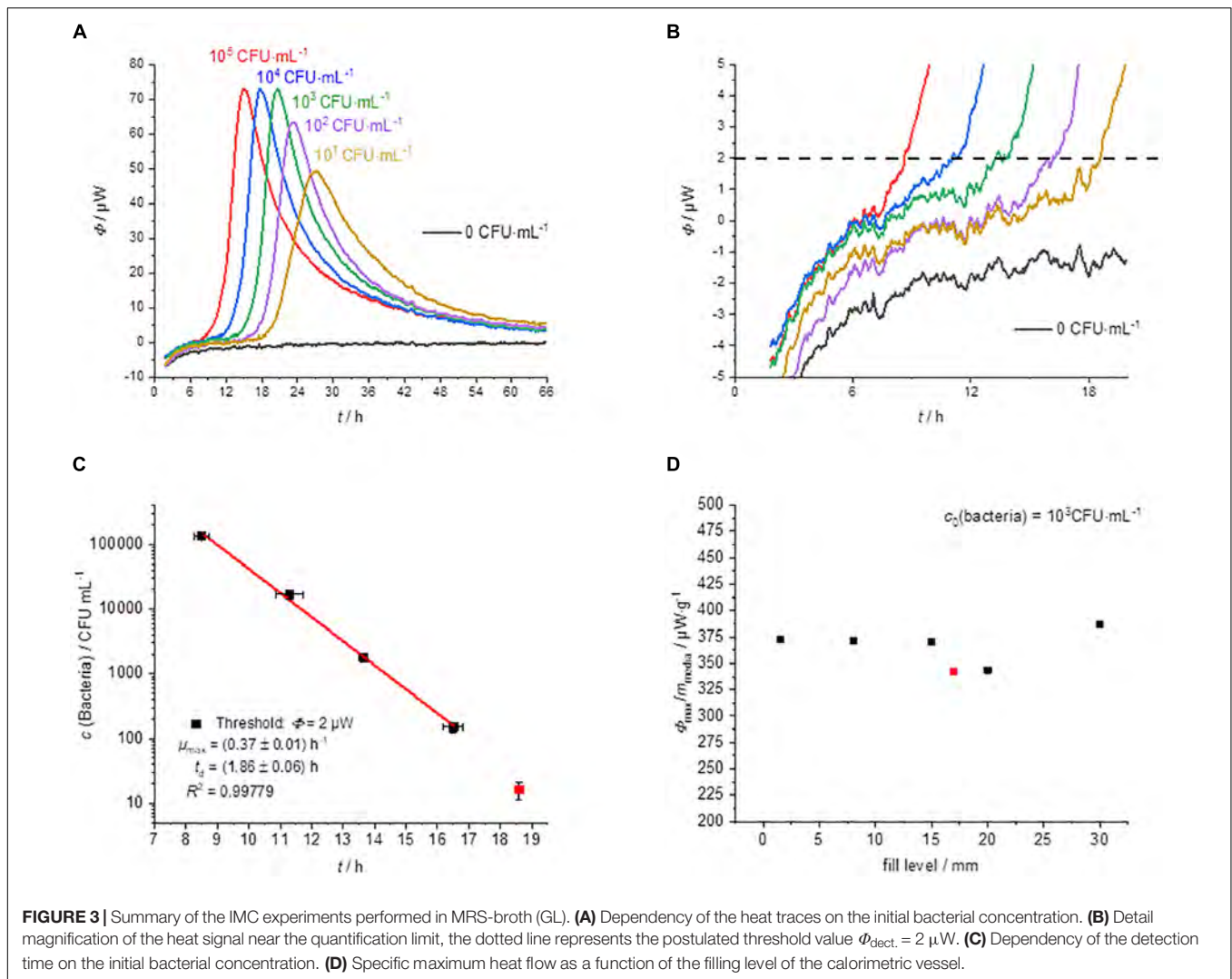
The results of CFU determinations are given in the **Supplementary Material**. For the highest concentration of bacteria, the detection took place after approximately 8 h and for

the lowest concentration after approximately 17 h. Derived from the slope microbiological information like the specific growth rate μ_{max} was obtained. **Table 1** summarize calorimetrically determined growth parameters and compare the calorimetric detection times of the different cultivation techniques.

TABLE 1 | Summary of the results with different cultivation techniques combined with IMC experiments.

Cultivation technique	V (inoculum)/mL	$\mu_{\text{max}}/\text{h}^{-1}$	$t_{\text{dect,high}}/\text{h}$	$t_{\text{dect,low}}/\text{h}$
GOA	0.01	(0.34 ± 0.03)	8.3	16.8 ^b
GL	0.01	(0.37 ± 0.01)	8.5	16.5 ^b
GF	1.8	(0.33 ± 0.02)	4.7	15.9 ^c
GIA	0.01	(0.40 ± 0.03)	8.9	13.6 ^d
Reference (Wegkamp et al., 2010)	n.d.	(0.40 ± 0.03) ^a	n.d.	n.d.

^a*L. plantarum* WCFS1 growth on MRS-medium in 96-wells microtiter plates at 37°C; ^b10² CFU·mL⁻¹; ^c10 CFU·mL⁻¹; ^d10³ CFU·mL⁻¹.



If only cheaper and less accurate calorimeters are available, the loss of accuracy can be compensated by a larger filling level of the calorimetric vessel. However, the correlation between the filling level (in mm) and the corresponding metabolic heat flow must be known. Interestingly, the specific maximum heat flow signals (in $\mu\text{W}\cdot\text{g}^{-1}$) versus the filling level of the calorimetric vessel is approaching asymptotically a border value (Figure 2D). Small amounts of solid nutrient medium with a low filling level show a comparatively larger specific maximum heat flow. However, if the filling level increases, the specific maximum heat flow decreases and reaches a constant value of about $30 \mu\text{W}\cdot\text{g}^{-1}$. This behavior seems to be independent of the applied calorimeter, because the red measuring point (Figure 2D), determined by a less powerful calorimeter (MC-Cal/100 P, C3 Prozess- und Analysetechnik GmbH, Munich, Germany) fits perfectly into the correlation determined with the high-performance calorimeter.

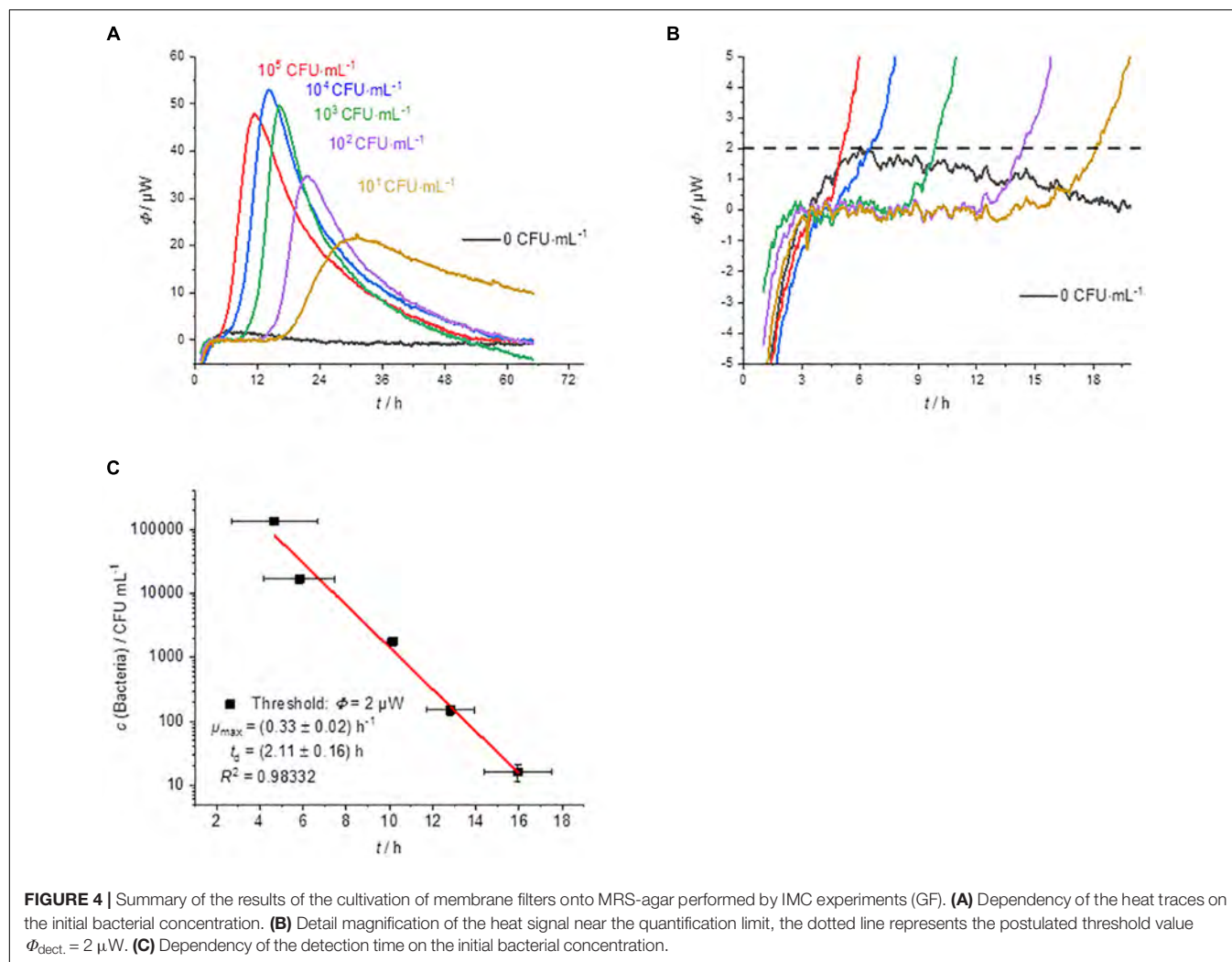
The asymptotic limit value approach during GOA-filled ampoules can be explained as follow. The maximum heat production is determined by the number of bacteria and their access to the substrate. The substrates are supplied by diffusion.

At low fill levels, the diffusion paths are short and the number of bacteria produced depends on the absolute amount of substrate. At high fill levels, the maximum number of bacteria is limited by the surface of the agar and the delivery rates of the substrate are slow due to the long diffusion path. An improved surface to filling volume ratio and thereby a shorter diffusion pathway can be achieved by using slanted agar (Braissant et al., 2010b).

This GOA cultivation technique is preferably suitable for aerobic mesophiles as well as aerotolerant microorganisms such as our model strain. The method is also applicable to strict anaerobic microorganisms if oxygen is excluded during both preparation and the conduction of the experiments. This can be achieved by purging with an inert gas (e.g., N_2) (Maskow and Babel, 2003) or by overcoating of the culture with paraffin oil as described by Xu et al. (2018).

Growth in Liquid (GL)

The usual IMC approach is the cultivation in liquid medium (broth) (Boling et al., 1973; Trampuz et al., 2007b; Maskow et al., 2012; Braissant et al., 2015; Miyake et al., 2016;



Dandé et al., 2018). The results with the liquid medium are summarized in **Figure 3**.

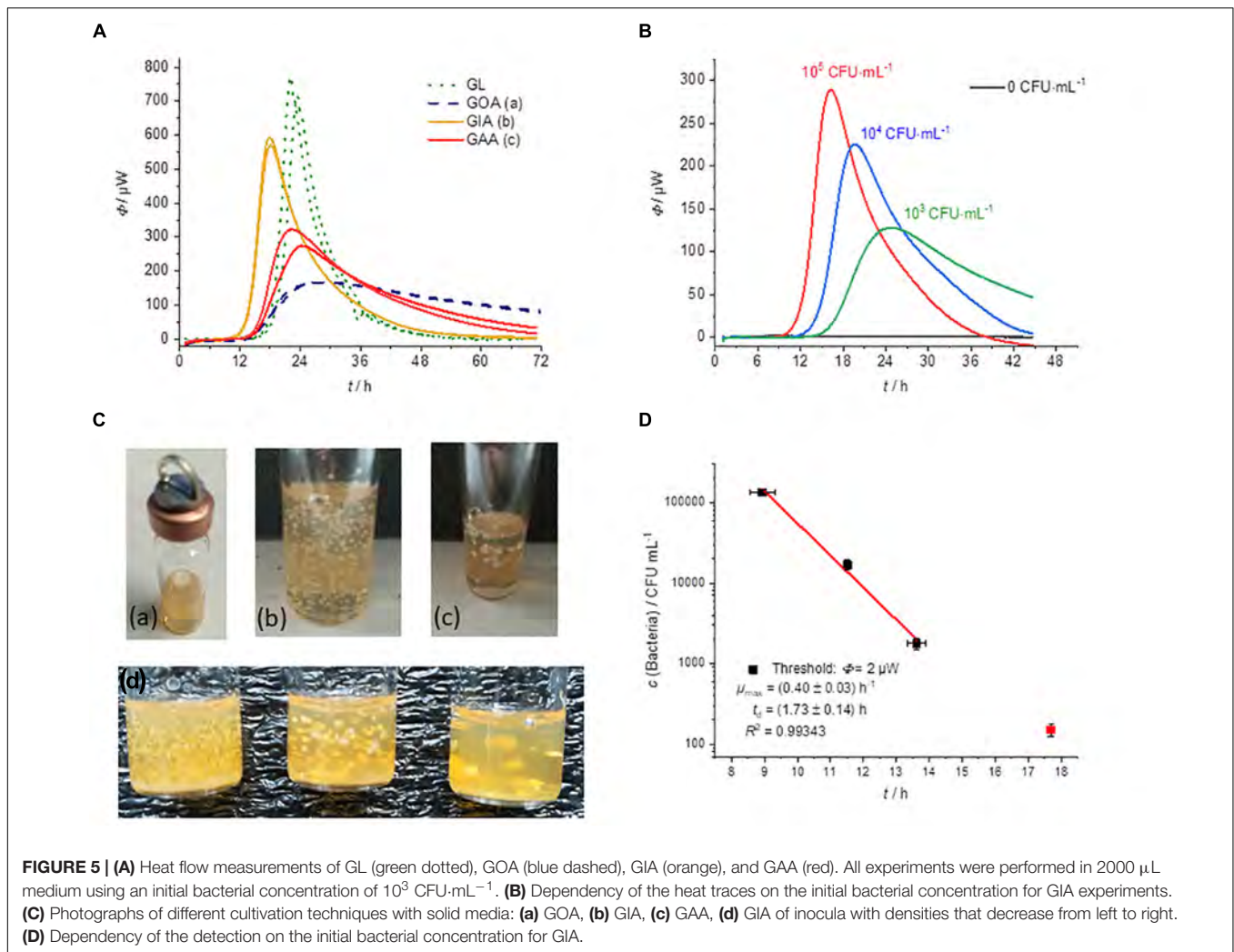
The shape of the heat flow signals is similar to that of the solid medium (**Figure 3A**). However, the standard deviation of the detection time is slightly smaller than for measurements on solid agar (**Figure 3C**). One reason might be the better homogeneity of bacteria and substrate in the liquid medium.

The detection times were between 8 h (for the highest concentration of bacteria) and 18.5 h (for the lowest concentration) using liquid media (**Figure 3C**). Garcia et al. (2017) were also able to find similar detection times for the microcalorimetric investigation of *Lactobacillus reuteri*. The lowest concentration ($10 \text{ CFU}\cdot\text{mL}^{-1}$) was only detectable once of three measurements. At a concentration of 10 bacteria per mL, the usual inoculum of $10 \mu\text{L}$ contains statistically only one of a tenth of a bacterium. A comparison with the literature data shows that the specific growth rate ($0.40 \pm 0.03 \text{ h}^{-1}$) (Wegkamp et al., 2010) measured for *L. plantarum* WCFS1 is very similar compared to our specific growth rate ($0.37 \pm 0.01 \text{ h}^{-1}$). The obtained microbiological information from this experiment is summarized in **Table 1**.

In contrast to experiments on solid medium, the specific maximum heat flow is constant and independent of the filling volume (**Figure 3D**). This finding is confirmed by a further experiment using a less sensitive calorimeter (MC-Cal/100 P, C3 Prozess- und Analysetechnik GmbH, Munich, Germany) with different geometry of the calorimetric vessel and a filling volume of 10 mL (see the red measuring point in **Figure 3D**). Gysin et al. (2018) observed similar behavior for their sample volume optimization in the range from 0.25 to 2 mL. This is explainable because in liquid culture, the bacteria and the substrates are mainly homogeneously distributed and effects of the vessel size, therefore should not play a role.

Growth on Membrane Filter Onto Agar (GF)

Figure 4 summarizes the results of the cultivation of membrane filter onto MRS-agar. The heat flow signals again follow a simple peak curve. However, the peak width is much wider than in the previous measurements. Due to the larger sample volume, which can be applied due to the membrane filtration step, the initial bacterial concentration is much higher than with the other



techniques. As a result, the detection times are even shorter (Figures 4A,B).

As expected, the GF experiments also show a linear dependency between the detection time and the logarithm of the initial bacterial concentration (Figure 4C). The slightly lower correlation can be explained by the fact that the CFUs per mL were determined from the original samples. A better approach might be to use the counted CFU per mL directly from the membrane filtration since there might be differences in the growth of single colonies between plating and growth on membrane filters (Clark et al., 1951; Taylor et al., 1953).

Nevertheless, the specific growth rate and the doubling time of the bacteria fit to the previous GOA experiments. The bacterial growth is slightly slower compared to GL. For the highest concentration of bacteria, the detection takes place after approx. 4.5 h and for the lowest concentration after approx. 16 h. As already mentioned, the earlier detection is due to the larger volume (1.8 mL), which was filtered in these experiments. Measurements depending on the filling level of the calorimetric vessels were not performed due to the similarity to GOA experiments.

Growth in Agar (GIA)

In addition to the classical spreading (or plating) of bacteria, there is another approach: the so-called pour plate method (GIA). It is the preferred technique for counting CFUs per mL of bacteria in viscous fluids (Vansoestbergen and Lee, 1969). For IMC measurements it might also be the preferred technique for strict anaerobic as well as for microaerophilic microorganisms (if strong anaerobic conditions were not met). Figure 5 shows that GIA can be also combined with calorimetric monitoring.

Figure 5A compares the different cultivation techniques. Note, that in the case of GIA an inoculum volume of 100 μL was used. The mixing of inocula with the medium allows the using of larger sample size with a higher number of initial bacteria and thus a shorter detection time in comparison to the GOA approach.

Furthermore, with GIA higher heat flow signals in comparison of GOA can be observed, because the colonies are evenly distributed in three dimensions instead of being restricted to a surface (2D). Therefore, substrate availability is better for GIA. The homogeneous 3D-distribution can be seen in Figure 5C. In order to understand the observed effect better, we investigated a

TABLE 2 | Comparison of the detection times (in h) determined by conventional techniques and IMC measurements.

Measuring technique	10 ⁵ CFU·mL ⁻¹	10 ⁴ CFU·mL ⁻¹	10 ³ CFU·mL ⁻¹	10 ² CFU·mL ⁻¹	10 ¹ CFU·mL ⁻¹
IMC – GOA	(8.3 ± 0.3)	(11.5 ± 0.3)	(14.4 ± 0.3)	(16.8 ± 0.3)	n.d.
IMC – GL	(8.5 ± 0.2)	(11.3 ± 0.4)	(13.7 ± 0.1)	(16.5 ± 0.3)	18.6 ^d
IMC – GF	(4.7 ± 2.0)	(5.8 ± 1.6)	(10.2 ± 0.3)	(12.8 ± 1.1)	(15.9 ± 1.5)
Counting – GOA <i>t</i> _{dect.} ^a /h	13.7	13.7	15.7	15.7	17.7
<i>t</i> _{dect.} ^b /h	(15.8 ± 0.4)	(16.7 ± 0.6)	(17.0 ± 0.6)	(17.1 ± 0.5)	n.d.
OD ₆₀₀ – GL ^c	(13.1 ± 0.4)	(18.5 ± 1.3)	(24.3 ± 2.0)	(25.6 ± 3.1)	n.d.
Counting – GF ^b	11	12	15	17	18

n.d., Not detectable. ^aDetection time after colonies were countable by the eye – evaluation in real-time; ^bDetection time after colonies were countable by the eye – evaluation of the scanning images; ^cOnly four of nine measurements could be evaluated; ^dLess than three replicate heat flow signals were obtained, no standard deviation is indicated.

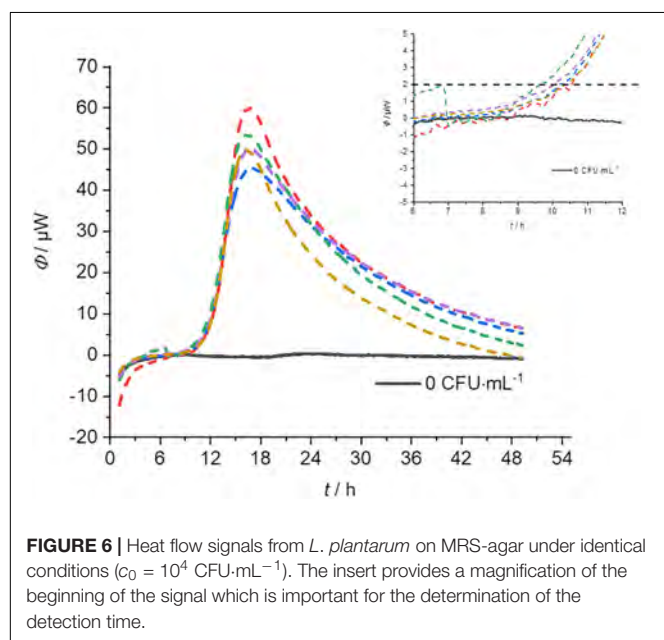


FIGURE 6 | Heat flow signals from *L. plantarum* on MRS-agar under identical conditions ($c_0 = 10^4$ CFU·mL⁻¹). The insert provides a magnification of the beginning of the signal which is important for the determination of the detection time.

case between GIA and GOA. The bacteria were placed between two agar layers (GAA). The availability of the substrates should therefore also be better than in the case of GOA. The red heat flow curves in **Figure 5A** illustrates that due to the better substrate

TABLE 3 | Summary of the reproducibility measurements of the different cultivation techniques combined with IMC measurements.

Cultivation technique	<i>m</i> (medium)/g	<i>c</i> ₀ /CFU·mL ⁻¹	<i>t</i> _{dect.} /h
GOA			
1	0.2	10 ⁴	(10.2 ± 0.3)
2	0.4	10 ⁵	(7.5 ± 1.1)
GL			
1	2	10 ⁷	(3.6 ± 0.4)
2	2	10 ⁷	(3.8 ± 0.6)
GF			
1	0.4	10 ⁵	(5.0 ± 0.7)
2 ^a	2	10 ⁵	(4.1 ± 0.4)

^aSixfold determination.

availability, the maximum heat flow is approx. twice as large as in GOA and half of that in GIA. The observations are very consistent with the IMC measurements of Kabanova et al. (2012, 2013). **Figures 5B,C** show the influence of the number on initial bacteria on the heat flow signal. In the case of a smaller initial number of bacteria, larger colonies were formed and the total heat flow was lower than for many bacteria (**Figure 5B**). At small bacterial concentrations, only one experiment was successful (red square, **Figure 5D**). We identified two potential reasons. Firstly, the inoculum volume (10 μL) might not have contained any bacterial cells. Secondly, the increased temperature of the still molten agar (~50°C) might have killed part of the initial bacteria.

A comparison of the specific growth rates revealed that the growth rate of the bacteria did not depend on the physical state of the medium and the localization of the inoculum. Kabanova came to the same conclusion when they investigated *Lactococcus lactis* (Kabanova et al., 2013). The reason for this is that glucose has a similar diffusion coefficient in water as in solid agar medium (Schantz and Lauffer, 1962).

Comparison With Conventional Techniques

A decisive question is what advantages (in terms of economy of time and accuracy) over conventional methods the IMC can achieve. In **Table 2**, IMC is compared with traditional counting and real-time measurement of the optical density.

If one first considers the high initial concentration (> 10² CFU·mL⁻¹), the great advantage of the IMC measurement over the visual counting of individual colonies and monitoring of the optical density becomes apparent. The exact determination of such a high concentration as CFU is error-prone even with small inoculum volumes such as 10 μL because the colonies cannot be clearly separated (an intermediate dilution is necessary). In the case of IMC, every bacteria contributes to the heat and, therefore, high bacteria concentrations do not falsify the measurement results. In addition, bacterial growth can be detected 5–7 h earlier by IMC in comparison to counting. On the other hand, low initial bacterial concentrations might also error-prone if one considers cell aggregation, is taking place. Just like a single cell, a cell aggregate delivers only one colony.

Comparing the IMC with the measurement of the optical density in a liquid medium (detection threshold value at

600 nm = 0.01) always an earlier detection (5–9 h) was possible. At low initial bacterial concentrations ($<10^2$ CFU·mL⁻¹), the IMC measurements on solid media were not significantly faster than the classical visual counting of colonies. For the liquid media, in all three measurements, no increase in the optical density was observed for the lowest initial concentration. As already discussed, the existing inoculum volume (10 µL) is too small to ensure the presence of bacteria (see **Supplementary Material**). It has been proven that the detection time could be greatly reduced by using GF. Here, the detection time for the smallest concentration could be reduced by almost 2 h.

Reproducibility

In order to determine the reproducibility of IMC measurements, five-fold determinations were performed with an identical initial concentration of bacteria for each cultivation technique (except pouring). **Figure 6** represents an example of a GOA measurement (for the other measurements see **Supplementary Material**). **Table 3** summarizes the results of these measurements. The error of the detection was roughly similar for GOA, GL and GF. Taking into account the results from **Tables 2, 3**, it is not surprising that the errors for the filtration technique (GF) were generally slightly higher, because of the difficult handling of the very small filters ($r = 5$ mm). Not every filter could be placed evenly and identically within the measuring ampoule on the nutrient medium. The error caused by the imperfect placement of the membrane filters can potentially be overcome by designing calorimeters that allow the use of standard filters (47 mm).

Relative errors in the calorimetric detection time in the same order as for our results were obtained by Bonkat et al. (2013) for bacteria infecting the urinal tract and by Zaharia et al. (2013) for *E. coli* and *Staphylococcus aureus*.

CONCLUSION

Our data demonstrate that conventional cultivation techniques like pouring (GIA) or plating on agar (GOA), inoculation of broth (GL) or membrane filter cultivation (GF) can be combined with IMC measurements. The great advantage of this technique is the preservation of simplified sample handling and easy evaluation of the data obtained. Only the detector is replaced, i.e., the human eye by a powerful thermoelectric element. In addition, these IMC measurements are non-invasive and non-destructive (Russel et al., 2009; Brueckner et al., 2016). Because the calorimetric experiment measures bacterial growth, an enrichment culture is available after the experiment that can be used for further molecular biological investigations.

It was shown in the case of *E. coli* that the detection time in a liquid medium measured by IMC is considerably faster than visual colony counting (Maskow et al., 2012). In order to verify the results, we compared for the first time IMC measurements on solid medium with classical visual colony counting and IMC measurements in liquid medium with classical OD₆₀₀ measurements. We were able to reduce the detection time for both approaches and we were also able to show that enrichment by membrane filtration, in

particular, enables a much faster detection time with IMC. When counting the colonies visually, it must be taken into account that further hours elapse before the colony is fully formed and optical identification is possible by morphological properties of the colony. This assumption could be confirmed by the real-time scanning of colony growth (see **Supplementary Material**). Furthermore, IMC measurements can be used to measure turbid starting solutions and a shaking of the sample is also not necessary.

We were also able to show that in the context of the anaerobic system investigated in this study, the quantity of substrate and the resulting fill level has an influence on the maximum heat flow. GL is preferable to GOA when less sensitive calorimeters are used for the detection of anaerobic microorganisms. However, it has been shown that solid media can also be used for quantification using GIA.

Using selective media, it might be possible to isolate targeted microorganisms from their natural environment and detect them quickly and reliably using IMC (Atlas, 2010). Furthermore, continuous success in the development of selective media for different species in microbiology can be recognized (Bujalance et al., 2006; Nwamaioha and Ibrahim, 2018; Veselá et al., 2019). The exchange of substrates, as well as the addition of antibiotics, enable in some cases the use of a highly selective media and suppressed the growth of accompanying microorganisms. Additionally, the pre-treatment of the sample with chemical treatment like in case of *Legionella* might also suppress the accompanying flora (Bopp et al., 1981). In this way, the lack of specificity of the IMC can potentially be overcome.

The next steps should be the development of simpler and cheaper calorimeters specifically designed for the detection of microbial contaminations in order to become competitive over the conventional approaches (Wadsö et al., 2011) and the investigation of an aerobic system to determine the limitations and applications regarding monitoring bacterial growth by IMC.

Finally, to overcome arbitrary threshold determinations for the heat flow signals mathematical models allowing to discriminate small biological signals from the physical background has to be developed. In this way, a further reduction of the detection time and of the measurement error can be potentially achieved.

DATA AVAILABILITY STATEMENT

All datasets generated for this study are included in the article/**Supplementary Material**.

AUTHOR CONTRIBUTIONS

TM developed the project idea. CF designed the experimental setup, performed the laboratory work as well as analyzed the data, and edited the manuscript. TM and HH provided consultation for the work and contributed significantly to the preparation of the manuscript. All authors reviewed the manuscript and agreed with the content.

FUNDING

This work was funded by the German Federation of Industrial Research Associations (AiF BMWi, AiF-Nr. ZF4315807RH7).

ACKNOWLEDGMENTS

The authors acknowledge M. Kolbe (UFZ, Department of Environmental Microbiology) and K. Lübke (UFZ, Department of Environmental Microbiology) for preparing

REFERENCES

- Astasov-Frauenhoffer, M., Braissant, O., Hauser-Gerspach, I., Daniels, A. U., Weiger, R., and Waltimo, T. (2012). Isothermal microcalorimetry provides new insights into biofilm variability and dynamics. *FEMS Microbiol. Lett.* 337, 31–37. doi: 10.1111/1574-6968.12007
- Astasov-Frauenhoffer, M., Braissant, O., Hauser-Gerspach, I., Weiger, R., Walter, C., Zitzmann, N. U., et al. (2014). Microcalorimetric determination of the effects of amoxicillin, metronidazole, and their combination on in vitro biofilm. *J. Periodontol.* 85, 349–357. doi: 10.1902/jop.2013.120733
- Atlas, R. M. (2010). *Handbook of Microbiological Media*. Hoboken: CRC Press.
- Boling, E. A., Blanchard, G. C., and Russell, W. J. (1973). Bacterial identification by microcalorimetry. *Nature* 241, 472–473. doi: 10.1038/241472a0
- Bonkat, G., Braissant, O., Rieken, M., Solokhina, A., Widmer, A. F., Frei, R., et al. (2013). Standardization of isothermal microcalorimetry in urinary tract infection detection by using artificial urine. *World J. Urol.* 31, 553–557. doi: 10.1007/s00345-012-0913-2
- Bonkat, G., Rieken, M., Braissant, O., Widmer, A. F., Feicke, A., Wyler, S., et al. (2011). Rapid detection of common causative pathogens of urinary tract infection by isothermal microcalorimetry. *Eur. Urol. Suppl.* 10, 162–162. doi: 10.1016/S1569-9056(11)60469-7
- Bopp, C. A., Sumner, J. W., Morris, G. K., and Wells, J. G. (1981). Isolation of legionella spp. from environmental water samples by low-pH treatment and use of a selective medium. *J. Clin. Microbiol.* 13, 714–719.
- Braissant, O., Keiser, J., Meister, I., Bachmann, A., Wirz, D., Gopfert, B., et al. (2015). Isothermal microcalorimetry accurately detects bacteria, tumorous microtissues, and parasitic worms in a label-free well-plate assay. *Biotechnol. J.* 10, 460–468. doi: 10.1002/biot.201400494
- Braissant, O., Wirz, D., Gopfert, B., and Daniels, A. U. (2010a). Biomedical use of isothermal microcalorimeters. *Sensors* 10, 9369–9383. doi: 10.3390/s101009369
- Braissant, O., Wirz, D., Gopfert, B., and Daniels, A. U. (2010b). The heat is on: rapid microcalorimetric detection of mycobacteria in culture. *Tuberculosis* 90, 57–59. doi: 10.1016/j.tube.2009.11.001
- Brueckner, D., Krähenbühl, S., Zuber, U., Bonkat, G., and Braissant, O. (2017). An alternative sterility assessment for parenteral drug products using isothermal microcalorimetry. *J. Appl. Microbiol.* 123, 773–779. doi: 10.1111/jam.13520
- Brueckner, D., Roesti, D., Zuber, U. G., Schmidt, R., Kraehenbuehl, S., Bonkat, G., et al. (2016). comparison of tunable diode laser absorption spectroscopy and isothermal micro-calorimetry for non-invasive detection of microbial growth in media fills. *Sci. Rep.* 6, 27894–27894. doi: 10.1038/srep27894
- Buckton, G., Russell, S. J., and Beezer, A. E. (1991). Pharmaceutical calorimetry: a selective review. *Thermochim. Acta* 193, 195–214. doi: 10.1016/0040-6031(91)80184-K
- Bujalance, C., Jiménez-Valera, M., Moreno, E., and Ruiz-Bravo, A. (2006). A selective differential medium for *Lactobacillus plantarum*. *J. Microbiol. Methods* 66, 572–575. doi: 10.1016/j.mimet.2006.02.005
- Chang-Li, X., Hou-Kuhan, T., Zhou-Hua, S., Song-Sheng, Q., Yao-Ting, L., and Hai-Shui, L. (1988). Microcalorimetric study of bacterial growth. *Thermochim. Acta* 123, 33–41. doi: 10.1016/0040-6031(88)80007-8
- Clais, S., Boulet, G., Van Kerckhoven, M., Lanckacker, E., Delputte, P., Maes, L., et al. (2015). Comparison of viable plate count, turbidity measurement and real-time PCR for quantification of *Porphyromonas gingivalis*. *Lett. Appl. Microbiol.* 60, 79–84. doi: 10.1111/lam.12341

the media, U. Lohse for performing the 16S ribosomal DNA analysis, and C. Heber, S. Paufler, and K.-T. Mühler (UFZ, Department of Environmental Microbiology) for technical support.

SUPPLEMENTARY MATERIAL

The Supplementary Material for this article can be found online at: <https://www.frontiersin.org/articles/10.3389/fmicb.2019.02530/full#supplementary-material>

- Clark, H. F., Geldreich, E. E., Jeter, H. L., and Kabler, P. W. (1951). The membrane filter in sanitary bacteriology. *Public Health Rep.* 66, 951–977. doi: 10.2307/4587804
- Dandé, Á, Nöt, L. G., Bücs, G., Wiegand, N., Kocsis, B., and Lörinczy, D. (2018). Examination of typical bacterial strains in septic arthritis by isoperibol calorimeter. *J. Therm. Anal. Calorim.* 131, 2041–2048. doi: 10.1007/s10973-017-6859-2
- Donoso, W., Castro, R. I., Guzmán, L., López-Cabaña, Z., Nachtigall, F. M., and Santos, L. S. (2017). Fast detection of *Listeria monocytogenes* through a nanohybrid quantum dot complex. *Anal. Bioanal. Chem.* 409, 5359–5371. doi: 10.1007/s00216-017-0481-9
- García, A. H., Herrmann, A. M., and Håkansson, S. (2017). Isothermal microcalorimetry for rapid viability assessment of freeze-dried *Lactobacillus reuteri*. *Process Biochem.* 55, 49–54. doi: 10.1016/j.procbio.2017.01.012
- Gram, L., and Sogaard, H. (1985). The potentiality of microcalorimetry as a rapid method for monitoring the microbiological quality of raw meat and fish. *Thermochim. Acta* 95, 375–381. doi: 10.1016/0040-6031(85)85298-9
- Gysin, M., Braissant, O., Gillingwater, K., Brun, R., Maser, P., and Wenzler, T. (2018). Isothermal microcalorimetry - a quantitative method to monitor *Trypanosoma congolense* growth and growth inhibition by trypanocidal drugs in real time. *Int. J. Parasitol. Drugs Drug Resist.* 8, 159–164. doi: 10.1016/j.ijpddr.2018.03.003
- Hazan, R., Que, Y.-A., Maura, D., and Rahme, L. G. (2012). A method for high throughput determination of viable bacteria cell counts in 96-well plates. *BMC Microbiol.* 12:259. doi: 10.1186/1471-2180-12-259
- Jami Al-Ahmadi, G., and Zahmatkesh Roodsari, R. (2016). Fast and specific detection of *Pseudomonas Aeruginosa* from other *pseudomonas* species by PCR. *Ann. Burns Fire Disasters* 29, 264–267.
- Jay, J. M., Loessner, M. J., and Golden, D. A. (2005). *Modern Food Microbiology*. New York, NY: Springer.
- Kabanova, N., Stulova, I., and Vilu, R. (2012). Microcalorimetric study of the growth of bacterial colonies of *Lactococcus lactis* IL1403 in agar gels. *Food Microbiol.* 29, 67–79. doi: 10.1016/j.fm.2011.08.018
- Kabanova, N., Stulova, I., and Vilu, R. (2013). Microcalorimetric study of growth of *Lactococcus lactis* IL1403 at low glucose concentration in liquids and solid agar gels. *Thermochim. Acta* 559, 69–75. doi: 10.1016/j.tca.2013.02.013
- Khalef, N., Campanella, O., and Bakri, A. (2016). Isothermal calorimetry: methods and applications in food and pharmaceutical fields. *Curr. Opin. Food Sci.* 9, 70–76. doi: 10.1016/j.cofs.2016.09.004
- Koch, A. L. (1970). Turbidity measurements of bacterial cultures in some available commercial instruments. *Anal. Biochem.* 38, 252–259. doi: 10.1016/0003-2697(70)90174-0
- Law, J. W.-F., Ab Mutalib, N.-S., Chan, K.-G., and Lee, L.-H. (2015). Rapid methods for the detection of foodborne bacterial pathogens: principles, applications, advantages and limitations. *Front. Microbiol.* 5:770. doi: 10.3389/fmicb.2014.00770
- Levin, K. (1977). Calorimetry, a time-honored technique with a potential in analytical work and cellular biology. *Clin. Chem.* 23, 929–937.
- Maskow, T., and Babel, W. (2003). Thermokinetic description of anaerobic growth of halomonas halodenitrificans using a static microcalorimetric ampoule technique. *J. Biotechnol.* 101, 267–274. doi: 10.1016/S0168-1656(02)00341-3
- Maskow, T., Schubert, T., Wolf, A., Buchholz, F., Regestein, L., Buechs, J., et al. (2011). Potentials and limitations of miniaturized calorimeters for bioprocess

- monitoring. *Appl. Microbiol. Biotechnol.* 92, 55–66. doi: 10.1007/s00253-011-3497-7
- Maskow, T., Wolf, K., Kunze, W., Enders, S., and Harms, H. (2012). Rapid analysis of bacterial contamination of tap water using isothermal calorimetry. *Thermochim. Acta* 543, 273–280. doi: 10.1016/j.tca.2012.06.002
- Miyake, H., Maeda, Y., Ishikawa, T., and Tanaka, A. (2016). Calorimetric studies of the growth of anaerobic microbes. *J. Biosci. Bioeng.* 122, 364–369. doi: 10.1016/j.jbiosc.2016.02.006
- Nwamaioha, N. O., and Ibrahim, S. A. (2018). A selective medium for the enumeration and differentiation of *Lactobacillus delbrueckii* ssp. *bulgaricus*. *J. Dairy Sci.* 101, 4953–4961. doi: 10.3168/jds.2017-14155
- Ren, Y., Zhang, P., Yan, D., Yan, Y., Chen, L., Qiu, L., et al. (2012). Application of microcalorimetry of *Escherichia coli* growth and discriminant analysis to the quality assessment of a Chinese herbal injection (Yinzhihuang). *Acta Pharm. Sin. B* 2, 278–285. doi: 10.1016/j.apsb.2012.02.013
- Russel, M., Yao, J., Chen, H., Wang, F., Zhou, Y., Choi, M. M. F., et al. (2009). Different technique of microcalorimetry and their applications to environmental sciences: a review. *J. Am. Sci.* 5, 194–208. doi: 10.7537/marsjas050409.29
- Schantz, E. J., and Lauffer, M. A. (1962). Diffusion measurements in agar gel. *Biochemistry* 1, 658–663. doi: 10.1021/bi00910a019
- Sieuwert, S., De Bok, F. A., Mols, E., De Vos, W. M., and Vlieg, J. E. (2008). A simple and fast method for determining colony forming units. *Lett. Appl. Microbiol.* 47, 275–278. doi: 10.1111/j.1472-765X.2008.02417.x
- Solokhina, A., Bruckner, D., Bonkat, G., and Braissant, O. (2017). Metabolic activity of mature biofilms of *Mycobacterium tuberculosis* and other non-tuberculous mycobacteria. *Sci. Rep.* 7:9225. doi: 10.1038/s41598-017-10019-4
- Taylor, E. W., Burman, N. P., and Oliver, C. W. (1953). Use of the membrane filter in the bacteriological examination of water. *J. Appl. Chem.* 3, 233–240. doi: 10.1002/jctb.5010030508
- Trampuz, A., Salzmann, S., Antheaume, J., and Daniels, A. U. (2007a). Microcalorimetry: a novel method for detection of microbial contamination in platelet products. *Transfusion* 47, 1643–1650. doi: 10.1111/j.1537-2995.2007.01336.x
- Trampuz, A., Steinhuber, A., Wittwer, M., and Leib, S. L. (2007b). Rapid diagnosis of experimental meningitis by bacterial heat production in cerebrospinal fluid. *BMC Infect. Dis.* 7:116. doi: 10.1186/1471-2334-7-116
- Tsuneishi, N., and Goetz, A. (1958). A method for the rapid cultivation of *Desulfovibrio-aestuarii* on filter membranes. *Appl. Microbiol.* 6, 42–44.
- Vansoestbergen, A. A., and Lee, C. H. (1969). Pour plates or streak plates. *Appl. Microbiol.* 18, 1092–1093.
- Velusamy, V., Arshak, K., Korostynska, O., Oliwa, K., and Adley, C. (2010). An overview of foodborne pathogen detection: in the perspective of biosensors. *Biotechnol. Adv.* 28, 232–254. doi: 10.1016/j.biotechadv.2009.12.004
- Veselá, K., Kumherová, M., Klojdová, I., Solichová, K., Horáčková, Š., and Plocková, M. (2019). Selective culture medium for the enumeration of *Lactobacillus plantarum* in the presence of *Lactobacillus delbrueckii* subsp. *bulgaricus* and *Streptococcus thermophilus*. *LWT* 114:108365. doi: 10.1016/j.lwt.2019.108365
- Vine, G. J., and Bishop, A. H. (2005). The analysis of microorganisms by microcalorimetry in the pharmaceutical industry. *Curr. Pharm. Biotechnol.* 6, 223–238. doi: 10.2174/1389201054022878
- Von Stockar, U., and Liu, J. S. (1999). Does microbial life always feed on negative entropy? thermodynamic analysis of microbial growth. *Biochim. Biophys. Acta Bioenerg.* 1412, 191–211. doi: 10.1016/S0005-2728(99)00065-1
- Wadsö, I. (1995). Microcalorimetric techniques for characterization of living cellular systems. Will there be any important practical applications?. *Thermochim. Acta* 26, 337–350. doi: 10.1016/0040-6031(95)02673-8
- Wadsö, L., and Galindo, F. G. (2009). Isothermal calorimetry for biological applications in food science and technology. *Food Control* 20, 956–961. doi: 10.1016/j.foodcont.2008.11.008
- Wadsö, L., Salamanca, Y., and Johansson, S. (2011). Biological applications of a new isothermal calorimeter that simultaneously measures at four temperatures. *J. Therm. Anal. Calorim.* 104, 119–126. doi: 10.1007/s10973-010-1140-y
- Wang, Y., and Salazar, J. K. (2016). Culture-independent rapid detection methods for bacterial pathogens and toxins in food matrices. *Compr. Rev. Food Sci. Food Saf.* 15, 183–205. doi: 10.1111/1541-4337.12175
- Wegkamp, A., Teusink, B., De Vos, W. M., and Smid, E. J. (2010). Development of a minimal growth medium for *Lactobacillus plantarum*. *Lett. Appl. Microbiol.* 50, 57–64. doi: 10.1111/j.1472-765X.2009.02752.x
- Xie, C. L., Wang, H., and Qu, S. S. (1995). Microcalorimetric study on the aerobic growth of *Escherichia coli*. *Thermochim. Acta* 253, 175–182. doi: 10.1016/0040-6031(94)01972-J
- Xu, J., Kiesel, B., Kallies, R., Jiang, F.-L., Liu, Y., and Maskow, T. (2018). A fast and reliable method for monitoring of prophage-activating chemicals. *Microb. Biotechnol.* 11, 1112–1120. doi: 10.1111/1751-7915.13042
- Zaharia, D. C., Muntean, A. A., Popa, M. G., Steriade, A. T., Balint, O., Micut, R., et al. (2013). Comparative analysis of *Staphylococcus aureus* and *Escherichia coli* microcalorimetric growth. *BMC Microbiol.* 13:171. doi: 10.1186/1471-2180-13-171

Conflict of Interest: The authors declare that the research was conducted in the absence of any commercial or financial relationships that could be construed as a potential conflict of interest.

Copyright © 2019 Fricke, Harms and Maskow. This is an open-access article distributed under the terms of the Creative Commons Attribution License (CC BY). The use, distribution or reproduction in other forums is permitted, provided the original author(s) and the copyright owner(s) are credited and that the original publication in this journal is cited, in accordance with accepted academic practice. No use, distribution or reproduction is permitted which does not comply with these terms.

3.1.2 How to speed up the detection of aerobic microbial contaminations by using isothermal microcalorimetry

Fricke C, Harms H, Maskow T. (2020):

How to speed up the detection of aerobic microbial contaminations by using isothermal microcalorimetry

J. Therm. Anal. Calorim. **142**, 1933–1949.

<https://doi.org/10.1007/s10973-020-09986-0> (published, Original research)

Significance: Calorimetric detection is primarily performed in small, airtight and static ampoule systems. In order to achieve the fastest possible detection of aerobically growing bacteria, it is crucial to know the variables influencing the detectable heat flow. Within the scope of this publication, parameters (including methodical and technical) and their interplay affecting the detection time of aerobic growing contaminations were investigated using *Pseudomonas putida* mt-2 KT2440 as an example. The results demonstrated that the interplay between the amount and state of medium (solid or liquid), the contamination level (CFU per ampoule) and the applied detection limit strongly affect the calorimetric detection time. The poor solubility of oxygen in liquid media and oxygen diffusion from the gas to the liquid phase would lead to delayed detection, especially with less sensitive calorimeters (detection limit > 10 μ W). On solid media, the data showed that low contamination levels (< 10 CFU per ampoule) cause a linear heat flow (diffusion-controlled growth of colonies), which also results in a significant delay in detection if less sensitive calorimeters were employed.

How to speed up the detection of aerobic microbial contaminations by using isothermal microcalorimetry

Christian Fricke¹ · Hauke Harms¹ · Thomas Maskow¹ 

Received: 20 January 2020 / Accepted: 22 June 2020 / Published online: 3 July 2020
© The Author(s) 2020

Abstract

Isothermal microcalorimetry (IMC) is regarded as a promising diagnostic tool for fast detection of bacterial contaminations in various matrices. Based on a reference detection time determined by visual inspection of bacterial growth on solid medium, we investigated the strict aerobically growing *Pseudomonas putida* mt-2 KT2440 in a static 4-mL ampoule system on solid and liquid media by IMC to evaluate the three main options to reduce the detection time of bacterial contamination. Firstly, the sample preparation (e.g. membrane filtration) leads to an elevated number of bacteria in the measuring ampoule and thus to a reduced detection time. Secondly, the amount of substrate and oxygen has been investigated by varying the filling volume of medium in the calorimetric ampoule. Here, we were able to show how biophysical characteristics like the substrate and oxygen diffusion determined the shape of heat flow signals and thus the detection time. Finally, the technical framework determines the sensitivity of the IMC instrument. We examined the impact of four different detection threshold values (2, 10, 50 and 100 μW) on the detection time as a function of the initial number of bacteria presented in the ampoule and the filling volume.

Keywords Aerobic system · Calorimetric detection · Isothermal microcalorimetry · *Pseudomonas putida* KT2440 · Real-time monitoring

List of symbols

c_0	Initial bacterial concentration of each dilution determined by CFU counting (CFU mL^{-1})
c_{O_2}	Concentration of the dissolved oxygen in the liquid medium (mg L^{-1})
LC	Liquid cultivation
LOD	Limit of thermal detection (W)
MF	Membrane filtration
N_0	Initial number of bacteria (CFU)
n_{TEG}	Number of thermocouples
SC	Solid cultivation
SD	Standard deviation
t	Time (h)
t_{dect}	Detection time (h)

U	Voltage (V)
V_i	Inoculum volume (mL)
V_{medium}	Filling volume of medium (mL)
α	Seebeck coefficient (V K^{-1})
$\Delta_k H_{\text{O}_2}$	Oxycaloric equivalent of -455 kJ mol^{-1}
ε	Calibration coefficient (V W^{-1})
κ	Specific thermal conductivity (W K^{-1})
μ	Specific growth rate (h^{-1})
Φ_{dect}	Detection threshold value (W)
Φ	Heat flow (W)
φ_0	Cell-specific heat production rate (W)

Introduction

In general, a calorimeter is capable of detecting the reaction heat released or taken up by any type of physical, chemical or biological process in real-time [1]. This has led to numerous applications in a wide range of fields, including life sciences [2–6], materials science [7], biotechnology [8, 9] and medical diagnostics [10, 11]. As one of the first applications in biocalorimetry in 1780, Lavoisier and Laplace linked calorimetry to biology by studying the metabolism of

Electronic supplementary material The online version of this article (<https://doi.org/10.1007/s10973-020-09986-0>) contains supplementary material, which is available to authorized users.

✉ Thomas Maskow
thomas.maskow@ufz.de

¹ Department of Environmental Microbiology, Helmholtz-Centre for Environmental Research – UFZ, Leipzig, Germany

guinea pigs [12]. Even the tiny heat released during bacterial growth can be monitored using modern high-performance calorimeters. These micro- or nanocalorimeters operate typically in isothermal mode and allow high resolutions in the nano- to microwatt range [1].

The increase in biomass during bacterial growth proceeds along with the formation of metabolic end products such as water or carbon dioxide. At the molecular level, numerous enzymatically controlled reactions take place that break down energy-rich organic molecules (catabolism) or synthesize biomolecules to maintain metabolism and biomass production (anabolism) [13]. Part of the assimilated Gibbs energy is released into the environment in the form of heat [2, 14]. One application focus of biocalorimetry is the qualitative and quantitative detection of bacterial contaminations in food [5], drinking water [15] or for sterility testing of pharmaceuticals [16]. Current isothermal microcalorimeters (IMC) do not allow the detection of a single bacterial cell, due to the low heat production rate of bacterial cells (a few pW) [17] which overstrains the efficiency of current heat flow sensors [18]. Detecting bacterial contaminations is possible by monitoring the growth of the bacteria in real time by cultivation in liquid (LC) [15, 19–22] or solid (SC) [23–25] medium. This benefits from the exponential growth forming substantial biomass from a single bacterial cell within a short time [26]. In this study, we identify the factors influencing the detection time in 4-mL static ampoules in microcalorimetric real-time monitoring using the example of *Pseudomonas putida* mt-2 KT2440.

Our emphasis is on the interplay between initial bacterial numbers, their substrate provision in LC and SC, and the performance of the calorimeter. Detection times are compared with those achieved by conventional visual detection (i.e. the counting of colony-forming units; CFUs).

Materials and methods

Bacterial strain, medium and cultivation

Pseudomonas putida mt2-KT2440 (German Collection of Microorganisms and Cell Cultures, DSMZ, Braunschweig, Germany) was used for the microcalorimetric experiments. The strain was cultivated on DSM-1 medium, recommended by DSMZ which is composed of (in g L⁻¹): peptone (5.0), meat extract (3.0) and agar (15.0). The liquid pre-cultures of *P. putida* were inoculated by a single colony of a pre-grown Petri dish culture. The liquid pre-culture was incubated overnight at room temperature. The identity of the species was regularly checked by the morphology of the colonies as well as by microscopy before and after the calorimetric experiments.

Calorimetric monitoring

The microcalorimeter TAM III (TA Instruments, New Castle, USA) with 12-channels as well as the cement calorimeter with 14-channels MC-Cal/100 P (C3 Prozess- und Analysetechnik GmbH, Munich, Germany) and 4.2-mL glass ampoules were used to perform the bacterial growth experiments. The glass ampoules and the caps were autoclaved at 121 °C for 40 min, subsequently filled with DSM-1 medium or DSM-1 agar and stored in the fridge. The ampoules were warmed up to room temperature before measurements and inoculated with bacteria. In the case of larger filling volumes of medium, the glass ampoules were warmed up in an incubator (30 ± 0.2 °C) to ensure fast thermal equilibration of the whole sample. The prepared ampoules were then placed into the channels of the microcalorimeter and thermally equilibrated for 15 min in the pre-heating position. After further 45 min for thermal equilibration in the measuring position, the heat flow was recorded. Before the experimental set-up was changed (e.g. for modification of filling volume), a gain calibration was performed to ensure the precision of measurements. A single pulse of 1 mW was generated in each channel by an integrated electrical calibration heater. As a result of the calibration, a gain factor and the offset of the respective channel were calculated.

In the case of the cement calorimeter, an internal electrical calibration was performed before the experiments were conducted, and gain factors, as well as the offset of each channel, were determined. Unlike the microcalorimeter, the prepared ampoules were directly placed in the measuring position. One channel was selected as reference and contained a reference ampoule (filled with 1 mL sterile medium). All measurements were conducted at 30.0 °C. After the heat flow had returned to the baseline, the measurements were completed and the ampoules were stored in the refrigerator for final microscopic examination.

The final data evaluation was carried out using the *Origin 2018* software. Baseline corrections followed the procedure described by [25].

Experimental

The experiments were divided into two sets: firstly CFU counting on solid culture as reference (Fig. 1) and secondly monitoring bacterial growth on solid culture (SC) (Fig. 2a) as well as in liquid culture (LC) (Fig. 2b) using IMC. In the case of reference experiments, we performed CFU counting experiments to investigate the influence of the initial concentration of bacteria on the detection time (Fig. 1).

Fig. 1 Experimental set-up for visual inspection (CFU counting) of bacterial growth on solid medium

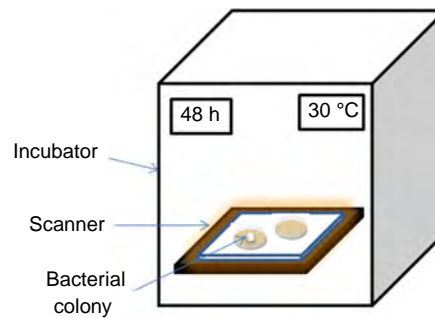
Medium: DSM-1

$V_{\text{medium}} \approx 25 \text{ mL}$

$T = 30 \text{ }^\circ\text{C}$

scan rate = 10 min

Visual inspection of CFUs by solid cultivation (SC)



Evaluation of obtained images by visual counting of colonies



initial concentration of bacteria, C_0

$c_0 = 10^5 - 10^1 \text{ CFU}\cdot\text{mL}^{-1}$

$v_i = 0.1 - 1 \text{ mL}$

CFU determination and CFU counting

Starting from a diluted pre-culture with an OD_{600} of approx. 0.2 a dilution series in 10-fold steps were prepared. To determine the initial concentration of bacteria c_0 in CFU mL^{-1} for each dilution, conventional CFU countings were conducted in parallel. Initial bacterial concentrations were ranging between 10^5 and 10^1 CFU mL^{-1} .

Common DSM-1 agar plates were inoculated with the abovementioned concentrations (including a sterile blank). As an exception, in one series of experiments, the same initial bacterial concentration (10^1 CFU mL^{-1}) but different inoculum volumes $V_i = 0.01, 0.1, 0.25, 0.5$ and 1 mL were used (result see S1 in Supporting Information, SI). After inoculation, the progress of colony formation was monitored at 10-min intervals using a scanner. The scanner was located in a temperature-controlled incubator (TH 30, Edmund Bühler GmbH, Bodelshause, Germany), at $30 \pm 1 \text{ }^\circ\text{C}$ (see Fig. 1). The resulting images were saved as jpg-files and subsequently evaluated. For this purpose, five independent observers inspected the obtained images. The detection time was defined as the time at which colonies were first discovered. The resulted detection time served as reference values for the IMC experiments and allowed us to compare CFU counting directly with IMC.

Microcalorimetric experiments

The IMC experiments on solid and in liquid medium (experimental set-up is shown in Fig. 2) were subdivided into three parts: The first part dealt with the initial number of bacteria N_0 (CFU in the ampoule). Here, the calorimetric ampoules were filled with 1 mL medium. In the case of SC and LC, 0.01 mL of each concentration (10^5 – 10^1 CFU mL^{-1} , including a sterile blank) were added to the medium for inoculation V_i (in mL). The initial number of bacteria N_0 results from the initial concentration c_0 and the inoculum volume V_i . The experiments were performed in triplicates. Further experiments were performed by membrane filtration (SC and LC, $n = 1$) as well as a range of higher inoculum volumes (LC, $n = 1$). In the former, the influence of the enrichment procedure was investigated and 10 mL of each concentration (10^5 – 10^1 CFU mL^{-1} , including a sterile blank) were membrane filtrated and subsequently purged with 2 mL sterile DSM-1 medium. Therefore, compatible sterile membrane filters (pore size $0.45 \text{ }\mu\text{m}$, cellulose nitrate, Sartorius AG, Göttingen, Germany) were prepared under sterile conditions using a punch (diameter 10 mm , Locheisen-Satz, BGS Technic KG, Wermelskirchen, Germany). The punched membrane filters were placed in specially made sealed adapters which were integrable into a 100-mL

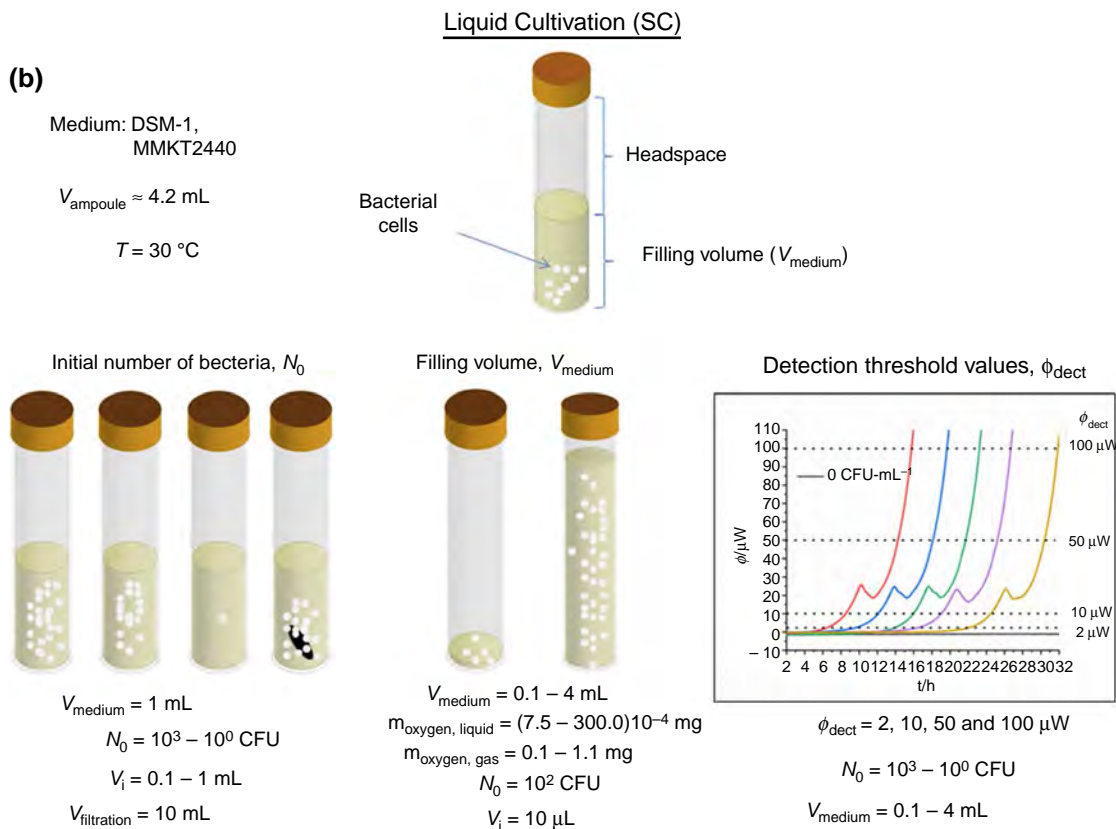
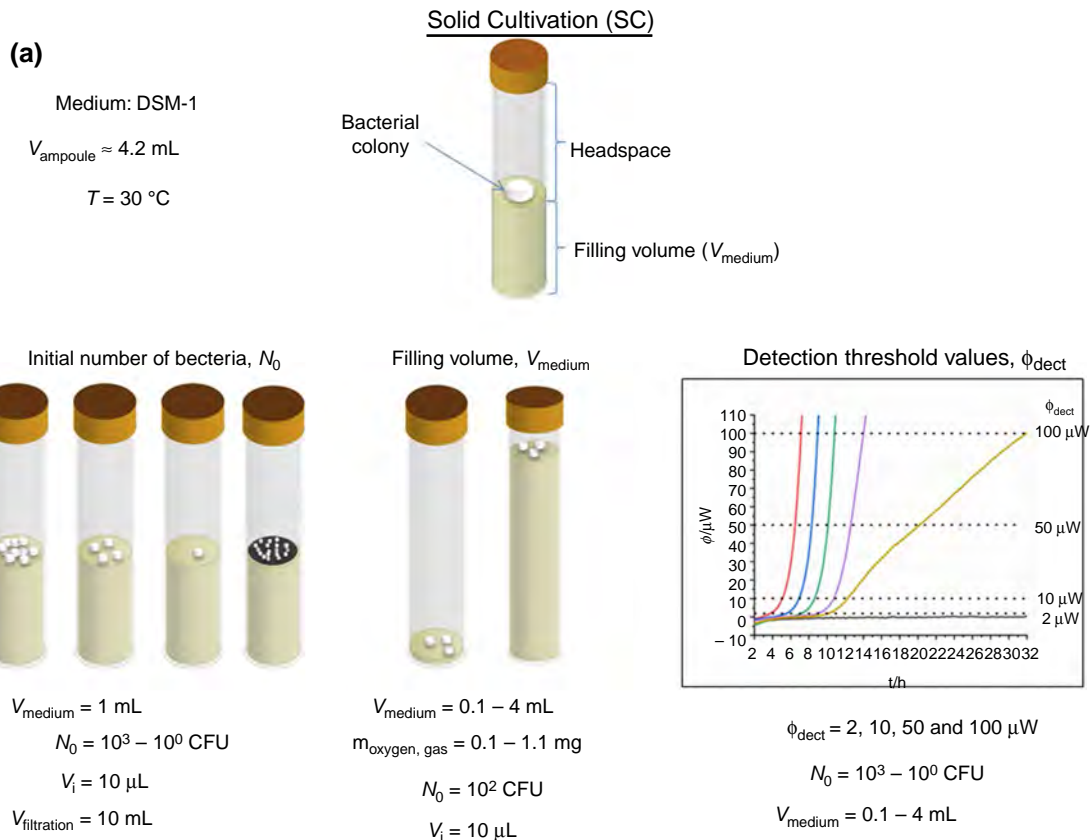


Fig. 2 Summary of the experimental set-up for IMC experiments to detect bacterial growth. **a** In solid (SC) and **b** in liquid cultivation (LC). Each of the two cultivations is subdivided into two separate experiments: an investigation of the heat flow measurements as a function of the initial number of bacteria N_0 (in CFU) as well as of the filling volume V_{medium} (in mL). Finally, the measured heat flows are evaluated by different detection threshold values Φ_{dect} (in μW)

glass filtration device (diameter 25 mm, Sartorius AG, Göttingen, Germany). Membrane filtration was performed under low pressure. Afterwards, the membrane filters were placed on top of the solid surface or submerged in the liquid medium using sterile tweezers.

Experiments with varying the inoculum volume V_i in LC were performed based on the lowest concentration ($c_0 = 10^1$ CFU mL⁻¹). Different volumes ($V_i = 0.01, 0.1, 0.25, 0.5$ and 1 mL) of this concentration (including a sterile blank) were added to 1 mL DSM-1 medium (results, see S1 in SI).

The second series of IMC experiments dealt with the filling volume V_{medium} of the calorimetric ampoules. Different filling volumes created different initial conditions concerning the amount of substrate and oxygen (see Fig. 2) so that we were able to investigate the influence on bacterial growth and consequently on the detection of the bacteria. Amounts of oxygen in headspace and liquid phase (see Fig. 2) were calculated based on a mass fraction of oxygen in the air atmosphere of 23.14% [27] and a concentration of dissolved oxygen in the liquid phase of 7.5 mg L⁻¹ [28] at 30 °C. An inoculum volume of 0.01 mL of the same concentration ($c_0 = 10^3$ CFU mL⁻¹ and including a sterile blank) was added to ampoules which were filled with different volumes of medium ($V_{\text{medium}} = 0.1, 0.5, 2, 3$ and 4 mL). In the 4.2-mL ampoules, a residual headspace was thus always present. To evaluate the practical value of the N_0 - and V_{medium} -dependent measured heat flows, they were regarded in the light of different detection threshold values ($\Phi_{\text{dect}} = 2, 10, 50$ and 100 μW).

The last series of experiments were performed in minimal medium (MMKT2440) instead of DMS-1 medium for calorimetric measurements (LC, $n = 2$). MMKT2440 consisted of (in g L⁻¹): (NH₄)₂SO₄ (0.5), Na₂HPO₄ (0.6), KH₂PO₄ (1.4), MgCl₂·H₂O (0.25), CaCl₂·H₂O (0.07) and glucose (0.5). Again, 1 mL of the medium and 0.01 mL of each concentration (10^5 – 10^1 CFU mL⁻¹, including a sterile blank) were added to 4.2 mL glass ampoules.

In total, we thus investigated how the initial number of bacteria N_0 , the filling volume of the calorimetric ampoules V_{medium} , the composition of the growth medium as well as detection threshold values Φ_{dect} influences the detection of bacterial growth in a 4.2 mL static ampoule system.

Results and discussion

Visual detection of colonies as a function of initial bacterial concentration

The proof of bacterial contaminations in microbiological analysis is still predominated by conventional cultivation mainly on solid culture media [29, 30]. As our study dealt with the detection time of aerobic bacterial growth using microcalorimetry, a reference value for the detection time of *P. putida* mt-2 KT2440 was determined by CFU counting by five independent observers (see for detailed results S4 in SI). The first appearance of colonies was defined as detection time, and results are shown in Fig. 3. The average CFU detection time of 13.3 ± 1.3 h was nearly independent of the initial concentration of bacteria, as expected. The subsequent detection times, determined by IMC experiments, are compared and related to this reference.

Factors influencing the detection time in IMC

In the following, we define the detection time t_{dect} as the time required from the insertion of the sample into the IMC instrument until the metabolically determining heat flow signal exceeds statistically significant the noise of the applied IMC. Manufacturers of IMCs specify a limit of detection (LOD), but in practice, however, a fixed value for the detectable heat flow Φ_{dect} (detection threshold value) of the respective instrument is typically defined empirically.

On this occasion, it is important to mention that our study aims at the earliest detection of bacterial growth; thus, our considerations are restricted to exponential growth at the beginning of the metabolically determining heat flow. In the following, we assume that the heat output of a growing culture starting from an initial cell number N_0 is determined by the specific growth rate μ (in h⁻¹) of an exponentially growing culture [26], and by a mean cell-specific heat production rate φ_0 (in W) [17, 21] (see both equations in Fig. 4). At this point, we have to differentiate between two scenarios: (1) at $t = 0$, the sample already contains so many bacteria that the actual metabolic heat production rate exceeds the detection threshold value $\Phi(t) \geq \Phi_{\text{dect}}$ or (2) at $t = 0$, the sample contains so few bacteria that the metabolic heat production is below the detection threshold value and heat can only be detected after exponential growth (if sufficient nutrients are available). The heat production rate will rise a detectable heat flow at time $t = t_{\text{dect}}$. Equation (1) relates the detection time t_{dect} (in h) and the detectable heat flow Φ_{dect} (in W).

$$t_{\text{dect}} = \frac{\ln\left(\frac{\Phi_{\text{dect}}}{\varphi_0}\right) - \ln(N_0)}{\mu} \quad (1)$$

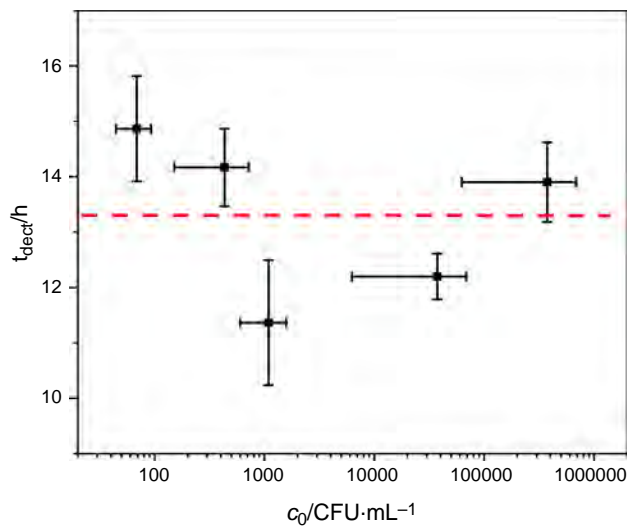


Fig. 3 Detection times t_{dect} as a function of the initial concentration of bacteria c_0 obtained. The red dash line represents the average CFU detection time. (Color figure online)

The meanings and derivation of the variables are given in Fig. 4.

In principle, preparative, technical and biological factors of influence on the detection time can be distinguished. These factors will be examined in the following.

Calorimetric detection time as a function of sample preparation and inoculum size

The initial number of bacteria N_0 (in CFU) can be influenced by sample preparation. Compared with classical CFU counting, where the inoculum size does not affect the time

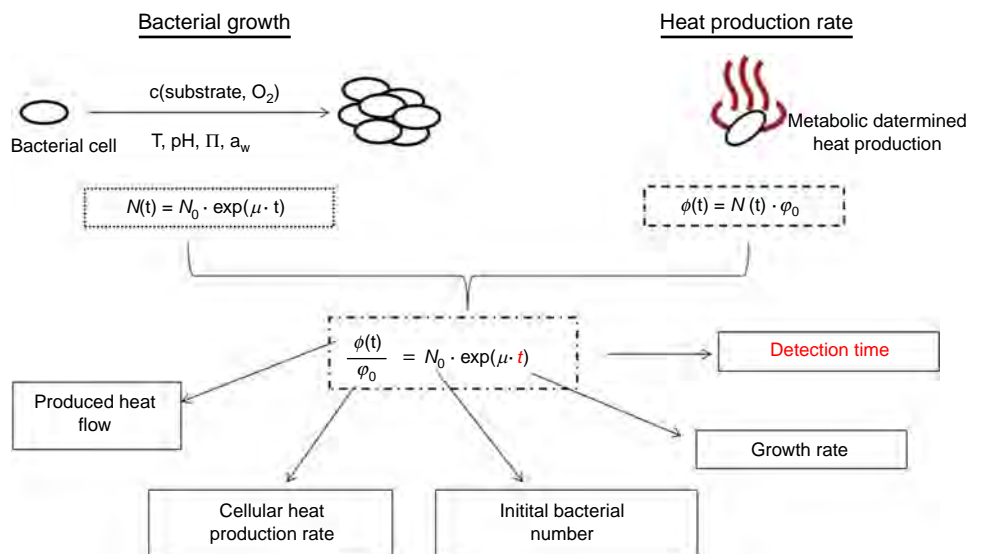
needed for detection of colonies (see Fig. 1 and S1 in SI), IMC detection depends on N_0 according to Eq. (1). Short detection times require high N_0 values which in principle can be achieved in two ways. First, the sample volume added for inoculation can be increased. However, this is generally restricted by the small size of common calorimetric vessels (typically in the range from 4 to 125 mL). In the case of LC, inoculum volumes of > 1 mL are applicable but for SC the upper limit even in large calorimetric vessels is approx. 1 mL because of their relatively small cross-sectional areas. Second, N_0 can be increased from a larger volume, for example by membrane filtration (MF). The reduction of IMC detection time by MF enrichment was recently shown with bacteria (i.e. *L. plantarum*) grown anaerobically in SC [25]. In principle, there are two common cultivation techniques (SC and LC) which will be investigated in the following.

Solid cultivation (SC)

The initial number of bacteria (N_0) dependency of heat flow measurements obtained on solid medium is shown in Fig. 5. All heat flow signals could be roughly divided into five stages: I. baseline, II. exponential (high N_0) or linear (low N_0) increase in heat flow, III. maximum heat flow, IV. decreasing heat flow and V. return to the baseline. All heat flow signals consisted of a single peak of varied shape. Heat flow signals were broader when N_0 was lower (Fig. 5a). Comparing these measurements with literature data revealed that other bacteria (*Lactobacillus plantarum* [25], *Mycobacterium* species [23] and *E. coli* [24]) displayed similar heat flow pattern on solid medium.

Shape and amplitude of the heat flow signals depend on the inocula size (i.e. initial number of bacteria). Larger N_0 consumed substrate and oxygen faster; thus, the bacteria

Fig. 4 Factors influencing the time needed to detect bacterial contaminations by IMC measurements



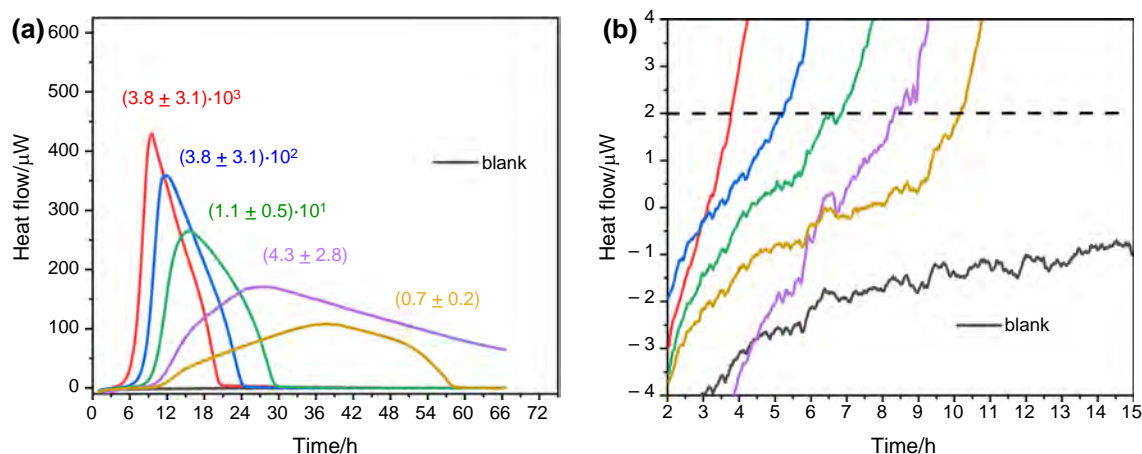


Fig. 5 IMC experiments performed on SC. The N_0 (mean \pm SD) in CFU are indicated next to the heat flow signals and based on the inoculum volume (10 μ L). **a** Dependency of heat traces on the N_0 . **b** Mag-

nification of heat flow signals near the detection zone, the dotted line representing the predefined detection threshold value of 2 μ W

reached early the maximum specific growth rate and consequently produced a larger heat flow (see Fig. 5a). This finally results in a sharper peak. Independent of N_0 , the average total amount of heat released was (12.0 ± 0.6) J. This value was confirmed by using the oxycaloric equivalent calculated for aerobic growth (see for details chapter S3.1 in SI). The total heat produced by oxygen-limited aerobic bacteria should thus be in the same range irrespective of species and inoculum size.

Following Eq. (1), the metabolically determining heat flow signals were detected earlier when the N_0 was higher (Fig. 5b). BRAISSANT and co-workers performed bacterial concentration-dependent IMC experiments with *Mycobacterium tuberculosis* and observed similar results [23]. For the determination of the detection time, a detection threshold value of 2 μ W was assumed for TAM III. This is 10 times higher than the instrument noise specified by the manufacturer (www.tainstrument.com). The resulting detection times are summarized in Table 1.

Liquid cultivation (LC)

The N_0 dependency of heat flows measured for LC are shown in Fig. 6. Here, six stages in all heat flow signals can be distinguished: (1) baseline, (2) a first exponential increase in heat flow, (3) a slight decrease (a phase being absent for SC), (4) a second exponential increase, (5) maximum in heat

flow and (6) return to baseline level (Fig. 6a). This heat flow pattern was also observed by BONKAT and co-workers for fast-growing mycobacteria *Mycobacterium smegmatis* and *Mycobacterium phlei* [31]. All heat flow signals had two peaks, a small initial one with a magnitude of approx. 25 μ W followed by a large one of approx. 500 μ W (500 mW L^{-1}). The first peak can be explained by the consumption of oxygen dissolved in liquid medium (approx. 23.4 μmol at 30 $^\circ\text{C}$) [28]. Using the oxycaloric equivalent ($-455 \text{ kJ mol}^{-1} \text{ O}_2$) [32], this corresponds to a heat production of approx. 0.1 J. This value was confirmed by integrating the heat flow curve up to the maximum of the first peak (see chapter S3.2 in SI).

The second peak might reflect dynamics of substrate or oxygen depletion. Unlike, the different times of onset, the form of the heat flow signals was independent of N_0 variation making LC more promising for the detection of low N_0 than SC. The different growth behaviour of the bacteria LC versus SC determines the shape of the heat flow signal. A bacterial colony relies on substrate (or oxygen) diffusing towards the substratum-colony interface, whereas in LC, bacteria are surrounded by dissolved substrate and oxygen, though provision with oxygen may be limited by diffusion from the headspace.

As expected from Eq. (1), the onset of heat flow signals depended on N_0 (Fig. 6b). The detection time was determined in the same way as for SC and is given in Table 1. Interestingly, cultivation in liquid or on solid medium (using

Table 1 Summary of the detection times (mean \pm SD) determined at a detection threshold value of 2 μ W

Growth condition	t_{dect}/h 3.8×10^3 CFU	t_{dect}/h 3.8×10^2 CFU	t_{dect}/h 1.1×10^1 CFU	t_{dect}/h 4.3 CFU	t_{dect}/h 0.7 CFU
SC	(3.9 ± 0.1)	(5.4 ± 0.2)	(7.2 ± 0.3)	(8.7 ± 0.3)	(10.5 ± 0.4)
LC	(3.9 ± 0.1)	(5.6 ± 0.1)	(7.8 ± 0.1)	(9.4 ± 0.2)	(11.1 ± 0.6)

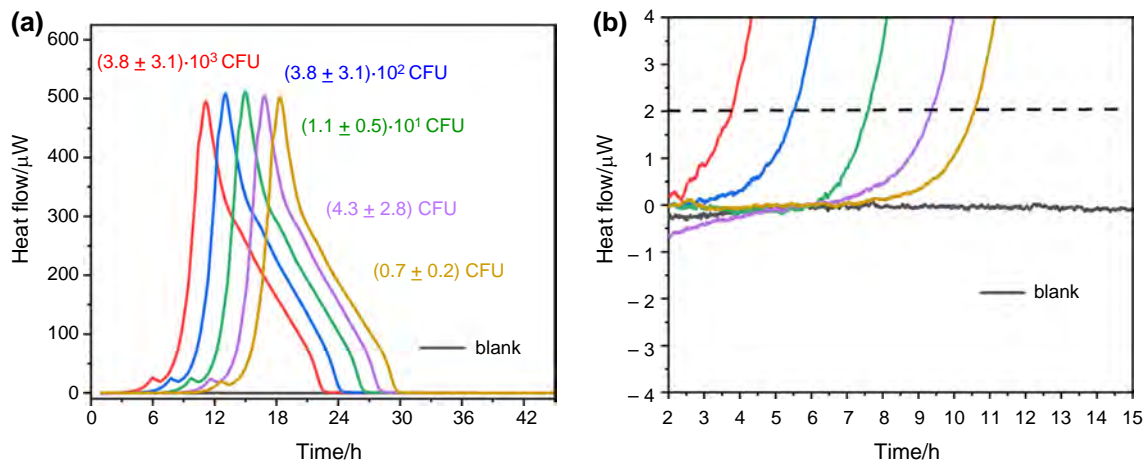


Fig. 6 IMC experiments performed in LC. The N_0 (mean \pm SD) in CFU are indicated next to the heat flow signals and based on the inoculum volume (10 μL). **a** Dependency of heat traces on the N_0 . **b** Mag-

nification of heat flow signals near the detection zone, the dotted line representing the predefined detection threshold value of 2 μW

the same inoculum volume of 10 μL) did not influence the detection time much at the predefined detection threshold value of 2 μW . For such a low heat flow, the provision of substrates and oxygen does not limit the growth. However, to achieve the earliest possible detection time, LC offers the major advantage that the inoculum volume can easily adapt to the overall volume of the calorimetric vessel.

Based on the CFU detection time determined by visual inspection (13.3 ± 1.3 h) of bacterial growth on solid medium, we could show with our results that a faster detection by IMC is possible. High N_0 ($(3.8 \pm 3.1) \times 10^3$ CFU) were detectable after 3.9 h for both on solid as well as in liquid medium and low N_0 (0.7 ± 0.2 CFU) after 10.6 h for solid medium and 11.1 h for liquid medium (considering a detection threshold value of 2 μW). Furthermore, if one compares the error of the detection times, it became apparent that calorimetric detections have a smaller error independent of N_0 . This difference can be attributed to the subjective evaluation of colony detection in the case of visual inspection. Similar conclusions were drawn during the visual inspection of pharmaceutical products utilizing sterility testing [16]. A summary of all N_0 -dependent heat flow signals measured on SC and LC is given in chapter S5 in the SI.

Enrichment via membrane filtration (MF)

One possibility to increase N_0 and to shorten detection is the enrichment from a larger sample volume using membrane filtration (MF). Depending on the background of the analysed sample, N_0 can range from a few bacteria cells (e.g. drinking water) to more than 10^6 (e.g. foodstuff) per mL sample volume [33]. Using the MF process thus larger sample volumes (e.g. 10 mL instead of 0.01 mL) could be subjected to calorimetric measurements. Figure 7

compares the heat flow signals with and without MF for SC and LC (taken from Figs. 5a, 6a).

Considering the enrichment factor of 1000, the obtained heat flow signals showed two substantial changes. Firstly, an increase in N_0 led to a reduction in detection time (Fig. 7b, d) independently of the detection threshold value (10, 50 μW). The highest N_0 (solid red curve) corresponded probably to an N_0 of approx. 10^6 (assumption based on the enrichment factor of 1000 and an initial number of approx. 10^3 bacteria in 0.01 mL inoculum volume) in the filter produced an initial heat flow of 25 μW . These results are very consistent with literature assumptions that 10.000 to 100.000 active bacteria are necessary to produce a heat flow above the limit of thermal detection ($\text{LOD} = 0.2$ μW for the TAM III, www.tainstruments.com) [34]. Secondly, the shape of the heat flow signals varied strongly between SC (Fig. 7a) and LC (Fig. 7c). Interestingly, the shape of the heat flow signals obtained on SC with (solid curves) and without (dash curves) MF varied especially for the lowest N_0 (yellow curves). In theory, the heat flow curves with the highest N_0 (red and blue dashed curves) contain the same number of bacteria as the two curves with the lowest N_0 (violet and yellow solid curves) due to MF. Consequently, curves should coincide. However, there is some small variation. Small inaccuracies in the placement of the filter on the agar surface and the consequence that not all bacteria have same access to the solid medium could be the cause. In the case of LC, the two heat flow signals with the same N_0 (red and blue dash curves, and violet and yellow solid curves, Fig. 7d) overlapped. This may indicate that the bacteria were able to detach themselves from the filter surface and access the substrates and oxygen via free movement in liquid phase. The increase in turbidity after the measurement confirmed this assumption.

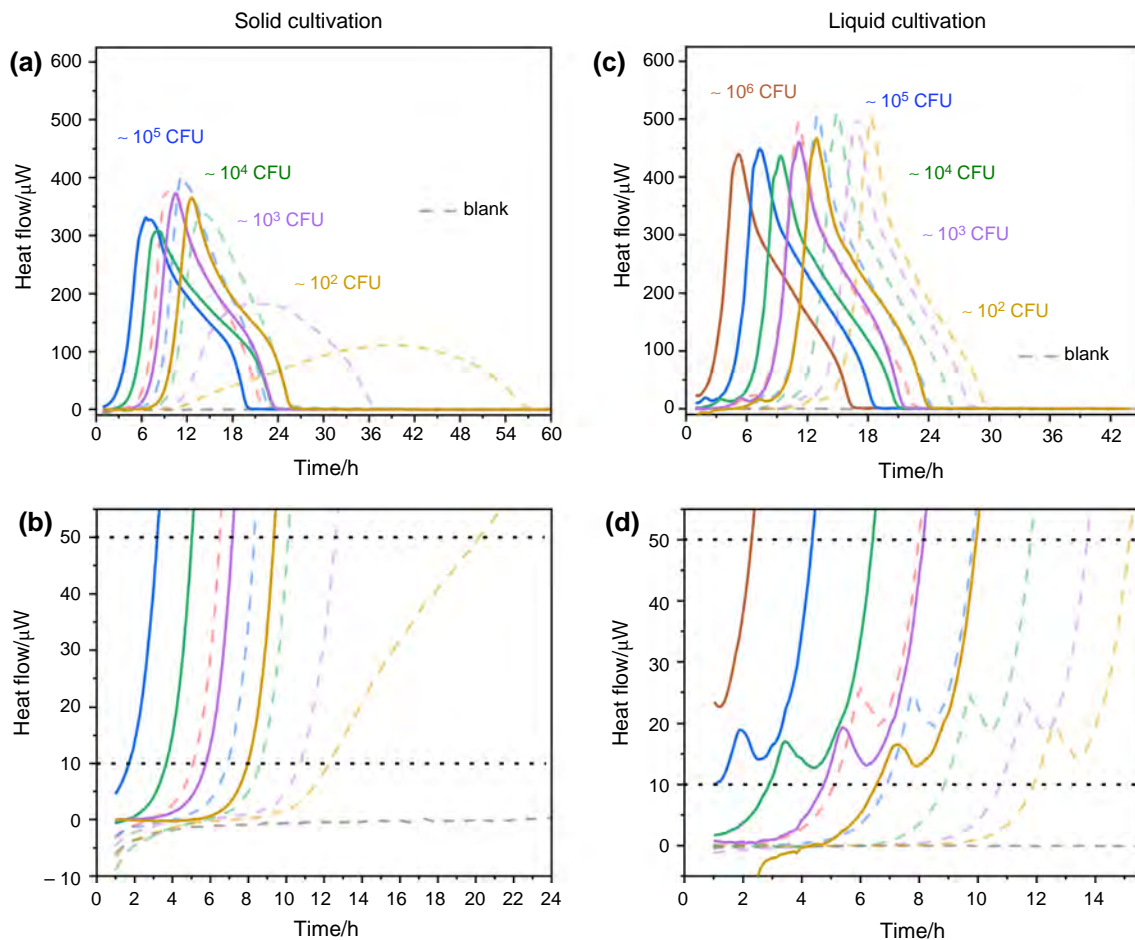


Fig. 7 IMC experiments performed after enrichment by MF. **a** Comparison of heat flow signals on SC with MF (solid curves) and without MF (dashed curves, approximated N_0 in CFU are indicated next to the heat flow signals and based on the filtration volume, 10 mL). **b** Magnification of the heat flow signals (SC) near the detection thresh-

old values 10 and 50 μW . **c** Comparison of heat flow signals in LC with MF (solid curves) and without MF (dashed curves). **d** Magnification of the heat flow signals (LC) near the detection threshold values 10 and 50 μW

It is important to mention here that membrane filtration is accompanied by a certain sample preparation time, and this should be taken into account for detection. However, there is also an argument for membrane filtration. For slowly growing bacteria, the time gained through enrichment can compensate for the loss through sample preparation time.

Influence of IMC performance on the detection time

Influences of technical specifications

The detectable heat flow $\Phi_{\text{dect}}(t)$ is mainly determined by the accuracy (lowest resolution in temperature difference which can still convert into voltage) of the detector, a thermoelectric generator (TEG), and the temperature constancy in the entire system. The TEG consists of several serially connected thermocouples. The most common microcalorimeters used to investigate cellular systems are based on

the principle of heat conduction and work in isothermal operation mode [8]. The aim is to ensure that as much of the metabolic heat as possible flows through the detector (TEG). Mathematically, this can be expressed as follows [35]:

$$\Phi(t) = \kappa \cdot n_{\text{TEG}} \cdot \Delta T \quad (2)$$

where κ (in W K^{-1}) is the thermal conductivity of a thermocouple, n_{TEG} the number of thermocouples and ΔT (in K) the temperature difference between the upper and lower surface of the TEG. The voltage $U(t)$ generated at the TEG can be described by Eq. (3) [35]:

$$U(t) = \alpha \cdot n_{\text{TEG}} \cdot \Delta T \quad (3)$$

where α (in V K^{-1}) is the Seebeck coefficient of the thermocouples. According to the difference in temperature between the upper surface (increase in temperature due to metabolic heat caused by bacteria) and the lower surface (constant

temperature of the heat sink given by the system), a voltage is generated (Seebeck effect). In other words, the heat conducted via the TEG $\Phi(t)$ is proportional to the measured voltage $U(t)$ (Eq. 4) [36]:

$$\Phi(t) = \varepsilon \cdot U(t) \quad (4)$$

The proportionality factor ε (in W V^{-1}), also referred to as the calibration constant, is composed as follows:

$$\varepsilon = \frac{\kappa}{\alpha} \quad (5)$$

Since these are two material constants, there are possibilities to influence this quotient and to keep the value of ε as small as possible. A low specific thermal conductivity and a large Seebeck coefficient are aimed for [37].

As already mentioned, the bottom side of the TEG is kept constant by a temperature-controlled heat sink. Due to the small temperature increase caused by the metabolic heat of the growing bacterial cultures [9], already small temperature fluctuations on the heat sink of the instruments can have a direct effect on the performance of the IMC measurement. As a result of such fluctuations, noise or drifts may superpose the metabolic heat flow signals and a delayed detection time would be determined.

Interestingly, most applications on bacteria detection by IMC in literature were performed in 4 mL static ampoules using high-performance microcalorimeters (low detection thresholds are applicable) [15, 19, 22, 23, 31]. In calorimeters with a high detection threshold, this deficit is typically compensated by large sample volumes containing more heat-producing bacteria [38]. However, due to the larger sample volume, only a few simultaneous measurements are possible. For the practitioner, however, in addition to short detection times and simple calorimeters, the number of simultaneous measurement possibilities is also decisive. Thus, it is a big difference to measure up to 48 samples in

a high-performance calorimeter or up to 12 samples using a simple calorimeter having the same volume-related limit of detection or to measure up to 48 samples in a simple calorimeter with a lower limit of detection as long as the bacterial contamination is detected early enough. To address these issues, we simulated the effect of calorimeter detection thresholds as well as the sample volumes on the detection time directly, assuming different empirical threshold values ($\Phi_{\text{dect}} = 2, 10, 50$ and $100 \mu\text{W}$) in the context of a static 4-mL ampoule system. These assumptions are supported by manufacturer information and literature data and selected to cover almost all commercially available IMC devices used for biocalorimetry (see Table 2).

Influence of the initial number of bacteria on the detectable heat flow

To relate detectable heat flows to common microcalorimeters (see Table 2), detection threshold values (2, 5, 10, 50 and $100 \mu\text{W}$) were used to establish detection times for LC and SC in conventional static 4-mL glass ampoules. Figure 8 summarizes the results. For the sake of simplicity, only the results obtained with the highest (red curves) and the lowest N_0 (yellow curves) are discussed.

Two cases will be considered: first, the difference between high and low N_0 at different detection threshold values and different cultivation modes (LC vs. SC) and second, the influence of different detection threshold values at constant N_0 .

The difference in the detection time between highest (red curve) and lowest (yellow) N_0 was independent of the detection threshold for LC (approx. 7 h). For SC, the same delay was observed at detection thresholds $\leq 10 \mu\text{W}$ (Fig. 8a). Whereas the difference in detection times at a threshold value of $50 \mu\text{W}$ was already twice as long (approx. 13 h) and at $100 \mu\text{W}$ almost four times as long (approx. 26 h).

Table 2 Typical detection threshold values for IMC instruments used in biocalorimetry

Calorimeter	Manufacturer	Empirical threshold/ μW	Filling volume of ampoule/mL	Volume-specific threshold ^a / mW L^{-1}	References
TAM 48	TA instruments	2	n.a.	–	[23]
TAM III		10, 2	3, 0.2	3, 10	[19, 25]
TAM air		25	7 - 5	4 - 5	[38]
MC-Cal/100 P	C3 Prozess- und Analysentechnik GmbH	100 ^b , 28 ^c	1 ^b , 0.4 ^c	100 ^b , 70 ^c	[39]
BioCal 2000	Calimetrix Inc.	100	n.a.	–	www.calimetrix.com
calScreener	Symcel AB	1	0.3	3	[40]

n.a. not available

^aCalculated by using the filling volume of the ampoules

^bDetermined in our study

^cCalculated from the available data

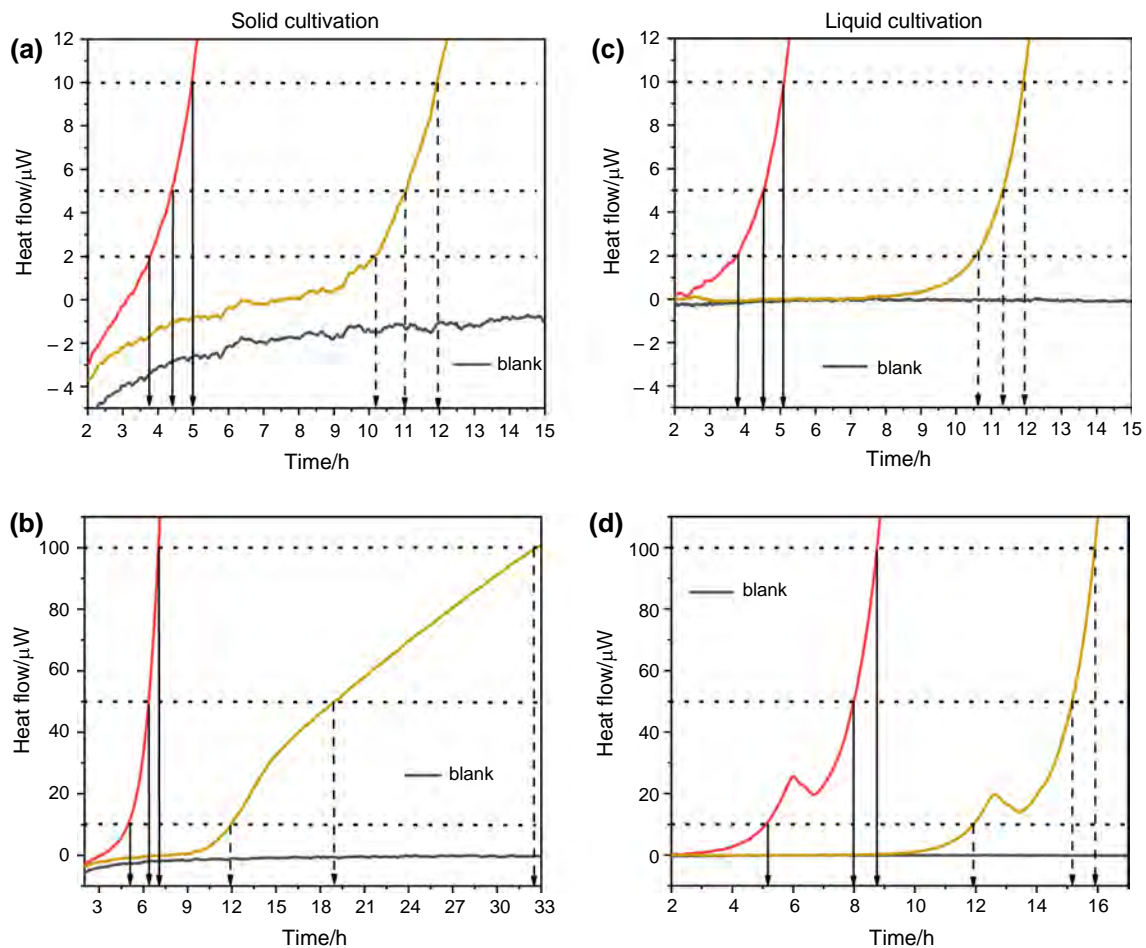


Fig. 8 Influence of simulated detection thresholds on detection times achieved in IMC experiments depending on N_0 in solid (a, b) as well as in liquid (c, d) medium. Red: $(3.8 \pm 3.1) \cdot 10^3$ CFU. Yellow: (0.7 ± 0.2) CFU. **a** Magnification of the heat flow signals measured in SC near detection threshold value, the dotted lines representing Φ_{dect}

of 2, 5 and 10 μW . **b** Heat flow signals measured in SC near Φ_{dect} of 10, 50 and 100 μW . **c** Magnification of the heat flow signals measured in LC near detection threshold value, the dotted lines representing Φ_{dect} of 2, 5 and 10 μW . **d** Heat flow signals measured in LC near Φ_{dect} of 10, 50 and 100 μW . (Color figure online)

Considering now a constant N_0 , the heat flow signals showed that, regardless of the cultivation mode (solid or liquid), the detection time between high-performance microcalorimeters (threshold values of 2 to 10 μW) varied by roughly 2 h following Eq. (1) (Fig. 8a, c). The exponential increase in the heat flow confirms the assumption of exponential growth. At high N_0 (red curve), the delay in detection with 100 μW versus 2 μW was 3 h with SC (Fig. 8a, c) and was 5 h with LC (Fig. 8c, d). The difference in detection time of 2 h between LC and SC might be caused by the influence of oxygen diffusion on the metabolic response of *P. putida* mt-KT2440 [41]. The growth process slows down under conditions influenced by diffusion. Simulations [42] point to the special role of oxygen diffusion in static, closed ampoules.

At low N_0 (yellow curve), the delay in detection with threshold values of 100 μW versus 2 μW increased by 22 h with SC (Fig. 8a, b) and by 5 h with LC (Fig. 8c, d). The

difference in LC has already been discussed. However, a completely different picture is obtained at low N_0 in the case of SC. The difference in detection time of 22 h was caused by a change from exponential to substrate diffusion-limited linear growth at about 30 μW (or after 14 h). This growth behaviour is characteristic for the formation of bacterial colonies on solid substrate [43, 44]. This effect was also reflected in the size of the colonies formed (see for details SI).

Finally, to confirm the detection times simulated here, we used a less powerful cement calorimeter (LOD of 20 μW for the MC-Cal/100 P, <https://www.c3-analysentechnik.de>) to perform the same N_0 -dependent measurements in LC ($n=2$) under the same conditions as described in Fig. 2b. The detection times are summarized in Table 3, and the corresponding heat flow signals are given in chapter S6 in the SI.

If we now compare the detection times in Table 3 (detection threshold 100 μW) with the CFU detection time

Table 3 Comparison of detection times determined with two different calorimeters at a detection threshold value of 100 μ W

Calorimeter	t_{dect}/h 3.8×10^3 CFU	t_{dect}/h 3.8×10^2 CFU	t_{dect}/h 1.1×10^1 CFU	t_{dect}/h 4.3 CFU	t_{dect}/h 0.7 CFU
TAM III ^a	$(8.8 \pm 0.1)^c$	(10.7 ± 0.1)	(12.6 ± 0.1)	(14.5 ± 0.1)	(16.1 ± 0.5)
MC-Cal/100 P ^b	9.1	11.6	13.5	15.4	16.4
	8.9	11.8	13.7	15.8	n.d.

n.d. not detected

^aSimulated detection times at a threshold value of 100 μ W

^bOnly measured in duplicates

^cMean \pm SD

(13.3 ± 1.3) determined by visual inspection, it must be concluded that if only less than ten bacteria cells are presented at the beginning of the measurement, visual inspection might be slightly faster. However, the time needed to form all countable colonies on a plate that are visible for the naked eye is mostly higher.

Influence of the filling volume of medium on the detectable heat flow

To investigate the influence of oxygen and substrate on the detection time being a function of the detectable heat flow, IMC experiments were performed with different filling volumes of liquid and solid medium (V_{medium}) in the calorimetric ampoules. The change in V_{medium} resulted in different amounts of oxygen and substrate, which are available to the bacteria for growth. Due to the close relation between bacterial growth and metabolic heat according to Eq. (1), we expect an influence on detection time, especially in LC. Here, the metabolic response of the bacteria to oxygen-limiting conditions should be more noticeable. But first, we examine the heat flow signals recorded at different V_{medium}

on solid medium (Fig. 9). Both factors, substrate and oxygen quantity, influenced the growth of bacteria on solid medium. At low filling volumes ($V_{\text{medium}} = 0.1$ mL), the bottom of the ampoule was not completely and evenly covered by the medium as well as by V_i ; hence, the shape of the heat flow curve (red curve, Fig. 9a) differed in comparison to the other.

If one compares only the increase of the heat flow curves in Fig. 9a considering detection threshold values, all heat flows show exponential shape (except for the red curve). Depending on the total amount of oxygen (determined by V_{medium}), the maximum heat flow varied and reached at $V_{\text{medium}} = 0.5$ mL (blue curve) a maximum value of 575 μ W (1150 mW L^{-1}). Detection times were the same for different V_{medium} regarding constant threshold value (Fig. 9b). However, decreasing performance of the instrument caused later detection, regardless of V_{medium} (Fig. 9b). The difference in detection time at threshold values of 2 and 100 μ W was approx. 4 h and almost independently of the respective V_{medium} .

The shape of heat flows obtained from V_{medium} -dependent experiments in LC (Fig. 10) showed a stronger variation compared with those obtained from SC. To describe the

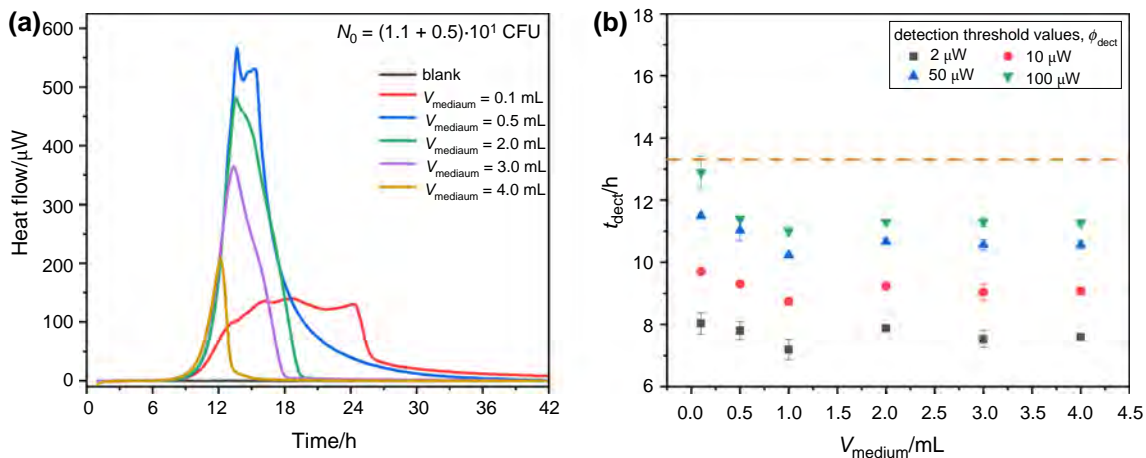


Fig. 9 Influence of V_{medium} on the heat flow signals obtained from IMC experiments conducted on solid medium. **a** Heat flow traces depending on V_{medium} . **b** Relationship between detection time and

V_{medium} as a function of different detection threshold values $\Phi_{\text{dect}} = 2, 10, 50$ and 100μ W. For comparison, the dashed line in B indicates the mean CFU detection time determined by visual inspection

shape of the heat flow curves, we have to distinguish between dissolved oxygen in the liquid phase which is immediately available to the bacteria, and oxygen in the gas phase which is only available to the bacteria through slow transport from gas phase into liquid phase and thus with delay [42]. The initial ratio between dissolved and unsolved oxygen was determined by V_{medium} of the liquid. Besides, a higher V_{medium} , as mentioned before, led to an overall decrease in the total amount of oxygen in the calorimetric ampoule (minimum and maximum oxygen quantities are shown in Fig. 2b). The lowest filling volume ($V_{\text{medium}} = 0.1$ mL) showed a slightly different heat flow signal (Fig. 10a, red curve) compared to the others. Possibly the interplay between substrate and oxygen limitation changed the metabolic response of the bacteria, thus causing a diffuse heat flow signal was obtained (Fig. 10a, red curve). Detection times were the same for different V_{medium} at threshold values of 2 and 10 μW (black and red points, Fig. 10b). Additionally, average detection times were in the same magnitude 7.5 h at 2 μW and 9.5 h at 10 μW for both SC and LC (Figs. 9b, 10b). The reason for this was that at time of these detectable heat flows sufficient oxygen and substrate were available to the bacteria. This corresponds to our assumption of a constant cell-specific heat production rate.

However, instruments with a worse threshold value (> 10 μW) led to later detection but unlike SC, a V_{medium} -dependent behaviour was observed (Fig. 10b). At a detection threshold value of 100 μW (green points, Fig. 10b), an almost linear relationship between the detection time and V_{medium} was observed. An assumption for this might be the extended diffusion path (caused by an increase in V_{medium}) for oxygen which diffused by transport from gas phase into liquid phase and the bacteria freely moving in medium. This would also explain the shift of the second peak depending on

V_{medium} (see Fig. 10a). However, the maximum of the second peak was determined by oxygen transferred from the headspace. Another exception was found at a threshold value of 50 μW (blue points, Fig. 10b). For low V_{medium} , the detection time followed the linear trend from the previous observation. However, the detection time decreased at a V_{medium} of 3 mL and dropped to a value of approx. 10.5 h at a V_{medium} of 4.0 mL (Fig. 10b). When using 3 or 4 mL instead of 2 mL filling volume, the dissolved amount of oxygen was so large that the initial peak reached a detectable heat flow of more than 50 μW . The large error bars in the case of the measurement point at 3 mL (Fig. 10b) are since only in one of three measurements a heat flow of the initial peak exceeded 50 μW and was therefore detectable. The detection of the other two curves only occurred at the second peak (temporally delayed, see explanation above) which then exceeded 50 μW . A summary of all V_{medium} -dependent heat flow signals measured on SC and LC is given in chapter S7 in the SI. As our data showed, for aerobic bacteria to be detected in LC it is important to know how much dissolved oxygen is needed to produce a detectable heat flow. This value can be estimated by using the following eq:

$$\Phi_{\text{dect}} < \mu \cdot c_{\text{O}_2} \cdot \Delta_k H_{\text{O}_2} + N_0 \cdot \varphi_0 \quad (6)$$

where c_{O_2} and $\Delta_k H_{\text{O}_2}$ are the amount of dissolved oxygen in the aqueous medium and the oxycaloric equivalent (-455 kJ mol $^{-1}$ O $_2$) [32], respectively. The derivation of Eq. (6) is given in chapter S8 of the SI.

Influencing biological heat production

Cell-specific heat production rate φ_0 and specific growth rate μ are characteristic of the respective bacterial strain.

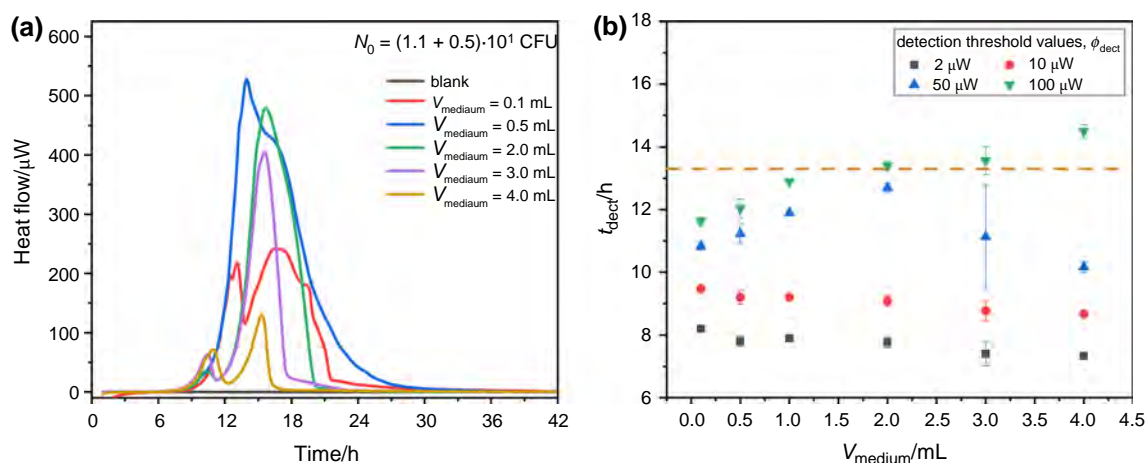


Fig. 10 Influence of V_{medium} on the heat flow signals obtained from IMC experiments conducted in liquid medium. **a** Heat flow traces depending on V_{medium} . **b** Relationship between the detection time and

V_{medium} as a function of different detection threshold values $\Phi_{\text{dect}} = 2, 10, 50$ and 100 μW . For comparison, the dashed line in **b** indicates the mean CFU detection time determined by visual inspection

High values of both favour early calorimetric detection. The growth rate likewise favours conventional visual detection and is affected by environmental conditions like temperature, pH, salinity or substrate availability [45–47]. All of these factors can be adjusted to achieve optimal growth. It is worth mentioning here that IMC can be advantageous for screening of optimal growth conditions [48], as all the factors mentioned influence the metabolism of the bacterial cell which is strongly correlated with the heat released [49].

A simple method to achieve fast growth is the use of complex media (e.g. lysogeny broth LB or trypticase soy broth TSB) [50]. These media contain important building blocks and provide all necessary components such as amino acids, carbohydrates and vitamins etc. [51] for the biosynthesis (anabolism) [52]. Thus, the build-up of bacterial biomass can take place faster and more energy efficiently than by synthesis from one or a small set of substrate molecules. To demonstrate this difference in terms of detection, we performed another IMC experiment in LC by using a minimal medium (MMKT2440) instead of DMS-1 medium. Everything else remained the same as described in Fig. 2b. For comparison, Fig. 11 shows the heat flow signals of bacterial growth in minimal medium as well as in DMS-1 medium (taken from Fig. 6a). For details, the corresponding heat flow signals measured in MMKT2440 are shown in chapter S9 in the SI.

A comparison of the heat flow signals showed that bacterial growth can be easily stimulated by a selective choice of the medium composition. Consequently, it is beneficial for the practitioner if metabolic processes of the desired target microorganisms are known and thus the detection time might be reduced via the medium composition. Complementary to this, it should be emphasized that this consideration also applies to temperature and pH as demonstrated by KATARAO et al. using the example of *E. coli* [49].

The cell-specific heat production rate is poorly investigated since metabolic processes of bacteria involve heat flows in the picowatt range. The mean cell-specific heat production rate is used, but this was only determined for a few bacteria under different growth conditions (e.g. aerobic, anaerobic, exponentially growing, resting) [4, 53–55]. Any possibility to increase the cellular heat with, e.g. selective substrates or reagents would favour an IMC detection of bacterial contaminations as they would allow earlier, more sensitive and more selective detection. The kind of metabolism might also play a key role since respiratory growth often releases more heat than fermentative growth [42]. One would thus cultivate facultative anaerobes under oxic conditions to increase the mean cell-specific heat production rate. For instance, the cell-specific heat production rate for *E. coli* is 0.8 pW/cell during aerobic growth as opposed to 0.2 pW/cell during anaerobic growth [17].

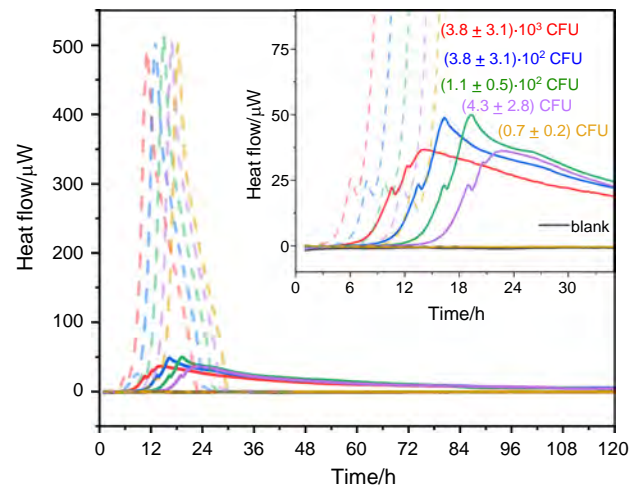


Fig. 11 Influence of the medium composition on the heat flow signals obtained by using complex medium (DSM-1, dashed lines) and chemical defined minimal medium (MMKT2440, solid lines). The insert provides a magnification of the heat flow signals. The N_0 (mean \pm SD) in CFU are indicated next to the heat flow signals and based on the inoculum volume (10 μ L)

Conclusions

Our study analysed the three factors determining the detection time in microcalorimetric measurements of aerobic bacterial contaminations in 4-mL static ampoules: (1) the initial number of bacteria (N_0), (2) the performance of the applied isothermal microcalorimeter (IMC) and (3) the provision of substrate and oxygen in the solid- or liquid-based cultivation set-up. This study used the aerobically growing *P. putida* mt-2 KT2440 as an example and complements an analogous study conducted with an anaerobic system [25]. This is important because numerous pathogenic or other bacterial contaminants grow aerobically.

The current trend in the field of IMC detection of bacterial contaminations is that, on the one hand, less powerful calorimeters (applicable detection thresholds $> 10 \mu$ W) use large sample vessels (up to 125 mL sample volume) but have only a few measuring channels. On the other hand, powerful calorimeters (applicable detection thresholds $< 10 \mu$ W) are used which have small sample vessels and allow up to 48 simultaneous measurements. Our results, together with the applications already known from the literature, e.g. *E. coli* produced a max. heat flow of 100 μ W (33 mW L^{-1}) in the concentration range of 10^5 to $10^0 \text{ CFU} \cdot \text{mL}^{-1}$ [56] or approx. 650 μ W (217 mW L^{-1}) in the concentration range of 10^5 to 10^0 CFU mL^{-1} [19] (depending on the cultivation conditions, for details see the respective reference), *Staphylococcus aureus* produced a max. heat flow of 100 to 350 μ W (33 to 117 mW L^{-1}) depending on the concentration (10^5 to 10^0 CFU mL^{-1}) [19] and *Legionella pneumophila* produced a max. heat flow of 175 μ W (58 mW L^{-1}) in the

concentration range of 10^5 to 10^2 CFU mL⁻¹ [57], show that it might be possible to develop a simple calorimeter that is less powerful (high detection threshold), uses small sample vessels (4–5 mL) and has a sufficient number of channels. The detection of metabolically induced heat flows in the range of 50–100 μ W and the use of 4-mL ampoules might be sufficient for most applications. Due to the exponential growth behaviour of the bacteria, the detection delay is only a few hours compared to powerful but also very expensive IMCs. We were also able to show that an increase in the initial number of bacteria can be a feasible solution. As an extension, especially for low contaminations or if larger sample volumes are investigated which would not be appropriate for 4-mL ampoules, membrane filtration would be a reasonable option. Additionally, if membranes with selectively antimicrobial surfaces or pore sizes [58] would be used, calorimetric detection could even be combined with the reduction of the influence of a potential accompanying bacterial flora. This should be the subject of follow-up research because bacterial contaminations are sometimes caused by bacterial communities and not only by single strains. However, there are already some potentially alternative enrichment methods such as biomagnetic separation (BMS) which has been successfully applied in the rapid detection of *E. coli* [59].

We were able to show that even less powerful calorimeters which only recognize a detectable heat flow of 50 μ W and more, can show comparatively early detection despite oxygen diffusion problems in the case of liquid cultivation (LC). However, very low N_0 on solid cultivation (SC) were critical, since our experiments have shown that if only a few colonies grow on the solid medium, a transition between exponential and linear heat flow can be observed. This behaviour is due to substrate diffusion-limited linear growth of colonies. Cultivation on solid substrate can be considered as a useful alternative, especially for microorganisms that grow better or only on solid medium. In the case of strictly aerobic growing bacteria, SC offers better access to oxygen [23]. Furthermore, larger V_i might be also applicable in SC by increasing the cross-sectional area of calorimetric vessels.

Finally, it should be noted that a deeper understanding in biological characteristics like stimulating specific growth rate μ through medium composition, temperature or pH as well as the cell-specific heat production rate φ_0 which is still comparatively little investigated, bears an enormous potential to further reduce detection times. Concerning φ_0 , one possibility could be the action of targeted substrates to stimulate the metabolic response of the microorganisms to yield a greater cell-specific heat production rate.

Acknowledgements Open Access funding provided by Projekt DEAL. The authors acknowledge M. Kolbe (UFZ, Department of Environmental Microbiology) and K. Lübke (UFZ, Department of Environmental

Microbiology) for preparing the media and N. Ghanem, T. Mainka, S. Paufler, C. Heber, A. Krämer and M. Reichard (UFZ Department of Environmental Microbiology) for technical support.

Funding This work was funded by the German Federation of Industrial Research Associations (AiF BMWi, AiF-Nr. ZF4315807RH7).

Compliance with ethical standards

Conflict of interest The authors declare that the research was conducted in the absence of any commercial or financial relationships that could be construed as a potential conflict of interest.

Open Access This article is licensed under a Creative Commons Attribution 4.0 International License, which permits use, sharing, adaptation, distribution and reproduction in any medium or format, as long as you give appropriate credit to the original author(s) and the source, provide a link to the Creative Commons licence, and indicate if changes were made. The images or other third party material in this article are included in the article's Creative Commons licence, unless indicated otherwise in a credit line to the material. If material is not included in the article's Creative Commons licence and your intended use is not permitted by statutory regulation or exceeds the permitted use, you will need to obtain permission directly from the copyright holder. To view a copy of this licence, visit <http://creativecommons.org/licenses/by/4.0/>.

References

1. Wadsö I, Goldberg RN. Standards in isothermal microcalorimetry (IUPAC Technical Report). *Pure Appl Chem.* 2001;73:1625–39.
2. Gustafsson L. Microbiological calorimetry. *Thermochim Acta.* 1991;193:145–71.
3. Ladbury JE, Chowdhry BZ. Sensing the heat: the application of isothermal titration calorimetry to thermodynamic studies of biomolecular interactions. *Chem Biol.* 1996;3:791–801.
4. Kemp RB. An historical review of developments in cellular microcalorimetry. *Pure Appl Chem.* 1993;65:1875–80.
5. Wadsö L, Gómez GF. Isothermal calorimetry for biological applications in food science and technology. *Food Control.* 2009;20(10):956–61.
6. Bruylants G, Wouters J, Michaux C. Differential scanning calorimetry in life science: thermodynamics, stability, molecular recognition and application in drug design. *Curr Med Chem.* 2005;12:2011–20.
7. Ozawa T. Thermal analysis—review and prospect. *Thermochim Acta.* 2000;355:35–42.
8. Wadsö I. Microcalorimetric techniques for characterization of living cellular systems. will there be any important practical applications? *Thermochim Acta.* 1995;269–270:337–50.
9. Maskow T, Kemp R, Buchholz F, Schubert T, Kiesel B, Harms H. What heat is telling us about microbial conversions in nature and technology: from chip- to megacalorimetry. *Microbiol Biotechnol.* 2010;3:269–84.
10. Lorinczy D. Thermal analysis in biological and medical applications. *J Therm Anal Calorim.* 2017;130:1263–80.
11. Braissant O, Wirz D, Göpfert B, Daniels AU. Biomedical use of isothermal microcalorimeters. *Sensors.* 2010;10:9369–83.
12. Lamprecht I. Calorimetry and thermodynamics of living systems. *Thermochim Acta.* 2003;405:1–13.
13. Stenesh J. Introduction to metabolism biochemistry. Boston: Springer; 1998. p. 203–19.

14. von Stockar U, Liu JS. Does microbial life always feed on negative entropy? Thermodynamic analysis of microbial growth. *Biochim Biophys Acta Bioenerg.* 1999;1412:191–211.
15. Maskow T, Wolf K, Kunze W, Enders S, Harms H. Rapid analysis of bacterial contamination of tap water using isothermal calorimetry. *Thermochim Acta.* 2012;543:273–80.
16. Brueckner D, Krähenbühl S, Zuber U, Bonkat G, Braissant O. An alternative sterility assessment for parenteral drug products using isothermal microcalorimetry. *J Appl Microbiol.* 2017;123:773–9.
17. Maskow T, Schubert T, Wolf A, Buchholz F, Regestein L, Buechs J, et al. Potentials and limitations of miniaturized calorimeters for bioprocess monitoring. *Appl Microbiol and Biotechnol.* 2011;92:55.
18. Chen J, Li K, Liu C, Li M, Lv Y, Jia L, et al. Enhanced efficiency of thermoelectric generator by optimizing mechanical and electrical structures. *Energies.* 2017;10:1329.
19. Trampuz A, Salzmann S, Antheaume J, Daniels AU. Microcalorimetry: a novel method for detection of microbial contamination in platelet products. *Transfusion.* 2007;47:1643–50.
20. Boling EA, Blanchard GC, Russell WJ. Bacterial identification by microcalorimetry. *Nature.* 1973;241:472–3.
21. Chang-Li X, Hou-Kuhan T, Zhau-Hua S, Song-Sheng Q, Yao-Ting L, Hai-Shui L. Microcalorimetric study of bacterial growth. *Thermochim Acta.* 1988;123:33–41.
22. Bonkat G, Braissant O, Rieken M, Solokhina A, Widmer AF, Frei R, et al. Standardization of isothermal microcalorimetry in urinary tract infection detection by using artificial urine. *World J Urol.* 2013;31:553–7.
23. Braissant O, Wirz D, Gopfert B, Daniels AU. “The heat is on”: rapid microcalorimetric detection of mycobacteria in culture. *Tuberculosis.* 2010;90:57–9.
24. Koga K, Nishizawa YU, Matsumoto Y-I, Hara T, Takahashi K. Evaluation of the growth activity of *Escherichia coli* and *Staphylococcus aureus* colonies on solid medium using microbial calorimetry. *Biocontrol Sci.* 2004;9:21–8.
25. Fricke C, Harms H, Maskow T. Rapid calorimetric detection of bacterial contamination: influence of the cultivation technique. *Front Microbiol.* 2019;10:1–12.
26. Monod J. The growth of bacterial cultures. *Annu Rev Microbiol.* 1949;3:371–94.
27. Saha K. *The Earth’s atmosphere: its physics and dynamics.* Berlin: Springer; 2008.
28. Benson BB, Krause D Jr. The concentration and isotopic fractionation of oxygen dissolved in freshwater and seawater in equilibrium with the atmosphere. *Limnol Oceanogr.* 1984;29:620–32.
29. Hazan R, Que Y-A, Maura D, Rahme LG. A method for high throughput determination of viable bacteria cell counts in 96-well plates. *BMC Microbiol.* 2012;12:1–7.
30. Hoffmann S, Walter S, Blume A-K, Fuchs S, Schmidt C, Scholz A, et al. High-throughput quantification of bacterial-cell interactions using virtual colony counts. *Front Cell Infect Microbiol.* 2018;8:1–10.
31. Bonkat G, Bachmann A, Solokhina A, Widmer AF, Frei R, Gasser TC, et al. Growth of mycobacteria in urine determined by isothermal microcalorimetry: implications for urogenital tuberculosis and other mycobacterial infections. *Urology.* 2012;80:1163.e9–e12.
32. Gnaiger E, Kemp RB. Anaerobic metabolism in aerobic mammalian cells: information from the ratio of calorimetric heat flux and respirometric oxygen flux. *Biochim Biophys Acta Bioenerg.* 1990;1016:328–32.
33. Bartram J, Cotruvo JA, Exner M, Fricker C, Glasmacher A. *Heterotrophic plate counts and drinking-water safety.* Geneva: World Health Organization; 2003.
34. Braissant O, Wirz D, Göpfert B, Daniels AU. Use of isothermal microcalorimetry to monitor microbial activities. *FEMS Microbiol Lett.* 2010;303:1–8.
35. Bäckman P, Bastos M, Hallén D, Lönnbro P, Wadsö I. Heat conduction calorimeters: time constants, sensitivity and fast titration experiments. *J Biochem Biophys Methods.* 1994;28:85–100.
36. Wadsö I. Isothermal microcalorimetry near ambient temperature: an overview and discussion. *Thermochim Acta.* 1997;294:1–11.
37. Lee W, Fon W, Axelrod BW, Roukes ML. High-sensitivity microfluidic calorimeters for biological and chemical applications. *Proc Natl Acad Sci USA.* 2009;106:15225–30.
38. Rodríguez D, Daniels AU, Urrusti JL, Wirz D, Braissant O. Evaluation of a low-cost calorimetric approach for rapid detection of tuberculosis and other mycobacteria in culture. *J Appl Microbiol.* 2011;111:1016–24.
39. Altwasser V, Patz RR, Lemke T, Paufler S, Maskow T. A simple method for the measurement of metabolic heat production rates during solid-state fermentations using ss-carotene production with *Blakeslea trispora* as a model system. *Eng Life Sci.* 2017;17:620–8.
40. Braissant O, Theron G, Barnard M, Friedrich SO, Diacon AH, Bonkat G. Comparison of isothermal microcalorimetry and BACTEC MGIT960 for detection of the metabolic activity of *Mycobacterium tuberculosis* in sputum samples. *J Appl Microbiol.* 2019;128:1497–502.
41. Crabbé A, Leroy B, Wattiez R, Aertsen A, Leys N, Cornelis P, et al. Differential proteomics and physiology of *Pseudomonas putida* KT2440 under filament-inducing conditions. *BMC Microbiol.* 2012;12:1–9.
42. Maskow T, Morais FM, Rosa LFM, Qian YG, Harnisch F. Insufficient oxygen diffusion leads to distortions of microbial growth parameters assessed by isothermal microcalorimetry. *RSC Adv.* 2014;4:32730–7.
43. Tronolone H, Tam A, Szenczi Z, Green JEF, Balasuriya S, Tek EL, et al. Diffusion-limited growth of microbial colonies. *Sci Rep.* 2018;8:1–11.
44. Warren M, Hwa T. The growth of bacterial colonies. *Biophys J.* 2012;102:152a.
45. Stoward PJ. Thermodynamics of biological growth. *Nature.* 1962;194:977–8.
46. Egli T. Microbial growth and physiology: a call for better craftsmanship. *Front Microbiol.* 2015;6:1–12.
47. Antoniou P, Hamilton J, Koopman B, Jain R, Holloway B, Lyberatos G, et al. Effect of temperature and pH on the effective maximum specific growth rate of nitrifying bacteria. *Water Res.* 1990;24:97–101.
48. Zaharia DC, Muntean AA, Popa MG, Steriade AT, Balint O, Micut R, et al. Comparative analysis of *Staphylococcus aureus* and *Escherichia coli* microcalorimetric growth. *BMC Microbiol.* 2013;13:1–14.
49. Katarao A, Yamato N, Takahashi K. Calorimetric study of *Escherichia coli* growth on Bouillon medium. *Agric Biol Chem.* 1987;51:2437–42.
50. Sezonov G, Joseleau-Petit D, D’Ari R. *Escherichia coli* physiology in Luria-Bertani broth. *J Bacteriol.* 2007;189:8746–9.
51. Burrows W. The nutritional requirements of bacteria. *Q Rev Biol.* 1936;11:406–24.
52. Russell JB, Cook GM. Energetics of bacterial growth: balance of anabolic and catabolic reactions. *Microbiol Rev.* 1995;59:48–62.
53. Loesberg C, van Miltenburg JC, van Wuk R. Heat production of mammalian cells at different cell-cycle phases. *J Therm Biol.* 1982;7:209–13.
54. Kimura T, Takahashi K. Calorimetric studies of soil microbes: quantitative relation between heat evolution during microbial

- degradation of glucose and changes in microbial activity in soil. *Microbiology*. 1985;131:3083–9.
55. Robador A, LaRowe DE, Finkel SE, Amend JP, Nealson KH. Changes in microbial energy metabolism measured by nanocalorimetry during growth phase transitions. *Front Microbiol*. 2018;9:1–7.
56. Bonkat G, Braissant O, Widmer AF, Frei R, Rieken M, Wyler S, et al. Rapid detection of urinary tract pathogens using microcalorimetry: principle, technique and first results. *BJU Int*. 2012;110:892–7.
57. Fricke C, Xu J, Jiang FL, Liu Y, Harms H, Maskow T. Rapid culture-based detection of *Legionella pneumophila* using isothermal microcalorimetry with an improved evaluation method. *Microbiol Biotechnol*. 2020;13:1262–72.
58. Bobbitt JA, Betts RP. The removal of bacteria from solutions by membrane filtration. *J Microbiol Methods*. 1992;16:215–20.
59. Lerchner J, Schulz A, Poeschel T, Wolf A, Hartmann T, Mertens F, et al. Chip calorimetry and biomagnetic separation: fast detection of bacterial contamination at low cell titers. *Eng Life Sci*. 2012;12:615–20.

Publisher's Note Springer Nature remains neutral with regard to jurisdictional claims in published maps and institutional affiliations.

3.1.3 Rapid culture-based detection of *Legionella pneumophila* using isothermal microcalorimetry with an improved evaluation method

Fricke C, Xu J, Jiang F-L, Liu Y, Harms H, Maskow T. (2020):

Rapid culture-based detection of *Legionella pneumophila* using isothermal microcalorimetry with an improved evaluation method


Microb. Biotechnol. **13** (4), 1262-72.

<https://doi.org/10.1111/1751-7915.13563> (published, Brief report)

Significance: ISO 11731:2017 is a culture-based standard method for the detection of *Legionella pneumophila*. According to the ISO, a positive result of a contaminated sample is confirmed after a cultivation period of 10 days. This procedure is a time-consuming detection method. It would be desirable to have an equivalent faster approach that can reduce the cultivation time and detect potential outbreaks earlier. In this publication, a culture-based detection of *L. pneumophila* using isothermal microcalorimetry was demonstrated for the first time. Detectable heat flows of highly concentrated samples (1000 CFU per ampoule) were determined after 24 h. Low contamination levels (4 CFU per ampoule) were detected after 45 h. Additionally, an improved evaluation method was presented by analysing the first derivative of the heat flow curve. Finally, the findings are discussed in the context of establishing an early warning system for drinking water samples based on microcalorimetry.

Brief report

Rapid culture-based detection of *Legionella pneumophila* using isothermal microcalorimetry with an improved evaluation method

Christian Fricke,¹ Juan Xu,² Feng-Lei Jiang,² Yi Liu,² Hauke Harms¹ and Thomas Maskow^{1*} 

¹Department of Environmental Microbiology, Helmholtz-Centre for Environmental Research – UFZ, Leipzig, Germany.

²Key Laboratory of Analytical Chemistry for Biology and Medicine (Ministry of Education), College of Chemistry and Molecular Sciences, Wuhan University, Wuhan, 430072, China.

Summary

The detection and quantification of *Legionella pneumophila* (responsible for legionnaire's disease) in water samples can be achieved by various methods. However, the culture-based ISO 11731:2017, which is based on counts of colony-forming units per ml (CFU·ml⁻¹) is still the gold standard for quantification of *Legionella* species (spp.). As a powerful alternative, we propose real-time monitoring of the growth of *L. pneumophila* using an isothermal microcalorimeter (IMC). Our results demonstrate that, depending on the initial concentration of *L. pneumophila*, detection times of 24–48 h can be reliably achieved. IMC may, therefore, be used as an early warning system for *L. pneumophila* contamination. By replacing only visual detection of growth by a thermal sensor, but otherwise maintaining the standardized protocol of the ISO 11731:2017, the new procedure could easily be incorporated into existing standards. The exact determination of the beginning of metabolic heat is often very difficult because at the beginning of the calorimetric signal the thermal stabilization and the metabolic heat development overlap. Here, we

propose a new data evaluation based on the first derivation of the heat flow signal. The improved evaluation method can further reduce detection times and significantly increase the reliability of the IMC approach.

Introduction

Legionnaire's disease, caused by pathogenic bacteria of *Legionella* spp., manifests itself as an atypical form of pneumonia (Fraser *et al.*, 1977; McDade *et al.*, 1977; Fields *et al.*, 2002; Hilbi *et al.*, 2010). Besides this, a less dangerous, non-pneumonic form, the so-called Pontiac fever (Rowbotham, 1980a; Tossa *et al.*, 2006; Ward *et al.*, 2010) can be caused by *Legionella* spp.. The best-characterized species of the genus is *Legionella pneumophila*, which comprises 16 serogroups (Kazandjian *et al.*, 1997; Yu *et al.*, 2002; Aurell *et al.*, 2003). It is a Gram-negative bacterium that is omnipresent in the environment, especially in aquatic systems (Rowbotham, 1980b). Here, amoebae act as host cells for *L. pneumophila* to protect and multiply them (Rowbotham, 1980b; Rowbotham, 1983; Thomas *et al.*, 2010). However, the greatest danger is posed by *L. pneumophila* when it invades technical water systems (private and public buildings), air conditioners, cooling towers, etc. (Fliermans *et al.*, 1981; Orrison *et al.*, 1981; Stout *et al.*, 1985; Fields *et al.*, 2002). The transmission occurs by inhalation of small water droplets containing *L. pneumophila* (Bollin *et al.*, 1985). The aerosols are then able to enter the respiratory tract and infect human macrophages in which *L. pneumophila* multiplies. Finally, the human macrophages are killed and the replicated *L. pneumophila* bacteria are released and can attack further macrophages (Segal and Shuman, 1999; Khweek and Amer, 2010).

Since the first recognition of *L. pneumophila* in 1976, several methods were developed for the detection of this pathogen (Villari *et al.*, 1998; Díaz-Flores *et al.*, 2015; Mobed *et al.*, 2019). One of the earliest diagnostic tools was based on immunofluorescence labelling (Cherry

Received 25 October, 2019; accepted 2 March, 2020.

*For correspondence. E-mail Thomas.Maskow@ufz.de; Tel. +49341 2351328; Fax +49 341 235 1351.

Microbial Biotechnology (2020) 13(4), 1262–1272

doi:10.1111/1751-7915.13563

Funding Information

This work was funded by the German Federation of Industrial Research Associations (AIF BMWi, AIF-Nr. ZF4315807RH7).

© 2020 The Authors. *Microbial Biotechnology* published by John Wiley & Sons Ltd and Society for Applied Microbiology.

This is an open access article under the terms of the Creative Commons Attribution License, which permits use, distribution and reproduction in any medium, provided the original work is properly cited.

et al., 1978; Berdal *et al.*, 1979). The semi-selective nutrient medium developed by Edelstein and co-workers in 1979, based on charcoal yeast extract (CYE) agar allowed the first selective enrichment of *L. pneumophila* cultures from contaminated specimens (Edelstein and Finegold, 1979). Later, more sensitive and selective nutrient media were explored (Warren and Miller, 1979; Ristoph *et al.*, 1980), which are admixed with antibiotics (e.g. as Glycine Vancomycin Polymyxin Cycloheximide (GVPC) agar) to suppress the growth of accompanying microorganisms (Edelstein 1981). The common present-day practice is to determine the number of *L. pneumophila* cells in environmental samples as prescribed in the standardized protocol of the ISO 11731:2017. This ISO method describes standardized cultivation of *L. pneumophila* on selective culture media (GVPC Agar). The degree of contamination is determined quantitatively as CFU per 100 ml sample.

Besides this, there are several other techniques known for the detection of *L. pneumophila*: for instance, urinary antigen tests (UAT) (Bibb *et al.*, 1984; Samuel *et al.*, 1988; Dominguez *et al.*, 1996), indirect and direct fluorescent antibody (IDFA) staining (Winn *et al.*, 1980; Makin and Hart, 1989; Alary and Joly, 1992), a high number of different qualitative and quantitative polymerase chain reaction (PCR) approaches (Starnbach *et al.*, 1989; Bej *et al.*, 1991; Catalan *et al.*, 1994; Matsiotabernard *et al.*, 1994; MatsiotaBernard *et al.*, 1997; Ballard *et al.*, 2000; van der Zee *et al.*, 2002; Fiume *et al.*, 2005; Boss *et al.*, 2018) and a variety of biosensors like surface plasmon resonance (SPR) immunosensor, electrochemical as well as genosensors etc. (Oh *et al.*, 2003; Li *et al.*, 2012; Mobed *et al.*, 2019). Especially, qPCR techniques are becoming more and more used in practice. One example is the ISO norm (ISO/TS 12869:2019) which deals with the detection and quantification of *L. pneumophila* (Omiccioli *et al.*, 2015). All these diverse techniques are able to detect *Legionella* spp. much faster (minutes to a few hours) compared with the conventional cultivation approach (3–7 days) (Mobed *et al.*, 2019). However, they have in common that expensive agents and a high level of expertise are required for their execution and data interpretation. Therefore, it is not surprising that the cultivation-dependent detection of *L. pneumophila* is still the gold standard.

For this reason and in contrast to the general research trend towards molecular biological techniques in the field of *L. pneumophila* detection, we propose a culture-based method using an isothermal microcalorimeter (IMC) to track the growth of *L. pneumophila* in real-time. We suggest replacing visual detection by the human eye through a highly sensitive thermoelectric device (*i.e.* Peltier element) of an IMC

and exploit the metabolic heat evolved for early detection of bacterial growth (Wadsö and Goldberg, 2001; von Stockar 2010; Maskow *et al.*, 2014; Braissant *et al.*, 2015a,2015b). Additionally, if IMC experiments are performed on solid medium further inspections like checking the colony morphology after the experiment are possible if glass ampoules are used. Depending on the bacterial strain as well as on the medium this subsequent visual inspection might provide some information on potential accompanying bacterial flora. Like colony counts, IMC recognizes only active and cultivable bacteria as the harmful fraction of the pathogen. Advantageously, IMC is very easy to implement and data interpretation does not require specific expertise. Furthermore, using IMC is fully compatible with ISO 11731:2017 sample preparation. Hence, it can be easily integrated into the existing standard protocols with the added benefit of potentially reduced detection times, especially for high concentrations of *L. pneumophila* ($> 10^4$ CFU L⁻¹) (WHO 2007). The three objectives of our study are therefore firstly to show the applicability of calorimetric monitoring to *L. pneumophila* contamination, secondly to optimize the data evaluation and thirdly, to analyse the dependence of the detection time on pathogen concentration.

Results and Discussion

Principles of heat flow measurements of bacterial growth

Medium and sample are held by a sealable glass ampoule (calorimetric vessel) which is put into a calorimeter. The metabolic heat flows via a Peltier element to a thermally controlled heat sink. The Peltier element provides a voltage which is proportional to the metabolic heat production rate $\Phi(t)$ (in W) (see Fig. 1).

The conversion factor of measured voltage to heat output signal is determined by electrical calibration. The actual heat flow $\Phi(t)$ depends on the number of active *L. pneumophila* cells at any point in time $N(t)$ and the cell-specific heat evolved by each cell φ_0 (in W) (Eq. 1, Chang-Li *et al.*, 1988):

$$\Phi(t) = N(t) \cdot \varphi_0. \quad (1)$$

It is well known that bacterial growth if all nutrients are available in excess follows the following exponential function:

$$N(t) = N_0 \cdot \exp(\mu \cdot t). \quad (2)$$

where N_0 is the initial bacterial concentration in the sample under investigation, μ is the specific growth rate (in h⁻¹) and t the elapsed time (in h). Combining Eqs 1 and 2 leads to:

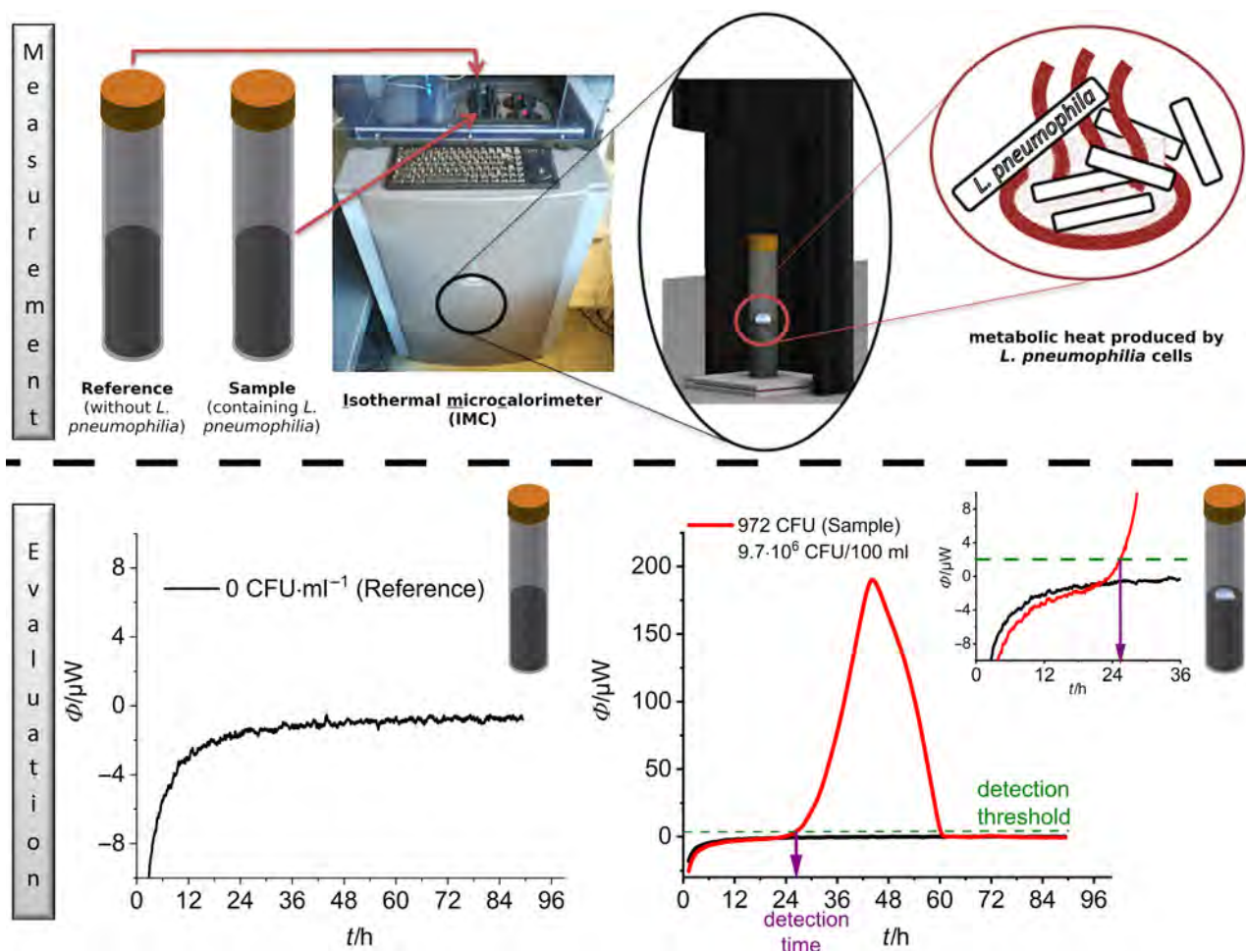


Fig. 1. Experimental setup and data evaluation for the microcalorimetric investigation of the growth of *L. pneumophila*.

$$\Phi(t) = N_0 \cdot \varphi_0 \cdot \exp(\mu \cdot t) \text{ or } \ln(N_0) = -\mu \cdot t + \ln\left(\frac{\Phi(t)}{\varphi_0}\right). \quad (3)$$

The logarithmized form of Eq. 3 makes it possible to establish a linear relationship between the initial concentration N_0 and the time t (in h) that passes until a given heat production rate $\Phi(t)$ is detected. Assuming a certain value as thermal detection limit (e.g. $2 \mu\text{W}$) (Braissant *et al.*, 2010), the corresponding time could be called detection time t_{dect} . It could be shortened by using a more sensitive calorimeter with a smaller thermal detection limit or a higher starting concentration of *L. pneumophila*. However, it has to be noted that not all commercially available microcalorimeters achieve this thermal detection limit. Nevertheless, the latter can be achieved by concentrating the sample, for example by membrane filtration. Membrane filtration of 100 ml sample volume is also used for the ISO 11731:2017 standard. When interpreting the results of plating $10 \mu\text{l}$

(in the case of the IMC experiments), the enrichment by a factor of 10^4 should be kept in mind. The t_{dect} is used to calculate the number of *L. pneumophila* cells in the calorimetric vessel and by considering the enrichment in the sample according to Eq. 3.

The thermal signal is essentially determined by two counteracting effects (see also Supporting information). First, the ampoule is entering the calorimeter with a temperature T_0 slightly deviating from the calorimeter temperature T_C and needs to be thermally equilibrated (typically an endothermal signal). Second, heat is evolved due to metabolic activity (exothermal signal). As a result of these two effects, there is a shift in the baseline, which is clearly noticeable at the beginning of all measurements. To ensure a reliable determination of the detection time, additional baseline corrections are necessary. Another possibility, which to our knowledge has never been tested before in measuring metabolic activity, is the analysis of the first derivative of the heat flow (see Fig. 2), which potentially eliminates the shift of the

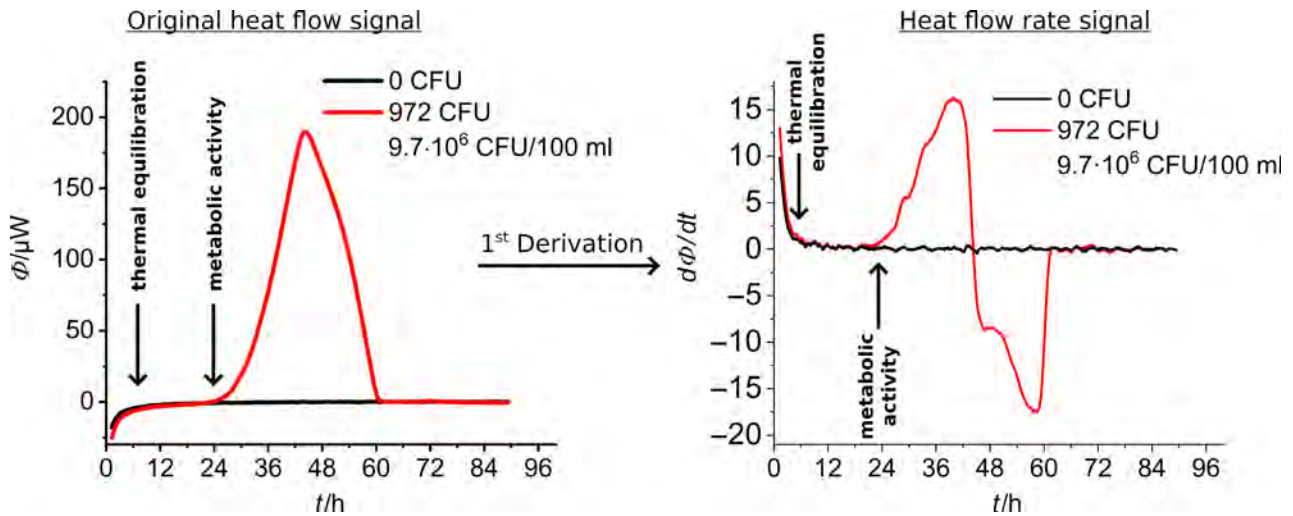


Fig. 2. Derivation of the original heat flow signal. Left: First derivation of the heat flow after the time (heat flow rate, ϕ). Right: The original signal, the red line stands for a metabolically influenced heat signal and the black line for the blank.

baseline and allows to distinguish the physical from the metabolic effect. In other words, such an approach does not require arbitrary baseline correction.

If necessary, additional information about the growth kinetic of *L. pneumophila* can be obtained via integration of the heat flow signal. The integrated heat flow shown in Fig. 3 follows a classical sigmoidal bacterial growth curve, which can be divided into lag phase, exponential growth phase and stationary phase (Monod, 1949).

However, more sophisticated models like the Gompertz equation (Eq. 4) describe lag phase and stationary phase and allows to derive important kinetic growth parameter from the observed integrated heat flow curve (Braissant *et al.*, 2013).

$$Q(t) = Q_{\max} \cdot \exp(-\exp(-\mu_{\max} \cdot (t - \gamma))). \quad (4)$$

In this equation, Q_{\max} (in J) represents the total amount of heat evolved during the growth. The parameter μ_{\max} (in h^{-1}) corresponds to the maximum growth rate during the exponential phase and γ (in h) corresponds to the duration of the lag phase, that is the lag time.

Applicability of *L. pneumophila* detection by IMC measurement

At first, the calorimetric signal has to be interpreted (Fig. 4). All initial bacterial concentrations are given in CFU (number of bacteria per ampoule) and CFU/100 ml

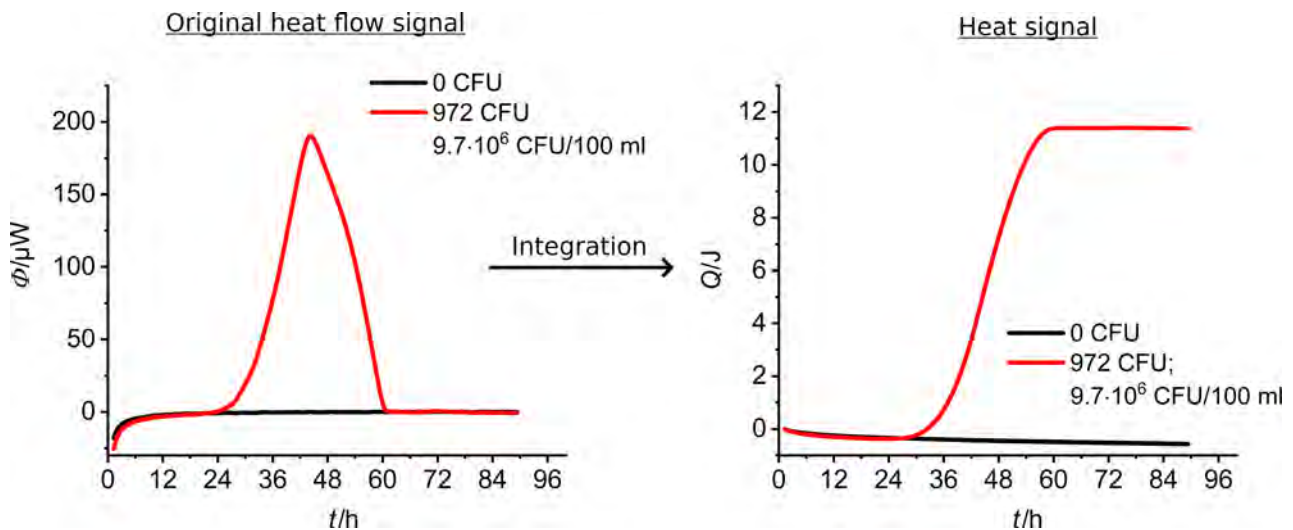


Fig. 3. Integration of the original heat flow signal. Left: Integral of the heat flow (total heat, Q). Right: The original signal, the red line stands for a metabolically influenced heat signal and the black line for the blank.

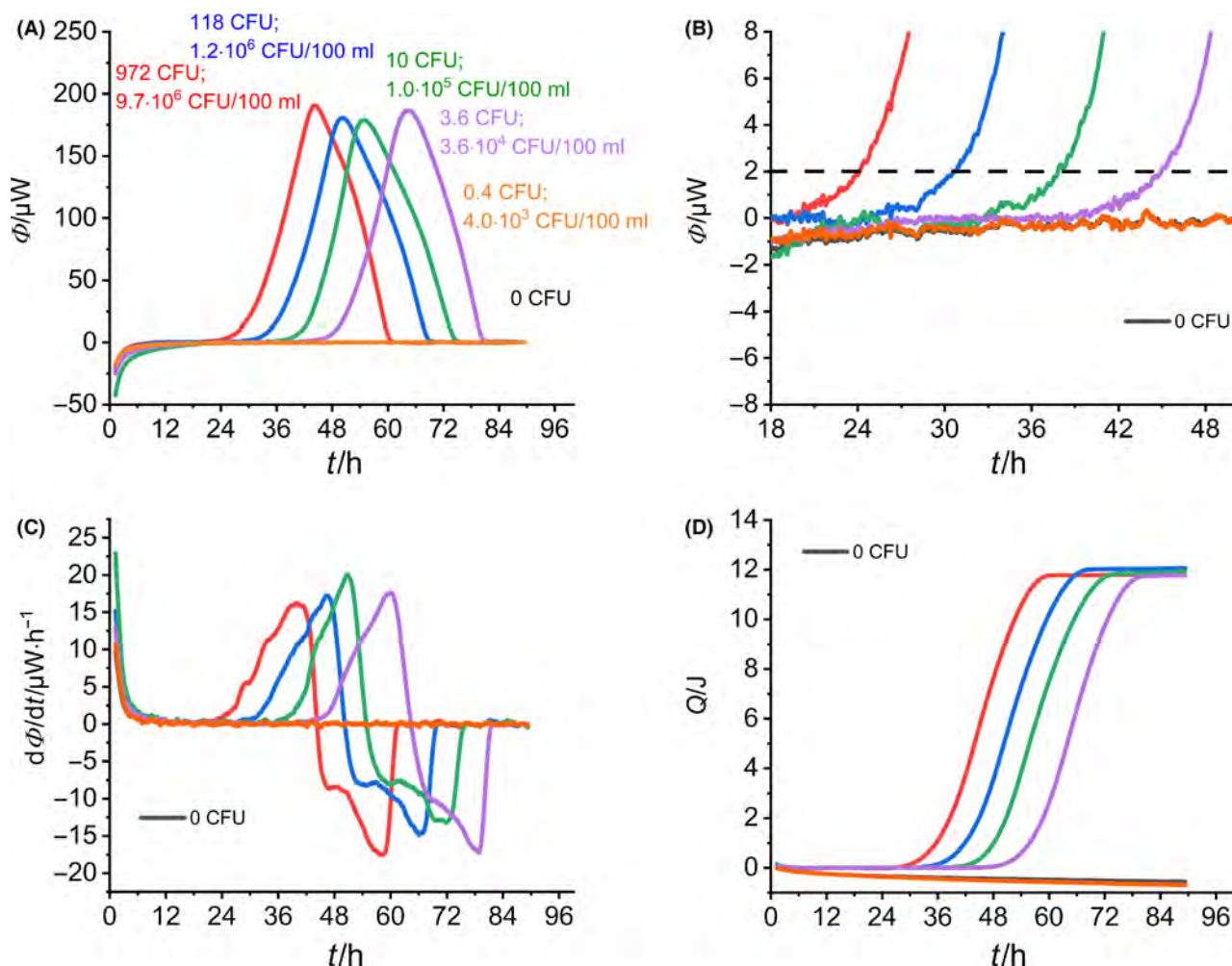


Fig. 4. Summary of the IMC monitoring of the growth of *L. pneumophila*. A. Heat flow over time depending on the initial bacterial concentration. B. Magnification of the heat flow near the threshold value. C. First derivatives of the heat flow signals depending on the initial bacterial concentration. D. Integrals of the heat flow signals depending on the initial bacterial concentration.

(as specified by ISO). Independent of the initial number of *L. pneumophila* cells, the heat flow signals had the same shape and displayed only a single peak. After reaching the maximum, all heat flow signals returned to the baseline (Fig. 4A). With increased initial bacterial concentration, the heat flow signals appeared earlier, according to Eq. 3.

Braissant *et al.* (2010) obtained similar results with their concentration-dependent investigation of *Mycobacterium tuberculosis*. The lowest initial concentration (0.4 CFU per calorimetric ampoule) did not result in an increase in the heat flow signal. This can be explained by the inoculum volume of 10 μl , which statistically contains only approx. 0.1 CFU so that only one CFU in every tenth sample is expected. To determine a corresponding detection time for each heat flow signal, we set

the threshold value at $\Phi(t) = 2 \mu\text{W}$ according to literature recommendations (Braissant *et al.*, 2010). If the respective heat flow signal reaches this value, the detection time can be read off directly (Fig. 4B).

If one considers the beginning of the heat flow signals, a sharp increase in all signals was observed (Fig. 4A). All heat flows showed the transient process from thermal equilibration of the calorimetric vessel to a metabolic heat signal. This kind of transitions led apparently to strong baseline drifts at the beginning of the signal and complicated the whole data evaluation because arbitrary baseline corrections are necessary to quantify the corresponding detection times correctly. In order to avoid baseline corrections, we calculated the first derivative of the heat flow signals (Fig. 4C). The first derivative provided a good baseline (the flat line linking the two effects).

Further information (such as maximum specific growth rate, total heat generated and the duration of the lag phase) can be derived from the integration of the heat flow signal and the parameter adjustment to the Gompertz model (eq. 4, see Supporting information). The integrated heat curves can be seen in Fig. 4D. The integrated curves show typical sigmoidal behaviour. The exponential part corresponds to the growth/proliferation phase of the bacteria. Reaching the plateau indicates that the existing media (e.g. oxygen and substrates) are depleted.

Improved data evaluation

To illustrate the effect of baseline correction, Fig. 5A shows the uncorrected (red) and baseline-corrected (black) heat flow signal. The interfering endothermal signal obviously has a significant influence on the definition of the baseline and thus on the detection time.

The uncorrected baseline reaches the threshold value ($2 \mu\text{W}$, dotted line) approx. 1.5 h later than the baseline-corrected signal. If a linear baseline is to be assumed, two points are needed where the heat production rate is set to zero. One point is obviously after the metabolism is finished. Here, a final signal appeared, which is approximately in the expected range of $0 \mu\text{W}$ with a signal noise of approx. ($\pm 0.2 \mu\text{W}$) as described for the used calorimeter type (TAM III, www.tainstruments.com) (Fig. 5B). The other point should be the beginning of the metabolically determined heat flow signal. However, it is difficult to define this point because the signal is interfered by the thermal equilibration (Fig. 5C). The data evaluation proposed by us, simple to practice, considers the first derivative of the total signal with both effects (thermal equilibration and metabolic activity) (Fig. 5D). The result is a broad minimum between the two effects, which can be

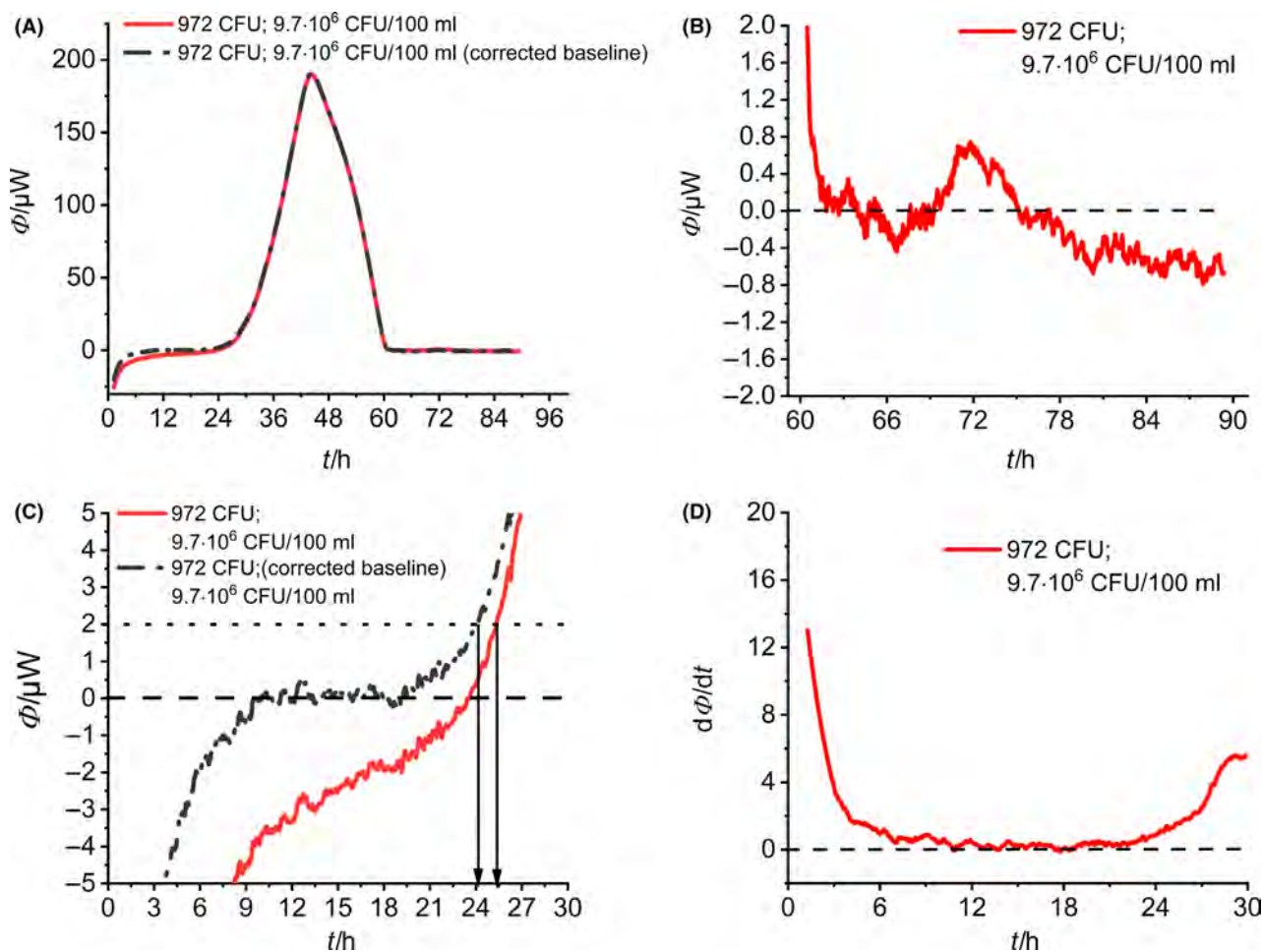


Fig. 5. Problems and improvements in data evaluation.

A. Total heat flow over time without (red) and with baseline corrections (black).

B. End of the heat flow signal.

C. Beginning of the heat flow signal. Due to incomplete thermal equilibration, the beginning suggests negative heat flow. The black curve with baseline correction results in a detection time of 24.1 h, whereas the uncorrected red curve gives a longer detection time of 25.3 h.

D. The first derivation of the heat flow signal obviating the need for baseline correction.

taken to define a comparatively constant baseline. Due to the on-line character of the heat signal, the measuring points can be placed very tightly, which enables good signal smoothing (Savitzky–Golay filter, 200 measuring points) and thus good differentiation.

Dependence of the detection speed on *L. pneumophila* concentrations

We obtained a linear relationship when plotting the detection time against the logarithm of the initial bacterial concentration (Fig. 6A) according to Eq. 3.

Using this correlation, it is now possible to determine the initial bacterial concentration for each unknown sample of *L. pneumophila*. In order to demonstrate that this linear relationship is not a question of the threshold definition, we additionally determined the corresponding detection times at different threshold values $\Phi(t) = 5, 10, 100 \mu\text{W}$ as well as at the maximum of the heat flow

signal Φ_{max} . The results are summarized in Fig. 6B and all thresholds show the aforementioned linear dependency. To demonstrate that the improved data evaluation might ease the whole evaluation process, the detection time was also determined for the first derivative of the respective heat flow signals (threshold: $0.75 \mu\text{W h}^{-1}$). In this way, a reduced detection time is obtained (approx. 1 hour).

Characteristic quantities derived from heat flow measurements

All information received from Fig. 4 is compiled in Table 1. A comparison of the specific growth rates shows that there is no significant relationship between the growth rate and the initial bacterial concentration according to the expectations expressed in Eq. 3. Based on the growth rates, the doubling times t_d between 4.2 and 4.6 h were calculated. These doubling times are in

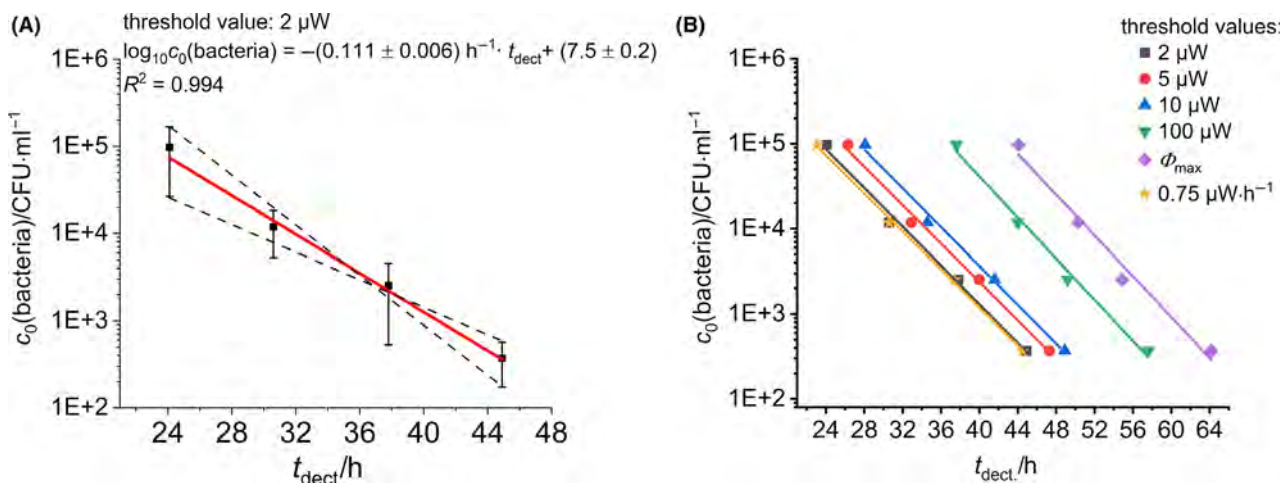


Fig. 6. Summary of the data evaluation of the concentration-dependent measurement.

A. Best-fit line with border-straight (lower and upper limit of the slope) plotted by the initial bacterial concentration and the detection time for a threshold value at $2 \mu\text{W}$.

B. Best-fit lines for different threshold values.

Table 1. Summary of the derived data from the heat flow measurements.

	972 CFU ^b ; 9.7 × 10 ⁶ CFU/100 ml ^c	118 CFU; 1.2 × 10 ⁶ CFU/100 ml	10 CFU; 1.0 × 10 ⁵ CFU/100 ml	3.6 CFU; 3.6 × 10 ⁴ CFU/100 ml
Integral				
$\mu_{\text{max}}/\text{h}^{-1}$	0.1650 ± 0.0005	0.1496 ± 0.0004	0.1500 ± 0.0002	0.1507 ± 0.0004
Q_{max}/J	11.97 ± 0.01	12.33 ± 0.01	12.23 ± 0.01	12.41 ± 0.01
γ/h	42.65 ± 0.01	49.25 ± 0.01	54.87 ± 0.01	62.93 ± 0.01
Measured data				
$\Phi_{\text{max}}(t)/\mu\text{W}$	190.7 (44.1 h)	180.3 (50.3 h)	178.9 (54.9 h)	186.6 (64.2 h)
$t_{\text{dect}}^{\text{a}}$	24.1	30.6	37.8	44.9

a. Threshold value: $2 \mu\text{W}$.

b. Number of bacteria per ampoule.

c. Enrichment due to the ISO 11731:2017 specification.

good agreement with literature data (4 to 6 h) (Donohue *et al.*, 2014). The total amount of heat can easily be derived from the integral of the heat flow signals (Fig. 4D). The magnitude of Q_{\max} can be estimated by using the oxycaloric equivalent $\Delta_k \cdot H_{O_2} = - (455 \pm 25) \text{ kJ} \cdot \text{mol}^{-1} \text{ O}_2$ (Gnaiger and Kemp, 1990). The volume of oxygen in the headspace was approx. 3 ml. The theoretical heat evolved during aerobic growth is $(11.2 \pm 0.6) \text{ J}$ and thus in good accordance with our finding of 12.0 to 12.4 J (for the calculation, see Supporting information). The lag time γ correlates indirectly with the initial bacterial concentration. The parameter of the Gompertz equation might be a powerful tool for the quantification of the susceptibility of *L. pneumophila* to antibiotics or biocides. Energy-dependent efflux pumps, for example should express themselves in a change of Q_{\max} , while bacteriostatic agents should be recognizable by an extension of the lag time γ and a reduction of the specific growth rate μ_{\max} .

The maximum heat flow demonstrates that only small amounts of medium (1000 μL) and a small volume of air (3000 μl) are sufficient for these fastidious bacteria to grow in such a way that enough heat is evolved, to be detected even by less sensitive calorimeters. The greatest benefit of the calorimetric method is faster detection (24 to 45 hours depending on initial bacterial concentration) than by conventional cultivation on plates (3 to 7 days). Depending on the initial bacterial concentration, detection within one day is also possible. If one considers less sensitive calorimeters, with a thermal detection limit of only 10–100 μW , detection times for 100 CFU/ml between 56 and 63 h will be achieved. IMC experiments do not require counting and handling plates thus led to a reduction in workload. Additionally, closed ampoules support safer handling of pathogenic bacteria (Braissant *et al.*, 2010).

Conclusion

In summary, our data demonstrate that IMC might be a powerful analytic tool for fast and reliable detection of *L. pneumophila*. Critical concentrations (100 CFU/ml) can be detected after two days and concentrated samples ($> 10^6$ CFU/100 ml) resembling harmful doses can be detected within a few hours up to one day. Regarding the analytical procedures of *L. pneumophila*, an on-line warning might be easily integrated when using microcalorimeters for detection. In addition to the short detection times, the main advantages of calorimetric detection are easy handling and easy data evaluation. From a legal point of view, it might be important for approval that our method is consistent and compatible with ISO 11731:2017 protocol as only the detection deviates.

Isothermal microcalorimetry, a non-specific method, becomes highly selective through the application of chemical and thermal pre-treatments (Leoni and Legnani, 2001) and the use of selective media (Descours *et al.*, 2014). The application of membrane filtration as an enrichment process and subsequential cultivation with the aim of shortening detection times was firstly demonstrated in liquid medium by Brueckner and co-workers using IMC (Brueckner *et al.*, 2017). Recently, heat flow measurements demonstrating the potential of membrane filtration were performed on solid medium after enrichment via membrane filtration for anaerobic cultures (Fricke *et al.*, 2019). In the case of *L. pneumophila* additionally, the availability and the transport of oxygen from the gas to the liquid phase have to be considered because the calorimetric vessel is usually airtight closed and unstirred. However, from first experiments with *P. putida* mt-2 KT2440 we know that the membrane technique also works for aerobic cultures in liquid and on solid media (unpublished results). In the face of *Legionella* detection, this might be of significance since the ISO 11731:2017 prescribe for samples containing low initial number of *Legionella* enrichment by membrane filtration.

Uncertainties in the definition of the thermal threshold can be overcome by evaluating the 1st derivative of the heat flow instead of the thermal signal itself.

In order to make this technology applicable for microbiological-analytical purposes, three main practical aspects are important: First, microcalorimeters have to be developed specifically for clinical microbiological issues. For instance, conventional IMC cover a large temperature range (e.g. 15–150°C in case of the TAM III, 5–90°C in case of TAM Air (www.tainstruments.com), 5–70°C in case of BioCal 2000/4000 (www.calmetrix.com)) at the expense of a high price of the instrument or limited thermal sensitivity. For most clinical applications, a narrow temperature range around 37°C will be sufficient improving these specifications. This idea has already been taken up, during the development of a multichannel instrument like the calScreener™ (37°C, www.kan-tht.com/images/pdf/calScreener4page.pdf). Second, the small tubes usually applied in calorimetry differ in size and sample vessel surface considerably from conventional Petri dishes, which allow an easy follow-up analysis of the colony material. Third, the throughput of conventional calorimeters still does not meet the requirements of commercial laboratories (Maskow *et al.*, 2012; Braissant *et al.*, 2015a, 2015b). A calorimeter with a moderate price that allows the application of conventional cultivation containers and high-throughput measurements would certainly find broad acceptance for *L. pneumophila* analysis, particularly since calorimetry complies with

the enrichment and cultivation conditions fixed in the ISO 11731:2017.

Experimental procedure

Legionella pneumophila ATCC 33152 (Guangdong Microbial Culture Center, GDMCC, Guangdong, China) was used for the calorimetric investigation. The strain was cultivated on BCYE (buffered charcoal yeast extract) medium, which is composed of (in g l⁻¹): charcoal (2), yeast extract (10), agar (15), ACES buffer (5), KOH (1.4), iron pyrophosphate (0.125), potassium- α -ketoglutarate (2) and L-cysteine hydrochloride (0.2). The pH value was stabilized to 6.8 ± 0.5 by the ACES buffer. A few colonies of a pre-grown Petri dish were used for liquid pre-culture of *L. pneumophila* on BYE-broth (without charcoal), which was incubated overnight at 37.0 ± 0.2 °C (HQ45Z, Zhongke Scientific Instrument and Technology Development Co. Ltd., Wuhan, China) and cells were harvested immediately before the calorimetric experiment was performed. The identity of the species was regularly checked by the morphology of the colonies.

The calorimetric measurements were performed in 4 ml glass ampoules in a high-performance IMC (TAM III, TA Instruments, New Castle, DE, USA). The ampoules and caps were autoclaved at 121°C for 40 min and then filled with 1000 μ l warm (~ 50°C), molten BCYE-agar medium, closed and stored at 4°C. The prepared glass ampoules with the solid media were cooled down to room temperature before the bacteria were added to the medium. Meanwhile, starting from the pre-culture (OD₆₀₀ = 0.18, 1:10 dilution) a dilution series was performed in 1:10 dilution steps (dilution factor $f_a = 10^5$ – 10^8). 10 μ l of each dilution step was added into a glass ampoule. After adding the bacteria, the glass ampoules were closed and set into a pre-heating position (to reach thermal equilibrium) for 15 min in the IMC. In the last step, the glass ampoules were pushed into the measuring position and after further 45 min (to reach thermal equilibrium), the heat flow signal was recorded.

Acknowledgements

The authors thank the Federal Ministry for Economic Affairs and Energy and the German Federation of Industrial Research Associations for the financial support of this research under the grant number (ZF4315807RH7). We would also like to thank the College of Chemistry and Molecular Sciences at Wuhan University for the opportunity to conduct our experiments there and further support.

Conflict of interest

The authors declare that the research was conducted in the absence of any commercial or financial relationships that could be construed as a potential conflict of interest.

References

- Alary, M., and Joly, J.R. (1992) Comparison of culture methods and an immunofluorescence assay for the detection of *Legionella-Pneumophila* in domestic hot water devices. *Curr Microbiol* **25**: 19–23.
- Aurell, H., Etienne, J., Forey, F., Reyrolle, M., Girardo, P., Farge, P., et al. (2003) *Legionella pneumophila* serogroup 1 strain Paris: endemic distribution throughout France. *J Clin Microbiol* **41**: 3320–3322.
- Ballard, A.L., Fry, N.K., Chan, L., Surman, S.B., Lee, J.V., Harrison, T.G., and Towner, K.J. (2000) Detection of *Legionella pneumophila* using a real-time PCR hybridization assay. *J Clin Microbiol* **38**: 4215–4218.
- Bej, A.K., Mahbubani, M.H., and Atlas, R.M. (1991) Detection of viable *Legionella-Pneumophila* in water by polymerase chain-reaction and gene probe methods. *Appl Environ Microb* **57**: 597–600.
- Berdal, B.P., Farshy, C.E., and Feeley, J.C. (1979) Detection of *Legionella-Pneumophila* antigen in urine by enzyme-linked immunospecific assay. *J Clin Microbiol* **9**: 575–578.
- Bibb, W.F., Arnow, P.M., Thacker, L., and Mckinney, R.M. (1984) Detection of soluble *Legionella-Pneumophila* antigens in serum and urine specimens by enzyme-linked immunosorbent-assay with monoclonal and polyclonal antibodies. *J Clin Microbiol* **20**: 478–482.
- Bollin, G.E., Plouffe, J.F., Para, M., and Hackman, B. (1985) Aerosols containing *Legionella pneumophila* generated by shower heads and hot-water faucets. *Appl Environ Microb* **50**: 1128–1131.
- Boss, R., Baumgartner, A., Kroos, S., Blattner, M., Fretz, R., and Moor, D. (2018) Rapid detection of viable *Legionella pneumophila* in tap water by a qPCR and RT-PCR-based method. *J Appl Microbiol* **125**: 1216–1225.
- Braissant, O., Wirz, D., Gopfert, B., and Daniels, A.U. (2010) "The heat is on": Rapid microcalorimetric detection of mycobacteria in culture. *Tuberculosis* **90**: 57–59.
- Braissant, O., Bonkat, G., Wirz, D., and Bachmann, A. (2013) Microbial growth and isothermal microcalorimetry: growth models and their application to microcalorimetric data. *Thermochim Acta* **555**: 64–71.
- Braissant, O., Bachmann, A., and Bonkat, G. (2015a) Microcalorimetric assays for measuring cell growth and metabolic activity: methodology and applications. *Methods* **76**: 27–34.
- Braissant, O., Keiser, J., Meister, I., Bachmann, A., Wirz, D., Göpfert, B., et al. (2015b) Isothermal microcalorimetry accurately detects bacteria, tumorous microtissues, and parasitic worms in a label-free well-plate assay. *Biotechnol J* **10**: 460–468.
- Bruেকner, D., Krähenbühl, S., Zuber, U., Bonkat, G., and Braissant, O. (2017) An alternative sterility assessment

- for parenteral drug products using isothermal microcalorimetry. *J Appl Microbiol* **123**: 773–779.
- Catalan, V., Moreno, C., Dasi, M.A., Munoz, C., and Apraiz, D. (1994) Nested polymerase chain-reaction for detection of *Legionella-Pneumophila* in water. *Res Microbiol* **145**: 603–610.
- Chang-Li, X., Hou-Kuhan, T., Zhou-Hua, S., Song-Sheng, Q., Yao-Ting, L., and Hai-Shui, L. (1988) Microcalorimetric study of bacterial growth. *Thermochim Acta* **123**: 33–41.
- Cherry, W.B., Pittman, B., Harris, P.P., Hebert, G.A., Thomason, B.M., Thacker, L., and Weaver, R.E. (1978) Detection of Legionnaires disease bacteria by direct immunofluorescent staining. *J Clin Microbiol* **8**: 329–338.
- Descours, G., Cassier, P., Forey, F., Ginevra, C., Etienne, J., Lina, G., and Jarraud, S. (2014) Evaluation of BMPA, MWY, GVPC and BCYE media for the isolation of *Legionella* species from respiratory samples. *J Microbiol Meth* **98**: 119–121.
- Díaz-Flores, Á., Montero, J.C., Castro, F.J., Alejandres, E.M., Bayón, C., Solís, I., et al. (2015) Comparing methods of determining *Legionella* spp. in complex water matrices. *BMC Microbiology* **15**: 91.
- Dominguez, J.A., Manterola, J.M., Blavia, R., Sopena, N., Belda, F.J., Padilla, E., et al. (1996) Detection of *Legionella pneumophila* serogroup 1 antigen in nonconcentrated urine and urine concentrated by selective ultrafiltration. *J Clin Microbiol* **34**: 2334–2336.
- Donohue, M.J., O'Connell, K., Vesper, S.J., Mistry, J.H., King, D., Kostich, M., and Pfaller, S. (2014) Widespread molecular detection of *Legionella pneumophila* Serogroup 1 in cold water taps across the United States. *Environ Sci Technol* **48**: 3145–3152.
- Edelstein, P.H. (1981) Improved semiselective medium for isolation of *Legionella-Pneumophila* from contaminated clinical and environmental specimens. *J Clin Microbiol* **14**: 298–303.
- Edelstein, P.H., and Finegold, S.M. (1979) Use of a semi-selective medium to culture *Legionella-Pneumophila* from contaminated lung specimens. *J Clin Microbiol* **10**: 141–143.
- Fields, B.S., Benson, R.F., and Besser, R.E. (2002) *Legionella* and Legionnaires' disease: 25 years of investigation. *Clin Microbiol Rev* **15**: 506–526.
- Fiume, L., Bucca Sabattini, M.A., and Poda, G. (2005) Detection of *Legionella pneumophila* in water samples by species-specific real-time and nested PCR assays. *Let Appl Microbiol* **41**: 470–475.
- Fliermans, C.B., Cherry, W.B., Orrison, L.H., Smith, S.J., Tison, D.L., and Pope, D.H. (1981) Ecological distribution of *Legionella-Pneumophila*. *Appl Environ Microb* **41**: 9–16.
- Fraser, D.W., Tsai, T.R., Orenstein, W., Parkin, W.E., Beecham, H.J., Sharrar, R.G., et al. (1977) Legionnaires' disease: description of an epidemic of pneumonia. *N Engl J Med* **297**: 1189–1197.
- Fricke, C., Harms, H., and Maskow, T. (2019) Rapid calorimetric detection of bacterial contamination: influence of the cultivation technique. *Front Microbiol* **10**: 1–12.
- Gnaiger, E., and Kemp, R.B. (1990) Anaerobic metabolism in aerobic mammalian cells: information from the ratio of calorimetric heat flux and respirometric oxygen flux. *Biochimica et Biophysica Acta (BBA) - Bioenergetics* **1016**: 328–332.
- Hilbi, H., Jarraud, S., Hartland, E., and Buchrieser, C. (2010) Update on Legionnaires' disease: pathogenesis, epidemiology, detection and control. *Mol Microbiol* **76**: 1–11.
- Kazandjian, D., Chiew, R., and Gilbert, G.L. (1997) Rapid diagnosis of *Legionella pneumophila* serogroup 1 infection with the Binax enzyme immunoassay urinary antigen test. *J Clin Microbiol* **35**: 954–956.
- Khweek, A.A., and Amer, A. (2010) Replication of *Legionella pneumophila* in human cells: why are we susceptible? *Front Microbiol* **1**: 133–133.
- Leoni, E., and Legnani, P.P. (2001) Comparison of selective procedures for isolation and enumeration of *Legionella* species from hot water systems. *J Appl Microbiol* **90**: 27–33.
- Li, N., Brahmendra, A., Veloso, A.J., Prashar, A., Cheng, X.R., Hung, V.W.S., et al. (2012) Disposable immunochips for the detection of *Legionella pneumophila* using electrochemical impedance spectroscopy. *Anal Chem* **84**: 3485–3488.
- Makin, T., and Hart, C.A. (1989) Detection of *Legionella-Pneumophila* in environmental water samples using a fluorescein conjugated monoclonal-antibody. *Epidemiol Infect* **103**: 105–112.
- Maskow, T., Wolf, K., Kunze, W., Enders, S., and Harms, H. (2012) Rapid analysis of bacterial contamination of tap water using isothermal calorimetry. *Thermochim Acta* **543**: 273–280.
- Maskow, T., Morais, F.M., Rosa, L.F.M., Qian, Y.G., and Harnisch, F. (2014) Insufficient oxygen diffusion leads to distortions of microbial growth parameters assessed by isothermal microcalorimetry. *RSC Advances* **4**: 32730–32737.
- Matsiotabernard, P., Pitsouni, E., Legakis, N., and Nauciel, C. (1994) Evaluation of commercial amplification kit for detection of *Legionella-Pneumophila* in clinical specimens. *J Clin Microbiol* **32**: 1503–1505.
- MatsiotaBernard, P., Vrioni, G., and Nauciel, C. (1997) Use of the polymerase chain reaction for the detection of *Legionella pneumophila* DNA in serum samples. *Clin Infect Dis* **25**: 939–939.
- McDade, J.E., Shepard, C.C., Fraser, D.W., Tsai, T.R., Redus, M.A., and Dowdle, W.R. (1977) Legionnaires' disease: isolation of a bacterium and demonstration of its role in other respiratory disease. *N Engl J Med* **297**: 1197–1203.
- Mobed, A., Hasanzadeh, M., Agazadeh, M., Mokhtarzadeh, A., Rezaee, M.A., and Sadeghi, J. (2019) Bioassays: The best alternative for conventional methods in detection of *Legionella pneumophila*. *Int J Biol Macromol* **121**: 1295–1307.
- Monod, J. (1949) The growth of bacterial cultures. *Annu Rev Microbiol* **3**: 371–394.
- Oh, B.K., Lee, W., Bae, Y.M., Lee, W.H., and Choi, J.W. (2003) Surface plasmon resonance immunosensor for detection of *Legionella pneumophila*. *Biotechnol Bioproc E* **8**: 112–116.
- Omiccioli, E., Schiavano, G.F., Ceppetelli, V., Amagliani, G., Magnani, M., and Brandi, G. (2015) Validation according to ISO/TS 12869:2012 of a molecular method for the

- isolation and quantification of *Legionella* spp. in water. *Mol Cell Probes* **29**: 86–91.
- Orrison, L.H., Cherry, W.B., and Milan, D. (1981) Isolation of *Legionella-Pneumophila* from cooling-tower water by filtration. *Appl Environ Microb* **41**: 1202–1205.
- Ristroph, J.D., Hedlund, K.W., and Allen, R.G. (1980) Liquid-medium for growth of *Legionella-Pneumophila*. *J Clin Microbiol* **11**: 19–21.
- Rowbotham, T.J. (1980a) Pontiac fever explained? *The Lancet* **316**: 969.
- Rowbotham, T.J. (1980b) Preliminary-report on the pathogenicity of *Legionella-Pneumophila* for fresh-water and soil amoebas. *J Clin Pathol* **33**: 1179–1183.
- Rowbotham, T.J. (1983) Isolation of *Legionella pneumophila* from clinical specimens via amoebae, and the interaction of those and other isolates with amoebae. *J Clin Pathol* **36**: 978–986.
- Samuel, D., Harrison, T.G., and Taylor, A.G. (1988) Detection of *Legionella-Pneumophila* serogroup-1 urinary antigen using an enhanced chemi-luminescence elisa. *J Biol Chem* **263**: 251–251.
- Segal, G., and Shuman, H.A. (1999) *Legionella pneumophila* utilizes the same genes to multiply within *Acanthamoeba castellanii* and human macrophages. *Infect Immun* **67**: 2117–2124.
- Starnbach, M.N., Falkow, S., and Tompkins, L.S. (1989) Species-specific detection of *Legionella-Pneumophila* in water by DNA amplification and hybridization. *J Clin Microbiol* **27**: 1257–1261.
- von Stockar, U. (2010) Biothermodynamics of live cells: a tool for biotechnology and biochemical engineering. *J Non-Equilibrium Thermodyn* **35**: 415.
- Stout, J.E., Yu, V.L., and Best, M.G. (1985) Ecology of *Legionella pneumophila* within water distribution systems. *Appl Environ Microb* **49**: 221–228.
- Thomas, V., McDonnell, G., Denyer, S.P., and Maillard, J.-Y. (2010) Free-living amoebae and their intracellular pathogenic microorganisms: risks for water quality. *FEMS Microbiol Rev* **34**: 231–259.
- Tossa, P., Deloge-Abarkan, M., Zmirou-Navier, D., Hartemann, P., and Mathieu, L. (2006) Pontiac fever: an operational definition for epidemiological studies. *BMC Public Health* **6**: 112–112.
- Villari, P., Motti, E., Farullo, C., and Torre, I. (1998) Comparison of conventional culture and PCR methods for the detection of *Legionella pneumophila* in water. *Lett Appl Microbiol* **27**: 106–110.
- Wadsö, I., and Goldberg, R.N. (2001) Standards in isothermal microcalorimetry (IUPAC Technical Report). *Pure App Chem* **73**: 1625–1639.
- Ward, M., Boland, M., Nicolay, N., Murphy, H., McElhiney, J., Collins, C., et al. (2010) A cluster of Legionnaires' disease and associated Pontiac fever morbidity in office workers, Dublin, June–July 2008. *J Environ Public Health* **2010**: 463926–463926.
- Warren, W.J., and Miller, R.D. (1979) Growth of legionnaires disease bacterium (*Legionella-Pneumophila*) in chemically defined medium. *J Clin Microbiol* **10**: 50–55.
- WHO (2007) *Legionella and the prevention of legionellosis*. Geneva: WHO, p. 95.
- Winn, W.C., Cherry, W.B., Frank, R.O., Casey, C.A., and Broome, C.V. (1980) Direct immunofluorescent detection of *Legionella-Pneumophila* in respiratory specimens. *J Clin Microbiol* **11**: 59–64.
- Yu, V.L., Plouffe, J.F., Pastoris, M.C., Stout, J.E., Schousboe, M., Widmer, A., et al. (2002) Distribution of *Legionella* species and serogroups isolated by culture in patients with sporadic community-acquired legionellosis: an international collaborative survey. *J Infect Dis* **186**: 127–128.
- van der Zee, A., Verbakel, H., de Jong, C., Pot, R., Bergmans, A., Peeters, M., et al. (2002) Novel PCR-probe assay for detection of and discrimination between *Legionella pneumophila* and other *Legionella* species in clinical samples. *J Clin Microbiol* **40**: 1124–1125.

Supporting information

Additional supporting information may be found online in the Supporting Information section at the end of the article.

Fig. S1. Heat over time diagram. The black line describes the integrated heat signal determined by metabolic activity. The red line shows the Gompertz fit.

Fig. S2. The schematic structure of the ampoules for monitoring *L. pneumophila* growth.

Table S1. Summary of the physical quantities for calculating the total heat production.

3.2 Numerical heat flow and transport simulation as a development tool for the design of isothermal microcalorimeters

Fricke C, Klee T, Richter S, Paufler S, Harms H, Maskow T. (2021)

Numerical heat flow and transport simulation as a development tool for the design of isothermal microcalorimeters

Thermochim. Acta (submitted, Original research)

Significance: Detection of bacteria by calorimetric measurements is usually performed in commercial high-performance microcalorimeters with precise temperature control systems. Unfortunately, such calorimeters were designed for low detection limits of the heat flow and not for optimum bacterial growth. Since the smallest temperature differences need to be measured, it is essential to develop such a micro(bio-)calorimeter to gain as much information as possible about the calorimetric system during the design phase. Testing under laboratory conditions usually provides only little discrete information about the entire system, such as local temperature in the heat sink (determined by a temperature sensor). In order to overcome this issue, the submitted manuscript presents numerical heat flow and transport simulations of an early-stage micro(bio-)calorimetric test system specifically designed for routine microbiological analysis. The performance of the test system was investigated under laboratory conditions. Internal and external sensor data (time-dependent temperature and voltage profiles) were evaluated at local and discrete points within the system.

Further information, especially concerning spatially temperature distributions, was obtained from a reconstructed 3D numerical model of the test system. Numerical heat flow and transport simulations revealed weak points of the test system, which cannot be obtained under laboratory conditions. Experimental data validated the predictive power of the 3D numerical model. Finally, preliminary simulations addressing optimization of the test systems were conducted in advance.

Numerical heat flow and transport simulation as a development tool for the design of isothermal microcalorimeters

Christian Fricke¹, Toralf Klee², Sven Richter², Sven Paufler¹, Hauke Harms¹, Thomas Maskow¹

¹ Helmholtz Centre for Environmental Research – UFZ, Permoserstraße 15, 04318 Leipzig, Germany

² Loetec Elektronische Fertigungssysteme GmbH, Dresdener Straße 28, 06886 Lutherstadt Wittenberg

Abstract: Numerous processes in biology and chemistry are accompanied by heat emission or consumption, which can be measured by isothermal microcalorimetry in the nano- to microwatt range and used to quantify the corresponding stoichiometry and kinetics. Sometimes these applications require special isothermal microcalorimeter (IMC), which are unaffordable e.g. microbiological routine testing. The design, construction and optimization of an IMC can be tedious and cost-intensive. It is thus suggested to accelerate and fasten the development process by numerical simulation using the finite element method (FEM). The FEM provides a complete picture of all energy and material fluxes not only temporally but also spatially resolved, which are difficult to determine experimentally.

In the present work, numerical simulations starting from a rough computer design of an IMC test system were performed and combined with experimental investigations using a physical test system under laboratory conditions to better understand the heat flows in the IMC and to support the development process towards a high-performance customized IMC. A representative detailed 3D model of our physical test system was created and the numerical simulation results are compared by the measured data of the physical test system. Using our 3D numerical model, we can now simulate modifications to progressively enhance the performance of the current physical test system. We conclude that numerical simulations can help to reduce the time and costs associated with the development process of customised IMCs.

Keywords: Isothermal Microcalorimeter, CFD, heat flow and transfer, finite element method

Introduction

The development of high-performance isothermal microcalorimeters (IMCs) based on the heat conduction principle has a long tradition. The calorimeter developed first by Tian (1923) and further improved by Calvet (1948) can be seen as the beginning of modern IMCs [1-3]. The development process at that time is well documented by Calvet and Prat [4]. Since then several microcalorimeters for a wide variety of applications were designed and constructed [3, 5-12]. The focus of these works was on the design of components, the performance of heat flow sensors (tested by calibration) and the suppression of parasitic heat flows of the overall system [13-17]. Nowadays, hardly any making of process-specific calorimeters is described and the development of commercially available microcalorimeters is largely kept undisclosed [18] (except for those [19, 12]).

35 In general, an IMC is composed of a measurement unit that consists of three components: i) a
36 calorimetric vessel in which the investigated process takes place, ii) a heat sink whose temperature is
37 precisely regulated at the desired operating temperature and iii) a heat flow sensor, which links the vessel
38 and the heat sink [17, 20]. If there is a significant change in temperature caused by any physical,
39 chemical or biological reaction in the vessel, a temperature gradient is formed over the heat flow sensor
40 [1]. Heat flow from the vessel to the heat sink or vice versa correspond to an exothermic or an
41 endothermic reaction, respectively [5, 21]. Thermoelectric generators (*i.e.* thermopiles) were widely
42 employed as heat flow sensors [22]. To ensure measurements of heat flows in the range of a few
43 microwatts, the measurement unit has to be well isolated from the surrounding and parasitic heat flow
44 kept to a minimum. Besides, the temperature control unit has to precisely regulate the power output of
45 heating elements to achieve very accurate temperature stability [3].

46 Since the smallest temperature differences are measured, the temperature distribution in the entire
47 system plays a key role [19]. However, this is often difficult to capture during the construction process
48 due to the complexity of the calorimetric system and therefore only individual and local temperatures
49 of components can be measured by internal temperature probes (e.g. Pt100 sensors). Moreover, it may
50 prove difficult to quantify all relevant heat flow paths experimentally in full detail. To overcome this
51 bottleneck in the construction process of microcalorimeters, we propose to apply finite element method
52 (FEM) computational simulations as a development tool for IMCs. Briefly, in FEM the considered
53 object is split into many small but finite elements. For each element node, a set of ordinary and partial
54 differential equations (ODE and PDE) describing the underlying physical processes and characteristics
55 such as heat transfer, computation fluid flow (CFD), structural mechanics etc. are solved [23] based on
56 defined initial and boundary conditions [24].

57 Only a few published studies used numerical simulations to investigate heat transfer and temperature
58 distribution in microcalorimeters. For instance, Vilchiz et al. investigated the heat transfer during gas
59 dosing experiments in a 2D (two-dimensional) and 3D (three-dimensional) model of a Tian-Calvet
60 microcalorimeter [25]. In the numerical study of Koci et al., the calibration of a virtual 3D model of a
61 real isothermal heat flow calorimeter was simulated [26]. Gonzalez-Duran et al. performed numerical
62 CFD simulations of a 2D model to analyse the geometry of a combustion chamber for developing a
63 reference calorimeter [27]. These studies only addressed specific issues and selected components of the
64 respective instruments. To our knowledge, there are no numerical simulations that address the entire
65 complexity of an IMC, including the temperature control systems, and therefore might apply to any type
66 of customized IMC.

67 In order to examine the extent to which FEM can describe heat flows and temperature distributions in
68 an IMC and even be used for optimization, we developed a 3D numerical model in COMSOL
69 Multiphysics® and a corresponding real-world test system of an IMC specifically designed for
70 microbiological analysis. By performing numerical analyses of the 3D model and selected compounds
71 we were able to simulate the 3D temperature distribution in the entire calorimetric system and to test

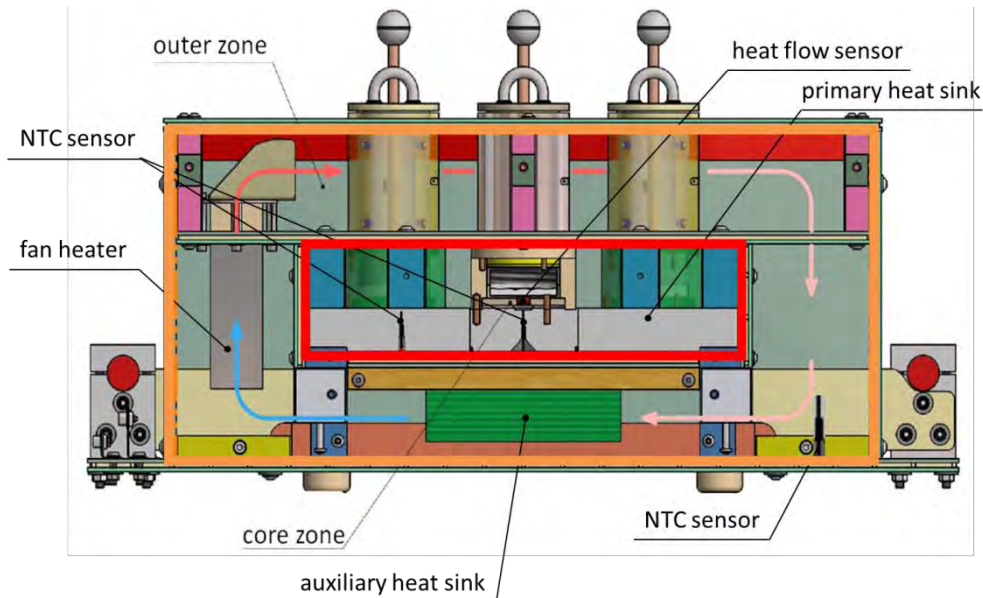
72 modifications of the system. Comparison of the simulations with temperature measurements at selected
73 points verified the adequacy of our model. Based on the comprehensive insight into the temperature
74 distribution in the system we were able to analyse the weak points of the test system as well as to
75 gradually introduce improvements.

76 **Material and Methods**

77 **Design of the IMC-test system**

78 The studied IMC-test system (670 x 351 x 261 mm) was manufactured by KEK GmbH and Loetec
79 Elektronische Fertigungssysteme GmbH. That system is divided into two separate thermal zones to
80 shield the measuring point from environmental temperature fluctuations (schematic section through the
81 instrument in Fig. 1). The borders of the outer zone are indicated by orange lines and those of the core
82 zone by red lines. Arrows in the outer zone indicate the direction of airflow caused by an internal fan
83 heater (Piccovent 70 W, RO/SE Blechverarbeitung GmbH & Co. KG, Bad Birnbach, Germany). The air
84 domain in the outer zone is heated by the heating element of the fan (Fig. 1 left). This heating element
85 is regulated by a PID controller. The actual temperature in the outer zone is measured by an internal
86 negative temperature coefficient (NTC) sensor (Amphenol Advanced Sensors Germany GmbH,
87 Pforzheim, Germany), which is located on the lower right side of the test system. The operating
88 temperature is set to 37 °C which is routinely used for many applications in microbiological analysis.
89 The IMC-test system has three measuring channels (arranged in a row). Each channel consists of an
90 upper part (aluminium) containing the sample holder (polyamide, PA) and a lower part (PA). The latter
91 is located in the core zone directly on top of the primary aluminium heat sink (300 x 300 x 30 mm). This
92 lower part of the channel encloses the actual measuring unit, a high-performance heat flow sensor (TGP-
93 651, Micropelt GmbH, Freiburg, Germany). The bottom of the heat flow sensors is thermally bonded to
94 the primary heat sink which provides a constant reference temperature for the sensor elements. Petri
95 dish like sample containers of different sizes and geometry can be placed on the top of the sensors and
96 thus fulfil the criteria for conventional microbiological analysis. Both the core as well as the outer zone
97 are surrounded by insulation plates (a sandwich construction made out of acrylonitrile butadiene styrene,
98 ABS, and air-filled honeycombs). The temperature of the heat sink is controlled via a PID control loop
99 using an NTC located directly below the central measuring channel as a sensor and a thermoelectric
100 cooler controller (LTC 1923, Linear Technology, Milpitas, California, USA) with two Peltier modules
101 (20 x 20 mm, CP60240, CUI Devices, Lake Oswego, Oregon, USA) as an actuator. The signal flow
102 diagram is shown in Fig. 2. An additional NTC sensor is located below channel 1. The heat generated
103 on the opposite side by the Peltier module is dissipated via the auxiliary heat sink (138 x 50 mm, SK466,
104 Fischer Elektronik GmbH & Co. KG, Lüdenscheid, Germany). In addition to those actuator Peltier
105 modules, two heater foils (THF-5095, Reichelt Elektronik, Sande, Germany) are used to support the

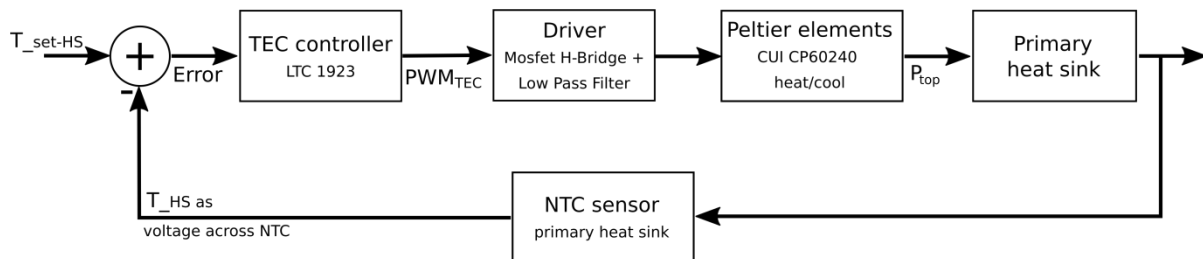
106 heat-up phase of the primary heat sink until the desired set temperature (37 °C) is reached (not shown
 107 in Fig. 1).



108

109 **Figure 1:** Section through the IMC-test system (orange line – outer thermal zone, red line – inner thermal zone).

110 The data acquisition and control unit with a graphical user interface is located in an external module
 111 connected to the IMC-test system. Temperature values and voltages of all NTC sensors and heat flow
 112 sensors, respectively, are displayed numerically and graphically in real time. All recorded data are stored
 113 in a database with the associated timestamp that can be assessed externally.



114

115 **Figure 2:** Signal flow diagram of the control loop in the microcalorimetric test system using the TEC controller, which regulates
 116 the temperature on the primary heat sink.

117 Experimental procedure

118 Performance test

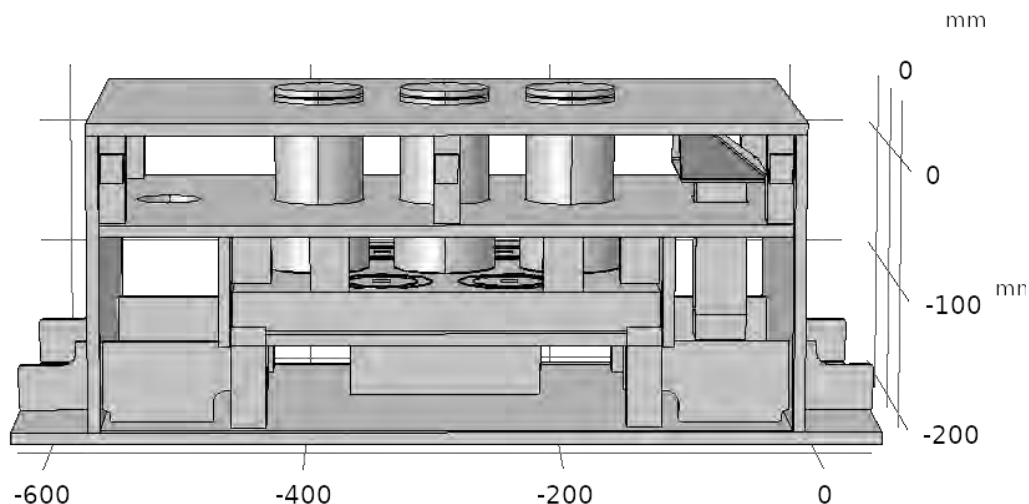
119 In order to determine the overall performance of the IMC test system, the calorimeter was run for approx.
 120 72 h (long-term response). All experiments started at room temperature (20 to 23 °C) to ensure equal
 121 starting conditions. During this test phase, the following parameters were determined: time to meet set-
 122 temperature of air and heat sink, the temperature stability of the heat sink as well as the performance of
 123 the heat flow sensors.

124 In addition to the three internal temperature measuring points, three flexibly positionable Pt100 sensors
 125 (1/3 DIN 4-wire thin-film platinum sensors connected to the LabBox (HiTec Zang GmbH,

126 Herzogenrath, Germany)) were installed to measure the temperature profile at various points in the test
127 system. The calorimeter was again tested for approx. 6 h (short-term response, sufficient to reach
128 thermal equilibrium) starting at room temperature. In this way, we were able to roughly map the
129 temperature distribution in the test system. All data, both internal and external, were evaluated in
130 *OriginPro* 2018 (OriginLab Corporation, Northampton, USA). For details, see supplementary material,
131 SM.

132 Numerical model of the IMC-test system

133 The FEM simulations were run on COMSOL[®] Version 5.5 (COMSOL Multiphysics GmbH, Göttingen,
134 Germany). Fig. 3 illustrates the three-dimensional geometry reconstructed in the simulation software.
135 The material assignment of all components is given in Tab. S1 in the SM. All components have been
136 created true to scale from a CAD design. The dimensions of the individual components were determined
137 in Autodesk[®] *Inventor Professional 2017* (Autodesk, Mill Valley, California, USA) and incorporated as
138 input for the creation of the 3D model in the simulation software.



139
140 **Figure 3:** The geometry of the 3D numerical model. Insulation plates were removed to visualise the internal details of the 3D
141 model.

142 Nevertheless, the following simplifications were made: insulation plates were rebuilt only of one
143 material instead of an air-filled sandwich structure. Holes, screws, wires and bar magnets were
144 neglected. The sample holder structure was simplified through a cylindrical stopper. Heat flow sensors,
145 Peltier modules, heater foils and the air heater were reconstructed simplified. The interior fan is
146 displayed as a square surface at the lower end of the air heater. These simplifications and neglections
147 have two reasons. First, the elements have little or no influence on the physical properties of the system.
148 Second, these fragmented components exhibiting many small domains, which would increase the
149 computation time enormously.

150 Modelling and simulation

151 The simulations were separated into two different phases. In the first phase, the performance and
152 interactions of the most important components were studied focusing on the heat sink configuration and

153 its temperature regulation via the Peltier modules and the respective feedback control loop (see chapter
 154 S4 and S5 in the SI). Here, the method for determining the control parameters is demonstrated. The
 155 obtained results are used for the control loop on the heat sink in the complete model simulation.
 156 Additionally, the temperature distribution in the upper part of the model was investigated in detail, as
 157 this strongly influences the behaviour of the measurement channels. For this purpose, the velocity
 158 magnitude of air flowing through the fan was first determined in a preliminary simulation (see for details
 159 chapter S6 in the SI). The numerical solution obtained then served as input for the simulations of the
 160 temperature distribution in the upper part.

161 The second phase analyses the temperature distribution of the complete test system. In particular, such
 162 temperature distributions are considered that cannot be obtained experimentally, such as on the heat sink
 163 or the cross-section through the entire test system. Therefore, all heating elements (see Tab. 1) and their
 164 control loops were included in the numerical simulation.

165

166 **Table 1:** Heat source components, their power output and control loop parameters applied in the numerical simulations

component	Parameters	controller	COMSOL implementation
Peltier ^a modules	$q_{\max} = 13.8 \text{ W}$, $q_{\min} = -13.8 \text{ W}$ $K_{p1} = 162$, $K_{i1} = 18$, $K_{d1} = 0$, $T_{t1}^c = 25 \text{ s}$, $T_{\text{set}1} = 310.22 \text{ K}$	PI	ODE and DAE interface, PID interface with domain point probe as input temperature
air heater ^b	$q_{\max} = 70 \text{ W}$, $q_{\min} = 0 \text{ W}$ $K_{p2} = 15.25$, $K_{i2} = 0.19375$ $K_{d2} = 75.5$, $T_{t2} = 5 \text{ s}$ $T_{\text{set}2} = 310.15 \text{ K}$	PID	ODE and DAE interface, PID interface with domain point probe as input temperature
heater foil	$q_{\text{on}} = 5 \text{ W const.}$	on-off	ODE and DAE interface, Event interface for on/off switch with domain probe as a temperature input

167 ^aPI controller parameters are determined in the present work.

168 ^bPID controller parameters were determined experimentally under laboratory conditions.

169 ^c time tracking constant

170

171 For simplicity, we assumed an on-off controller for the heating foils, although a PID controller was used
 172 in the test system because in practice the PID controller delivers almost 100% heating power below the
 173 setpoint and almost 0 % above it (see Fig. S4 in the SM).

174 For the consideration of all physical effects of influence, a programme in COMSOL using two interfaces
 175 was written. The airflow regime caused by an interior fan of the air thermostat was computed in
 176 stationary study steps using the *fluid flow* interface. For the sake of simplicity and to reduce
 177 computational effort, we assumed laminar flow. Heat transfer phenomena like conduction, natural and
 178 forced convection (the latter strongly occurred on the heat source of the fan heater) were mostly solved
 179 time-dependent in a second study step with the *heat transfer in solids and fluids* interface. Both

180 interfaces are coupled in the *non-isothermal* interface. In the case of the upper part, we performed one-
181 way coupled stationary studies of laminar flow and heat transfer, to reduce the computational time [28].

182 **Governing equations and boundary conditions**

183 ***Solid physics - Heat Transfer***

184 Solid physics are restricted to the *heat transfer* interface. The conductive heat flux is assumed to
185 dominate and to obey Fourier's law:

$$186 \quad q = -k\nabla T \quad (1)$$

187 Where k is the thermal conductivity (in $\text{W}\cdot\text{m}^{-1}\cdot\text{K}^{-1}$), q is the heat flux (in $\text{W}\cdot\text{m}^{-2}$) and ∇T is the
188 temperature gradient (in $\text{K}\cdot\text{m}^{-1}$). The development of the temperature field is computed by solving the
189 heat balance:

$$190 \quad \rho C_p \frac{\partial T}{\partial t} = \nabla \cdot (k\nabla T) + Q \quad (2)$$

191 Where ρ is the density (in $\text{kg}\cdot\text{m}^{-3}$), C_p the specific heat capacity ($\text{J}\cdot\text{kg}^{-1}\cdot\text{K}^{-1}$), and Q the sum of heat
192 sources (in $\text{W}\cdot\text{m}^{-3}$). All material-dependent constants used are provided in Tab. S1 in the SM. Potential
193 contributions of heat radiation are neglected. The following initial and boundary conditions were
194 defined. The initial temperature was set to 294.15 K (ambient temperature under laboratory conditions).
195 The heat exchange with the environment is assumed as convective heat flux q_0 (in $\text{W}\cdot\text{m}^{-2}$, eq. 3).

$$196 \quad q_0 = h \cdot (T_{\text{ext}} - T) \quad (3)$$

197 Where h is the heat transfer coefficient (in $\text{W}\cdot\text{m}^{-2}\cdot\text{K}^{-1}$) and T_{ext} the external temperature (in K). In order
198 to model laboratory conditions, h and T_{ext} were parameterized to $20 \text{ W}\cdot\text{m}^{-2}\cdot\text{K}^{-1}$ [25] and 294.15 K. All
199 heat sources were assigned by a heat rate P_0 (in W) that corresponds to the regulated power output. In
200 the case of the air heater and the Peltier modules, the heat rate is a variable of the implemented controller
201 algorithm (see Tab.1).

202 ***Fluid physics - Laminar Flow***

203 The physics of fluid motions are described by the Navier-Stokes equation (eq. 4, conservation of
204 momentum). By solving this equation together with the continuity equation (eq. 5, conservation of mass)
205 and the energy equation (eq. 6, conservation of energy) we can predict the air velocity, pressure and
206 temperature in our numerical model. To simplify the complex nature of fluid dynamics in our numerical
207 model, we made the following assumptions in respect to the fluid flow regime: i) incompressible, ii)
208 laminar and iii) steady. These assumptions were made mainly to reduce the computation time and to
209 achieve convergence of the numerical model. Further assumptions are made regarding the
210 incompressibility (see below). Viscous heating is neglected.

$$211 \quad \rho \mathbf{u} \cdot \nabla(\mathbf{u}) = -\nabla p + \mu \nabla^2 \mathbf{u} + F \quad (4)$$

$$\nabla \cdot \mathbf{u} = 0 \quad (5)$$

$$\rho C_p \frac{\partial T}{\partial t} + \rho C_p \mathbf{u} \cdot \nabla T = \nabla \cdot (k \nabla T) + Q \quad (6)$$

Where ρ (in $\text{kg} \cdot \text{m}^{-3}$), u (in m/s), p (in Pa) and μ (in $\text{Pa} \cdot \text{s}$), C_p (in $\text{J} \cdot \text{kg}^{-1} \cdot \text{K}^{-1}$), k (in $\text{W} \cdot \text{m}^{-1} \cdot \text{K}^{-1}$) are the fluid density, velocity, pressure, dynamic viscosity, specific heat capacity and thermal conductivity, respectively. T stands for the temperature. F and Q represent the volume force as well as the sum of all heat sources.

The fluid velocity is formed on the interior fan. The fan is defined as an interior boundary, which is composed of an in- and outlet [29]. Here, a pressure difference between the inlet and outlet of the fan caused the fluid velocity (eq. 7). The pressure difference is a function of static pressure, p_{nf} (in Pa) as well as flow rate, $V_{0,\text{fd}}$ (in $\text{m}^3 \cdot \text{s}^{-1}$).

$$\Delta p_{\text{pc}} = f(p_{\text{nf}}, V_{0,\text{fd}}) = [p - n^T K n + \rho (\mathbf{u} \cdot \mathbf{n})^2]_{\pm}^{\pm} \quad (7)$$

Where \mathbf{n} is the normal vector, ρ (in $\text{kg} \cdot \text{m}^{-3}$) the density, p (in Pa) the pressure. Both parameters were taken over from the datasheet of the fan (MagLev Motor fan, MF40202V1-1000U-A99, Sunon, Kaohsiung, Taiwan). We added an additional pressure point constraint to the air domain to define the reference pressure p_0 . Again, to obtain a unique numerical solution by solving the eq. 4-6 for our numerical model, we have to determine initial and boundary conditions. The velocity field $\mathbf{u}(t=0)$, as well as the reference pressure $p_0(t=0)$, was initially set to 0. Finally, by default settings, the no-slip boundary condition (eq. 8) on the walls is applied.

$$\mathbf{u} = 0 \quad (8)$$

This boundary condition considers that the velocity of the air domain becomes zero at the boundary. Due to the different heat sources, forced and natural convection is occurring in the fluid flow regime. Natural convection occurs through density variations caused by different temperature fields in the air domain. The latter phenomenon cannot physically be described by eq. 4. However, when gravity is considered, the Navier-Stokes equation is extended through the buoyancy force:

$$\rho \mathbf{u} \cdot \nabla(\mathbf{u}) = -\nabla p + \mu \nabla^2 \mathbf{u} + \rho \mathbf{g} \quad (9)$$

Using the Boussinesq-approximation (a detailed derivation is found in [30]) density variations in the buoyance term can be considered and the Navier-Stokes equation leads to:

$$\rho_0 \mathbf{u} \cdot \nabla(\mathbf{u}) = -\nabla P + \mu \nabla^2 \mathbf{u} - \rho_0 \frac{T - T_0}{T_0} \mathbf{g} \quad (10)$$

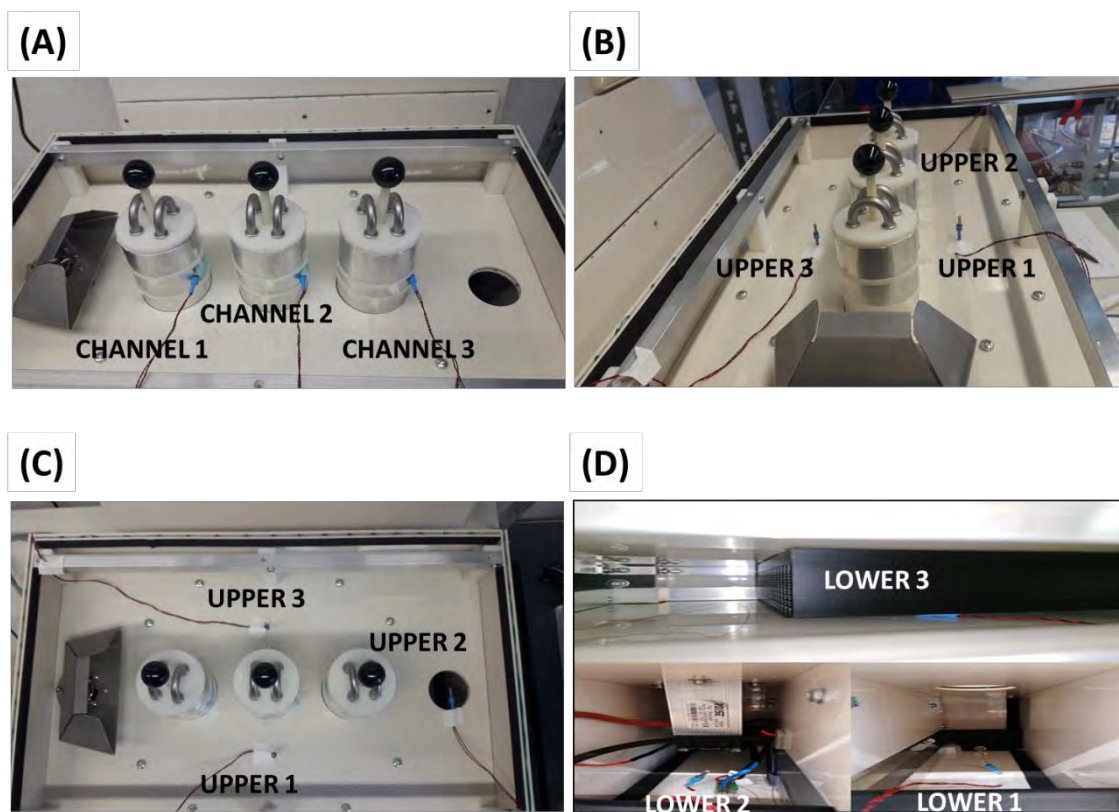
Where ρ_0 is the reference density (in $\text{kg} \cdot \text{m}^{-3}$), T_0 the reference temperature (in K), \mathbf{g} the gravitational constant, P represents the pressure shift (in Pa) expressed by the elevation h (in m):

242
$$P = p + \rho_0gh \tag{11}$$

243 **Results and discussion**

244 **Experimental performance test of the test system**

245 To investigate the overall performance of the test system, we evaluated the data obtained from the
 246 internal sensors (temperature and heat flow sensors) as well as from the supplementary (external) Pt100
 247 sensors. In total, we measured the local temperature at 12 different positions (all external positions are
 248 displayed in Fig. 4) and the generated voltage of the heat flow sensors. The obtained data were compared
 249 with the simulation results to validate the 3D numerical model.



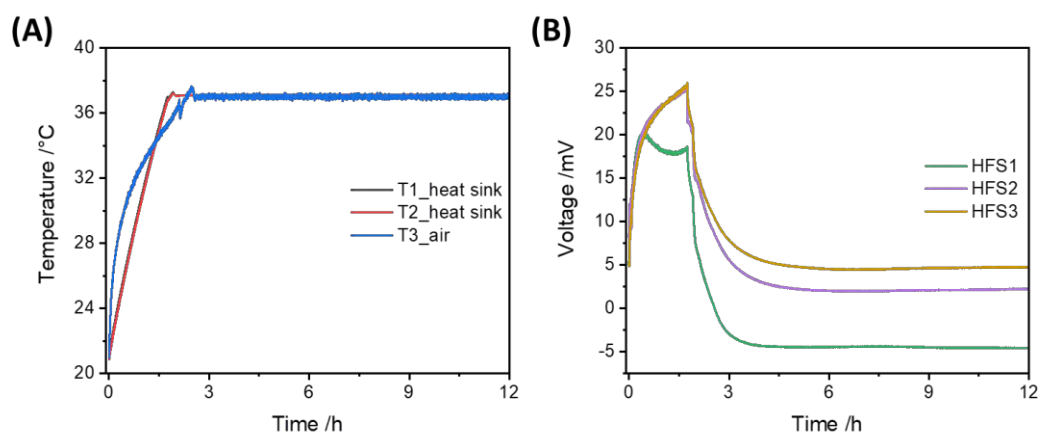
250
 251 **Figure 4:** Positions of all external temperature sensors located in the test system. **A):** Location of the Pt100 sensors connected
 252 to the channels. **B and C):** Location of the Pt100 sensors in the upper part of the test system. **D):** Location of the Pt100 sensors
 253 in the lower part of the test system.

254 **Evaluation of internal sensors**

255 Based on the signal flow diagram in Fig. 2, the measured temperatures on the heat sink and in the air
 256 domain were evaluated. The obtained temperature profiles are shown in Fig. 5A and the most valuable
 257 data (the heat flow) that can be internally extracted is the voltage of the heat flow sensors (HFS, Fig.
 258 5B). The voltage signal from the heat flow sensors U_{HFS} (in V) is given by:

259
$$U_{HFS} = \Delta T_{HFS} \cdot \alpha \tag{11}$$

260 Where α (in $V \cdot K^{-1}$) is the Seebeck coefficient and ΔT_{HFS} (in K) the temperature difference between the
 261 top and bottom of the HFS. Consequentially, the resulting voltage depends on material properties and
 262 the temperature gradient above the sensor. Since α is a constant it becomes obvious that fluctuations in
 263 the sensor signal are caused by temperature fluctuations occurring on the heat sink (in contact with the
 264 bottom side of the sensor) and the temperature of the air in the measuring chamber (in contact with the
 265 sensors top side). The desired operating temperature of $37\text{ }^{\circ}\text{C}$ was achieved after approx. 3 h (see Fig.
 266 5A). The mean air temperature (after thermal equilibration, considered time interval 6 to 72 h) was
 267 $(37.00 \pm 0.08)\text{ }^{\circ}\text{C}$. The mean heat sink temperature measured at the two NTC sensors (after thermal
 268 equilibration, considered time interval 6 to 72 h) were $(37.072 \pm 0.001)\text{ }^{\circ}\text{C}$ and $(37.107 \pm 0.001)\text{ }^{\circ}\text{C}$ (for
 269 details see SM).



270

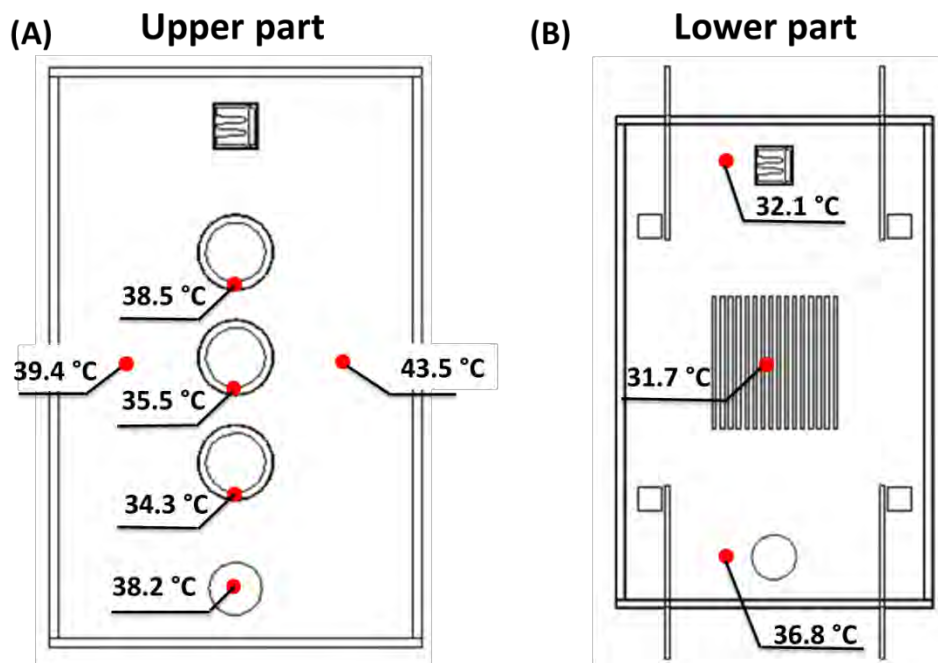
271 **Figure 5:** Summary of all obtained data from the internal sensors during the run-in phase of the test system. **A:** Temperature
 272 on the primary heat sink (T1_heat sink, black curve and T2_heat sink red curve) and of the flowing air (T3_air, blue curve). **B:**
 273 Generated voltage on the heat flow sensors (HFS1 green curve, HFS2, purple curve and HFS3 yellow curve).

274 After approx. 6 h a constant baseline at each HFS was achieved. Interestingly, the mean voltage signal
 275 varied strongly among the different HFS. The voltage profiles of HFS2 and 3 are almost equal. However,
 276 HFS1 showed the opposite profile. Even the sign between HFS1 as well as HFS2 and 3 is different. In
 277 general, two issues are affecting the generated voltages at the HFS. First, as mentioned earlier, there are
 278 time-dependent variations in temperature that have a direct impact on the variation of the voltage over
 279 time (detailed evaluation is given in the SI). In order to minimize such variations, better insulation to
 280 the environment and improved control of the temperature in the outer zone can be used. Second, signal
 281 differences between the three HFS are caused by spatial temperature gradients. Since U_{HFS} is
 282 proportional to ΔT_{HFS} (see eq. 11), we can calculate ΔT_{HFS} by using the Seebeck coefficient of the TEGs
 283 ($\alpha = 60\text{ mV} \cdot \text{K}^{-1}$). As a result, we obtained temperature differences for HFS 1 of -80 mK (the top is
 284 warmer than the bottom side), for HFS 2 of $+40\text{ mK}$ and for HFS 3 of $+100\text{ mK}$ (in both cases is the top
 285 colder than the bottom side). Unfortunately, from our experimental data, we cannot localize the cause
 286 of these temperature differences among the HFS. Therefore, FEM simulations are crucial to visualize
 287 spatial temperature gradients on the one hand and to test solutions by simulations in advance to improve
 288 the spatial temperature distribution on the other hand. The different voltage profiles, as well as the

289 differences in temperature between the heat flow sensors, will be explained in more detail when we
290 consider the corresponding heat transfer simulation results.

291 **Evaluation of external sensors**

292 Even if the internal data already revealed some information about the temperature distribution, this
293 information is mainly restricted to the inner zone of the test system. To obtain local temperatures in the
294 outer zone, we added external Pt100 sensors (see locations in Fig. 4). The mean steady-state
295 temperatures for the measuring point are mapped in Fig. 6. The corresponding temperature profiles are
296 given in the SM. By using the external sensors we get a more accurate estimation of the performance of
297 the test system and at the same time, we can use the measured temperatures for the validation of our
298 numerical model. By solving the heat transfer and fluid flow equations numerically in our 3D model,
299 we can explain the underlying causes of the measured effects by the internal and external sensors.



300

301 **Figure 6:** Steady-state temperatures of all external Pt100 sensors in the IMC test system. **A:** Local temperatures in the upper
302 part. Three sensors were placed on the wall of the channels. Two sensors were located next to the reference (Ch2) channel and
303 a third sensor was placed in the centre of the transition between the upper and lower part. **B:** Local temperatures in the lower
304 part. One sensor was located below the auxiliary heat sink. The second sensor was placed next to the internal NTC sensor that
305 measures the temperature in the outer zone and the third sensor was placed on at the level of the fan.

306 Figure 6 shows large temperature differences ranging from 31.7 °C (in the outer zone, lower part) to
307 43.5 °C (in the upper part, next to the reference channel 2). The lowest temperature (31.7 °C) is caused
308 by the Peltier modules that regulate the temperature of the primary heat sink. Since this cool spot is
309 below the core zone no influence on the performance of the overall IMC system is expected. However,
310 strong temperature differences were also observed in the upper part. Depending on the location of the
311 external Pt100 sensor (at the level of channel 2), temperature differences (in steady-state) of 4 °C were
312 observed (39.4 °C left side vs. 43.5 °C right side). Again, we will discuss the influence of these
313 deviations on the overall system in the context of the numerical simulation results. The temperature

314 difference between channel 1 and channel 2 or 3 can simply be explained by the lateral arrangement of
315 the channels related to the fan heater.

316 **Numerical results**

317 As the test system is restricted to three internal temperature probes that are used as input signals for the
318 temperature control loops. Only at those three discrete points, the temperature can be measured to
319 characterize the system. Consequentially, spatial temperature gradients, heat accumulations and thermal
320 bridges cannot be detected system-wide without installing additional sensors. However, all these
321 phenomena affect directly the performance and thus the sensitivity of heat flow measurements by the
322 sensors. Especially, variances regarding voltage signals between heat flow sensors remain inexplicable.
323 In the following, numerical results from two selected models are presented. In order to understand the
324 different behaviour of the heat flow sensors (see data obtained under laboratory conditions, Fig. 5B),
325 heat flow and transfer simulations of the upper part are conducted. Additionally, modifications of the
326 upper part are simulated in advance to demonstrate the predictive power of numerical simulations.
327 Finally, to get insight into the overall temperature distribution, the complete model was solved
328 numerically. Here, control parameters obtained from simulations of the control loop of the heat sink (see
329 chapter S4 and S5 in the SI) are used for this simulation. To validate our numerical results temperatures
330 are compared with experimental data.

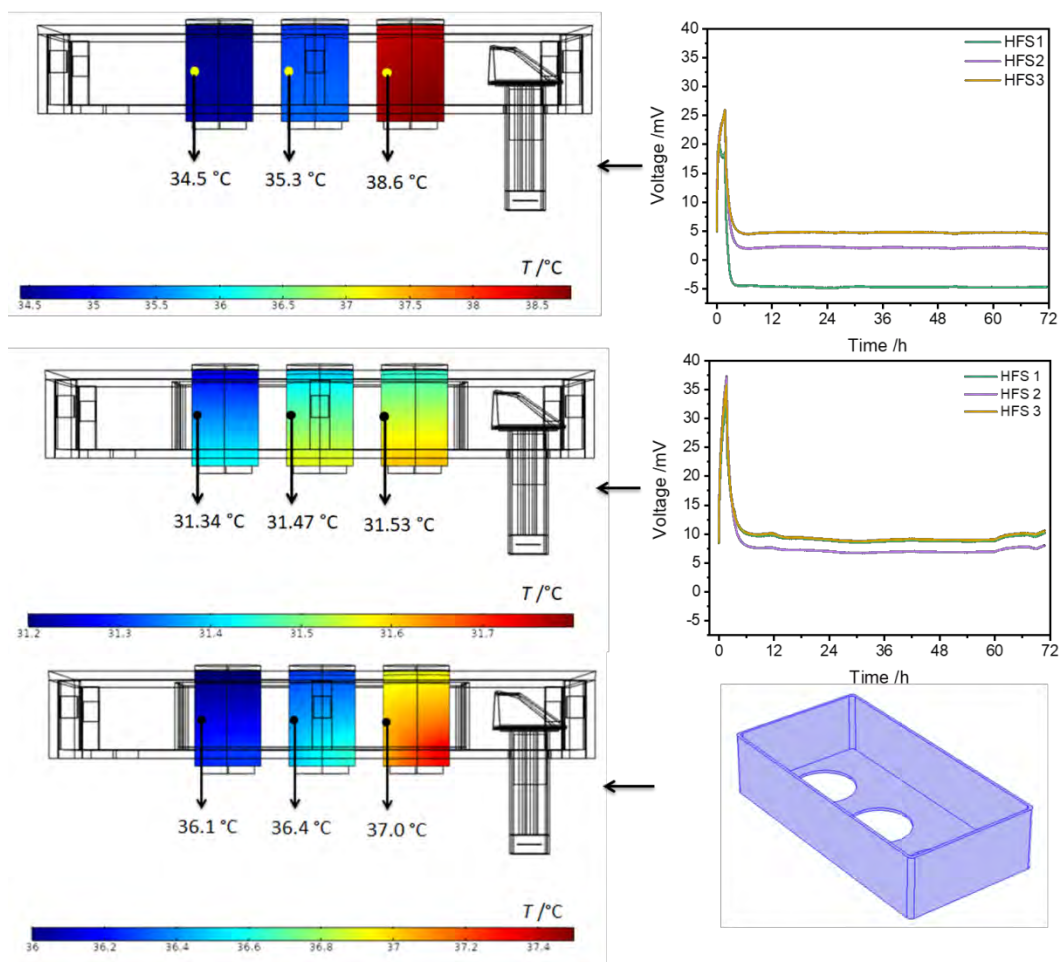
331 **Temperature distribution in the upper part**

332 As the experimental data already revealed, strong temperature gradients can be observed in the upper
333 part of the IMC test system (see Fig. 6A). Since the temperature of the channels has a significant effect
334 on the heat flow sensors, simulations were performed on the upper part of the calorimetric system. The
335 numerical results are validated by experimental data and possible modifications in the upper part are
336 simulated with the aim of lower temperature differences between the channels and thus more equal
337 responses of the heat flow sensor.

338 In a preliminary study, the velocity magnitude v (in $\text{m}\cdot\text{s}^{-1}$, the magnitude of the velocity vector u) on the
339 boundary condition that represents the interior fan in our numerical model was determined (for details
340 see SI). Through this study, we were able to implement the average velocity magnitude $v = 4.2 \text{ m}\cdot\text{s}^{-1}$
341 as an inlet boundary condition at the height of the fan position. Thereby, we simplified the entire
342 simulation to the upper part without having to recreate the complete airflow in the test system.
343 Consequentially, an outlet boundary condition was set at the transition between the upper and lower
344 part. The considered geometry of the upper part of the calorimeter is shown in Fig. 7. In a stationary
345 study, the local temperature distribution was simulated with particular emphasis on the temperature
346 profiles of the channels.

347 The temperature distribution across the channels for the initial test system is shown in Fig. 7A. The
348 numerical results are in good agreement with the experimental data and confirm the validity of the
349 simulated numerical model. Deviation between simulation and experimental data is only $0.2 \text{ }^\circ\text{C}$ (Fig.

350 7A). Those deviations can be attributed to (i) non-ideal heat flux boundary conditions, since under
 351 laboratory conditions ambient temperature may vary with time. (ii) The influence of the necessary
 352 simplifications concerning geometry and airflow (laminar flow and incompressible fluid). (iii) The mesh
 353 might be too coarse, thus strong gradients, as they occur especially at the heating element of the fan,
 354 cannot be modelled perfectly. The latter reason can be largely excluded because the simulations were
 355 carried out exemplarily with different meshes. Due to the accuracy of our model, we can simulate
 356 specific modifications to achieve a more uniform temperature distribution across the channels. The first
 357 approach is the protection of the channels by an aluminium shield (300 x 150 x 70 mm) with a thickness
 358 of 3 mm around the channels (see Fig 7C). The corresponding numerical solution (Fig. 7B) shows a
 359 much more uniform temperature distribution. However, the simulated temperature (approx. 31.5 °C) is
 360 far away from the desired temperature (37 °C).
 361



362
 363 **Figure 7:** Numerical solutions of the temperature distribution among the channels obtained from the one-way coupled
 364 stationary studies. **A:** Temperature volume plots of the channels in the original reconstruction of the upper part. Next to it,
 365 the experimentally measured voltage curves in this configuration **B:** Temperature volume plots of the channels in a modified
 366 reconstruction of the upper part by adding a frame around the channels. Next to it, the experimentally measured voltage curves
 367 in this modified configuration **C:** Temperature volume plots of the channels in a modified reconstruction of the upper part by
 368 adding a frame with a bottom plate around the channels. Next to it, the geometry of this frame with the bottom plate.

369 Experimental data of this configuration confirms the simulation with a temperature difference among
370 the channels of approx. 1 °C ($T_{\text{ch1}} = 33.5$ °C, $T_{\text{ch3}} = 32.7$ °C, $T_{\text{ch2}} = 32.4$ °C). This behavior can be
371 attributed to the fact that by inserting the frame, the channels are surrounded by stagnant air, which is a
372 poor heat conductor. However, this modification leads also to a drastically reduced difference in the
373 generated voltage by the heat flow sensor performance. Moreover, by the fact that the channels are now
374 colder, the offset of the voltage is correspondingly higher, which correlated very well with the
375 experimental data (see Fig.7B). Here, one possibility might be to change the position of the temperature
376 probe in close contact with the aluminium shield.

377 To overcome this temperature issue, we simulated in another study a modified frame with a 3 mm thick
378 bottom plate as a heat conductor (geometry is shown in Fig. 7C). This time, we achieved a temperature
379 difference of 0.9 °C (Fig. 7C) which is slightly worse than the solution without the bottom plate (0.2
380 °C) but deviates from the desired temperature of 37 °C by only approx. 0.6 to 0.9 °C. Further approaches
381 and modifications can easily be simulated on this model to optimize the temperature value and
382 variations.

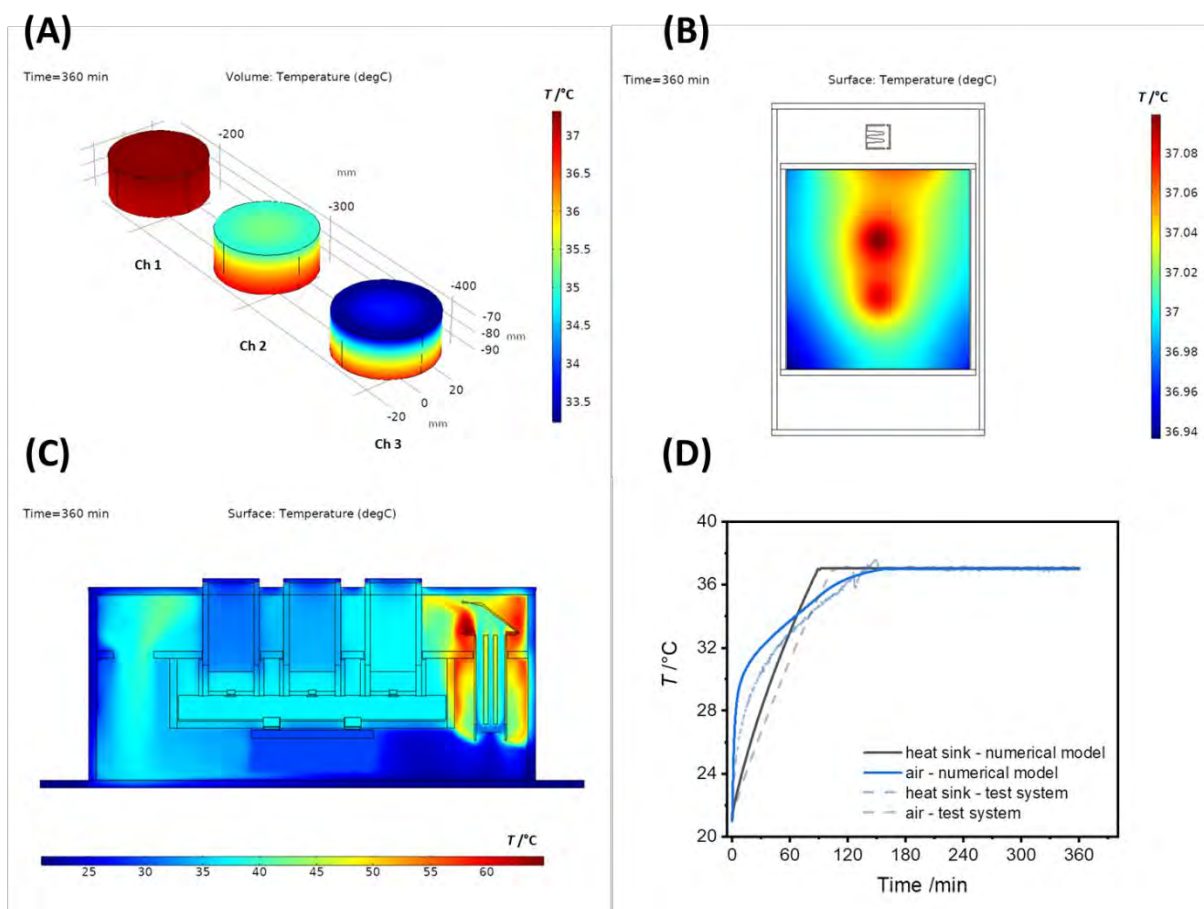
383 **Heat transfer and fluid flow simulations of the complete model**

384 In a final simulation, we reconstructed a complete 3D model of the initial test system (without any
385 modifications) in the simulation software (see Fig. 3) and performed numerical simulations to
386 investigate the overall temperature distribution. A particular selection of the simulation results is
387 gathered in Fig. 8 and 9.

388 In Fig. 8 volume and surface plots of the temperature distribution of selected compounds or parts of the
389 test system in 2 and 3D model are displayed. Additionally, the simulated temperature profile in the outer
390 zone and on the heat sink are compared with the experimental data (Fig. 8D). Fig. 8A shows the
391 simulated temperature variations across the channels in which the samples are finally placed on the heat
392 flow sensors. Based on these temperature plots, we can easily explain the observed different behavior
393 of the heat flow sensors (Fig. 5B). Additionally, entering a sample vessel into the measuring position
394 should increase the voltage signal of the heat flow sensors, since the temperature gradient in the
395 measuring chamber is transferred to the sample vessel. We observed this behavior in some preliminary
396 tests under laboratory conditions (data not shown).

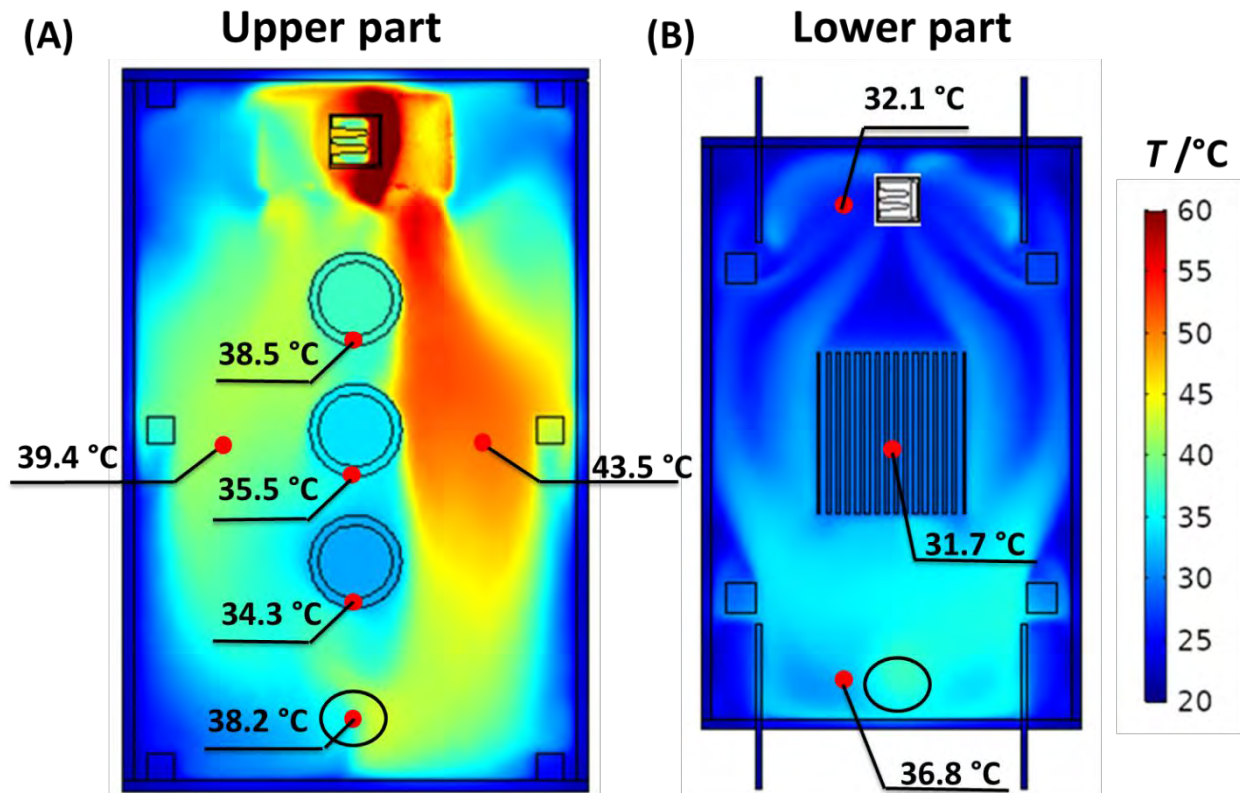
397 Fig. 8B shows a surface plot of the temperature distribution of the heat sink. The asymmetric temperature
398 distribution can be explained by the heat released by the fan heater (hot spot on the right side in Fig.
399 8C). The fan heater affects the temperature distribution on the heat sink. Here we can observe a strong
400 heat accumulation, which consequently influences the temperature on the right side of the heat sink by
401 convection. Two hotspots on the heat sink can be revealed by the numerical simulation. These
402 correspond to the position of the two Peltier modules below the heat sink. The temperature distribution
403 among the channels shown in Fig. 8C is in good agreement with the corresponding numerical data (see
404 Fig. 7). Additionally, the cooling effect of the auxiliary heat sink becomes visible. As a result, a cold
405 spot in the right corner of the device is created. The cold air has to be heated up again by the air heater.

406 In Figure 8D, we compared the numerical solution of the temperature increase measured by the internal
 407 probes with experimental data under laboratory conditions. Numerical simulations showed good
 408 agreement with the experimental data. The setpoint temperature is reached a bit earlier, especially for
 409 the temperature in the inner zone. This can be attributed to better insulation of the numerical model
 410 compared to the real world test system. Additionally, the Peltier modules heat with a constant power in
 411 the numerical model, whereas in the test system the heating power is influenced by the temperature-
 412 dependent Seebeck effect. Further deviations were already discussed and can be mainly attributed to the
 413 poor mesh quality of the air domain.



414
 415 **Figure 8:** Surface and volume plots of selected compounds from the complete 3D model obtained by numerical simulations.
 416 **A:** volume plot of the enclosed air volume in the lower part of the channel. **B:** surface plot of a cross-section through the heat
 417 sink. **C:** surface plot of a vertical cross-section through the complete 3D model. **D:** surface plot of a horizontal cross-section
 418 through the upper part.

419 Finally, Fig. 9 compares the numerical results of the steady-state (achieved after 360 min) with the
 420 experimental data from external temperature sensors. The surface plots are combined and mapped to
 421 local temperatures from the external sensors. A qualitative observation shows that numerical results are
 422 in good accordance with experimental data. These results together with the results from Fig. 8
 423 demonstrate the superiority of numerical simulations. On the one hand, using standard laboratory
 424 equipment (*i.e.* mainly temperature sensors) only a few local temperatures can be captured. On the other
 425 hand, numerical simulations provide simultaneously and time-dependent data available at each point
 426 within the considered geometry. Thus, spatial gradients can be visualized.



427

428 **Figure 9:** Comparison of numerical solutions of the 3D numerical model with experimental data obtained from the IMC test
 429 system under laboratory conditions. **A:** Mapped local temperatures in the upper part of the calorimetric test system. **B:** Mapped
 430 local temperatures in the lower part of the calorimetric test system.

431 Conclusion

432 The design and construction of isothermal microcalorimeters (IMC), whether for special applications or
 433 commercial multipurpose instruments, pose enormous challenges to the developer or manufacturer. Tiny
 434 heat fluxes in the range of a few microwatts or even nanowatts have to be measured. This places the
 435 highest demands on the temperature constancy of an IMC. During the development process of such an
 436 instrument early constructed test systems, prototypes and finally production device are built and tested
 437 under laboratory conditions. From an experimental point of view, only a few parameters such as local
 438 temperatures through e.g. Pt100 sensors, the control behavior of heating or cooling elements and the
 439 performance of the heat flow sensors can be recorded. Comprehensive temperature distributions in the
 440 entire system or selected components of it, local hotspots and their impact on the performance of the
 441 device remain mostly uncovered. However, these are crucial if the overall IMC system is to be
 442 optimized.

443 In the present study, we were able to demonstrate that numerical simulations can support experimental
 444 data and provide deeper insights into the contribution of single components to the overall performance
 445 of the entire system. Based on an IMC test system that is specifically designed for microbiological
 446 analysis, we determined in numerical simulations control parameters for a PI controller which regulates
 447 the temperature on the heat sink. Further, we investigated the temperature distribution among the

448 channels in the upper part of the 3D model. Here, we simulated the first modifications to investigate
449 their impact on the temperature homogeneity between the channels. Finally, we performed a time-
450 dependent simulation of the complete 3D model to obtain numerical data for the entire system. The
451 advantages of such numerical simulations are:

452 First, the time saved in determining control parameters for the different controller and their interplay.
453 For example, the windup or the influence of individual control variables on the control behavior can be
454 excellently investigated in this way.

455 Second, weak points of a test system can be visualized at an early stage and, depending on the
456 complexity of the 3D model, quantified to a certain extent. In this way, a better understanding of the
457 complex interplay of heat fluxes, temperature distributions and fluid dynamics in the entire IMC system
458 can be achieved.

459 Third, failure to design both specialized and multipurpose IMCs represents not only a considerable delay
460 for the respective research task but also an economic risk. Using simulations, it is conceivable to first
461 design and optimizes an IMC *in silico* and later builds it only if the required performance parameters
462 are predicted.

463 **Acknowledgments**

464 The authors thank the Federal Ministry for Economic Affairs and Energy and the German Federation of
465 Industrial Research Associations for the financial support of this research under the grant number
466 (ZF4315807RH7). We would also like to thank Hartwin Lier (KEK GmbH) for design and construction
467 of the microcalorimetric test system and Bernd Herrmann (UFZ) for the administrative support during
468 the simulations.

469 **Author Contributions**

470 **Christian Fricke:** Conceptualization, Methodology, Investigation, Writing - Original Draft,
471 Visualization, Formal analysis **Sven Richter:** Conceptualization, Software, Resources **Toralf Klee:**
472 Conceptualization, Software, Resources. **Sven Paufler:** Conceptualization, Visualization, Writing -
473 Review & Editing **Hauke Harms:** Supervision, Writing - Review & Editing **Thomas Maskow:**
474 Conceptualization, Supervision, Writing - Review & Editing.

475 All authors reviewed the manuscript and agreed with the content.

476 **Literature**

477

478 1. Wadsö, L. Isothermal Microcalorimetry. Current problems and prospects. *Journal of Thermal*
479 *Analysis and Calorimetry* **64**, 75–84 (2001). <https://doi.org/10.1023/A:1011576710913>.

- 480 2. Attree RW, Cushing RL, Ladd JA, Pieroni JJ. Differential Calorimeter of the Tian - Calvet Type.
481 *Review of Scientific Instruments*. **29**, 491-6 (1958). <https://doi.org/10.1063/1.1716233>.
- 482 3. Sarge SM, Höhne G, Hemminger W. *Calorimetry: Fundamentals, Instrumentation and*
483 *Applications*. Wiley-VCH: Weinheim, Germany, 2014.
- 484 4. Calvet E, Prat H. *Recent Progress in Microcalorimetry*. (ed) Skinner HA. Pergamon Press: Oxford.
485 1963.
- 486 5. Wadso I. Design and Testing of a Micro Reaction Calorimeter. *Acta Chemica Scandinavica*. **22**,
487 927-37 (1968). <https://doi.org/10.3891/acta.chem.scand.22-0927>.
- 488 6. Evans WJ, McCourtney EJ, Carney WB. A Microcalorimeter Using Semiconductors as the Sensing
489 Elements. *Instrumentation Science & Technology*. **2**, 249-55 (1969).
490 <http://doi.org/10.1080/10739146908543280>.
- 491 7. Stott JB. An isothermal micro-calorimeter. *Journal of Scientific Instruments*. **33**, 58-63 (1956).
492 <https://doi.org/10.1088/0950-7671/33/2/304>.
- 493 8. Ishikawa Y, Shoda M, Maruyama H. Design and performance of a new microcalorimetric system
494 for aerobic cultivation of microorganisms. *Biotechnology and Bioengineering*. **23**, 2629-40 (1981).
495 <https://doi.org/10.1002/bit.260231118>.
- 496 9. Bauer S, Ploss B. Design and properties of a microcalorimeter. *IEEE Transactions on Electrical*
497 *Insulation*. **27**, 861-6 (1992). <https://doi.org/10.1109/14.155811>.
- 498 10. Moreno-Pirajan JC, Gutierrez LG, Ordonez AG. A batch-type heat conduction microcalorimeter
499 for immersion heat determinations: design, calibration and applications. *Thermochimica Acta*. **290**, 1-
500 12 (1997). [https://doi.org/10.1016/S0040-6031\(96\)03066-3](https://doi.org/10.1016/S0040-6031(96)03066-3).
- 501 11. Wadsö, I., Wadsö, L. A second generation twin double microcalorimeter. *Journal of Thermal*
502 *Analysis and Calorimetry* **49**, 1045–1052 (1997). <https://doi.org/10.1007/BF01996792>
- 503 12. Wadsö I, Hallén D, Jansson M, Suurkuusk J, Wenzler T, Braissant O. A well-plate format
504 isothermal multi-channel microcalorimeter for monitoring the activity of living cells and tissues.
505 *Thermochimica Acta*. **652**, 141-149 (2017). <https://doi.org/10.1016/j.tca.2017.03.010>.
- 506 13. Parrillo DJ, Gorte RJ. Design parameters for the construction and operation of heat-flow
507 calorimeters. *Thermochimica Acta*. **312**, 125-32 (1998). [https://doi.org/10.1016/S0040-](https://doi.org/10.1016/S0040-6031(97)00446-2)
508 [6031\(97\)00446-2](https://doi.org/10.1016/S0040-6031(97)00446-2).
- 509 14. Zhang WS. Construction, calibration and testing of a decimeter-size heat-flow calorimeter.
510 *Thermochimica Acta*. **499**, 128-32 (2010). <https://doi.org/10.1016/j.tca.2009.11.013>.
- 511 15. Chen A-t, Wadsö I. A test and calibration process for microcalorimeters used a thermal power
512 meters. *Journal of Biochemical and Biophysical Methods*. **6**, 297-306 (1982).
513 [https://doi.org/10.1016/0165-022X\(82\)90011-2](https://doi.org/10.1016/0165-022X(82)90011-2).
- 514 16. X. Cui, Y. Li, X. Gao, A new design and evaluation technique of a microcalorimeter, *2012*
515 *Conference on Precision electromagnetic Measurements*, 736-738 (2012).
516 <https://doi.org/10.1109/CPEM.2012.6251140>.

- 517 17. Khaw MK, Mohd-Yasin F, Nguyen NT. Microcalorimeter: Design considerations, materials and
518 examples. *Microelectronic Engineering*. **158**, 107-17 (2016).
519 doi:<https://doi.org/10.1016/j.mee.2016.03.050>.
- 520 18. Hansen LD, Russell DJ. Which calorimeter is best? A guide for choosing the best calorimeter for a
521 given task. *Thermochimica Acta*. **450**,71-2 (2006). <https://doi.org/10.1016/j.tca.2006.08.001>.
- 522 19. Suurkuusk, J., Suurkuusk, M. & Vikegard, P. A multichannel microcalorimetric system. *Journal of*
523 *Thermal Analysis and Calorimetry* **131**, 1949–1966 (2018). [https://doi.org/10.1007/s10973-017-6684-](https://doi.org/10.1007/s10973-017-6684-7)
524 7.
- 525 20. Wadso L, Smith AL, Shirazi H, Mulligan SR, Hofelich T. The isothermal heat conduction
526 calorimeter: A versatile instrument for studying processes in physics, chemistry, and biology. *Journal*
527 *of Chemical Education*. **78**, 1080-6 (2001). <https://doi.org/10.1021/ed078p1080>.
- 528 21. Wadso I, Goldberg RN. Standards in isothermal microcalorimetry (IUPAC technical report). *Pure*
529 *and Applied Chemistry*. **73**, 1625-39 (2001). <https://doi.org/10.1351/pac200173101625>.
- 530 22. Giraldo L, Moreno JC. Thermal and Electric Characterization of the Sensor System in the
531 Microcalorimetry of Heat Conduction. *Instrumentation Science & Technology*. **28**, 223-31 (2002).
532 <https://doi.org/10.1081/CI-100100973>.
- 533 23. Rao SS. Chapter 1 - Overview of Finite Element Method. In: Rao SS, editor. *The Finite Element*
534 *Method in Engineering (Fifth Edition)*. Boston: Butterworth-Heinemann; 2011. p. 3-50.
- 535 24. Pepper DW, Heinrich JC. *The finite element method : basic concepts and applications with*
536 *MATLAB, MAPLE, and COMSOL*. 2017.
- 537 25. Vilchiz LE, Pacheco-Vega A, Handy BE. Heat-flow patterns in Tian–Calvet microcalorimeters:
538 Conductive, convective, and radiative transport in gas dosing experiments. *Thermochimica Acta*.
539 **439**,110-8 (2005). <https://doi.org/10.1016/j.tca.2005.09.014>.
- 540 26. Koci V, Madera J, Jerman M, Cerny R. Computational analysis of heat transport and storage
541 processes in large-volume isothermal heat flow calorimeter. *Applied Thermal Engineering*. **121**, 547-
542 53 (2017). <https://doi.org/10.1016/j.applthermaleng.2017.04.118>.
- 543 27. Gonzalez-Duran JEE, Zamora-Antunano MA, Lira-Cortes L, Rodriguez-Resendiz J, Olivares-
544 Ramirez JM, Lozano NEM. Numerical Simulation for the Combustion Chamber of a Reference
545 Calorimeter. *Processes*. **8**, 575 (2020). <https://doi.org/10.3390/pr8050575>.
- 546 28. Oberdorfer P. *How to Save Computational Time with One-Way Coupling Approach*. 2017.
547 Accessed 26.05.2021.
- 548 29. COMSOL Multiphysics®. *CFD Module User's Guide 5.5*.
549 <https://doc.comsol.com/5.5/doc/com.comsol.help.cfd/CFDModuleUsersGuide.pdf>. Accessed
550 26.05.2021.
- 551 30. COMSOL Multiphysics. *The Boussinesq Approximation*. 2015.
552 <https://www.comsol.com/multiphysics/boussinesq-approximation>. Accessed 26.01.2021.

3.3 Further experiments related to instrument development and selective detection of bacteria

The following unpublished results deal with the ongoing development of the calorimetric test system and the first applications of monitoring bacterial growth by improved versions of the test system. In the final section of the experimental part of this thesis, unpublished experiments related to the selective detection of *L. pneumophila* from drinking water samples by IMC are given. The selectivity of calorimetric detection of frequent accompanying pathogens in drinking water such as *E. coli*, *P. aeruginosa* and *E. faecalis* is investigated.

3.3.1 Development process towards an improved calorimetric test system

As part of the development processes for the test system, numerical simulations were performed in addition to experimental measurements under laboratory conditions. Through such simulations, the spatially resolved temperatures of the entire test system were visualized (**section 3.2**). Thus weaknesses caused mainly by the arrangement of the channels concerning the air thermostat were revealed. Experimental temperature measurements at discrete points in the test system confirmed the accuracy of the numerical simulation. Hence, it was possible to make initial modifications to the test system during the development process (adding an aluminium shield around the channels) to improve the performance of the calorimeter (1st modified version of the test system). In order to understand the entire development process over time, **Figure 9** shows a flow chart, starting with the first design concept and ending with the final version of the current test system (3rd modified version).

Despite these numerical simulations, experiments under laboratory conditions show that the insulation to the ambient of the test system is insufficient (see microbiological measurements in **section 3.3.2**). For instance, more substantial fluctuations appear in the first measurement channel independently of the aluminium shield around the channels. These fluctuations are strongly linked to the fan heater and the overall insulation of the test system. The better the temperature can be maintained in the test system (good insulation from the ambient), the less the output of the fan heater will fluctuate. As a result, small fluctuations in the channels are also to be expected. Therefore, further modifications are made to the test system affecting the insulation to improve the temperature stability in the overall system. Thus, the 2nd modified version of the test system includes a Styrofoam box placed around the entire calorimetric unit. In addition, a bottom plate is added to the aluminium frame in the upper part of the test system. The heat of the frame should be transferred to the channels through the bottom plate. The Styrofoam box is somewhat bulky and takes up much space. Therefore, improved insulation to the ambient is achieved by sticking 40 mm Styrofoam panels around the original test system (3rd modified version).

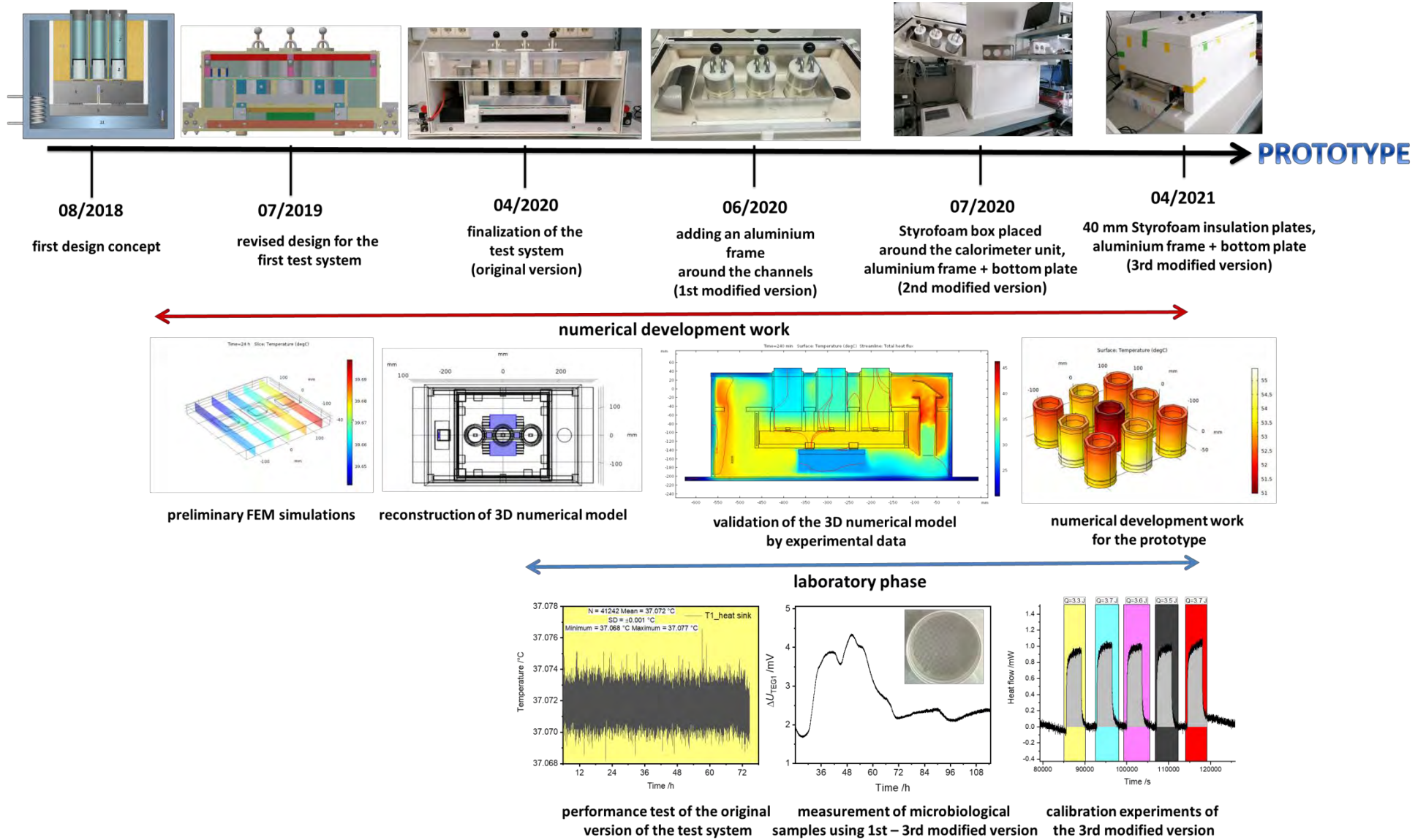


Figure 9: Summary of the chronological progression of the calorimeter development.

In order to demonstrate the influence of modifications on the performance of the calorimeter, the temperature profiles (**Figure 10**) and voltage profiles (**Figure 11**) of the heat flow sensors are compared between the original and 3rd modified version of the test system (under almost equal laboratory conditions, room temperature was approx. $(20 \pm 1) \text{ }^\circ\text{C}$). Due to the additional insulation in the modified test system, the temperature stability is enormously improved. Now the maximum fluctuations are approx. $\pm 0.1 \text{ }^\circ\text{C}$ compared to $\pm 0.3 \text{ }^\circ\text{C}$ in the original test system (**Figure 10A**). In contrast, the heat sink is less affected by the modification, which indicates that good insulation to the outer zone has already been established with the original design. Nevertheless, slightly better temperature stability can be recognized (**Figure 10B**). This improvement is also reflected in the percentage power output of each heating element. The fan heater has reduced its heating output from 35 % to approx. 15 % (maximum fluctuations only $\pm 5 \%$, **Figure 10C**). Consequentially, the power output of the Peltier modules was also reduced and more stable in the 3rd modified test system (**Figure 10D**).

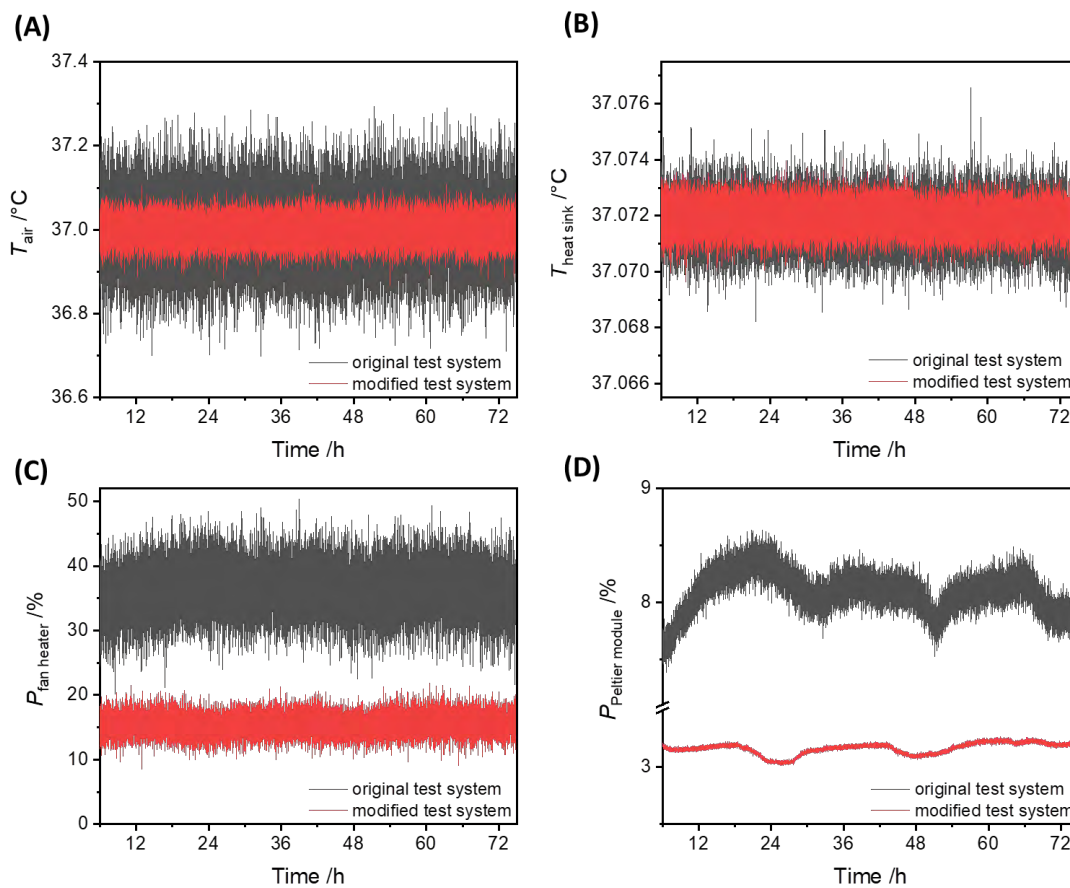


Figure 10: Comparison of internal sensor data between the original test system and the 3rd modified version. **A:** Temperature profiles of the air measured by the internal NTC sensor in the outer zone. **B:** Temperature profiles of the heat sink measured by the internal NTC sensor located below the reference channel. **C:** Percental power output of the fan heater. **D:** Percental power output of the Peltier modules, which regulate the temperature on the heat sink (unpublished data).

Since the heat flow sensors are the most crucial component of an isothermal microcalorimeter, the impact of the abovementioned modifications on the voltage profile of the heat flow sensor is given in **Figure 11**. Here, the differential signals ΔU (in mV) of the heat flow sensor 1, HFS1 (in channel 1) and HFS3 (in channel 3) are displayed. In order to obtain a net value, the reference signal of HFS2 (in channel 2) was subtracted from the signal of HFS1 and 3, respectively. Due to the modification of the test system (3rd modified version), two changes from the original configuration can be identified. First, HFS1 shows only minimal fluctuations (compare yellow and green curves). This reduction in fluctuations results from the aluminium shield around the channels so that the heated air of the fan heater no longer directly affects channel 1 (see **section 3.2**). Second, the offsets of HFS 1 and 3 are now closer to 0 mV. This change can be attributed to a better temperature distribution among the channels caused by the bottom plate. Especially between channel 1 and the reference channel (channel 2) since the resulting ΔU_{HFS1} is approx. 0 mV. The larger offset of HFS 3 (0.76 mV) results from a temperature gradient along with the bottom plate. The baseline stability over 24 h (determined in the interval from 24 to 48 h) in the original test system is ± 0.1 mV (HFS 1) and ± 0.04 mV (HFS 2). In the modified version, the baseline stability is ± 0.01 mV (HFS1) and ± 0.03 mV (HFS 2) in the same time interval.

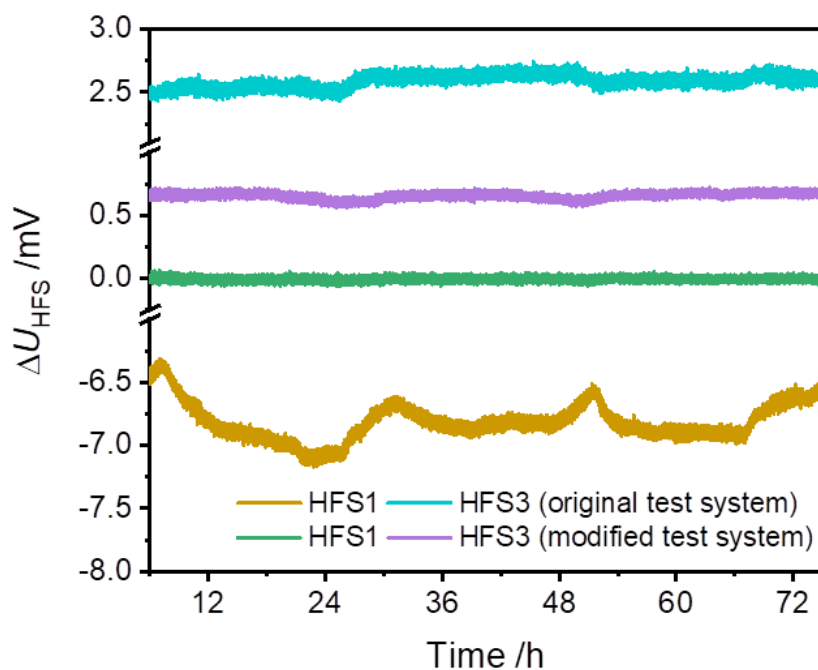


Figure 11: Internal heat flow sensor data in the original test system and the 3rd modified version (unpublished data).

Based on the experimental data of the modified test system, it can be seen that both temperature stability and the performance of the heat flow sensors needs to be improved. All these data, together with

the ongoing numerical development work, will be incorporated into the design of the planned prototype.

Finally, electrical calibration experiments are conducted, and the 3rd modified version of the test system is further characterized (**Figure 12**). A uniquely prepared calorimetric vessel equipped with a $100 \Omega \pm 0.1 \%$ precision thin film chip resistor (Vishay Serie PCAN, Vishay Intertechnology, Malvern, Pennsylvania, US) and a dummy stopper (made out of polyvinyl chloride) are used in these kind of experiments (**Figure 12A**). Steady-state calibrations ($P = 1 \text{ mW}$ for 60 min) with five replicates were measured (**Figure 12B**). For each measurement, the $\Delta\Delta U$ -value was determined after reaching steady-state (**Figure 12C**). From this, the experimental calibration constant is $\varepsilon_{\text{exp}} = 1.7 \text{ W V}^{-1}$. Additionally, the integration provides the total amount of heat released during these experiments (theoretically 3.6 J). This total heat could also be confirmed experimentally and was on average $(3.6 \pm 0.4) \text{ J}$ for channel 1 and $(3.6 \pm 0.1) \text{ J}$ for channel 3.

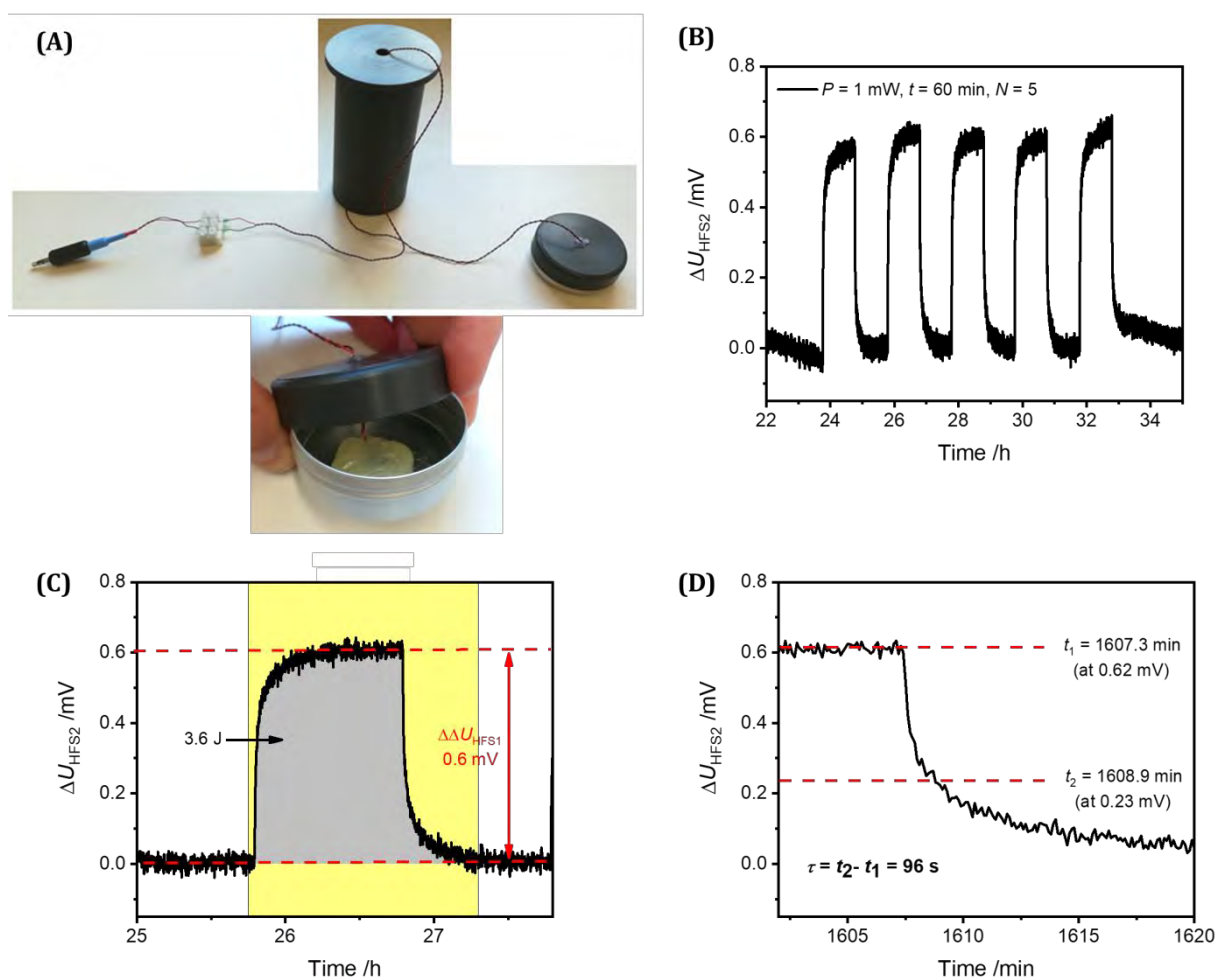


Figure 12: Electrical calibration procedure. **A:** Experimental setup and the prepared calorimetric vessel. **B:** Steady-state calibration experiments conducted in channel 3. **C:** Determination of the $\Delta\Delta U_{\text{HFS2}}$ in steady-state. Additionally, the integral reflects the total heat released during this calibration (theoretically 3.6 J). **D:** Determination of the time constant τ (unpublished data).

In the final evaluation step, the time constants for both measuring channels were determined from the decay rate of the voltage signal after switching off the electrical calibration heater ¹³⁶. (**Figure 12D**). For this purpose, t_1 was determined (signal in steady-state) and t_2 (decrease of signal to 36.8 % compared to the initial value, which corresponds to $\exp(-1)$ ¹⁴⁵). The time difference between t_1 and t_2 corresponds to the time constant τ . Its value for both channels are $\tau_{\text{ch1}} = (106 \pm 37)$ s and $\tau_{\text{ch3}} = (82 \pm 10)$ s. In the following section, the applicability of the micro(bio-)calorimeter on the detection of microbial activity is experimentally investigated. Additionally, experiments addressing the selectivity of non-selective and selective Legionella media are given.

3.3.2 Detection of bacterial activity using the novel micro(bio-)calorimeter

As mentioned in **section 3.2**, the calorimeter was designed to meet the prerequisites for detecting bacterial contamination in routine microbiological testing. Therefore, two microbiological samples were tested to prove the applicability of the calorimeter. **Figure 13** displays the first microbiological measurement performed by the 1st modified version of the test system (only an aluminium shield around the channels). Here, the growth of *P. putida* mt-2 KT2440 in LB broth was monitored in real-time (duplicate determination).

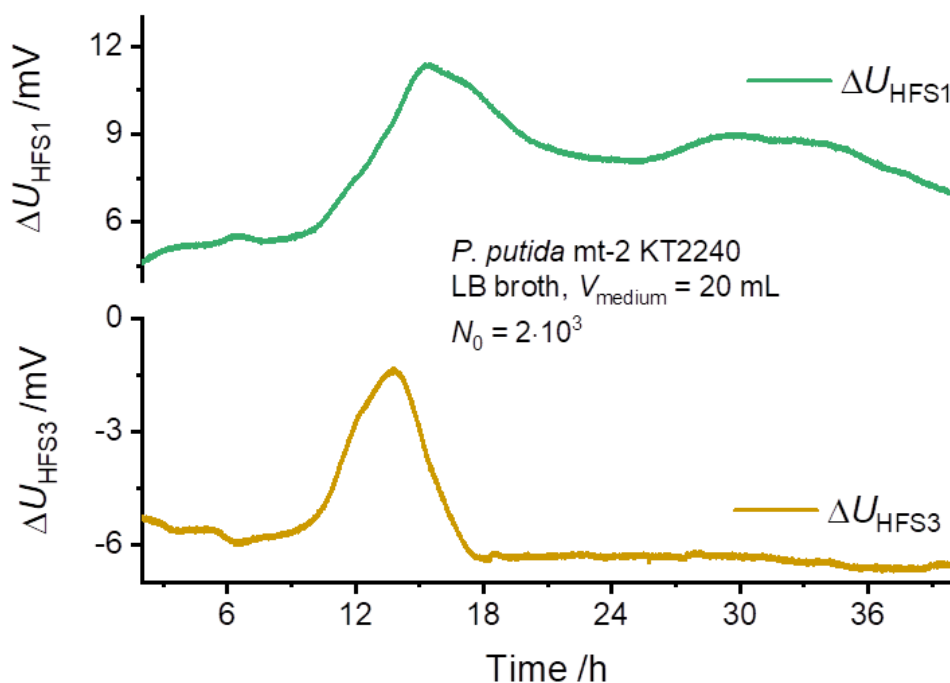


Figure 13: Micro(bio-)calorimetric measurement of *P. putida* mt-2 KT2440 in 20 mL LB broth performed by a 1st modified version of the test system (unpublished data).

The increase of the signal after approx. 8 h is caused by the metabolic activity of the bacteria. It can be seen as the earliest detection time of bacterial growth.

Based on the modification, both channels showed a similar voltage profile. The signal height is almost equal in both measurements (approx. 4 mV). This voltage corresponds to a heat flow of 6.8 mW using the experimental calibration constant $\varepsilon_{\text{exp}} = 1.7 \text{ W V}^{-1}$. However, the HFS1 signal (green curve) does not abruptly return to the baseline compared to the signal of HFS3 (yellow curve). This different behavior might be attributed to the insufficient insulation of the 1st modified version used in this experiment. However, the aluminium frame alone provides somewhat better stability of the voltage signal at the heat flow sensors. Channel 1 exhibits less stability of the signal due to the significant fluctuation of the fan heater (see **Figure 10A, C**).

In addition, and for the first time, a real cooling tower sample (duplicate determination) was also measured on a selective Legionella medium by plating 0.5 mL on 10 to 15 mL GVPC agar. The corresponding voltage profiles can be seen in **Figure 14**. In reference measurements (count plates according to ISO 11731:2017), the concentration of *L. pneumophila* in the sample was determined to $7.8 \cdot 10^3 \text{ CFU/100 mL}$. The corresponding micro(bio-)calorimetric measurements detected an increase in the voltage signal after about 10 h. The curve profile is very similar for both measurements, which suggests good reproducibility. The maximum of ΔU_{HFS} is in both curves approx. 5 mV (corresponds to a heat flow of 8.5 mW using $\varepsilon_{\text{exp}} = 1.7 \text{ W V}^{-1}$). This measurement shows that waterborne contaminations can be detected quickly (within a few hours) using the designed micro(bio-)calorimeter.

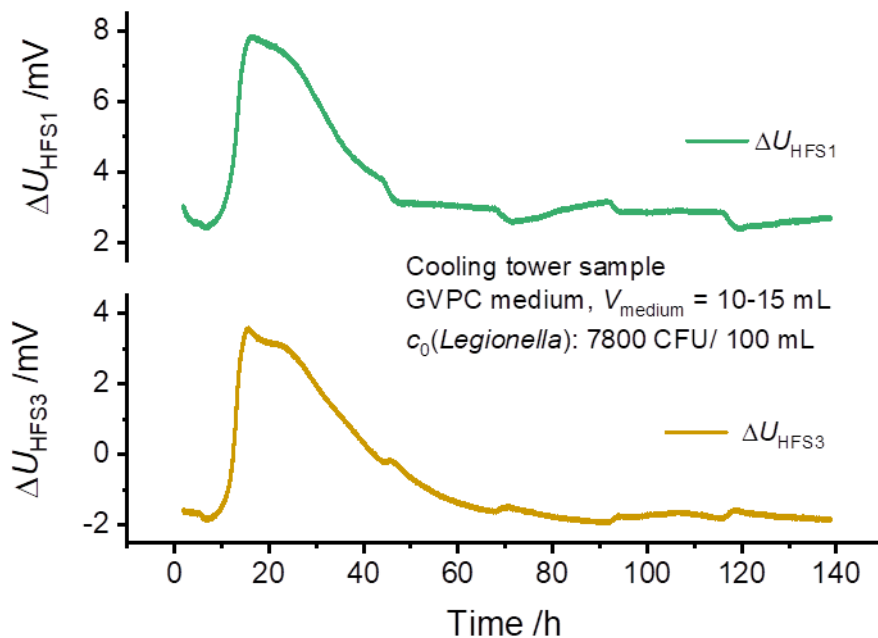


Figure 14: Micro(bio-)calorimetric measurement of a real cooling tower sample on 10 mL selective GVPC agar performed by the 2nd modified version of the test system (unpublished data).

However, despite the selective medium, GVPC, recommended by ISO 11731, it is possible that other accompanying bacteria may grow in addition to *L. pneumophila* and thus contribute to the heat flow signal. In order to investigate the influence of the selective medium on accompanying microorganisms, further calorimetric measurements were conducted. The results are given in the next section.

3.3.3 Calorimetric measurements on the selectivity of conventional Legionella media for accompanying pathogens

Additional heat flows of three common accompanying pathogens, *Escherichia coli* (ATCC 8739), *Enterococcus faecalis* (ATCC 19433) and *Pseudomonas aeruginosa* (ATCC 27853), were measured on non-selective BCYE agar (**Figure 15A**) and selective, i.e. BCYE-Ab (supplemented with 9 mg L⁻¹ cefazolin, 70 mg L⁻¹ pimericin and 80000 IU L⁻¹ polymyxin B) and GVPC (3 g L⁻¹ glycine, 1 mg L⁻¹ vancomycin, 80000 IU L⁻¹ polymyxin B, 80 mg L⁻¹ cycloheximide) agar (**Figure 15B, C**). For comparison, measurements of *L. pneumophila* (ATCC 33152) on these media were also performed (**Figure 15D**).

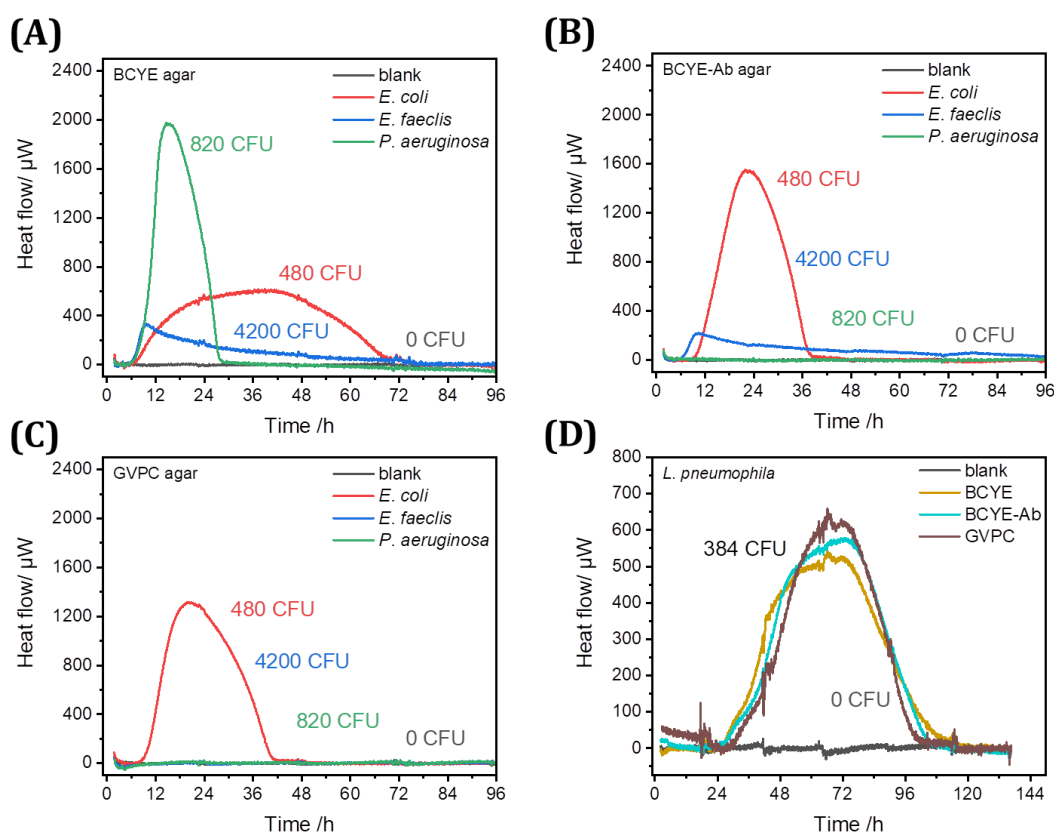


Figure 15: Summary of selective microcalorimetric detection of waterborne pathogens using different Legionella media. **A:** Heat flow measurements of *E. coli*, *E. faecalis* and *P. aeruginosa* on non-selective BCYE agar, **B:** on selective BCYE-Ab agar, **C:** on selective GVPC agar. **D:** Heat flow measurements of *L. pneumophila* on different selective and non-selective media. The *N*₀ in CFU are indicated next to the heat flow signals. In all measurements, a blank (0 CFU) was used as a reference (unpublished data).

The experiments (single determination for the accompanying bacteria and triplicates for *L. pneumophila*) were performed in 30-mL calorimetric ampoules (filled with 5 mL medium) using the MC-Cal/100 P (C3 Prozess- und Analysetechnik GmbH, Munich, Germany). The inoculum volume was 20 μ L. **Figure 15A** demonstrates that all bacteria grow on non-selective BCYE agar. *P. aeruginosa* showed the highest maximum heat flow of approx. 2000 μ W, followed by *E. coli*. The slightly broader heat flow curve of *E. coli* can be attributed to the growth of few and well-separated colonies (the same effect was observed with *P. putida* mt-2 KT2440 on solid medium in **section 3.1.2**). The typical maximum heat flow for *E. coli* on BCYE agar is approx. 1300 μ W (data not shown). This corresponds well with the maximum heat flow measured on BCYE-Ab and GVPC agar. Interestingly, despite the slower growth, *L. pneumophila* showed a higher maximum heat flow (approx. 600 μ W) than *E. faecalis* (approx. 400 μ W), which is probably due to the different metabolism of the bacteria (strictly aerobic growth versus facultative anaerobe).

On the BCYE-Ab medium, only *P. aeruginosa* was inhibited entirely (**Figure 15B**). GVPC shows the best performance since *E. faecalis* and *P. aeruginosa* were inhibited entirely (**Figure 15C**). On the contrary, *L. pneumophila* (ATCC 33152) showed, as expected, growth on all applied media (**Figure 15D**). Likewise, *E. coli* showed no inhibition. These results correspond well with microbiological tests from manufactures of such selective media¹⁵⁸⁻¹⁵⁹. However, it must be pointed out that these are only single determinations for the accompanying bacteria. In order to obtain statistically significant results, further measurements are necessary.

4. Discussion

4.1 Micro(bio-)calorimetry - A culture-based detection technique for bacterial contamination

The most crucial criterion for the detection of microbial contamination is the time that elapses between sampling and confirmation of whether a positive (contaminated) or negative (non-contaminated) sample is present (qualitative approach)²². The earlier the contamination is detected, the faster and more targeted countermeasures can be taken. Subsequently, it is necessary to receive immediately a quantity that can be used to determine the level of contamination (quantitative approach). Further, this quantity should reflect the actual threat of contamination. Consequentially, the microbiological analysis information must include the viable and active cells that may pose an immediate threat should they enter the human organism. At the moment, culture-based techniques with a subsequent visual inspection, predominantly performed by the naked eye, are standard in microbiological laboratories²². Different cultivation techniques specified for different kinds of samples and bacteria are performed¹⁶⁰⁻¹⁶¹.

The 4-mL ampoule system predominantly used in microcalorimetric detection of bacteria was considered as the reference system. In the context of this thesis, it was therefore methodically investigated whether conventional cultivation techniques are compatible with microcalorimetric measurements and which advantages and drawbacks may arise concerning the detection time. Therefore, systematic studies on two model strains, *Lactobacillus plantarum* DSM 20205 (representative for an anaerobic system, **section 3.1.1**) and *Pseudomonas putida* mt-2 KT2440 (representative for an aerobic system, **section 3.1.2**), were conducted in this thesis. The main findings are discussed and compared with the visual inspection of bacterial contaminations (**section 4.1.1**).

Based on the first heat flow measurements of *Legionella pneumophila* ATCC 33152 (**section 3.1.3**) and complementary measurements of pathogens also present in drinking water, the calorimetric approach is discussed in the context of establishing an early warning system in drinking water analysis (**section 4.1.2**).

Due to the lack of commercially available microcalorimeters that fulfil the criteria for microbiological analysis, an early stage developed micro(bio-)calorimeter was designed and constructed. Here, numerical simulations supported the development process (**section 3.2**). On the one hand, weak spots of the micro(bio-)calorimetric test system were revealed, and on the other hand, modifications were simulated in advance to stepwise improve the entire system's performance. Such modifications led to an improved version of the test system (**section 3.3**). Features of the micro(bio-)calorimeter are discussed in the final part and compared with commercially available calorimeters (**section 4.2**).

4.1.1 Compatibility of cultivation techniques with calorimetric detection - Potential and limitations

Almost all available data and studies addressing microcalorimetric detection of bacteria represent just a proof of concept (**Table 2, section 2.2.3**). Further, measurements are exclusively performed in liquid medium (exceptions are ¹¹²⁻¹¹³), mainly using 4-mL static ampoules. In addition, there has been little discussion of the advantages and limitations of this static ampoule system on detectable heat flows in the study of bacterial contaminations. Perhaps this is also the reason why a microcalorimetric method is not yet used as an alternative to conventional microbiological analysis. This is somewhat surprising since it is precisely the growth of bacteria that forms the essential common ground of both methods.

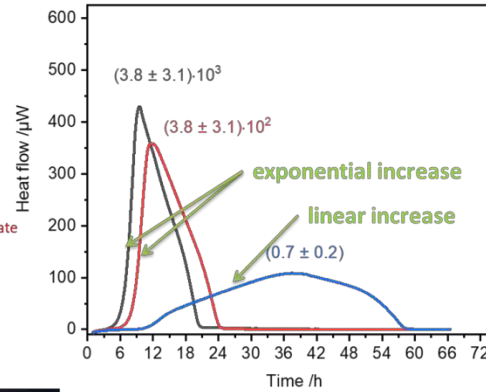
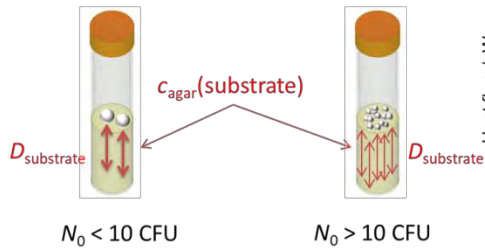
For the first time, systematic investigations were conducted on two model systems, *L. plantarum* DSM 20205 (**section 3.1.1**) and *P. putida* mt-2 KT2440 (**section 3.1.2**). The data demonstrated the compatibility of conventional cultivation techniques in the context of microcalorimetric detection of bacteria. Pouring, plating and membrane filtration (**Figure 1**) were successfully applied to microcalorimetric measurements. Interestingly, detection times obtained from experiments performed on solid medium differ hardly or only minimal from those in liquid medium if very sensitive calorimeters (limit of detection, $\text{LOD} \leq 10 \mu\text{W}$) are used ^{124, 162}. This makes the use of solid media attractive since most ISO standards prescribe cultivation on solid media for conventional microbiological analysis.

However, it was found that with a small initial number of bacteria (< 10 CFU), diffusion limits the exponential growth of bacteria on solid medium. This issue was reflected in the shape of the monitored heat flow. The initial exponential increase changed to a linear course, and smaller, broader heat flow curves were obtained. Hence, leading to the conclusion that less sensitive calorimeters ($\text{LOD} \geq 100 \mu\text{W}$) might not detect the produced heat flow ¹²⁴. This issue can be ascribed to the 4-mL static ampoule system and diffusion-controlled growth of colonies ¹²⁴. **Figure 16** summarizes all limitations of the 4-mL ampoule system that affecting the detection of bacterial contamination in microcalorimetry. Further, Braissant et al. observed the same phenomena for *Mycobacterium tuberculosis* on Lowenstein-Jensen agar ¹¹². Their experiments on slanted solid medium (to minimize diffusion problems) showed that the incubation of samples contaminated with 2 CFU per ampoule produced a maximum heat flow of approx. $10 \mu\text{W}$ ¹¹². For comparison, a higher contamination level of *M. tuberculosis* (2300 CFU per ampoule) resulted in a maximum heat flow of approx. $45 \mu\text{W}$ ¹¹².

In the case of *L. plantarum* DSM 20205, it was shown that there is a strong relationship between the height of the filling volume that correlates with the diffusion path of the substrate (glucose) and the maximum heat flow produced during growth on a solid medium ¹⁶².

Limitations on solid medium

(a) Initial number of bacteria



(b) Enumeration



The small surface area ($d = 10$ mm) only allows enumeration of low contamination levels (< 10 CFU).

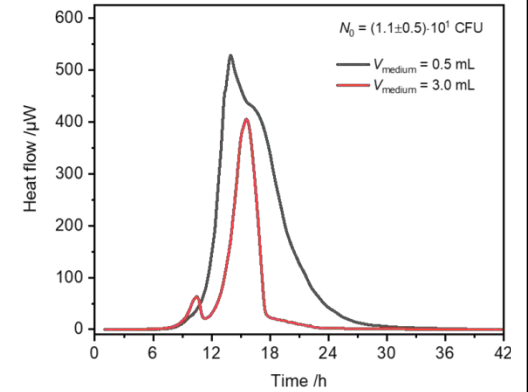
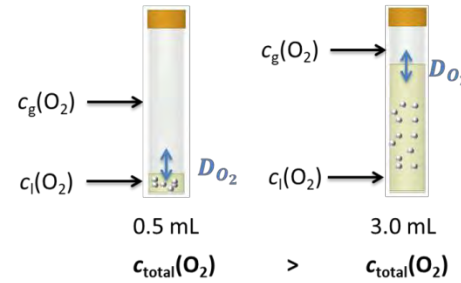
(c) Sample volume



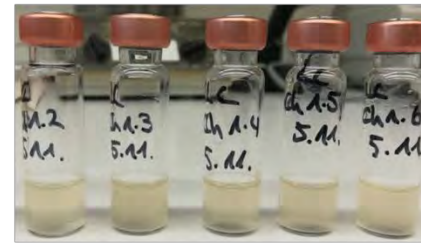
The maximum sample volume is restricted to approx. 10 to 25 μL , otherwise colonies cannot be formed, and bacteria grow in the liquid supernatant.

Limitations in liquid medium

(a) Available amount of oxygen

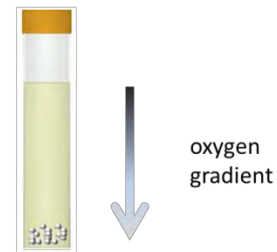


(b) Enumeration



Enumeration is not possible since no conclusion can be drawn about the initial cell number based on the appearance of the sample after measurement.

(c) Anoxic conditions



Sedimentation of non-motile bacteria may limit the detectable heat flow ¹⁶⁴.

Figure 16: Limitations on solid and in liquid medium for detecting bacteria in 4-mL static ampoules.

The enumeration of colonies formed after the calorimetric experiment is only partially feasible. The prerequisite for this is that they are well distributed on the small surface and no more than approx. 10 CFUs have formed. This situation can be further complicated since a convex shape reduces the effective surface area. Similar issues were reported in another study where 20 mL static ampoules were used, and higher inocula also made counting of separate colonies impossible¹¹³. However, the main limiting factor concerns the sample volume. In order to enable bacterial growth on solid medium (colony formation), only 10 to 25 μL are applicable to 4-mL static ampoules. Otherwise, the cells will grow in the supernatant, and no colonies will appear. Additionally, such small sample volumes are impractical for microbiological analysis. This limitation is perhaps one of the main drivers for the dominance of liquid cultures in previous studies.

For aerobic systems, the 4-mL static ampoule system also has some limitations. The filling volume, especially in liquid medium (low solubility of oxygen, 7.5 mg L^{-1} at $30 \text{ }^\circ\text{C}$ ¹⁶³), restricted the amount of available oxygen, and this strongly affects the heat flow and might limit the use of less sensitive calorimeters ($\text{LOD} > 10 \text{ } \mu\text{W}$)¹²⁴. The experimental data in this thesis are in good agreement with numerical simulations concerning oxygen availability in 4-mL static ampoule systems¹⁶⁴.

Basically, when using liquid medium for the calorimetric detection of bacteria, no quantitative evaluation (e.g. enumeration) is possible that would indicate the degree of contamination. Another limitation that corresponds to the amount of available oxygen in liquid medium might be the sedimentation of non-motile bacteria⁸³. Since *P. putida* mt-2 KT2440 is motile, this effect was not considered in this thesis. Maskow et al. investigated sedimentation processes of *P. putida* MM1 through numerical models and demonstrated that the location of bacteria (bottom, top and homogeneously distributed) in the static ampoule affects the total heat produced during microbial growth¹⁶⁴. Bacteria growing on the bottom produced less total heat than those on the top, and the slope of the total heat curve was much flatter¹⁶⁴. If one referred this to the corresponding heat flow curve, a flat, broad peak would result (similar to the experiments with few cells growing on solid medium). This issue can be circumvented if the density of liquid medium increases, e.g., using Percoll¹⁶⁴.

Microcalorimetric measurements provide a real-time signal based on heat flow measurements related to the kinetics and stoichiometry of the ongoing process in the calorimetric ampoule¹¹⁹⁻¹²⁰. Depending on the level of contamination, heat flow signals can immediately be obtained by entering the sample into the measurement position of very sensitive microcalorimeters ($\text{LOD} \leq 10 \text{ } \mu\text{W}$)¹²⁴. In the case of *P. putida* mt-2 KT2440, a directly detectable heat flow was obtained if approx. 10^5 CFU are presented in the sample¹²⁴. This is in substantial agreement with literature data^{32, 100}. It should be considered that less sensitive calorimeters ($\text{LOD} \geq 10 \text{ } \mu\text{W}$) may lead to a slightly delayed detection time, despite the high initial number of bacteria present in the sample. Nevertheless, the systematic investigations in the thesis show, supported by a few previous studies^{32, 112, 125}, that microcalorimetric detection is superior to conventional microbiological analysis in terms of detection time.

Most importantly, these studies show that calorimetric detections in 4-mL static ampoules are inadequate to compete with conventional microbiological analysis. However, recent reports follow this type of systematic study. For example, Corvec et al. investigated the influence of the filling volume of 4-mL ampoules and the selection of the medium composition on the detection time of anaerobically growing pathogens³⁶. Such investigations are necessary to optimize the calorimetric detection method. Comparisons of microcalorimetric detection times and molecular biological (PCR) or immunological techniques (ELISA) are not reported yet. Hence, they cannot be discussed in connection with the detection time of bacterial contamination. One reason for this is certainly the deviating nature of detectable quantities of these techniques. For instance, PCR detects molecules. IMC, in contrast, detects whole, metabolically active cells as only these produce heat and might pose immediate danger⁵³. Undoubtedly, molecular biological techniques and immunological assays provide faster and sometimes more reliable detection of pathogens than conventional techniques such as counting plates²⁶. Nevertheless, only a few standardized protocols consider other detection methods (mostly PCR) than cultivation and enumeration on solid medium^{71, 165}. One possible reason might be the complexity of the sample matrix.

Interestingly, in IMC measurements, the sample matrix might not play a crucial role as an interfering factor compared with other techniques¹⁰⁰. For instance, in food samples, part of the matrix can limit the applicability of PCR and biosensors to detect bacteria²⁶. In contrast, the complexity of the biological composition (mixed culture) of the sample might be crucial in IMC since each bacterium present in the sample that grows under the given conditions (operating temperature, medium composition) consequently contributes to the measured heat flow (non-specificity)^{34, 83}. Therefore, discrimination between heat production rates from different species is not possible. Conventional microbiological analysis is facing a similar problem since the colonies formed and visually inspected afterwards are not always distinguishable by their colors or morphological characteristics.

Further, the initial number of bacteria correlates with the detection time (defined at an empirically determined threshold value)^{32, 53, 133, 162}. This relation might enable quantitative measurements if (i) selective detection of this microorganism can be guaranteed through the use of selective culture medium and (ii) a standard curve (logarithm of the initial number of bacteria versus detection time) for a targeted microorganism is established. The latter requires that the bacteria in the sample grow exponentially. Again, the compatibility between IMC and conventional microbiological analysis is evident, as this would allow the use of known quantities, namely CFU mL⁻¹, for calibration.

In contrast, culture-independent detection methods also provide quantitative data for detecting bacteria, such as GUs in qPCR^{27, 69}. However, there are currently no legal and technical thresholds based on this unit¹⁶⁶. Additionally, GUs are not directly translatable to CFU since DNA from both live and dead cells is detected¹⁶⁷.

In the next section, the discussion of a microcalorimetric detection of bacteria will focus on drinking water contaminated with *Legionella pneumophila*.

4.1.2 An early warning system for *Legionella pneumophila* in drinking water based on calorimetry?

Microcalorimetric data for waterborne pathogens are rare. Maskow et al. suggested to perform microcalorimetric measurements as part of the drinking water analysis³². In the context of this thesis, the question arises, how and why can a microcalorimetric approach contribute to the rapid detection of *Legionella pneumophila* in drinking water?

First, it has already demonstrated that IMC can detect bacterial contamination more quickly than conventional microbiological analysis^{32, 112}. In this thesis, heat flow measurements of *L. pneumophila* are presented for the first time. Despite the fastidious growth conditions for this pathogen, substantial heat flows ($\Phi_{\max} \approx 175 \mu\text{W}$) were detected in the 4-mL static ampoule system (containing 1 mL BCYE agar and approximately 3 mL air headspace), and concentration-dependent detection times ranged from 24 (10^3 CFU) to 45 h (4 CFU)⁵³. This is a substantial reduction compared to conventional diagnostics, where visible colonies are detected not until 72 to > 300 h of incubation^{81, 168}. For comparison, qPCR enables detection of *L. pneumophila* after 3 h^{165, 169}. However, Whiley and Taylor pointed out that it is difficult to compare the culture-based approach with qPCR because of many inconsistencies between the two methods²⁷ (see also discussion in **section 4.1.1**). A better comparison here is rather Legiolert, another culture-based approach performed in liquid medium, where the increase in turbidity and/or brown color change confirms positive samples¹⁷⁰⁻¹⁷¹. However, Legiolert detects *L. pneumophila* after 168 h of incubation¹⁷². Therefore, both ISO 11731 and Legiolert are time-consuming culture-based detection techniques compared to IMC. Especially if we consider the incubation period until the onset of the first symptoms of Legionnaires disease usually takes 5 to 6 days¹⁷³.

Furthermore, membrane filtration is an easy way to handle the pre-enrichment method for *L. pneumophila*, speeding up the calorimetric detection in samples with low cell numbers^{124, 162}. Although ISO 11731:2017 suggests membrane filtration as an approach for detecting *L. pneumophila*, it has no detection time advantage since the culture-based approach is a concentration-independent detection method¹²⁴. Again, IMC is superior, as shown in the example of *P. putida* mt-2 KT2440 (**section 3.1.2**) and *L. plantarum* DSM 20205 (**section 3.1.1**). Membrane filtration is an efficient method to increase the initial cell number and reduce the detection at the same time. This procedure should be readily applicable to the calorimetric measurement of *L. pneumophila*.

Besides the qPCR approach mentioned above, there are several other techniques for the rapid detection of *L. pneumophila* in water samples, such as immunomagnetic separation followed by flow cytometric analysis (2 h)¹⁷⁴, SPR (detection time not given)¹⁷⁵, immunofluorescent microscopy (few hours)¹⁷⁶, immunofluorescence assay (72 h)¹⁷⁷, on-chip fluorescent staining (1.5 h)¹⁷⁸, Optical Waveguide Lightmode Spectroscopy (0.5 h)¹⁷⁹. These methods have comparatively short detection times but are not yet used for routine testing of *L. pneumophila* in drinking water analysis. Indeed, a fast detection time is crucial, but at what price? The main exclusion criterion, such as expensive instruments as well

as reagents, bulky devices and complex data evaluation, were already addressed in the introduction of this thesis (**section 2.1**). Another aspect briefly mentioned in the previous discussion is the amount of information obtained from the microbiological analysis. For example, the ScanVIT-Legionella can differentiate between *L. pneumophila* and other *Legionella* spp., but the analysis requires three days¹⁷⁷. qPCR, in turn, provides GUs within a few hours, although it is yet not possible to estimate how many GUs pose a direct threat and only proposed threshold values are mentioned in the literature¹⁶⁶. A culture-based approach such as IMC, by contrast, provides less information and reflects only active, proliferating cells. However, this information might be sufficient to make a comparatively straightforward and inexpensive estimate of the risk posed by the sample under investigation. More selective information about the content of the sample would undoubtedly be desirable in the context of a calorimetric detection of *L. pneumophila*.

Therefore, the second reason why calorimetry might be a suitable tool for an early warning system of *L. pneumophila* contaminations in drinking water is that selective media such as GVPC, BCYE-Ab^{168, 180-182} and additional treatments (chemical and physical)¹⁸³ are well-known to reduce the number of accompanying bacteria (see **section 2.1.1**). However, even a small selection of possible accompanying pathogens such as *P. aeruginosa*, *E. coli* and *E. faecalis* showed that complete inhibition is not possible with the current recommended selective media in the context of calorimetric measurements of drinking water samples (**section 3.3.3**). The best performance was shown on GVPC agar, where two out of three bacteria were inhibited (except for *E. coli*). In general, this topic is very controversial discussed in the literature, and a few studies have examined the selectivity of different *Legionella* media from different manufacturers^{168, 181-182, 184-186}.

In a comparative study of different isolation and cultivation procedures of tap water samples, Reintaler et al. also found that GVPC showed the highest selectivity for *L. pneumophila*¹⁸⁴. Scatturo et al. concluded that GVPC shows higher efficiency in detecting *Legionella* in potable water samples than on BCYE¹⁸¹. Recently, Ditommaso et al. recommended modified Wadowsky-Yee (MWY) medium to detect *Legionella* spp. in hospital water¹⁶⁸. The latter contains antibiotics (3 g L⁻¹ glycine, 50000 IU L⁻¹ polymyxin B, 1 mg L⁻¹ vancomycin and 80 mg L⁻¹ anisomycin) to inhibit the accompanying flora and uses two dyes (10 mg L⁻¹ bromothymol blue and 10 mg L⁻¹ bromocresol purple) those stain colonies and thus facilitate identification¹⁶⁸.

Concerning the selectivity of the calorimetric method, follow-up studies are necessary to obtain statistically significant results on the one hand and to investigate different approaches such as chemical and physical treatment of samples and their influence on the heat flow signal on the other hand.

Indeed, IMC and conventional microbiological analyses are unspecific concerning the detection of a particular pathogen. Nevertheless, a screening method, i.e. early warning system based on IMC, would be suitable in drinking water analysis since bacterial activity can be detected much faster and is superior to conventional analysis. Identifying a pathogen from a positive sample must only be proved when the legal threshold has been exceeded, e.g. > 100 CFU /100 mL in the case of *L. pneumophila* accord-

ning to the ISO 11731:2017⁴⁸. Consequently, PCR or matrix-assisted laser desorption/ionisation - time of flight (MALDI-TOF) can further analyse those suspicious colonies formed during the calorimetric measurement due to the non-destructive nature of the calorimetric method³⁴. As previously discussed, 4-mL static ampoules (predominately used in applications) do not apply to this approach due to the small surface area (**Figure 16**). Petri dish-like sample vessels would be advantageous for obtaining well-separated colonies that can be further analyzed after calorimetric detection. The latter is already considered in the micro(bio-)calorimeter designed in this thesis.

One last aspect concerning an early warning system based on IMC has to be mentioned briefly, namely, detecting a positive (contaminated) sample, i.e. how the calorimeter indicates a positive finding. As mentioned in the introduction (**section 2.2.2**), empirical thresholds are currently being defined for different calorimeters. Despite the simplicity of this approach, possibly thermal disturbances at the beginning of the measurements might lead to false-positive signals. By using the first derivative, it was shown in this thesis (**section 3.1.3**) that the influence of thermal disturbances could be minimized, and a more constant baseline can be achieved⁵³. Nevertheless, the establishment of an empirical detection threshold is also required. Follow-up studies should address the threshold-setting issue, preferably on many real samples, to have a sufficient data basis for statistical methods.

The last section of this chapter addresses the newly developed micro(bio-)calorimeter. The discussion will focus on the main features and advantages of the designed calorimeter to commercial instruments and the applicability in the context of microbiological analyses.

4.2 A novel calorimeter designed for microbiological analysis

Based on the results from the method development, a calorimeter specially designed for microbiological analysis was constructed (**section 3.2**). It is essential to mention that the current test system developed here represents only a specific step in the overall development process (**Figure 9**). However, key features of this calorimetric test system are a fixed measuring temperature of 37 °C, the selection of sample vessel geometry that enables compatibility with conventional cultivation techniques and a comparatively compact and transportable design. The use of an air thermostat and the fixed measuring temperature reduces the overall weight of the test system and reduces the complexity of the temperature control unit.

The choice of sample vessel (consisting of an aluminium body, $V = 35$ mL, $d = 51$ mm and $h = 19$ mm and a plastic top) allows larger medium volumes and the application of membrane filters ($d = 47$ mm) commonly used in sample pre-enrichment (**Figure 1**). Due to the large surface area, sample volumes up to 0.5 mL can be plated out, and isolated colonies obtained during incubation in the calorimeter are countable afterwards. An image of a sample after incubation is shown in **Figure 17**. Due to the large surface area of the sample vessels, follow-up analytics, such as PCR, and MALDI-TOF, of colonies formed are easily accessible. Indeed, the small surface area is still, from a microbiological point of

view, a significant drawback in most commercially available microcalorimeters since small sample vessels (≤ 20 mL) are predominantly used, and well-separated colonies are not obtained after the measurement (**Figure 16**). Standard membrane filters have a diameter of 47 mm and are therefore not applicable to common sample vessels of commercial calorimeters currently used to detect bacteria (see **Table 2**).



Figure 17: Colonies formed on the membrane filter after incubation using the calorimetric vessel of the test system.

Another advantage is that diffusion problems of substrate and oxygen can be minimized due to the low filling height and larger surface area. Consequentially, the limitations found for the 4-mL static ampoule system (**Figure 16**) can be overcome by the sample vessels used for this novel micro(bio-)calorimeter.

Commercial instruments have either narrow ($d < 20$ mm), small ($V < 20$ mL) or wide ($d > 50$ mm), large ($V > 125$ mL) sample vessels (**Table 3**). The latter occupies a correspondingly large space, meaning that only a few measuring channels are available (< 5). Consequently, only a few samples can be measured simultaneously, and the number of replicates is also severely limited. Even though the test system currently has only three channels, the prototype is planned for nine channels (one will serve as a reference). Further, the restricted operating temperature of 37 °C is also dissimilar to commercial devices (except for ¹⁵⁷). From an economic point of view, this is probably the area where the greatest savings can be made since a broad temperature spectrum requires sophisticated temperature regulation systems and good insulation especially when measurements are conducted at low or high temperatures. Another exception is the reference system of the calorimeter developed in this thesis. Usually, commercial devices have a twin configuration, i.e. measuring and reference cell form a closed unit that can be arranged horizontally or vertically ¹⁰⁷. The developed micro(bio-)calorimeter has a reference channel located on the same heat sink as the measurement channels. It thus serves as a reference for all measuring channels. In this configuration, small temperature gradients along the large

heat sink are not an issue as long as the local temperatures at the bottom of the heat flow sensors in each channel have the same temperature stability. It is questionable whether a large heat sink is in sum heavier than several twin configurations. The heat sink, weighing about 8 kg, accounts for one-third of the total mass of the calorimeter. The total mass of approx. 25 kg corresponds to those of smaller commercial instruments such as the BioCal 2000 (<https://www.calmetrix.com/>).

Experimental and numerical investigations on the test system have shown weaknesses in the temperature distribution among the channels (**section 3.2**). Consequently, an aluminium frame was added to the upper part (1st modified version of the test system). With this modified version, microbiological samples were measured for the first time. The bacterial growth of *P. putida* mt-2 KT2440 in LB broth was monitored in real-time (**section 3.3.2**). The bacterial activity was detected after approx. 8 h. Maskow et al. investigated the detection time of *P. putida* PpG7 in LB medium at 37 °C, using the 4-mL static ampoule system³². Despite the high sensitivity of their applied microcalorimeter (TAM III), the bacterial contamination of $N_0 = 6 \cdot 10^3$ cells was detected not until approx. 6 h³². Even if a different strain (mt-2 KT2440) and slightly different inoculum ($N_0 = 2 \cdot 10^3$ cells) were employed (**Figure 13**), this clearly shows that the bacterial diagnostics performance of the 1st modified version of the test system is already comparable to much more powerful commercial instruments.

However, additional insulation (Styrofoam box, 50 mm thickness) was necessary to improve the overall temperature stability in the entire system. Further, the heat flow simulations illustrated another issue in the 1st modified version. The aluminium frame in the upper part caused a cold spot among the channels due to the stagnant air (a good isolator). In order to overcome this problem, a bottom plate was added to the aluminium frame to ensure thermal contact between the heated frame and the upper part of the channels (**section 3.2 & 3.3.1**). Both modifications lead to the 2nd modified version of the test system. With this modified version, the metabolic activity of *Legionella* and potentially accompanying bacteria from a real cooling tower sample was measured for the first time. This measurement reflects the discussion as mentioned above on an early warning system based on IMC. An increase in the heat flow signal was detected after approx. 10 h and can be interpreted as the earliest detection time of bacterial activity in the sample. The maximum heat flow measured for this sample is approx. 8.5 mW (using $\varepsilon_{\text{exp}} = 1.7 \text{ W V}^{-1}$). This value might be quite high for *L. pneumophila* (assuming selective detection) since heat flow measurements on 5 mL GVPC medium yielded a maximum heat flow of approx. 0.6 mW (**Figure 15D**), although a slightly different sample vessel geometry and less medium were used. From this, one could conclude that accompanying bacteria have also grown on the medium, which is in line with the limited selectivity found for GVPC (**Figure 15C**) and reported in the literature (see discussion in **section 4.1.2**). Cooling tower samples, in particular, often have diverse accompanying flora, making selective detection of *L. pneumophila* even more challenging⁴⁸. The next step should be to start a campaign with larger numbers of real water samples to get statistically significant results. It would be desirable to start this campaign with the prototype (eight measuring channels and one reference channel) under development since the current test system consists only of two

measuring channels. Thus, only a duplicate determination is possible, which would significantly limit the number of replicates and consequently the statistical power of the results.

In order to optimize the insulation of the 2nd modified version, the Styrofoam box was substituted by Styrofoam insulation panels (40 mm thickness), which were attached to the housing of the original test system. In this way, the 3rd modified version of the test system was created. **Table 4** summarizes some specifications and features of the 3rd modified version of the test system. The aluminium shield with the bottom plate and the additional insulation represent inexpensive and straightforward modifications that significantly impact the temperature stability throughout the system (**section 3.3.1**). Further, it also affects the baseline stability of the heat flow sensors so that presumably, the already investigated microbiological samples can be detected even earlier.

Table 4: Specification and features of the 3rd modified version

3rd modified version of the test system	
Sample vessel	
volume /mL	35
diameter /mm	51
Temperature	
range /°C	37
stability mK /24 h (air) ^a	± 30
stability mK /24 h (heat sink 1) ^b	± 0.5
stability mK /24 h (heat sink 2) ^c	± 0.6
Sensitivity^e	
long-term noise μ W /24 h (HFS1) ^d	± 24
long-term noise μ W /24 h (HFS2) ^d	± 43
limit of detection / μ W	n. d.
Number of measuring channels	2

n. d. = not determined

^a temperature determined by the NTC in the outer zone

^b temperature determined by the NTC below the reference channel in the heat sink

^c temperature determined by the NTC below channel 1 in the heat sink

^d the long-term noise was determined as the standard deviation of the baseline in the time interval of 24 h

^e determined without the calorimetric vessel

If we compare the specifications of the 3rd modified test system with those of commercial microcalorimeters (**Table 3**), it is clear that the temperature stabilities are competitive with commercial instruments such as the TAM Air and the BioCal 2000/4000. However, to compare baseline stabilities of the modified test system, follow-up studies with empty calorimetric vessels (no heat production) in the measurement position should be performed to determine long-term noise and other characteristics such as baseline drifts, short-term noise and the LOD.

In order to further characterize the performance of the test system, electrical calibration experiments (empty calorimetric vessel) were conducted on the 3rd modified version (**section 3.3.1**). In these steady-state calibrations, ε_{exp} was determined to 1.7 W V^{-1} . The theoretical calibration constant specified by the manufacturer is $\varepsilon_{\text{theo}} = 0.6 \text{ W V}^{-1}$ ¹⁸⁷. A larger experimental calibration constant implies that a significant portion of the heat generated in the sample vessel (approx. 65 %) does not flow through the heat flow sensor¹⁴⁵. The literature states that this proportion can also be over 50 % for microcalorimeters (batch type)¹⁸⁸. However, to understand the corresponding and dominant heat flow paths, numerical simulations might be necessary. These simulations could then be used to test modifications in the measuring chamber that minimize the proportion of heat flow that does not pass through the heat flow sensor. Further, additional calibrations, e.g. chemically¹⁴⁷ and single-pulse¹⁴⁵ should be performed as recommended by the technical report from the International Union of Pure and Applied Chemistry¹⁴¹.

Besides the calibration constant of the calorimeter, time constants for both measurement channels were determined using steady-state calibration experiments. The corresponding time constants are approx. 1.5 min for each channel. These are thus in the range of high-performance calorimeters, such as the TAM III (time constant around 100 s)⁹¹. Since the micro(bio-)calorimeter is intended to study slow processes, such as bacterial growth, the use of eq. 10 is sufficient, and no dynamic corrections (Tian equation, eq. 11) to the recorded heat flow signal are necessary (**section 2.2.4.1**).

The first modifications, characterizations and measurements of microbiological samples are promising, as fast detection times can be achieved, and the complete spectrum of possible cultivation techniques can be covered with the micro(bio-)calorimetric test system. Thus, moving the test system towards a prototype (already under development and supported by numerical simulations) can lead to absolute competitiveness with the less suitable but more expensive commercial microcalorimeters currently on the market.

5. Conclusion

Rapid and reliable detection of bacterial contaminations is one of the most critical challenges to ensure safe consumables and prevent damage to the health of us humans. The present thesis dealt with the method optimization and instrument development for micro(bio-)calorimetric measurements to rapidly detect bacterial contamination. Therefore, comprehensive and systematic studies on calorimetric detection of bacteria in static 4-mL ampoules (mainly used in research studies published in literature) on three model microorganisms, *Lactobacillus plantarum* DSM 20205 (**section 3.1.1**), *Pseudomonas putida* mt-2 KT2440 (**section 3.1.2**) and *Legionella pneumophila* ATCC 33152 (**section 3.1.3**) were performed for the first time. In addition, a specially designed micro(bio-)calorimetric test system was presented (**section 3.2**).

From the microbiological experiments, it can be concluded that:

- Conventional cultivation techniques such as pouring (recommended for anaerobic and microaerophilic bacteria), plating and membrane filtration are compatible with microcalorimetric detection of bacterial contaminations (**section 3.1.1 & 3.1.2**). The latter should be chosen especially when low contamination levels are suspected since calorimetric detection times depend on the initial cell number. The high compatibility should allow the implementation of the calorimetric approach into existing ISO standards.
- Calorimetric detection is superior to conventional microbiological analysis (visual inspection of plate counts) regarding the detection speed. All microorganisms studied in this work could be detected more reliably and rapidly using IMC (**section 3.1**). In addition, cultivation on solid medium achieves similar detection times as in liquid medium (so far preferred medium for calorimetric detection of bacteria). Since most ISO standards are based on cultivation on solid medium, it is recommendable to use a solid medium for the calorimetric detection of bacteria.
- The standard 4-mL static ampoule system (predominately used in calorimetric detection) has too many limitations (summarized in **Figure 16**) and is consequently less suitable for a routine microbiological analysis based on calorimetric detection. Smaller Petri dish vessels would be desirable, as standardized membrane filters ($d = 47$ mm) can then be employed and quantification in terms of plate counts (CFU) are also possible after successful calorimetric measurement. Commercial calorimetric vessels that meet this requirement are oversized ($V > 100$ mL) and occupy a relatively large amount of space, which is reflected in the low number of measuring channels (< 5) available (summarized in **Table 3**).

With the first investigation of *L. pneumophila*, following a previous study by Maskow et al. ³², the detection of bacterial contamination in drinking water was addressed in this thesis. This opportunistic pathogen is a recurrent cause of major outbreaks worldwide, especially in connection with drinking water contamination. From this proof of concept study, three prominent aspects can be deduced:

- Despite the challenging growth conditions for this slow-growing pathogen, metabolic activity ($\Phi_{\max} = 175 \mu\text{W}$) in 4-mL static ampoules (1 mL BCYE agar and 3 mL headspace) is successfully monitored by IMC. A fast calorimetric detection within one day is achievable and thus preferable to ISO 11731:2017, which prescribes ten days of incubation (**section 3.1.3**).
- The first derivation of the heat flow curve can be helpful in determining the detection time, especially if the sample vessel is not fully thermally equilibrated and the specimen under investigation contains few cells (**section 3.1.3**).
- Selective calorimetric detection of *L. pneumophila* might not be feasible with the currently available culture media and calorimetric methods. This lack of selectivity is partly due to the comparatively lower heat production rate of slow-growing *L. pneumophila* than fast-growing accompanying bacteria such as *P. aeruginosa* or *E. coli* (**section 3.3.3**). However, conventional microbiological analysis faces similar issues since colonies of different species cannot always be discriminated by their morphological properties. Since the cell count correlates with the detection time, co-contaminations in drinking water samples can also be detected more quickly using IMC (early warning system). If real drinking water samples were analysed in larger calorimetric vessels, fast and more advanced identification tools (PCR, MALDI-TOF) could be employed to identify suspicious colonies in the follow-up analysis.

Finally, in this thesis, the first step towards achieving a competitive detection method of bacteria by IMC is already made through the newly designed micro(bio-)calorimeter. From the development work for this calorimetric test system, it can be concluded that:

- The calorimeter aims to overcome the limitations of the 4-mL static ampoule systems and fulfil all requirements for a culture-based calorimetric detection of bacteria. Therefore, it has a compact and transportable format and uses sample vessels aimed explicitly at the cultivation of microbiological samples. Additionally, it includes a low-cost temperature unit (air thermostat) and achieves a sensitivity (long-term noise) that is already sufficient to detect bacterial activity rapidly (**section 3.2 & 3.3**). In addition, the temperature stability already achieved in the 3rd modified version can compete with commercial calorimeters.
- 3D numerical simulations are an essential tool for the development process since experimental data, in particular, reflects only local and limited information about the test system's performance. A platform is now available through the successful validation of the numerical model, which is crucial for further developing the prototype (**section 3.2**).

6. Outlook

In the framework of this thesis, the method optimization and instrument development of micro(bio-)calorimetric detection for bacterial contaminations was presented. Although calorimetric detection is superior in terms of speed of detection to conventional microbiological analysis (i.e. visual inspection of count plates), in the case of low contamination levels (a few CFU mL⁻¹) calorimetry showed a minimal advantage. Therefore, it would be desirable to detect even the lowest bacterial contaminations as quickly as possible using IMC. In order to address this issue, two approaches would be conceivable.

Firstly, the cellular heat production rate ϕ could provide a set point for the faster detection of bacteria. The provision of necessary building blocks such as vitamins, amino acids, and energy-rich compounds (e.g. sugars) ensure optimal heat production of the cellular machinery (**section 3.1.2**)¹²⁴. Therefore, the aim must be to achieve a maximal value of ϕ within the population under investigation for micro-calorimetric detection (according to eq. 3, **section 2.2.2**). In addition, this parameter has not yet attracted much attention, so that there may be an unknown potential to detect the produced heat flow more quickly. Another exciting approach regarding heat production would be purposefully induced side reactions that generate additional heat during bacterial growth by, e.g. metabolic products, oxygen or pH shifts in the medium. The idea is to amplify the net heat flow signal throughout these side reactions. Signal amplification is often used in other techniques to reduce the detection limit of bacteria¹⁸⁹⁻¹⁹¹.

Secondly, since the heat production rate of a single bacterium is relatively low, approx. 1-4 pW³², currently, there is no calorimeter capable of detecting the heat produced by a single bacterium. However, recently a micromachined picocalorimeter sensor showed excellent resolutions between 30 and 200 pW¹⁵⁶. Unfortunately, only minute sample volumes ($\leq 1 \mu\text{L}$) are applicable, which are difficult to handle in the context of bacterial contaminations. Nevertheless, this issue could be solved if selective pre-enrichment methods are applied. For instance, biomagnetic separation (BMS) has been applied in chip calorimetric measurements resulting in the detection of lower cell numbers¹⁹².

Further improvements in the future addressing the instrument development are expected for the detectors, i.e. the heat flow sensors. Almost all commercial microcalorimeters use high-sensitive TEGs. These are characterized by low thermal conductivity k (in W m⁻¹ K⁻¹), a high Seebeck coefficient α (in V K⁻¹), high electrical conductivity σ and a large ratio of voltage to power S (sensitivity in V W⁻¹). Since the first three parameters are material dependent, potentially new materials can improve the overall sensitivity of such heat flow sensors.

Besides the continuous improvements of method and instrument development for the rapid detection of bacteria, future studies of micro(bio-)calorimetric measurements should exclusively address real samples to detect bacterial contamination. Additionally, the ISO11731:2017 recommends further treatments such as chemical and physical. These treatments were not investigated in the present thesis.

However, they should be addressed in follow-up studies, as IMC is ideally suited to support studies towards a more selective procedure to detect *L. pneumophila*. For instance, new antibiotics could be tested to develop even more selective media. An IMC based antimicrobial susceptibility testing of bacteria was already shown on *E. coli* and *S. aureus*¹⁹³. The thermal response provides direct information on whether there is a possible inhibition of accompanied bacteria, and further, the minimal inhibitory concentration can be determined¹⁹³.

Hopefully, with the thesis presented here and the preliminary experiment on a real cooling tower sample, this approach might be applied to ISO standards in the field of food microbiology. The more application areas this method finds, the more the development of the instruments will be a benefit. Above all, the sample throughput must be increased. So far, microcalorimeters have been reported that allow a maximum of 48 simultaneous measurements^{107, 157}. The prototype, which is still under development, is expected to consist of eight measurement channels and one reference channel (**Figure 18**).

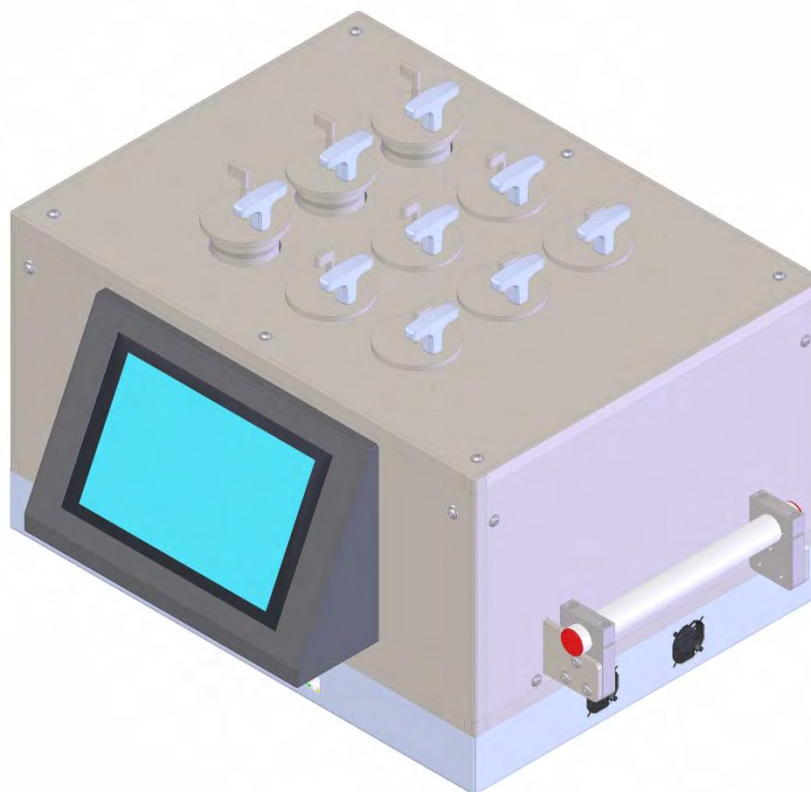


Figure 18: Design of the prototype (8+1 channels) under development.

Finally, the long-term goal should be to establish micro(bio-)calorimetry as an alternative method to conventional microbiological analysis for the rapid and reliable detection of bacteria.

7. References

1. Ferone, M.; Gowen, A.; Fanning, S.; Scannell, A. G. M., Microbial detection and identification methods: Bench top assays to omics approaches. *Compr. Rev. Food Sci. Food Saf.* **2020**, *19* (6), 3106-3129. DOI: 10.1111/1541-4337.12618
2. Balloux, F.; van Dorp, L., Q&A: What are pathogens, and what have they done to and for us? *BMC Biol.* **2017**, *15* (91), 1-6. DOI: 10.1186/s12915-017-0433-z
3. Alegbeleye, O. O.; Singleton, I.; Sant'Ana, A. S., Sources and contamination routes of microbial pathogens to fresh produce during field cultivation: A review. *Food Microbiol.* **2018**, *73*, 177-208. DOI: 10.1016/j.fm.2018.01.003
4. Brackett, R., Incidence, contributing factors, and control of bacterial pathogens in produce. *Postharvest Biol. Technol.* **1999**, *15* (3), 305-311. DOI: 10.1016/S0925-5214(98)00096-9
5. Flaum, I., Contamination of pharmaceutical products. *J. Pharm. Sci.* **1978**, *67* (1), 1-11. DOI: 10.1002/jps.2600670104
6. Jimenez, L., Molecular Diagnosis of Microbial Contamination in Cosmetic and Pharmaceutical Products: A Review. *J. AOAC Int.* **2019**, *84* (3), 671-675. DOI: 10.1093/jaoac/84.3.671
7. Charrois, J. W. A., Private drinking water supplies: challenges for public health. *Can. Med. Assoc. J.* **2010**, *182* (10), 1061-1064. DOI: 10.1503/cmaj.090956
8. Chowdhury, S., Heterotrophic bacteria in drinking water distribution system: a review. *Environ. Monit. Assess.* **2012**, *184* (10), 6087-6137. DOI: 10.1007/s10661-011-2407-x
9. Nabeela, F.; Azizullah, A.; Bibi, R.; Uzma, S.; Murad, W.; Shakir, S. K.; Ullah, W.; Qasim, M.; Häder, D.-P., Microbial contamination of drinking water in Pakistan—a review. *Environ. Sci. Pollut. Res.* **2014**, *21* (24), 13929-13942. DOI: 10.1007/s11356-014-3348-z
10. Pandey, P. K.; Kass, P. H.; Soupir, M. L.; Biswas, S.; Singh, V. P., Contamination of water resources by pathogenic bacteria. *AMB Express* **2014**, *4* (51), 1-16. DOI: 10.1186/s13568-014-0051-x
11. Wen, X.; Chen, F.; Lin, Y.; Zhu, H.; Yuan, F.; Kuang, D.; Jia, Z.; Yuan, Z., Microbial Indicators and Their Use for Monitoring Drinking Water Quality—A Review. *Sustainability* **2020**, *12* (6), 1-14. DOI: 10.3390/su12062249
12. Thakali, A.; MacRae, J. D., A review of chemical and microbial contamination in food: What are the threats to a circular food system? *Environ. Res.* **2021**, *194* (110635), 1-16. DOI: 10.1016/j.envres.2020.110635
13. Tauxe, R. V., Emerging foodborne pathogens. *Int. J. Food Microbiol.* **2002**, *78* (1), 31-41. DOI: 10.1016/S0168-1605(02)00232-5
14. Adley, C. C.; Ryan, M. P., Chapter 1 - The Nature and Extent of Foodborne Disease. In *Anti-microbial Food Packaging*, Barros-Velázquez, J., Ed. Academic Press: San Diego, 2016; pp 1-10. DOI: 10.1016/B978-0-12-800723-5.00001-2

15. Bintsis, T., Foodborne pathogens. *AIMS Microbiol.* **2017**, *3* (3), 529-563. DOI: 10.3934/microbiol.2017.3.529
16. Boling, E. A.; Blanchard, G. C.; Russell, W. J., Bacterial Identification by Microcalorimetry. *Nature* **1973**, *241* (5390), 472-473. DOI: 10.1038/241472a0
17. Forrest, W. W., Chapter X Microcalorimetry. In *Methods in Microbiology*, Norris, J. R.; Ribbons, D. W., Eds. Academic Press: 1972; Vol. 6, pp 285-318. DOI: 10.1016/S0580-9517(08)70601-9
18. Braissant, O.; Keiser, J.; Meister, I.; Bachmann, A.; Wirz, D.; Göpfert, B.; Bonkat, G.; Wadsö, I., Isothermal microcalorimetry accurately detects bacteria, tumorous microtissues, and parasitic worms in a label-free well-plate assay. *Biotechnol. J.* **2015**, *10* (3), 460-468. DOI: 10.1002/biot.201400494
19. Wadsö, L., Isothermal Microcalorimetry. Current problems and prospects. *J. Therm. Anal. Calorim.* **2001**, *64* (1), 75-84. DOI: 10.1023/A:1011576710913
20. Trampuz, A.; Salzmann, S.; Antheaume, J.; Daniels, A. U., Microcalorimetry: a novel method for detection of microbial contamination in platelet products. *Transfusion* **2007**, *47* (9), 1643-1650. DOI: 10.1111/j.1537-2995.2007.01336.x
21. Szewzyk, U.; Szewzyk, R.; Manz, W.; Schleifer, K.-H., Microbiological Safety of Drinking Water. *Annu. Rev. Microbiol.* **2000**, *54* (1), 81-127. DOI: 10.1146/annurev.micro.54.1.81
22. Rajapaksha, P.; Elbourne, A.; Gangadoo, S.; Brown, R.; Cozzolino, D.; Chapman, J., A review of methods for the detection of pathogenic microorganisms. *Analyst* **2019**, *144* (2), 396-411. DOI: 10.1039/C8AN01488D
23. World Health Organization (WHO). Food safety. <https://www.who.int/en/news-room/fact-sheets/detail/food-safety> (accessed May 07, 2021).
24. Ramírez-Castillo, F. Y.; Loera-Muro, A.; Jacques, M.; Garneau, P.; Avelar-González, F. J.; Harel, J.; Guerrero-Barrera, A. L., Waterborne Pathogens: Detection Methods and Challenges. *Pathogens* **2015**, *4* (2), 307-334. DOI: 10.3390/pathogens4020307
25. Stevens, K. A.; Jaykus, L.-A., Bacterial Separation and Concentration from Complex Sample Matrices: A Review. *Crit. Rev. Microbiol.* **2004**, *30* (1), 7-24. DOI: 10.1080/10408410490266410
26. Wang, Y.; Salazar, J. K., Culture-Independent Rapid Detection Methods for Bacterial Pathogens and Toxins in Food Matrices. *Compr. Rev. Food Sci. Food Saf.* **2016**, *15* (1), 183-205. DOI: 10.1111/1541-4337.12175
27. Whiley, H.; Taylor, M., Legionella detection by culture and qPCR: Comparing apples and oranges. *Crit. Rev. Microbiol.* **2016**, *42* (1), 65-74. DOI: 10.3109/1040841X.2014.885930
28. Sieuwerts, S.; De Bok, F. A. M.; Mols, E.; De Vos, W. M.; Van Hylckama Vlieg, J. E. T., A simple and fast method for determining colony forming units. *Lett. Appl. Microbiol.* **2008**, *47* (4), 275-278. DOI: 10.1111/j.1472-765X.2008.02417.x
29. Kim, S.-O.; Kim, S.-S., Bacterial pathogen detection by conventional culture-based and recent alternative (polymerase chain reaction, isothermal amplification, enzyme linked immunosorbent assay, bacteriophage amplification, and gold nanoparticle aggregation) methods in food samples: A review. *J. Food Saf.* **2021**, *41* (1), 1-12. DOI: 10.1111/jfs.12870

30. Benoit, P. W.; Donahue, D. W., Methods for Rapid Separation and Concentration of Bacteria in Food that Bypass Time-Consuming Cultural Enrichment. *J. Food Prot.* **2003**, *66* (10), 1935-1948. DOI: 10.4315/0362-028x-66.10.1935
31. Váradi, L.; Luo, J. L.; Hibbs, D. E.; Perry, J. D.; Anderson, R. J.; Orenge, S.; Groundwater, P. W., Methods for the detection and identification of pathogenic bacteria: past, present, and future. *Chem. Soc. Rev.* **2017**, *46* (16), 4818-4832. DOI: 10.1039/C6CS00693K
32. Maskow, T.; Wolf, K.; Kunze, W.; Enders, S.; Harms, H., Rapid analysis of bacterial contamination of tap water using isothermal calorimetry. *Thermochim. Acta* **2012**, *543*, 273-280. DOI: 10.1016/j.tca.2012.06.002
33. Gram, L.; Søgaard, H., The potentiality of microcalorimetry as a rapid method for monitoring the microbiological quality of raw meat and fish. *Thermochim. Acta* **1985**, *95* (2), 375-381. DOI: 10.1016/0040-6031(85)85298-9
34. Braissant, O.; Wirz, D.; Göpfert, B.; Daniels, A. U., Biomedical Use of Isothermal Microcalorimeters. *Sensors* **2010**, *10* (10), 9369-9383. DOI: 10.3390/s101009369
35. Baldoni, D.; Hermann, H.; Frei, R.; Trampuz, A.; Steinhuber, A., Performance of Microcalorimetry for Early Detection of Methicillin Resistance in Clinical Isolates of *Staphylococcus aureus*. *J. Clin. Microbiol.* **2009**, *47* (3), 774-776. DOI: 10.1128/jcm.02374-08
36. Corvec, S.; Seiler, E.; Wang, L.; Moreno, M. G.; Trampuz, A., Characterization of medical relevant anaerobic microorganisms by isothermal microcalorimetry. *Anaerobe* **2020**, *66* (102282), 1-6. DOI: 10.1016/j.anaerobe.2020.102282
37. Baron E. J. Chapter 3 Classification. In *Medical microbiology*, 4th ed.; Baron, S., Ed.; University of Texas Medical Branch at Galveston: Galveston, Texas, 1996.
38. Sandle, T., 9 - Microbial identification. In *Pharmaceutical Microbiology*, Sandle, T., Ed.; Woodhead Publishing: Oxford, 2016; pp 103-113. DOI: 10.1016/B978-0-08-100022-9.00009-8
39. Janda, J. M.; Abbott, S. L., Bacterial identification for publication: when is enough enough? *J. Clin. Microbiol.* **2002**, *40* (6), 1887-1891. DOI: 10.1128/JCM.40.6.1887-1891.2002
40. Proctor, C. H., A simple definition of detection limit. *J. Agric. Biol. and Environ. Stat.* **2008**, *13* (99), 99-120. DOI: 10.1198/108571108X273476
41. Kaufmann, S. H. E.; Schaible, U. E., 100th anniversary of Robert Koch's Nobel Prize for the discovery of the tubercle bacillus. *Trends Microbiol.* **2005**, *13* (10), 469-475. DOI: 10.1016/j.tim.2005.08.003
42. Blevins, S. M.; Bronze, M. S., Robert Koch and the 'golden age' of bacteriology. *Int. J. Infect. Dis.* **2010**, *14* (9), e744-e751. DOI: 10.1016/j.ijid.2009.12.003
43. Hitchens, A. P.; Leikind, M. C., The Introduction of Agar-agar into Bacteriology. *J. Bacteriol.* **1939**, *37* (5), 485-493. DOI: 10.1128/JB.37.5.485-493.1939
44. Hahn, M. W.; Koll, U.; Schmidt, J., Isolation and Cultivation of Bacteria. In *The Structure and Function of Aquatic Microbial Communities*, Hurst, C. J., Ed.; Springer: Cham, 2019; Vol. 7, pp 313-351. DOI: 10.1007/978-3-030-16775-2_10

45. Hameed, S.; Xie, L.; Ying, Y., Conventional and emerging detection techniques for pathogenic bacteria in food science: A review. *Trends in Food Sci. Technol.* **2018**, *81*, 61-73. DOI: 10.1016/j.tifs.2018.05.020
46. Lodish H; Berk A; Zipursky SL; Matsudaira P; Baltimore D; J, D., *Molecular cell biology*. 4th ed.; W.H. Freeman: New York, 2000.
47. Baylis, C. L.; MacPhee, S.; Betts, R. P., Comparison of two commercial preparations of buffered peptone water for the recovery and growth of Salmonella bacteria from foods. *J. Appl. Microbiol.* **2000**, *89* (3), 501-510. DOI: 10.1046/j.1365-2672.2000.01145.x
48. International Organization for Standardization (ISO), ISO 11731:2017 Water quality — Enumeration of Legionella. 2017.
49. Taylor, R. H.; Geldreich, E. E., A New Membrane Filter Procedure for Bacterial Counts in Potable Water and Swimming Pool Samples. *J. Am. Water Works Assoc.* **1979**, *71* (7), 402-405.
50. Chen, W.-B.; Zhang, C., An automated bacterial colony counting and classification system. *Inf. Sys. Front.* **2009**, *11* (4), 349-368. DOI: 10.1007/s10796-009-9149-0
51. Jung, J. H.; Lee, J. E., Real-time bacterial microcolony counting using on-chip microscopy. *Sci. Rep.* **2016**, *6* (21473), 1-8. DOI: 10.1038/srep21473
52. Donohue, M. J.; O'Connell, K.; Vesper, S. J.; Mistry, J. H.; King, D.; Kostich, M.; Pfaller, S., Widespread Molecular Detection of Legionella pneumophila Serogroup 1 in Cold Water Taps across the United States. *Environ. Sci. Technol.* **2014**, *48* (6), 3145-3152. DOI: 10.1021/es4055115
53. Fricke, C.; Xu, J.; Jiang, F.-L.; Liu, Y.; Harms, H.; Maskow, T., Rapid culture-based detection of Legionella pneumophila using isothermal microcalorimetry with an improved evaluation method. *Microb. Biotechnol.* **2020**, *13* (4), 1262-1272. DOI: 10.1111/1751-7915.13563
54. Brugger, S. D.; Baumberger, C.; Jost, M.; Jenni, W.; Brugger, U.; Mühlemann, K., Automated Counting of Bacterial Colony Forming Units on Agar Plates. *PLoS One* **2012**, *7* (3), 1-6. DOI: 10.1371/journal.pone.0033695
55. Siragusa, M.; Dall'Olio, S.; Fredericia, P. M.; Jensen, M.; Groesser, T., Cell colony counter called CoCoNut. *PLoS One* **2018**, *13* (11), 1-18. DOI: 10.1371/journal.pone.0205823
56. Frost, H. R.; Tsoi, S. K.; Baker, C. A.; Laho, D.; Sanderson-Smith, M. L.; Steer, A. C.; Smeesters, P. R., Validation of an automated colony counting system for group A Streptococcus. *BMC Res. Notes* **2016**, *9* (72), 1-8. DOI: 10.1186/s13104-016-1875-z
57. Clarke, M. L.; Burton, R. L.; Hill, A. N.; Litorja, M.; Nahm, M. H.; Hwang, J., Low-cost, high-throughput, automated counting of bacterial colonies. *Cytom. A* **2010**, *77A* (8), 790-797. DOI: 10.1002/cyto.a.20864
58. London, R.; Schwedock, J.; Sage, A.; Valley, H.; Meadows, J.; Waddington, M.; Straus, D., An Automated System for Rapid Non-Destructive Enumeration of Growing Microbes. *PLoS One* **2010**, *5* (1), 1-16. DOI: 10.1371/journal.pone.0008609
59. Khan, A. u. M.; Torelli, A.; Wolf, I.; Gretz, N., AutoCellSeg: robust automatic colony forming unit (CFU)/cell analysis using adaptive image segmentation and easy-to-use post-editing techniques. *Sci. Rep.* **2018**, *8* (7302), 1-10. DOI: 10.1038/s41598-018-24916-9

60. Austerjost, J.; Marquard, D.; Raddatz, L.; Geier, D.; Becker, T.; Scheper, T.; Lindner, P.; Beutel, S., A smart device application for the automated determination of *E. coli* colonies on agar plates. *Eng. Life Sci.* **2017**, *17* (8), 959-966. DOI: 10.1002/elsc.201700056
61. Frost, W. D., Improved technic for the micro or little plate method of counting bacteria in milk. *J. Infect. Dis.* **1921**, *28* (2), 176-184. DOI: 10.1093/infdis/28.2.176
62. Pönisch, W.; Eckenrode, K. B.; Alzurqa, K.; Nasrollahi, H.; Weber, C.; Zaburdaev, V.; Biaias, N., Pili mediated intercellular forces shape heterogeneous bacterial microcolonies prior to multicellular differentiation. *Sci. Rep.* **2018**, *8* (16567), 1-10. DOI: 10.1038/s41598-018-34754-4
63. Kuchibiro, T.; Hirano, A.; Ogasawara, S.; Nakamura, T., The microcolony detection method (MCD), a simple and rapid screening test for antimicrobial resistance bacteria on positive blood cultures. *Heliyon* **2020**, *6* (11), 1-7. DOI: 10.1016/j.heliyon.2020.e05494
64. Galat, A.; Dufresne, J.; Combrisson, J.; Thépaut, J.; Boumghar-Bourtchai, L.; Boyer, M.; Fourmestraux, C., Novel method based on chromogenic media for discrimination and selective enumeration of lactic acid bacteria in fermented milk products. *Food Microbiol.* **2016**, *55*, 86-94. DOI: 10.1016/j.fm.2015.11.005
65. Gunasekera, T. S.; Attfield, P. V.; Veal, D. A., A flow cytometry method for rapid detection and enumeration of total bacteria in milk. *Appl. Environ. Microbiol.* **2000**, *66* (3), 1228-1232. DOI: 10.1128/AEM.66.3.1228-1232.2000
66. Li, L.; Mendis, N.; Trigui, H.; Oliver, J. D.; Faucher, S. P., The importance of the viable but non-culturable state in human bacterial pathogens. *Front. Microbiol.* **2014**, *5* (258), 1-20. DOI: 10.3389/fmicb.2014.00258
67. Ricchi, M.; Bertasio, C.; Boniotti, M. B.; Vicari, N.; Russo, S.; Tilola, M.; Bellotti, M. A.; Bertasi, B., Comparison among the Quantification of Bacterial Pathogens by qPCR, dPCR, and Cultural Methods. *Front. Microbiol.* **2017**, *8* (1174), 1-15. DOI: 10.3389/fmicb.2017.01174
68. Garibyan, L.; Avashia, N., Polymerase chain reaction. *J. Invest. Dermatol.* **2013**, *133* (3), 1-4. DOI: 10.1038/jid.2013.1
69. Dusserre, E.; Ginevra, C.; Hallier-Soulier, S.; Vandenesch, F.; Festoc, G.; Etienne, J.; Jarraud, S.; Molmeret, M., A PCR-based method for monitoring *Legionella pneumophila* in water samples detects viable but noncultivable legionellae that can recover their cultivability. *Appl. Environ. Microbiol.* **2008**, *74* (15), 4817-4824. DOI: 10.1128/AEM.02899-07
70. Belgrader, P.; Benett, W.; Hadley, D.; Richards, J.; Stratton, P.; Mariella, R.; Milanovich, F., PCR Detection of Bacteria in Seven Minutes. *Science* **1999**, *284* (5413), 449-450. DOI: 10.1126/science.284.5413.449
71. De Medici, D.; Kuchta, T.; Knutsson, R.; Angelov, A.; Auricchio, B.; Barbanera, M.; Diaz-Amigo, C.; Fiore, A.; Kudirkiene, E.; Hohl, A.; Horvatek Tomic, D.; Gotcheva, V.; Popping, B.; Prukner-Radovic, E.; Scaramaglia, S.; Siekel, P.; To, K. A.; Wagner, M., Rapid Methods for Quality Assurance of Foods: the Next Decade with Polymerase Chain Reaction (PCR)-Based Food Monitoring. *Food Anal. Methods* **2015**, *8* (2), 255-271. DOI: 10.1007/s12161-014-9915-6
72. Cangelosi, G. A.; Meschke, J. S., Dead or Alive: Molecular Assessment of Microbial Viability. *Appl. Environ. Microbiol.* **2014**, *80* (19), 5884-5891. DOI: 10.1128/aem.01763-14

73. Law, J. W.-F.; Ab Mutalib, N.-S.; Chan, K.-G.; Lee, L.-H., Rapid methods for the detection of foodborne bacterial pathogens: principles, applications, advantages and limitations. *Front. Microbiol.* **2015**, *5* (770), 1-19. DOI: 10.3389/fmicb.2014.00770
74. Verma, J.; Saxena, S.; Babu, S. G., ELISA-Based Identification and Detection of Microbes. In *Analyzing Microbes: Manual of Molecular Biology Techniques*, Arora, D. K.; Das, S.; Sukumar, M., Eds. Springer Berlin Heidelberg: Berlin, Heidelberg, 2013; pp 169-186. DOI: 10.1007/978-3-642-34410-7_13
75. Mobed, A.; Baradaran, B.; Guardia, M. d. l.; Agazadeh, M.; Hasanzadeh, M.; Rezaee, M. A.; Mosafer, J.; Mokhtarzadeh, A.; Hamblin, M. R., Advances in detection of fastidious bacteria: From microscopic observation to molecular biosensors. *Trends Anal. Chem.* **2019**, *113*, 157-171. DOI: 10.1016/j.trac.2019.02.012
76. Ivnitski, D.; Abdel-Hamid, I.; Atanasov, P.; Wilkins, E., Biosensors for detection of pathogenic bacteria. *Biosens. Bioelectron.* **1999**, *14* (7), 599-624. DOI: 10.1016/S0956-5663(99)00039-1
77. Deisingh, A. K.; Thompson, M., Biosensors for the detection of bacteria. *Can. J. Microbiol.* **2004**, *50* (2), 69-77. DOI: 10.1139/w03-095 %M 15052308
78. Kotsiri, Z.; Vidic, J.; Vantarakis, A., Applications of biosensors for bacteria and virus detection in food and water—A systematic review. *J. Environ. Sci.* **2022**, *111*, 367-379. DOI: 10.1016/j.jes.2021.04.009
79. Bhalla, N.; Jolly, P.; Formisano, N.; Estrela, P., Introduction to biosensors. *Essays Biochem.* **2016**, *60* (1), 1-8. DOI: 10.1042/EBC20150001
80. Ahmed, A.; Rushworth, J. V.; Hirst, N. A.; Millner, P. A., Biosensors for whole-cell bacterial detection. *Clin. Microbiol. Rev.* **2014**, *27* (3), 631-646. DOI: 10.1128/CMR.00120-13
81. Lazcka, O.; Campo, F. J. D.; Muñoz, F. X., Pathogen detection: A perspective of traditional methods and biosensors. *Biosens. Bioelectron.* **2007**, *22* (7), 1205-1217. DOI: 10.1016/j.bios.2006.06.036
82. Gustafsson, L., Microbiological calorimetry. *Thermochim. Acta* **1991**, *193*, 145-171. DOI: 10.1016/0040-6031(91)80181-H
83. Wadsö, I., Bio-calorimetry. *Trends in Biotechnol.* **1986**, *4* (2), 45-51. DOI: 10.1016/0167-7799(86)90153-8
84. Chaires, J. B.; Hansen, L. D.; Keller, S.; Brautigam, C. A.; Zhao, H.; Schuck, P., Biocalorimetry. *Methods* **2015**, *76*, 1-2. DOI: 10.1016/j.ymeth.2015.02.001
85. Sivaprakasam, S.; Schuler, M. M.; Hama, A.; Hughes, K.-M.; Marison, I. W., Biocalorimetry as a process analytical technology process analyser; robust in-line monitoring and control of aerobic fed-batch cultures of crabtree-negative yeast cells. *J. Therm. Anal. Calorim.* **2011**, *104* (1), 75-85. DOI: 10.1007/s10973-010-1259-x
86. Wadsö, I., Biochemical calorimetry. *Pure Appl. Chem.* **1964**, *8* (2), 179-186. DOI: 10.1351/pac196408020179
87. Snyder, G. J.; Toberer, E. S., Complex thermoelectric materials. *Nat. Mater.* **2008**, *7* (2), 105-114. DOI: 10.1351/pac196408020179

88. O'Connor, C. M.; Adams, J. U., *Essentials of Cell Biology* [Online]; NPG Education: Cambridge, MA, 2010. <https://www.nature.com/scitable/ebooks/essentials-of-cell-biology-14749010/>. (accessed June 22, 2021).
89. Stockar, U. v.; Marison, I. W.; Liu, J.-S., Endothermic microbial growth. A calorimetric investigation of an extreme case of entropy-driven microbial growth. *Pure Appl. Chem.* **2000**, *72* (10), 1835-1838. DOI: 10.1351/pac200072101835
90. Blaxter, K. L., Adair Crawford and Calorimetry. *Proc. Nutr. Soc.* **1978**, *37* (1), 1-3. DOI: 10.1079/PNS19780002
91. Sarge, S. M.; Höhne, G.; Hemminger, W., *Calorimetry: Fundamentals, Instrumentation and Applications*, 1st ed.; Wiley VCH, 2014. DOI: 10.1002/9783527649365
92. Lamprecht, I., Calorimetry and thermodynamics of living systems. *Thermochim. Acta* **2003**, *405* (1), 1-13. DOI: 10.1016/S0040-6031(03)00123-0
93. Kőrösy, K. v., Mikrokalorimeter zur Bestimmung der Wärmeproduktion von Bakterien. **1913**, *86* (5), 383-400. DOI: 10.1515/bchm2.1913.86.5.383
94. Tangl, F., Beiträge zur Energetik der Ontogenese. *Archiv für die gesamte Physiologie des Menschen und der Tiere* **1903**, *98* (11), 475-489. DOI: 10.1007/BF01663663
95. Hill, A. V., A new form of differential micro-calorimeter, for the estimation of heat production in physiological, bacteriological, or ferment actions. *J. Physiol.* **1911**, *43* (3-4), 261-285. DOI: 10.1126/science.284.5413.449
96. Ud-Din, A.; Wahid, S., Relationship among *Shigella* spp. and enteroinvasive *Escherichia coli* (EIEC) and their differentiation. *Braz. J. Microbiol.* **2014**, *45* (4), 1131-1138. DOI: 10.1590/S1517-83822014000400002
97. Shearer, C., On the amount of heat liberated by bacillus coli when grown in the presence of free amino-acids. *J. Physiol.* **1921**, *55* (1-2), 50-60. DOI: 10.1113/jphysiol.1921.sp001955
98. Bayne-Jones, S.; Rhees, H. S., Bacterial calorimetry II. Relationship of heat production to phases of growth of bacteria. *J. Bacteriol.* **1929**, *17* (2), 123-140. DOI: 10.1128/jb.17.2.123-140.1929
99. Beezer, A. E., *Biological Microcalorimetry*. Academic Press London: New York, 1980.
100. Bastos, M., *Biocalorimetry Foundations and Contemporary Approaches*. 1st ed.; CRC Press: Boca Raton, 2016. DOI: 10.1201/b20161
101. Mortensen, U.; Norén, B.; Wadsö, I., Microcalorimetry in the Study of the Activity of Microorganisms. *Bulletins from the Ecological Research Committee* **1973**, (17), 189-197.
102. Spink, C. H.; Wadsö, I., Analytical Calorimetry in Biochemical and Clinical Applications. *Crit. Rev. Anal. Chem.* **1980**, *9* (1), 1-54. DOI: 10.1080/10408348008542716
103. C.-G. Heden, T. I., *New approaches to the identification of microorganisms*. Wiley: New York, 1975.

104. Berridge, N. J.; Cousins, C. M.; Cliffe, A. J., Microcalorimetry applied to certain species of bacteria growing in sterilized separated milk. *J. dairy Res.* **1974**, *41* (2), 203-15. DOI: 10.1017/s0022029900019622
105. Ripa, K. T.; Mårdh, P. A.; Hovellius, B.; Ljungholm, K., Microcalorimetry as a tool for evaluation of blood culture media. *J. Clin. Microbiol.* **1977**, *5* (4), 393-396. DOI: 10.1128/jcm.5.4.393-396.1977
106. Gram, L.; Søgaaard, H., Microcalorimetry as a Rapid Method for Estimation of Bacterial Levels in Ground Meat. *J. Food Prot.* **1985**, *48* (4), 341-345. DOI: 10.4315/0362-028x-48.4.341
107. Suurkuusk, J.; Suurkuusk, M.; Vikegard, P., A multichannel microcalorimetric system The third-generation Thermal Activity Monitor (TAM III). *J. Therm. Anal. Calorim.* **2018**, *131* (2), 1949-1966. DOI: 10.1007/s10973-017-6684-7
108. Wadsö, L.; Markova, N., A double twin isothermal microcalorimeter. *Thermochim. Acta* **2000**, *360* (2), 101-107. DOI: 10.1016/S0040-6031(00)00574-8
109. Wadsö, L.; Li, X., A simple rate law experiment using a custom-built isothermal heat conduction calorimeter. *J. Chem. Educ.* **2008**, *85* (1), 112-116. DOI: 10.1021/ed085p112
110. Wadsö, L.; Salamanca, Y.; Johansson, S., Biological applications of a new isothermal calorimeter that simultaneously measures at four temperatures. *J. Therm. Anal. Calorim.* **2011**, *104* (1), 119-126. DOI: 10.1007/s10973-010-1140-y.
111. Trampuz, A.; Steinhuber, A.; Wittwer, M.; Leib, S. L., Rapid diagnosis of experimental meningitis by bacterial heat production in cerebrospinal fluid. *BMC Infect. Dis.* **2007**, *7* (116), 1-6. DOI: 10.1186/1471-2334-7-116
112. Braissant, O.; Wirz, D.; Göpfert, B.; Daniels, A. U., "The heat is on": Rapid microcalorimetric detection of mycobacteria in culture. *Tuberculosis* **2010**, *90* (1), 57-59. DOI: 10.1016/j.tube.2009.11.001
113. Rodríguez, D.; Daniels, A. U.; Urrusti, J. L.; Wirz, D.; Braissant, O., Evaluation of a low-cost calorimetric approach for rapid detection of tuberculosis and other mycobacteria in culture. *J. Appl. Microbiol.* **2011**, *111* (4), 1016-1024. DOI: 10.1111/j.1365-2672.2011.05117.x
114. Bonkat, G.; Bachmann, A.; Solokhina, A.; Widmer, A. F.; Frei, R.; Gasser, T. C.; Braissant, O., Growth of Mycobacteria in Urine Determined by Isothermal Microcalorimetry: Implications for Urogenital Tuberculosis and Other Mycobacterial Infections. *Urology* **2012**, *80* (5), 1163.e9-1163.e12. DOI: 10.1016/j.urology.2012.04.050
115. von Stockar, U.; Liu, J. S., Does microbial life always feed on negative entropy? Thermodynamic analysis of microbial growth. *Biochim. Biophys. Acta Bioenerg.* **1999**, *1412* (3), 191-211. DOI: 10.1016/S0005-2728(99)00065-1
116. Goldberg, R. N., Thermodynamics of Enzyme-Catalyzed Reactions: Part 6—1999 Update. *J. Phys. Chem. Ref. Data* **1999**, *28* (4), 931-965. DOI: 10.1063/1.556041
117. Stenesh, J., Introduction to Metabolism. In *Biochemistry*, Springer US: Boston, MA, 1998; pp 203-219. DOI: 10.1007/978-1-4757-9427-4_8

118. Forrest, W. W., Entropy of Microbial Growth. *Nature* **1970**, 225 (5238), 1165-1166. DOI: 10.1038/2251165b0
119. Maskow, T.; Kemp, R.; Buchholz, F.; Schubert, T.; Kiesel, B.; Harms, H., What heat is telling us about microbial conversions in nature and technology: from chip- to megacalorimetry. *Microb. Biotechnol.* **2010**, 3 (3), 269-284.
120. Maskow, T.; Paufler, S., What does calorimetry and thermodynamics of living cells tell us? *Methods* **2015**, 76, 3-10. DOI: 10.1016/j.ymeth.2014.10.035
121. Chang-Li, X.; Hou-Kuhan, T.; Zhou-Hua, S.; Song-Sheng, Q.; Yao-Ting, L.; Hai-Shui, L., Microcalorimetric study of bacterial growth. *Thermochim. Acta* **1988**, 123, 33-41. DOI: 10.1016/0040-6031(88)80007-8
122. Maskow, T.; Schubert, T.; Wolf, A.; Buchholz, F.; Regestein, L.; Buechs, J.; Mertens, F.; Harms, H.; Lerchner, J., Potentials and limitations of miniaturized calorimeters for bioprocess monitoring. *Appl. Microbiol. Biotechnol.* **2011**, 92 (1), 55-66. DOI: 10.1007/s00253-011-3497-7
123. Kemp, R. B.; Guan, Y., Heat flux and the calorimetric-respirometric ratio as measures of catabolic flux in mammalian cells. *Thermochim. Acta* **1997**, 300 (1), 199-211. DOI: 10.1016/S0040-6031(96)03125-5
124. Fricke, C.; Harms, H.; Maskow, T., How to speed up the detection of aerobic microbial contaminations by using isothermal microcalorimetry. *J. Therm. Anal. Calorim.* **2020**, 142 (5), 1933-1949. DOI: 10.1007/s10973-020-09986-0
125. Bonkat, G.; Braissant, O.; Widmer, A. F.; Frei, R.; Rieken, M.; Wyler, S.; Gasser, T. C.; Wirz, D.; Daniels, A. U.; Bachmann, A., Rapid detection of urinary tract pathogens using microcalorimetry: principle, technique and first results. *BJU Int.* **2012**, 110 (6), 892-897. DOI: 10.1111/j.1464-410X.2011.10902.x
126. Wadsö, I., On the accuracy of results from microcalorimetric measurements on cellular systems. *Thermochim. Acta* **1993**, 219, 1-15. DOI: 10.1016/0040-6031(93)80479-T
127. Skoczowski, A.; Przemieniecki, S. W.; Oliwa, J.; Kula-Maximenko, M.; Rys, M.; Stawoska, I.; Karpiński, S., Estimation of microbiological contamination of maize seeds using isothermal calorimetry. *J. Therm. Anal. Calorim.* **2020**, 142 (2), 749-754. DOI: 10.1007/s10973-020-10011-7
128. Entenza, J. M.; Bétrisey, B.; Manuel, O.; Giddey, M.; Sakwinska, O.; Laurent, F.; Bizzini, A., Rapid Detection of *Staphylococcus aureus* Strains with Reduced Susceptibility to Vancomycin by Isothermal Microcalorimetry. *J. Clin. Microbiol.* **2014**, 52 (1), 180-186. DOI: 10.1128/jcm.01820-13
129. Lago, N.; Legido, J. L.; Paz Andrade, M. I.; Arias, I.; Casás, L. M., Microcalorimetric study on the growth and metabolism of *Pseudomonas aeruginosa*. *J. Therm. Anal. Calorim.* **2011**, 105 (2), 651-655. DOI: 10.1007/s10973-010-1175-0
130. Rivero, N. L.; Legido, J. L.; Santos, I. A.; Casás, L. M., Comparative Study of Microcalorimetric Behavior of *Escherichia coli*, *Proteus mirabilis* and *Klebsiella pneumoniae*. *Pol. J. Microbiol.* **2012**, 61 (3), 199-204. DOI: 10.1007/s10973-011-2052-1

131. Rivero, N. L.; Legido Soto, J. L.; Casás, L. M.; Santos, I. A., Microcalorimetric study of the growth of *Enterococcus faecalis* in an enriched culture medium. *J. Therm. Anal. Calorim.* **2012**, *108* (2), 665-670. DOI: 10.1007/s10973-011-2052-1
132. Brueckner, D.; Krähenbühl, S.; Zuber, U.; Bonkat, G.; Braissant, O., An alternative sterility assessment for parenteral drug products using isothermal microcalorimetry. *J. Appl. Microbiol.* **2017**, *123* (3), 773-779. DOI: 10.1111/jam.13520
133. Nykyri, J.; Herrmann, A. M.; Håkansson, S., Isothermal microcalorimetry for thermal viable count of microorganisms in pure cultures and stabilized formulations. *BMC Microbiol.* **2019**, *19* (65), 1-10. DOI: 10.1186/s12866-019-1432-8
134. Wadsö, L.; Smith, A. L.; Shirazi, H.; Mulligan, S. R.; Hofelich, T., The isothermal heat conduction calorimeter: A versatile instrument for studying processes in physics, chemistry, and biology. *J. Chem. Educ.* **2001**, *78* (8), 1080-1086. DOI: 10.1021/ed078p1080
135. Wadsö, I., Trends in isothermal microcalorimetry. *Chem. Soc. Rev.* **1997**, *26* (2), 79-86. DOI: 10.1039/CS9972600079
136. Bäckman, P.; Bastos, M.; Hallén, D.; Lönnbro, P.; Wadsö, I., Heat conduction calorimeters: time constants, sensitivity and fast titration experiments. *J. Biochem. Biophys. Methods* **1994**, *28* (2), 85-100. DOI: 10.1016/0165-022X(94)90023-X
137. Bäckman, P.; Bastos, M.; Briggner, L.-E.; Hagg, S.; Hallen, D.; Lonnbro, P.; Nilsson, S.-O.; Olofsson, G.; Schon, A.; Suurkuusk, J.; Teixeira, C.; Wadsö, I., A system of microcalorimeters. *Pure Appl. Chem.* **1994**, *66* (3), 375-382. DOI: 10.1351/pac199466030375
138. Wadsö, L., Temperature changes within samples in heat conduction calorimeters. *Thermo-chim. Acta* **2001**, *366* (2), 121-127. DOI: 10.1016/S0040-6031(00)00738-3
139. Wadsö, I., Design and Testing of a Micro Reaction Calorimeter. *Acta Chem. Scand.* **1968**, *22* (3), 927-937. DOI: 10.3891/acta.chem.scand.22-0927
140. Witting, I. T.; Chasapis, T. C.; Ricci, F.; Peters, M.; Heinz, N. A.; Hautier, G.; Snyder, G. J., The Thermoelectric Properties of Bismuth Telluride. *Adv. Electron. Mater.* **2019**, *5* (6), 1-20. DOI: 10.1002/aelm.201800904
141. Wadsö, I.; Goldberg, R. N., Standards in isothermal microcalorimetry (IUPAC Technical Report). *Pure Appl. Chem.* **2001**, *73* (10), 1625-1639. DOI: 10.1351/pac200173101625
142. Jaziri, N.; Boughamoura, A.; Müller, J.; Mezghani, B.; Tounsi, F.; Ismail, M., A comprehensive review of Thermoelectric Generators: Technologies and common applications. *Energy Rep.* **2020**, *6*, 264-287. DOI: 10.1016/j.egy.2019.12.011
143. Goldsmid, H. J., Bismuth Telluride and Its Alloys as Materials for Thermoelectric Generation. *Materials* **2014**, *7* (4), 2577-2592. DOI: 10.3390/ma7042577
144. Lee, W.; Fon, W.; Axelrod, B. W.; Roukes, M. L., High-sensitivity microfluidic calorimeters for biological and chemical applications. *Proc. Natl. Acad. Sci. U.S.A.* **2009**, *106* (36), 15225-15230. DOI: 10.1073/pnas.0901447106
145. Wadsö, L., Operational issues in isothermal calorimetry. *Cem. Concr. Res.* **2010**, *40* (7), 1129-1137. DOI: 10.1016/j.cemconres.2010.03.017

146. Chen, A. T.; Wadsö, I., A Test and Calibration Process for Micro-Calorimeters Used as Thermal Power Meters. *J. Biochem. Biophys. Methods* **1982**, *6* (4), 297-306. DOI: 10.1016/0165-022x(82)90011-2
147. Wadsö, I., Needs for standards in isothermal microcalorimetry. *Thermochim. Acta* **2000**, *347* (1), 73-77. DOI: 10.1016/S0040-6031(99)00418-9
148. González-Durán, J. E. E.; Zamora-Antuñano, M. A.; Lira-Cortés, L.; Rodríguez-Reséndiz, J.; Olivares-Ramírez, J. M.; Lozano, N. E. M., Numerical Simulation for the Combustion Chamber of a Reference Calorimeter. *Processes* **2020**, *8* (5), 1-15. DOI: 10.3390/pr8050575
149. Okereke, M.; Keates, S., Computational Mechanics and the Finite Element Method. In *Finite Element Applications: A Practical Guide to the FEM Process*, Springer: Cham, 2018; pp 3-25. DOI: 10.1007/978-3-319-67125-3_1
150. Rao, S. S., Chapter 1 - Overview of Finite Element Method. In *The Finite Element Method in Engineering*, 5th ed.; Rao, S. S., Ed. Butterworth-Heinemann: Boston, 2011; pp 3-50. DOI: 10.1016/B978-1-85617-661-3.00001-5
151. Pepper, D.; Heinrich, J., *The Finite Element Method: Basic Concepts and Applications with MATLAB®, MAPLE, and COMSOL*. 2017. DOI: 10.1201/9781315395104
152. Davids, N.; Berger, R. L., Computer simulation for deconvolution of a heat conduction batch microcalorimeter by the D-B Finite Element Technique. *J. Biochem. Biophys. Methods* **1982**, *6* (3), 205-17. DOI: 10.1016/0165-022x(82)90043-4
153. Vilchiz, L. E.; Pacheco-Vega, A.; Handy, B. E., Heat-flow patterns in Tian–Calvet microcalorimeters: Conductive, convective, and radiative transport in gas dosing experiments. *Thermochim. Acta* **2005**, *439* (1), 110-118. DOI: 10.1016/j.tca.2005.09.014
154. Cruz-Duarte, J.; Morega, A.; Garcia-Perez, A.; Correa-Cely, C., Numerical simulation of heat transfer process in a non-conventional calorimeter. *Rev. Roum. Sci. Tech - El* **2017**, *62*, 424-430.
155. Kočí, V.; Maděra, J.; Jerman, M.; Černý, R., Computational analysis of heat transport and storage processes in large-volume isothermal heat flow calorimeter. *Appl. Therm. Eng.* **2017**, *121*, 547-553. DOI: 10.1016/j.applthermaleng.2017.04.118
156. Bae, J.; Zheng, J.; Zhang, H.; Foster, P. J.; Needleman, D. J.; Vlassak, J. J., A Micromachined Picocalorimeter Sensor for Liquid Samples with Application to Chemical Reactions and Biochemistry. *Adv. Sci.* **2021**, *8* (5), 1-11. DOI: 10.1002/advs.202003415
157. Wadsö, I.; Hallén, D.; Jansson, M.; Suurkuusk, J.; Wenzler, T.; Braissant, O., A well-plate format isothermal multi-channel microcalorimeter for monitoring the activity of living cells and tissues. *Thermochim. Acta* **2017**, *652*, 141-149. DOI: 10.1016/j.tca.2017.03.010
158. Xebios Diagnostics GmbH. Legionella-BCYE+AB Agar (Bulk) (BCYE+AB). <https://www.xebios.de/items/legionella-bcye-ab-nen-agar.pdf> (accessed June 30, 2021).
159. Xebios Diagnostics GmbH. Legionella-GVPC-Selective-Agar. <https://www.xebios.com/items/legionella-gvpc-selektivagar.pdf> (accessed June 30, 2021).
160. Soestbergen, A. A. V.; Lee, C. H., Pour Plates or Streak Plates? *Appl. Microbiol.* **1969**, *18* (6), 1092-1093. DOI: 10.1128/am.18.6.1092-1093.1969

161. Goetz, A.; Tsuneishi, N.; Kabler, P. W.; Streicher, L.; Neumann, H. G., Application of Molecular Filter Membranes to the Bacteriological Analysis of Water. *J. Am. Water Works Assoc.* **1951**, *43* (12), 943-984.
162. Fricke, C.; Harms, H.; Maskow, T., Rapid Calorimetric Detection of Bacterial Contamination: Influence of the Cultivation Technique. *Front. Microbiol.* **2019**, *10*, 1-12. DOI: 10.3389/fmicb.2019.02530
163. Benson, B. B.; Krause Jr., D., The concentration and isotopic fractionation of oxygen dissolved in freshwater and seawater in equilibrium with the atmosphere. *Limnol. Oceanogr.* **1984**, *29* (3), 620-632. DOI: 10.4319/lo.1984.29.3.0620
164. Maskow, T.; Morais, F. M.; Rosa, L. F. M.; Qian, Y. G.; Harnisch, F., Insufficient oxygen diffusion leads to distortions of microbial growth parameters assessed by isothermal microcalorimetry. *RSC Adv.* **2014**, *4* (62), 32730-32737. DOI: 10.1039/C4RA03921A
165. Omiccioli, E.; Schiavano, G. F.; Ceppetelli, V.; Amagliani, G.; Magnani, M.; Brandi, G., Validation according to ISO/TS 12869:2012 of a molecular method for the isolation and quantification of *Legionella* spp. in water. *Mol. Cell. Probes* **2015**, *29* (2), 86-91. DOI: 10.1016/j.mcp.2014.12.004
166. Collins, S.; Stevenson, D.; Walker, J.; Bennett, A., Evaluation of *Legionella* real-time PCR against traditional culture for routine and public health testing of water samples. *J. Appl. Microbiol.* **2017**, *122* (6), 1692-1703. DOI: 10.1111/jam.13461
167. Young, C.; Smith, D.; Wafer, T.; Crook, B., Rapid Testing and Interventions to Control *Legionella* Proliferation following a Legionnaires' Disease Outbreak Associated with Cooling Towers. *Microorganisms* **2021**, *9* (3), 1-15. DOI: 10.3390/microorganisms9030615
168. Ditommaso, S.; Giacomuzzi, M.; Memoli, G.; Garlasco, J.; Zotti, C. M., Comparison of BCYE α +AB agar and MWY agar for detection and enumeration of *Legionella* spp. in hospital water samples. *BMC Microbiol.* **2021**, *21* (48), 1-6. DOI: 10.1186/s12866-021-02109-1
169. Krøjgaard, L. H.; Krogfelt, K. A.; Albrechtsen, H.-J.; Uldum, S. A., Detection of *Legionella* by quantitative-polymerase chain reaction (qPCR) for monitoring and risk assessment. *BMC Microbiol.* **2011**, *11* (254), 1-7. DOI: 10.1186/1471-2180-11-254
170. Monteiro, S. N.; Robalo, A. M.; Santos, R. J., Evaluation of Legiolert™ for the Detection of *Legionella pneumophila* and Comparison with Spread-Plate Culture and qPCR Methods. *Curr. Microbiol.* **2021**, *78* (5), 1792-1797. DOI: 10.1007/s00284-021-02436-6
171. Scaturro, M.; Buffoni, M.; Girolamo, A.; Cristino, S.; Girolamini, L.; Mazzotta, M.; Bucci Sabattini, M. A.; Zaccaro, C. M.; Chetti, L.; Laboratory, M. A. N.; Bella, A.; Rota, M. C.; Ricci, M. L., Performance of Legiolert Test vs. ISO 11731 to Confirm *Legionella pneumophila* Contamination in Potable Water Samples. *Pathogens* **2020**, *9* (9), 1-8. DOI: 10.3390/pathogens9090690
172. Rech, M. M.; Swalla, B. M.; Dobranic, J. K., Evaluation of Legiolert for Quantification of *Legionella pneumophila* from Non-potable Water. *Curr. Microbiol.* **2018**, *75* (10), 1282-1289. DOI: 10.1007/s00284-018-1522-0
173. Centers for Disease Control and Prevention. *Legionella* (Legionnaires' Disease and Pontiac Fever). <https://www.cdc.gov/legionella/clinicians/clinical-features.html> (accessed July 27, 2021).

174. Keserue, H.-A.; Baumgartner, A.; Felleisen, R.; Egli, T., Rapid detection of total and viable *Legionella pneumophila* in tap water by immunomagnetic separation, double fluorescent staining and flow cytometry. *Microb. Biotechnol.* **2012**, *5* (6), 753-763. DOI: 10.1111/j.1751-7915.2012.00366.x
175. Oh, B.-K.; Kim, Y.-K.; Lee, W.; Bae, Y. M.; Lee, W. H.; Choi, J.-W., Immunosensor for detection of *Legionella pneumophila* using surface plasmon resonance. *Biosens. Bioelectron.* **2003**, *18* (5), 605-611. DOI: 10.1016/S0956-5663(03)00032-0
176. Delgado-Viscogliosi, P.; Simonart, T.; Parent, V.; Marchand, G.; Dobbelaere, M.; Pierlot, E.; Pierzo, V.; Menard-Szczebara, F.; Gaudard-Ferveur, E.; Delabre, K.; Delattre, J. M., Rapid Method for Enumeration of Viable *Legionella pneumophila* and Other *Legionella* spp. in Water. *Appl. Environ. Microbiol.* **2005**, *71* (7), 4086-4096. DOI: 10.1128/AEM.71.7.4086-4096.2005
177. Ditommaso, S.; Giacomuzzi, M.; Gentile, M.; Zotti, C. M., Evaluation of the usefulness of a new direct immunofluorescence assay (ScanVIT-*Legionella*TM) for monitoring hospital water systems contaminated with *Legionella* spp. *Lett. Appl. Microbiol.* **2010**, *50* (4), 341-346. DOI: 10.1111/j.1472-765X.2010.02797.x
178. Yamaguchi, N.; Tokunaga, Y.; Goto, S.; Fujii, Y.; Banno, F.; Edagawa, A., Rapid on-site monitoring of *Legionella pneumophila* in cooling tower water using a portable microfluidic system. *Sci. Rep.* **2017**, *7* (3092), 1-8. DOI: 10.1038/s41598-017-03293-9
179. Cooper, I. R.; Meikle, S. T.; Standen, G.; Hanlon, G. W.; Santin, M., The rapid and specific real-time detection of *Legionella pneumophila* in water samples using Optical Waveguide Lightmode Spectroscopy. *J. Microbiol. Methods* **2009**, *78* (1), 40-44. DOI: 10.1016/j.mimet.2009.04.004
180. Descours, G.; Cassier, P.; Forey, F.; Ginevra, C.; Etienne, J.; Lina, G.; Jarraud, S., Evaluation of BMPA, MWY, GVPC and BCYE media for the isolation of *Legionella* species from respiratory samples. *J. Microbiol. Methods* **2014**, *98*, 119-121. DOI: 10.1016/j.mimet.2014.01.001
181. Scaturro, M.; Poznanski, E.; Mupo, M.; Blasior, P.; Seeber, M.; Prast, A.-M.; Romanin, E.; Girolamo, A.; Rota, M. C.; Bella, A.; Ricci, M. L.; Stenico, A., Evaluation of GVPC and BCYE Media for *Legionella* Detection and Enumeration in Water Samples by ISO 11731: Does Plating on BCYE Medium Really Improve Yield? *Pathogens* **2020**, *9* (9), 1-6. DOI: 10.3390/pathogens9090757
182. Ditommaso, S.; Giacomuzzi, M.; Memoli, G.; Garlasco, J.; Zotti, C. M., Sensitivity and Selectivity of Two Commercially Available Media for *Legionella* spp. Recovery from Environmental Water Samples. *Pathogens* **2020**, *9* (7), 1-9. DOI: 10.3390/pathogens9070523
183. Leoni, E.; Legnani, P. P., Comparison of selective procedures for isolation and enumeration of *Legionella* species from hot water systems. *J. Appl. Microbiol.* **2001**, *90* (1), 27-33. DOI: 10.1046/j.1365-2672.2001.01178.x
184. Reinthaler, F. F.; Sattler, J.; Schaffler-Dullnig, K.; Weinmayr, B.; Marth, E., Comparative study of procedures for isolation and cultivation of *Legionella pneumophila* from tap water in hospitals. *J. Clin. Microbiol.* **1993**, *31* (5), 1213-1216. DOI: 10.1128/jcm.31.5.1213-1216.1993
185. Lück, P. C.; Igel, L.; Helbig, J. H.; Kuhlisch, E.; Jatzwauk, L., Comparison of commercially available media for the recovery of *Legionella* species. *Int. J. Hyg. Environ. Health* **2004**, *207* (6), 589-593. DOI: 10.1078/1438-4639-00332

186. Edelstein, P. H., Comparative study of selective media for isolation of *Legionella pneumophila* from potable water. *J. Clin. Microbiol.* **1982**, *16* (4), 697-699. DOI: 10.1128/jcm.16.4.697-699.1982
187. Micropelt GmbH. TGP-651 ThermoGenerator-Package (TGP) Thin Film Thermogenerator inside standard package. http://www.micropelt.com/fileadmin/user_upload/_PDF_TGP_UK.pdf (accessed July 30, 2021).
188. Briggner, L.-E.; Wadsö, I., Test and calibration processes for microcalorimeters, with special reference to heat conduction instruments used with aqueous systems. *J. Biochem. Biophys. Methods* **1991**, *22* (2), 101-118. DOI: 10.1016/0165-022X(91)90023-P
189. Shukla, S. K.; López, P. R.; Sánchez, C. S.; Urréjola, J.; Segura, L. E., A new ultrasonic signal amplification method for detection of bacteria. *Meas. Sci. Technol.* **2012**, *23* (10), 1-8. DOI: 10.1088/0957-0233/23/10/105701
190. Qi, P.; Zhang, D.; Wan, Y.; Lv, D., A facile approach to construct versatile signal amplification system for bacterial detection. *Talanta* **2014**, *118*, 333-338. DOI: 10.1016/j.talanta.2013.10.040
191. Shen, J.; Zhou, X.; Shan, Y.; Yue, H.; Huang, R.; Hu, J.; Xing, D., Sensitive detection of a bacterial pathogen using allosteric probe-initiated catalysis and CRISPR-Cas13a amplification reaction. *Nat. Commun.* **2020**, *11* (267), 1-10. DOI: 10.1038/s41467-019-14135-9
192. Lerchner, J.; Schulz, A.; Poeschel, T.; Wolf, A.; Hartmann, T.; Mertens, F.; Boschke, E., Chip calorimetry and biomagnetic separation: Fast detection of bacterial contamination at low cell titers. *Eng. Life Sci.* **2012**, *12* (6), 615-620. DOI: 10.1002/elsc.201200029
193. von Ah, U.; Wirz, D.; Daniels, A. U., Isothermal micro calorimetry – a new method for MIC determinations: results for 12 antibiotics and reference strains of *E. coli* and *S. aureus*. *BMC Microbiol.* **2009**, *9* (106), 1-14. DOI: 10.1186/1471-2180-9-106

Declaration of Authorship

I, Christian Fricke, herewith declare that the present cumulative dissertation was written independently, without unauthorized assistance from external parties and using sources other than those indicated in the text. All ideas that have been taken directly or indirectly from other works are marked accordingly, and a complete reference of their source has been appropriately provided.

This cumulative dissertation includes three published articles and one submitted manuscript that were prepared in collaboration with several co-authors. The names of these authors and the respective shares of their contribution to the articles and manuscript have been stated, countersigned by the senior scientist, and listed in the section “**Author Contributions of Published Articles and Submitted Manuscript**” (Appendix A5).

I assure that no other persons have contributed to the intellectual preparation of this thesis. In particular, no PhD consultants were engaged, and no third party has received any neither indirect nor direct financial benefits in goods and services for work related to the content of this cumulative dissertation.

This work, either in full or in part, has never been submitted in an equal or similar form for examination in order to obtain the degree of doctorate or any other degree at another academic institution or has not been published.

I am the exclusive author of **section 3.2** “Numerical heat flow and transport simulation as a development tool for the design of isothermal microcalorimeters”, and **3.3** “Further experiments related to instrument development and selective detection of bacteria”.

I also confirm that no other unsuccessful doctoral examination processes have taken place.

Leipzig, September 14, 2021

Danksagung

An erster Stelle möchte ich mich bei Prof. Dr. Hauke Harms, Leiter des Departments für Umweltmikrobiologie am UFZ, für die Aufnahme im Department und die sehr gute wissenschaftliche Betreuung bedanken. Darüber hinaus bin ich sehr dankbar für die wertvollen Anregungen, die zum Erfolg dieser Arbeit beigetragen haben.

I would also like to thank Prof. Dr. Lars Wadsö for taking the effort to examine this dissertation.

Besonderer Dank gilt meinem Betreuer PD Dr. Thomas Maskow für die großartige Betreuung während meiner Promotion, vor allem aber für die lehrreichen und anregenden Diskussionen während der wöchentlichen Besprechungen. Auch möchte ich mich für die Ausdauer beim Korrekturlesen bedanken.

Weiterer Dank gilt vor allem Sven Paufler für die technische Unterstützung im Labor und Dr. Thore Rohwerder für die regelmäßigen, kritischen Auseinandersetzungen zu dem Thema der Doktorarbeit. Auch für das Korrekturlesen möchte ich mich bei Euch beiden bedanken.

Vielen Dank auch an die gesamte Arbeitsgruppe Ökothermodynamik / Biokalorimetrie sowie Nicole Steinbach (AG Mikrobielle Interaktionsökologie), Ute Lohse (AG Mikrobiologie anaerober Systeme), Martina Kolbe (AG Nährbodenstation), Dr. Anja Worrich (AG Mikrobielle Ökologie sich verändernder Umwelten), Lars Oehler (Poststelle), Bernd Herrmann, Stanley Rogowski, Karsten Seyfarth (WKDV), Daniel Karmowski, Manuel Kositzke, Björn Häberlein (BFM), Theo und Nawras für die freundliche und kompetente Unterstützung während meiner Promotion. Ganz besonders möchte ich mich aber bei Carola Riemenschneider (Sekretariat) für die vielen netten und aufbauenden Worte während der stressigen Phasen der Promotion, den schönen Unterhaltungen und vielen Unterstützungen, vor allem bei bürokratischen Problemen, sehr bedanken. Das Arbeitsklima im gesamten Department war sehr angenehm und ich habe mich sehr gefreut über die Hilfsbereitschaft bei auftretenden Problemen.

I would like to thank Prof. Dr. Liu and Prof. Dr. Fenglei as well as Xu Juan, for the excellent supervision during my research stay at the Wuhan University.

Des Weiteren möchte ich mich bei den Kooperationspartnern Hartwin Lier (KEK), Toralf Klee und Sven Richter (Loetec) seitens der Fertigstellung des Testsystems und bei Katrin Stahr (ÖHMI) für die unterstützende Betreuung in der Zeit in Magdeburg bedanken.

Zu guter Letzt möchte ich mich noch bei meinen Eltern, meiner gesamten Familie und meiner Freundin für den Rückhalt in dieser Zeit bedanken. Eure Worte und Unterstützungen haben mir sehr geholfen in dieser Zeit und ich bin glücklich, dass ich euch habe.

Curriculum Vitae

Personal Details

Name	Christian Fricke
Address	Kochstraße 56, 04275 Leipzig
Phone	+49 15739650552
E-Mail	F.Christian05@googlemail.com
Date of birth	28.05.1991
Place of birth	Staßfurt (Sachsen-Anhalt)

Education

since 07/2018	Doctoral studies at the University of Leipzig, Faculty of Biosciences, Pharma and Psychology degree: thesis: “ <i>Isothermal Micro(bio-)calorimetry - Method and Instrument Development for a Rapid and Reliable Detection Technique of Bacteria</i> ” (in cooperation with Helmholtz-Centre for Environmental Research GmbH)
10/2015 – 03/2018	Master studies in Chemistry at the Georg-August-University Göttingen degree: M. Sc. Chemistry (1.6) thesis: “ <i>Investigation of the phase separation behavior of a polymer solution for the production of macro-porous membranes</i> ” (in cooperation with Sartorius Stedim Biotech GmbH).
10/2012 – 07/2015	Bachelor studies in Chemistry at the Georg-August-University Göttingen degree: B. Sc. Chemistry (1.7) thesis: “ <i>Reflectometric interference spectroscopy study of the binding of ENTH domain to artificial membranes</i> ”.
08/2010 – 06/2012	Fachoberschule and Berufsoberschule at the Europaschule Schulzentrum SII Utbremen (Bremen) graduation: general qualification for university entrance (1.1)
09/2007 – 06/2010	Apprenticeship as Chemical Laboratory Technician at the training centre of the University Bremen professional qualification: Chemical Laboratory Technician (very good)

Work experiences/internship/stay abroad

08/2020 – 09/2020	Six-week research stay at the department Microbiology - Drinking water analysis ÖHMI Analytik GmbH in Magdeburg
02/2019 – 03/2019	Four-week research stay in the group of Prof. Yi Liu College of Chemistry and Molecular Science, University Wuhan
since 07/2018	Doctoral researcher at the Helmholtz-Centre for Environmental Research GmbH - UFZ (Leipzig) Working group: Ecothermodynamic / Biocalorimetry
04/2017	Three-week internship as Working Student at Daimler Location: Bremen
10/2015 – 02/2018	Handball trainer University sports at the Georg-August-University Göttingen, Level 1-2
06/2014 – 03/2016	Research assistant Poison Information Center North Forensic Toxicology Laboratory at the University Hospital in Göttingen
10/2013 – 02/2018	Teaching assistant Experimentalchemie I Nebenfach WiSe 13/14, WiSe 14/15, Experimentalchemie II Hauptfach SoSe 15, Experimentalchemie II Nebenfach SoSe 16, Chemie für Mediziner SoSe 15, WiSe 15/16, SoSe16, WiSe 16/17, SoSe 17, WiSe 17/18, Chemisches Praktikum für Studierende der Human- und Zahnmedizin WiSe 15/16, WiSe 16/17, Fachtutor für Chemie im Rahmen des Internationalen Herbstkurses an der Georg-August-Universität Göttingen WiSe 16/17, Propädeutikum: Chemie für Mediziner SoSe17, WiSe 17/18, Propädeutikum: Chemie für Biologen/Geo-/Agrar-/Forstwissenschaften WiSe 17/18
05/2006	Two-week internship as Chemical Laboratory Technician at the brewery Beck GmbH & Co. KG Location: Bremen

List of Publications

Journal Publications (peer review)

Fricke C, Klee T, Richter S, Paufler S, Harms H, Maskow T. (2021)

Numerical heat flow and transport simulation as a development tool for the design of isothermal microcalorimeters

Thermochim. Acta (submitted, Original research)

Fricke C, Harms H, Maskow T. (2020):

How to speed up the detection of aerobic microbial contaminations by using isothermal microcalorimetry

J. Therm. Anal. Calorim. **142**, 1933–1949.

<https://doi.org/10.1007/s10973-020-09986-0> (published, Original research)

Fricke C, Xu J, Jiang F-L, Liu Y, Harms H, Maskow T. (2020):

Rapid culture-based detection of *Legionella pneumophila* using isothermal microcalorimetry with an improved evaluation method

Microb. Biotechnol. **13** (4), 1262-72.

<https://doi.org/10.1111/1751-7915.13563> (published, Brief report)

Fricke C, Harms H, Maskow T. (2019):

Rapid Calorimetric Detection of Bacterial Contamination: Influence of the Cultivation Technique

Front. Microbiol. **10** (2530), 1-12.

<https://doi.org/10.3389/fmicb.2019.02530> (published, Methods article)

Kahrs C, Metze M, **Fricke C**, Schwellenbach J. (2019):

Thermodynamic analysis of polymer solutions for the production of polymeric membranes

J. Mol. Liq. **291**, 111351.

<https://doi.org/10.1016/j.molliq.2019.111351> (published, Original research)

Gleisner M, Kroppen B, **Fricke C**, Teske N, Kliesch TT, Janshoff A Meinecke M, Steinem C. (2016):

Epsin N-terminal Homology Domain (ENTH) Activity as a Function of Membrane Tension

J. Biol. Chem. **291** (38), 19953-61.

<https://doi.org/10.1074/jbc.M116.731612> (published, Original Research)

Conference contributions

Fricke C, Klee T, Richter S, Paufler S, Harms H, Maskow T. (05/2021) *Insights of an isothermal microcalorimeter - Flow and heat transfer simulations as a development tool for calorimeter design and construction*. Presentation at the 24. Kalorimetrietagen, Brunswick, Germany.

Fricke C, Klee T, Richter S, Paufler S, Harms H, Maskow T. (10/2020) *Flow And Heat Transfer Simulations As A Development Tool For A Novel Microcalorimeter*. Poster at the COMSOL Online-Conference 2020 Europe, Grenoble, France.

Fricke C, Harms H, Maskow T. (03/2020). *Combining isothermal microcalorimetry and microbiological analytics for fast and reliable detection of microbial contaminations*. Presentation at the 6. jointed Conference of DGHM & VAAM, Leipzig, Germany.

Fricke C, Harms H, Maskow T. (11/2019). *Using microcalorimetry as an early warning system for the detection of bacterial contaminations*. Poster at the 2nd joint IP-Day, Leipzig, Germany.

Fricke C, Harms H, Maskow T. (08/2019). *On the trail of heat - Isothermal microcalorimetry as a real-time monitor for bacterial contamination*. Presentation at the CEEC-TAC5 & MEDICTA2019, Rome, Italy.

Fricke C, Harms H, Maskow T. (06/2019). *Conventional microbiological cultivation techniques are under close scrutiny - Can all these techniques be applied in microcalorimetry?* Presentation at the 23. Kalorimetrietagen, Brunswick, Germany.

Fricke C, Harms H, Maskow T. (01/2019). *Sample preparation as key for the fast and reliable calorimetric detection of microbial contaminations*. Poster at the 15th Research Festival, Leipzig, Germany.

Appendix

A1 Supplementary material for section 3.1.1 (published article 1)

Supplementary material

Rapid Calorimetric Detection of Bacterial Contamination: Influence of the Cultivation Technique

Christian Fricke, Hauke Harms, Thomas Maskow*

Helmholtz-Centre for Environmental Research – UFZ, Department of Environmental Microbiology, Leipzig,
Germany

*Correspondence: Thomas Maskow: thomas.maskow@ufz.de

Table of contents

S1: Sample preparation

S2: Baseline correction

S3: CFU-counting results

S4: Heat flow curves of the reproducibility measurements

S5: Reference measurement for the bacterial growth on solid medium using the naked eye for detection

S6: Reference measurement for the bacterial growth on membrane filter using the naked eye for detection

S7: Reference measurements of bacterial growth in liquid medium using OD₆₀₀

S1 Sample preparation

Fig. 1 illustrates exemplary prepared glass ampoules with different cultivation approaches before and after an IMC experiment.

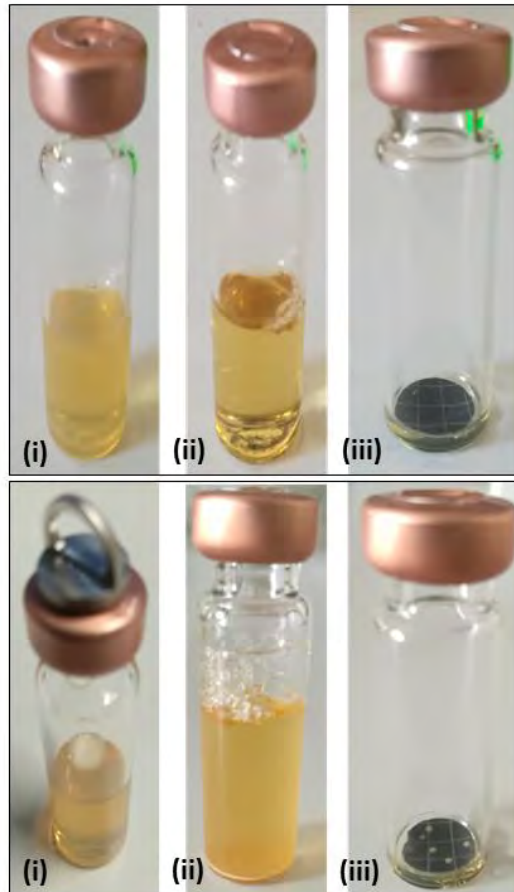


Figure 1: IMC ampoules for each cultivation technique after sample preparation (top) and after an IMC experiment (bottom). **i:** GOA. **ii:** GL. **iii:** GF.

S2 Baseline correction

Fig. 2 shows exemplarily the procedure for the baseline correction of a heat flow signal which deviates from the baseline. Using the baseline correction within *OriginPro 2018*, the heat flow signal was corrected.

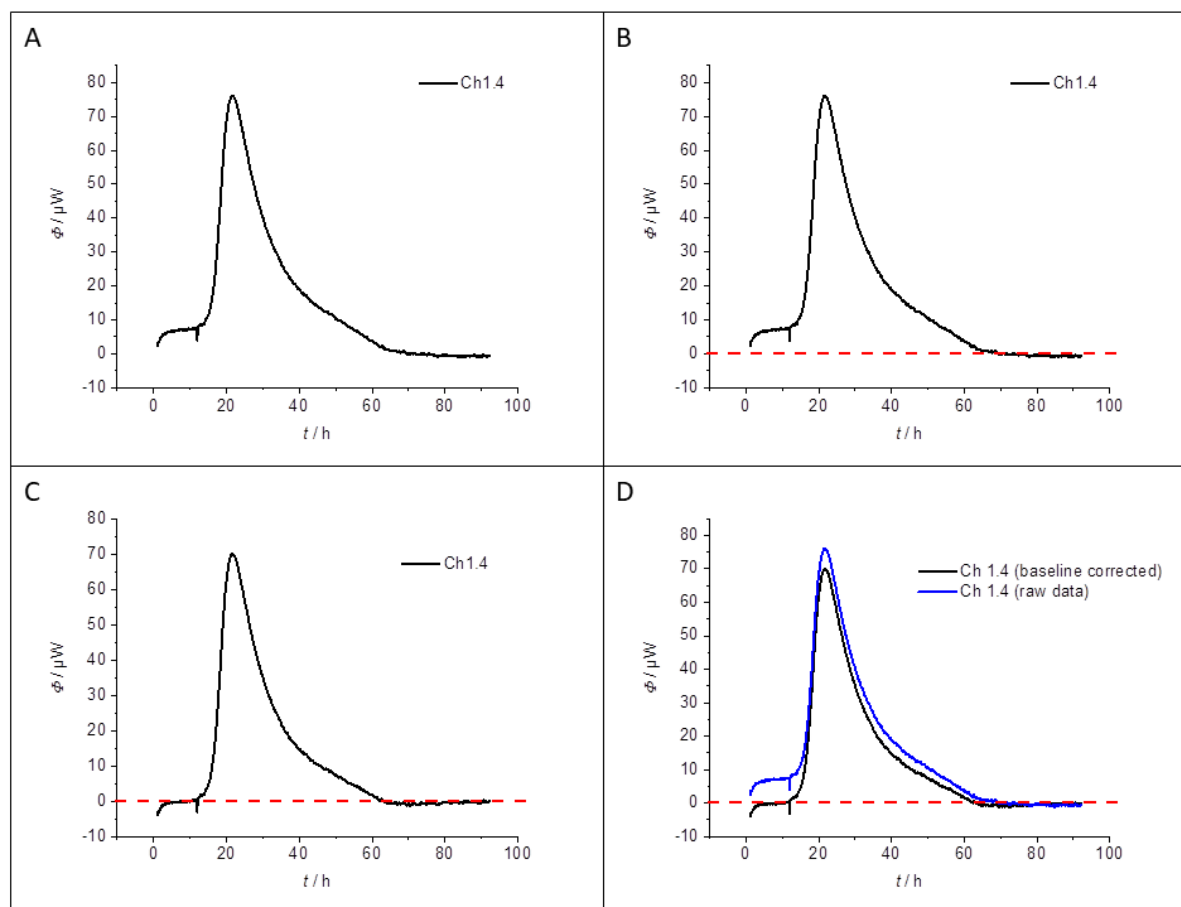


Figure 2: Procedure for linear baseline correction by *OriginPro 2018*. **A:** Raw heat flow signal after measurement. **B:** Red dotted line corresponds to the baseline. **C:** The heat flow signal after baseline correction by *OriginPro 2018* (menu option: Analysis \rightarrow Peaks and Baseline \rightarrow Peak Analyzer \rightarrow Subtract Baseline \rightarrow Baseline Mode: User defined). **D:** Comparison of heat flow signal before and after baseline correction.

S3 CFU-Counting results

Tab. 1 and **Tab. 2** summarize the results of the CFU-counting experiments. The results in **Tab. 1** are corresponding to the experiments for the fill level-dependent and reproducibility measurements as well as for the real-time monitoring after colonies became visible for the eye. The results in **Tab 2.** are corresponding to the investigations of the dependency of the heat traces on the initial bacterial concentration as well as for the real-time monitoring by scanning the plates at defined intervals.

Tab. 1: Summary of the replicates CFU-countings of fill level-dependent, reproducibility measurements and real-time monitoring by the naked eye.

f_a	1	2	3	4	5	mean	SD
10^4	366400 ^a	324000 ^a	-	-	-	345200	-
10^5	44400 ^b	46700 ^b	50700 ^b	-	-	47267	2603
10^6	4300 ^b	4500 ^b	4400 ^b	3130 ^c	4090 ^d	4084	82
10^7	300 ^b	420 ^b	360 ^b	278 ^e	-	340	49
10^8	20 ^b	80 ^b	90 ^b	56 ^e	-	62	27

^aOD₆₀₀ was not determined.

^bOD₆₀₀ = 0.18 (1:100 dilution).

^cOD₆₀₀ = 0.19 (1:100 dilution).

^dOD₆₀₀ = 0.20 (1:100 dilution).

^eOD₆₀₀ = 0.20 (1:100 dilution).

Tab. 2: Summary of the replicates CFU-countings of the concentration-dependent measurements and real-time monitoring by scanning.

f_a	1 ^a	2 ^b	3 ^b	4 ^b	mean	SD
10^4	129000	135300	121700	150200	134050	10493
10^5	15900	19400	18600	13200	16775	2438
10^6	1900	1400	2200	1600	1775	303
10^7	150	160	180	110	150	26
10^8	-	16	22	10	16	5

^aOD₆₀₀ = 0.16 (1:100 dilution).

^bOD₆₀₀ = 0.17 (1:100 dilution).

S4 Heat flow curves of the reproducibility measurements

Fig. 3-5 shows for each cultivation technique (GOA, GL and GF) the corresponding heat flow curves.

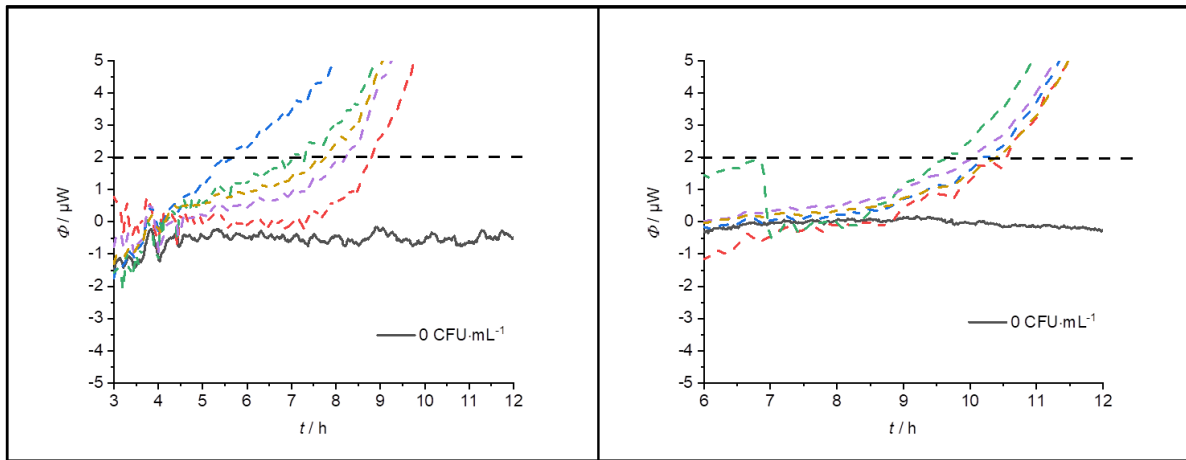


Figure 3: Heat flow curves of the reproducibility measurements of GOA.

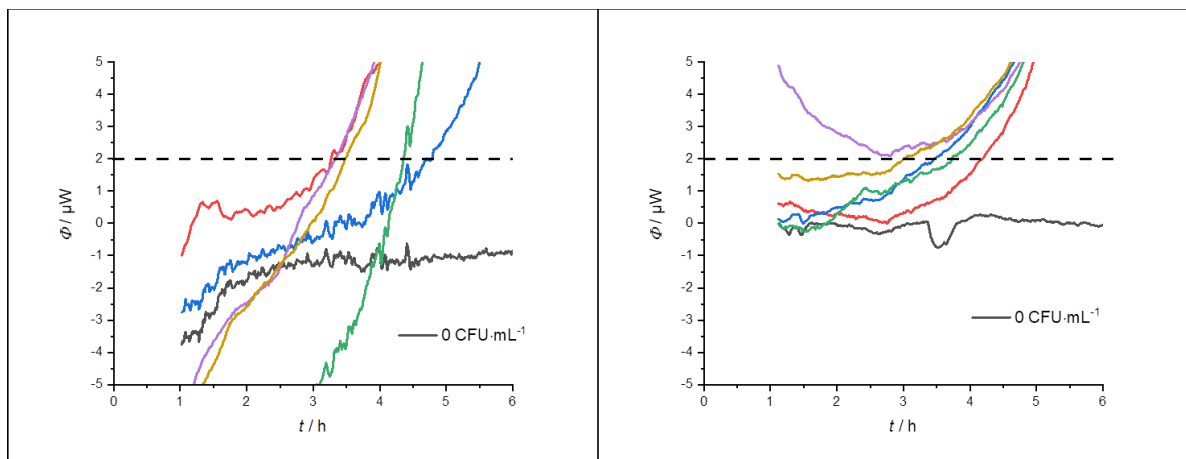


Figure 4: Heat flow curves of the reproducibility measurements of GL.

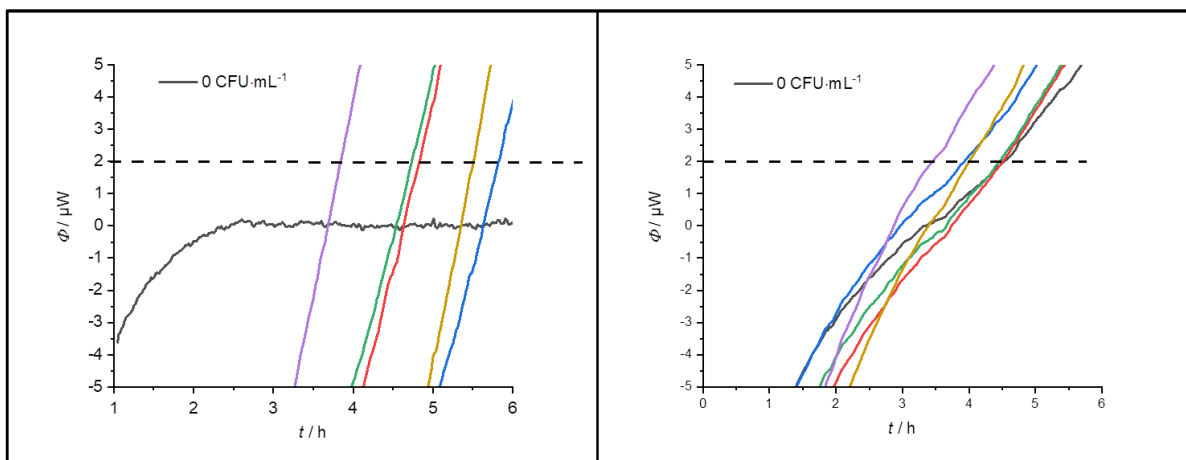


Figure 5: Heat flow curves of the reproducibility measurements of GF.

S5 Reference measurement for the bacterial growth on solid medium using the naked eye for detection

After the experiments, the files were then evaluated. For this purpose, 4 independent persons determined for each dilution level the time from which the colony was visible to the naked eye. The visual detection time was then determined from the results using standard deviation.



Figure 6: Time-dependent recording of the colony forming process on solid media at different initial bacterial concentrations in the time interval from 0 h to 22 h. The detection time t_{dect} was determined after a colony became visible for the naked eye.

S6 Reference measurement for the bacterial growth on membrane filter using the naked eye for detection



Figure 7: Time-dependent recording of the colony forming process on membrane filter at different initial bacterial concentrations in the time interval from 0 h to 19 h. The detection time t_{dect} was determined after a colony became visible for the naked eye.

S7 Reference measurements of bacterial growth in liquid medium using OD_{600}

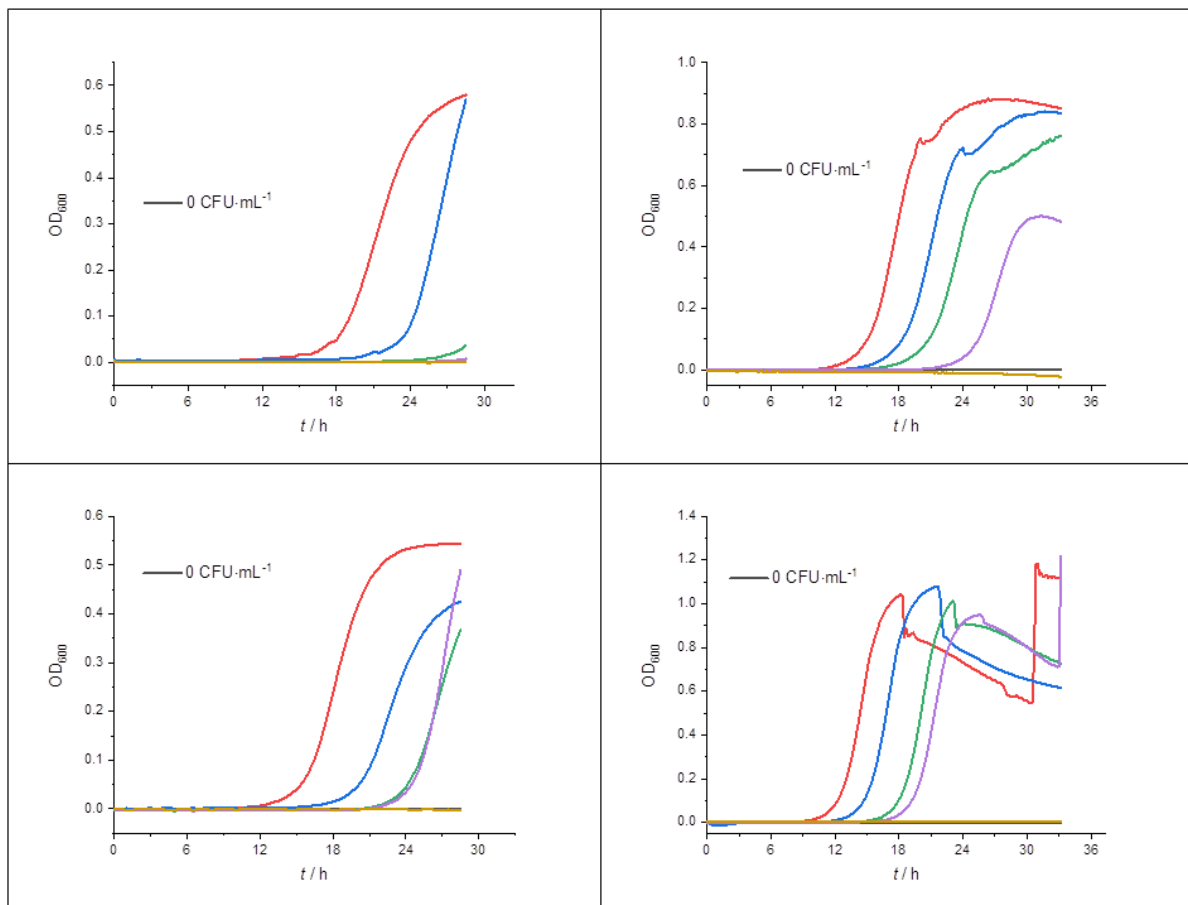


Figure 8: Replicates of a time-dependent recording of the OD_{600} at different initial bacterial concentrations under the same conditions. **Red:** $10^5 \text{ CFU}\cdot\text{mL}^{-1}$. **Blue:** $10^4 \text{ CFU}\cdot\text{mL}^{-1}$. **Green:** $10^3 \text{ CFU}\cdot\text{mL}^{-1}$. **Violet:** $10^2 \text{ CFU}\cdot\text{mL}^{-1}$. **Yellow:** $10^0 \text{ CFU}\cdot\text{mL}^{-1}$. **Black:** $0 \text{ CFU}\cdot\text{mL}^{-1}$. The corresponding detection threshold was set to $OD_{600} = 0.01$.

A2 Supplementary material for section 3.1.2 (published article 2)

Supporting information

How to speed up the detection of aerobic microbial contaminations by using isothermal microcalorimetry

Christian Fricke, Hauke Harms, Thomas Maskow*

Helmholtz-Centre for Environmental Research – UFZ, Department of Environmental Microbiology, Leipzig,
Germany

***Correspondence:**

Thomas Maskow
thomas.maskow@ufz.de

Table of Contents

S1 Influence of the inoculum volume on the detection time in IMC and visual inspection	2
S2 Influence of the size of colonies formed during IMC experiments on the heat flow pattern	4
S3 Calculation of the total heat	5
S3.1 Calculation of total heat for SC	6
S3.2 Calculation of total heat for LC	6
S4 Influence of the initial concentration of bacteria on the detection time in IMC experiments and visual inspection	8
S5 Summary of the initial number of bacteria-dependent heat flow measurements	10
S6 Summary of the initial number of bacteria-dependent heat flow measurements performed in MC-Cal 100P calorimeter	11
S7 Summary of the filling volume-dependent heat flow measurements	12
S8 Threshold value of the calorimeter and dissolved oxygen in the medium	14
S9 Summary of the N_0 -dependent heat flow measurements performed in minimal medium	15

S1 Influence of the inoculum volume on the detection time in IMC and visual inspection

We investigated the influence of the inoculum volume (V_i) on the detection time in both cultivations on solid medium by CFU-counting and IMC experiments in liquid medium (see **Fig. S1**). In the former case, the respective V_i were plated on DSM-1 agar plates and subsequently incubated at 30 °C. The samples possessed the same initial concentration of bacteria $(6.9 \pm 2.4) \cdot 10^1$ CFU·mL⁻¹. The plates were located within a scanner which was placed in a temperature-controlled incubator. Every ten minutes the plates were scanned and the resulting scan was saved as a jpg-file. **Fig. S2** displayed a certain selection of the obtained scans. Afterwards, the jpg-files were evaluated by five independent observers. The data evaluation aimed to identify the jpg-file which for the first time showed no change in the number of CFUs formed for the respective V_i . The corresponding detection time was then calculated from the selected jpg-file number. The resulting detection times determined by each observer for the respective V_i are summarized in **Tab S1**.

Finally, we compared the obtained detection times from the visual evaluation (CFU-counting) with the results from the IMC experiments in LC (see **Fig. S1**). As expected, in the case of visual detection V_i did not affect the detection time. The average CFU detection time after all colonies became visible for the naked eye was 15.5 ± 0.6 h. However, the corresponding detection times obtained from the IMC experiments indicate a dependency of V_i on the detection time. A larger V_i leads to a reduced detection time.

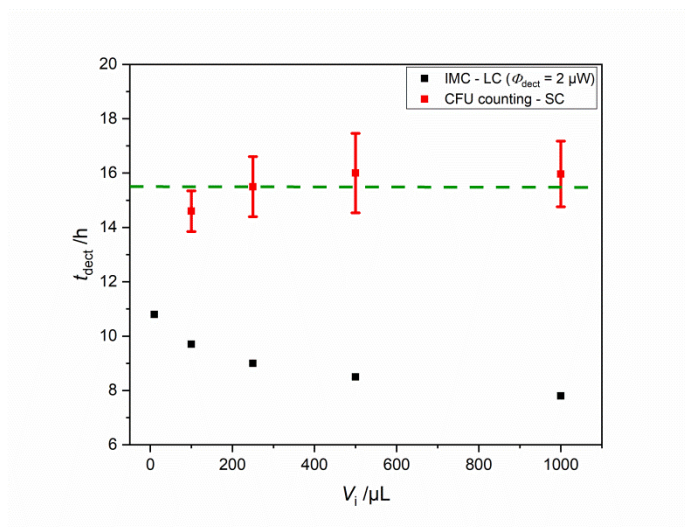


Figure S1: Comparison of the influence of the V_i on the detection time in visual inspection (CFU counting - SC) and IMC experiments performed in LC (detection threshold value, $\Phi_{\text{detect}} = 2 \mu\text{W}$).

Table S1: Summary of the detection times for the visual evaluation of the scanned images.

$V_i / \mu\text{L}$	observer	I	II	III	IV	V	mean	SD
		$t_{\text{dect}} / \text{h}$						
10		-	-	-	-	-	-	-
100		14.8	14.7	13.3	15.7	14.5	14.6	0.7
250		16.0	15.7	13.3	16.3	16.2	15.5	1.1
500		15.7	16.0	13.5	17.0	17.8	16.0	1.5
1000		16.5	16.0	13.7	16.5	17.2	16.0	1.2



Figure S2: A selection of the obtained scans from V_i -dependent experiments by visual inspection on solid medium.

Larger V_i increased the overall liquid volume so that the liquid phase contained more total oxygen, but it decreased the headspace volume. On the other hand, a higher inoculum size contained more active bacteria. The interplay of less total oxygen (due to poorly solubility of oxygen in liquid, $7.5 \text{ mg} \cdot \text{L}^{-1}$ at $30 \text{ }^\circ\text{C}$) [1] in the entire system and more active bacteria decreased the maximum heat flow (**Fig. S3A**). Besides, the latter led to a reduction in the detection of approx. 3 h. Using 1 mL inoculum, bacterial growth was detected after approx. 8 h. If the inoculum was reduced by a factor of 100, the detection took approx. 11 h (**Fig. S3B**).

Using larger V_i for LC might thus be an option for less sensitive IMCs such as the TAM Air, Calimetrix BioCal 2000 or similar instruments since sample vessels (125 mL) with a large liquid/gas interfacial area can be used.

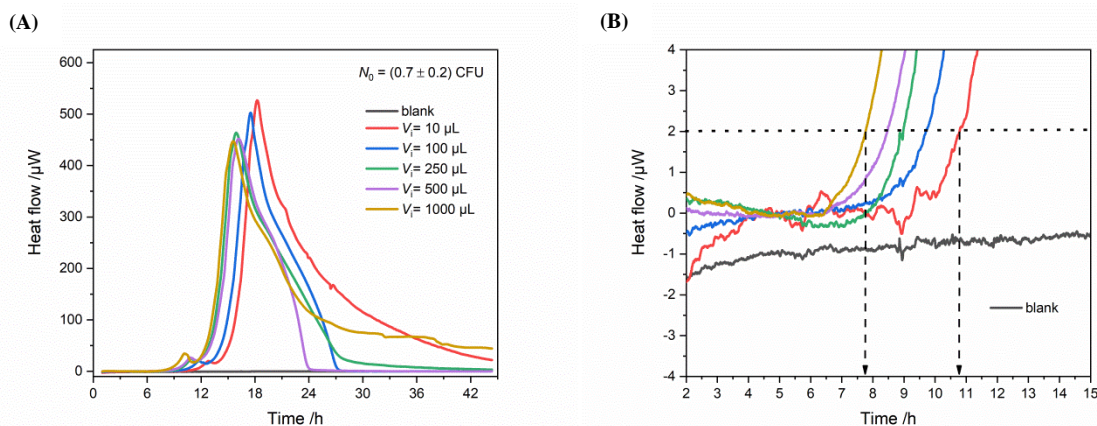


Figure S3: Influence of V_i on the detection time in LC. **A):** Heat flow signals of different $V_i = 10, 100, 250, 500$ and 1000 µL. **B):** Magnification of the heat flow signals near the detection threshold value of 2 µW.

S2 Influence of the size of colonies formed during IMC experiments on the heat flow pattern

Fig. S4 linked the heat flow signals with the respective images of the samples taken after the IMC experiment. Based on the initial number of bacteria N_0 , we observed different heat flow patterns as well as different size of colonies formed during the IMC experiment. The red curve was characterized by a sharp and slender peak (**Fig. S4**). The image of the sample looked like a perfectly large colony, but there were probably many tiny colonies of very small diameter connected. A look at the second sample (blue curve, **Fig. S4**) might clarify this situation, as small but well-separated colonies were visible on the edge of the large colony in the middle of the ampoule. The heat flow pattern seemed to be almost identical only the maximum heat flow was minimized. The green curve was wider compared to the earlier curves. The associated image revealed for the first time many middle size colonies which were almost well separated. The two last curves (violet and green, **Fig. S4**) showed a completely different heat flow pattern. Both curves were characterized by a flat and wide peak. The increase of the heat flow signal was only partially dominated by an exponential behavior. The corresponding images showed the formation of large colonies. In the case of the violet heat flow signal, probably less than 10 colonies were formed. The yellow heat flow signal can be related to two single colonies formed during the IMC experiment.

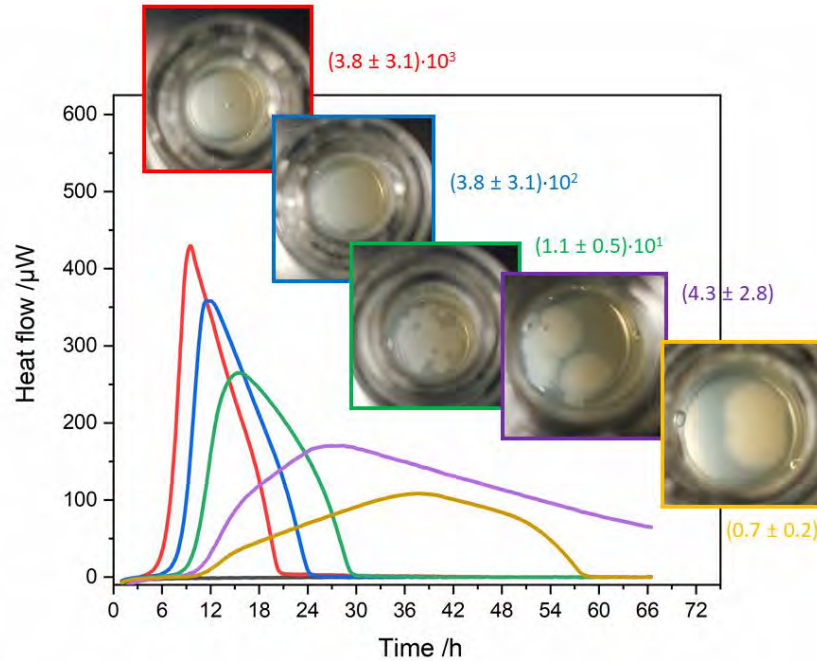


Figure S4: Summary of the N_0 -dependent IMC experiments performed on SC. The dependency of the heat traces on N_0 as well as associated images taken after the IMC experiment. N_0 (mean \pm SD) in CFU are indicated next to the heat flow signals.

S3 Calculation of the total heat

To confirm the amount of total heat Q_{exp} (in J) produced during the growth of *P. putida* mt-2 KT2440 in the N_0 -dependent IMC experiments, we used the initial situation outlined in **Fig. S5**. The corresponding necessary physical quantities are summarized in **Tab S2**. The calculations of the amount of total heat released during the growth experiments are described for both cases LC and SC in the following chapters.

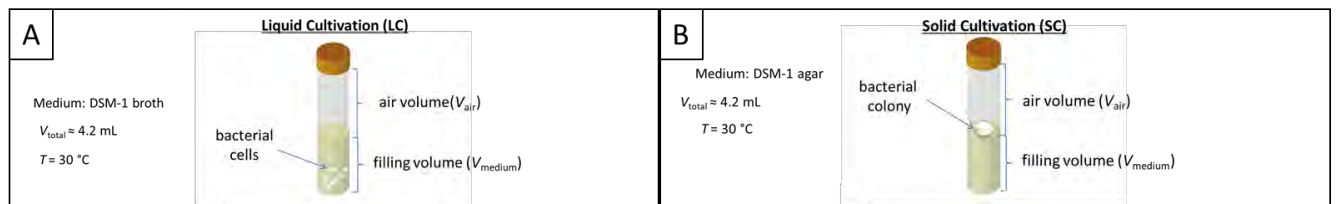


Figure S5: Illustration of the initial situation of N_0 -dependent growth experiments performed on SC (A) and in LC (B) by IMC.

Table S2: Summary of the physical quantities for calculating the total heat production

parameter	value	dimension	reference
$V(\text{air})$	0.0032	L	-
$V(\text{medium})$	0.001	L	-
$\rho(\text{air})$	1.1381 ^a	kg·m ³	-
$w(\text{O}_2)$	23.14	%	[2]
$\beta(\text{O}_2)$	$7.5 \cdot 10^{-3}$	g·L ⁻¹	[1]
$M(\text{O}_2)$	32	g·mol ⁻¹	-
$\Delta_k H_{\text{O}_2}$	(455 ± 25)	kJ·mol ⁻¹ O ₂	[3]

^a determined by the specific gas constant of dry air, $R_s = 287.058 \text{ J} \cdot \text{kg}^{-1} \cdot \text{K}^{-1}$ at 310.15 K

S3.1 Calculation of total heat for SC

The mass of air and molecular oxygen in the gas phase m_g can be calculated as follow:

$$m(\text{air}) = V(\text{air}) \cdot \rho(\text{air}) \quad (1)$$

$$m_g(\text{O}_2) = w(\text{O}_2) \cdot m(\text{air}) \quad (2)$$

The molar mass of molecular oxygen can be used to calculate the amount of molecular oxygen in the headspace.

$$n(\text{O}_2) = \frac{m(\text{O}_2)}{M(\text{O}_2)} \quad (3)$$

In the last step, the total heat released from the aerobic growth can be calculated using the oxycaloric equivalent $\Delta_k H_{\text{O}_2}$.

$$Q_{\text{theo}} = n(\text{O}_2) \cdot \Delta_k H_{\text{O}_2} \quad (4)$$

The theoretical heat evolved during aerobic growth under the circumstances was $Q_{\text{theo}} = (12.0 \pm 0.6) \text{ J}$.

S3.2 Calculation of total heat for LC

The mass of air and molecular oxygen in the gas phase m_g can be calculated by using **eq. 1** and **2**. The mass of dissolved oxygen in the liquid phase m_l can be calculated by **eq. 5**:

$$m_1(O_2) = \beta(O_2) \cdot V(\text{liquid}) \quad (5)$$

The sum of the mass in liquid and in gas phase are summarized as follow:

$$m_{\text{total}}(O_2) = m_g(O_2) + m_1(O_2) \quad (6)$$

The molar mass of molecular oxygen can be used to calculate the amount of molecular oxygen in the headspace.

$$n_{\text{total}}(O_2) = \frac{m_{\text{total}}(O_2)}{M(O_2)} \quad (7)$$

In the last step, the total heat released from the aerobic growth can be calculated using the oxycaloric equivalent $\Delta_k H_{O_2}$.

$$Q_{\text{theo}} = n_{\text{total}}(O_2) \cdot \Delta_k H_{O_2} \quad (8)$$

The theoretical heat evolved during aerobic growth under the circumstances was $Q_{\text{theo}} = (12.4 \pm 0.6)$ J.

The integration of the first peak (grey area in **Fig. S6**) allowed us to determine the partially heat production during the consumption of all dissolved oxygen in the liquid phase. The resulting heat of $Q_{\text{exp}} \approx 0.08$ J can be confirmed by the abovementioned calculations and yielded to $Q_{\text{theo}} = (0.11 \pm 0.01)$ J.

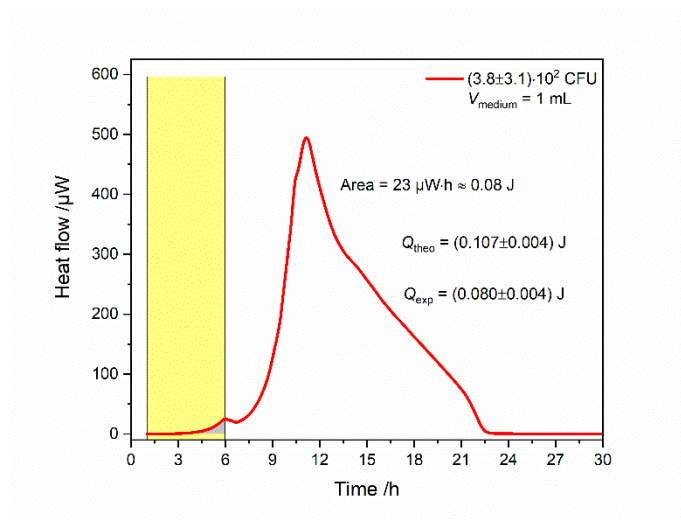


Figure S6: Heat flow signal obtained from monitoring growth of *P. putida* mt-2 KT2440 in LC. Integration of the first peak by *OriginPro 2018* (Gadgets → Integrate).

S4 Influence of the initial concentration of bacteria on the detection time in IMC experiments and visual inspection

We investigated the influence of the initial concentration of bacteria c_0 in $\text{CFU}\cdot\text{mL}^{-1}$ on the detection time in both visual inspection on solid medium and IMC experiments on SC (see **Fig. S7**). In the former case, the respective dilutions were plated on DSM-1 agar plates and subsequently incubated at $30\text{ }^\circ\text{C}$. The plates were located within a scanner which stood in a temperature-controlled incubator. Every ten minutes the plates were scanned and the resulting scan was saved as a jpg-file. **Fig. S8** displayed a certain selection of the obtained scans. Afterwards, the jpg-files were evaluated by five independent observers. The data evaluation aimed to identify the image which for the first time showed a colony which became visible for the naked eye of the respective concentration. The corresponding detection time was then calculated from the selected jpg-file number. The resulting detection times determined by each participant for the respective initial bacterial concentration are summarized in **Tab S3**.

Finally, we compared the obtained detection times from the visual inspections with the results from the IMC experiments on SC (see **Fig. S7**). As expected, in the case of visual inspection the concentration did not affect the detection time. The mean detection time after a colony became visible for the naked eye was 13.3 ± 1.3 h. However, the corresponding detection times obtained from the IMC experiments indicate a linear dependency of the logarithm of the initial bacterial concentration on the detection time.

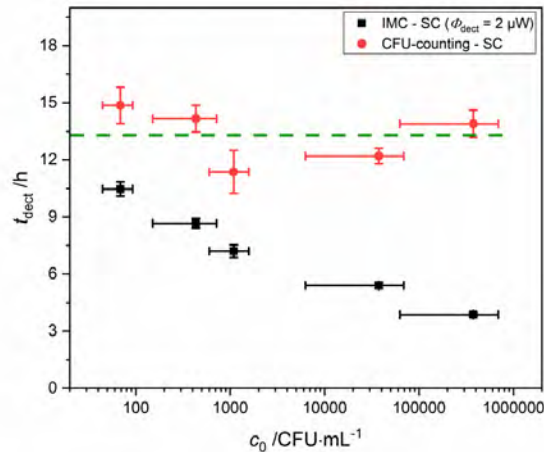


Figure S7: Comparison of the influence of the initial concentration of bacteria on the detection time in visual inspection (CFU counting - SC) and IMC experiments performed on SC ($\Phi_{\text{dect}} = 2\ \mu\text{W}$).

Table S3: Summary of the detection times for the visual evaluation of the scanned images.

$c_0 / \text{CFU} \cdot \text{mL}^{-1}$	observer	I	II	III	IV	V	mean	SD
		$t_{\text{dect}} / \text{h}$						
$(3.8 \pm 3.1) \cdot 10^5$		13.0	14.5	14.0	14.8	13.2	13.9	0.7
$(3.8 \pm 3.1) \cdot 10^4$		12.6	12.5	11.5	12.3	12.0	12.2	0.4
$(1.1 \pm 0.5) \cdot 10^3$		11.5	11.5	9.3	12.8	11.7	11.4	1.1
$(4.3 \pm 2.8) \cdot 10^2$		13.3	14.5	14.0	15.3	13.7	14.2	0.7
$(6.9 \pm 2.4) \cdot 10^1$		14.0	16.0	13.8	16.0	14.5	14.9	1.0



Figure S8: A selection of the obtained scans from concentration-dependent experiments by CFU-counting on solid medium.

S5 Summary of the initial number of bacteria-dependent heat flow measurements

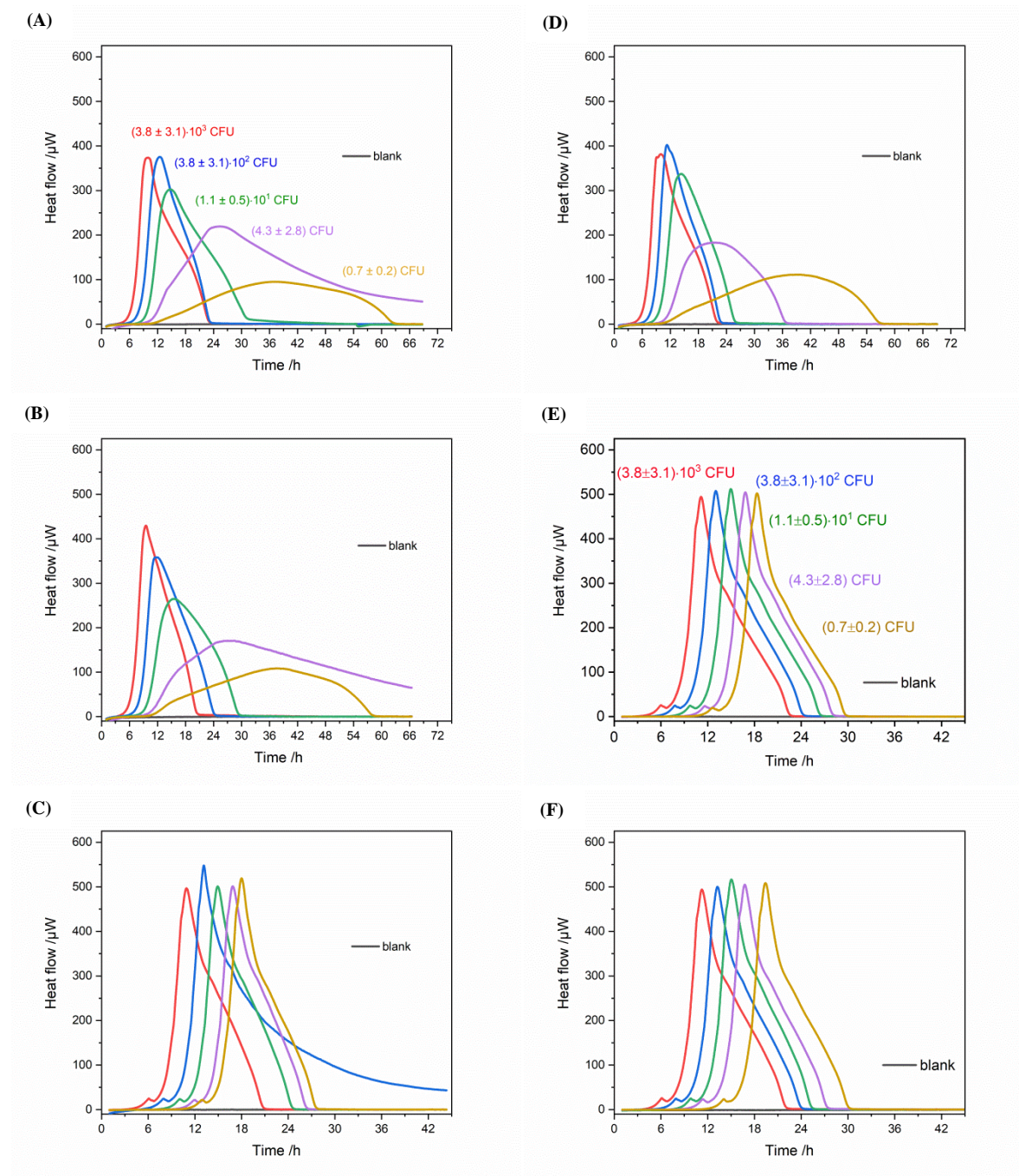


Figure S9: IMC experiments performed on SC and LC. The N_0 (mean \pm SD) in CFU are indicated next to the heat flow signals. **A), B), D):** Dependency of the heat traces on N_0 measured on SC. **C), E), F):** Dependency of the heat traces on N_0 measured on LC.

S6 Summary of the initial number of bacteria-dependent heat flow measurements performed in MC-Cal 100P calorimeter

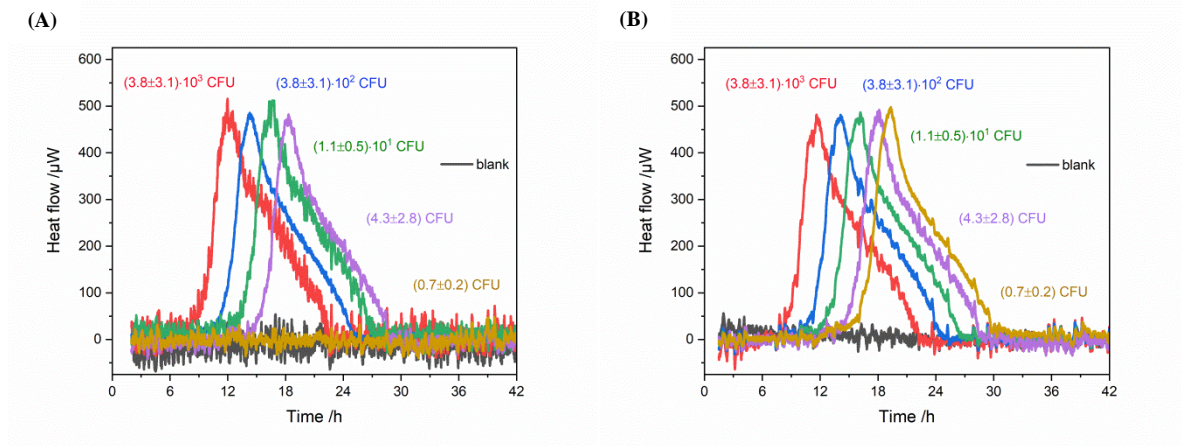


Figure S10: IMC experiments performed in LC using MC-Cal 100P calorimeter (A) and (B). The N_0 (mean \pm SD) in CFU are indicated next to the heat flow signals.

S7 Summary of the filling volume-dependent heat flow measurements

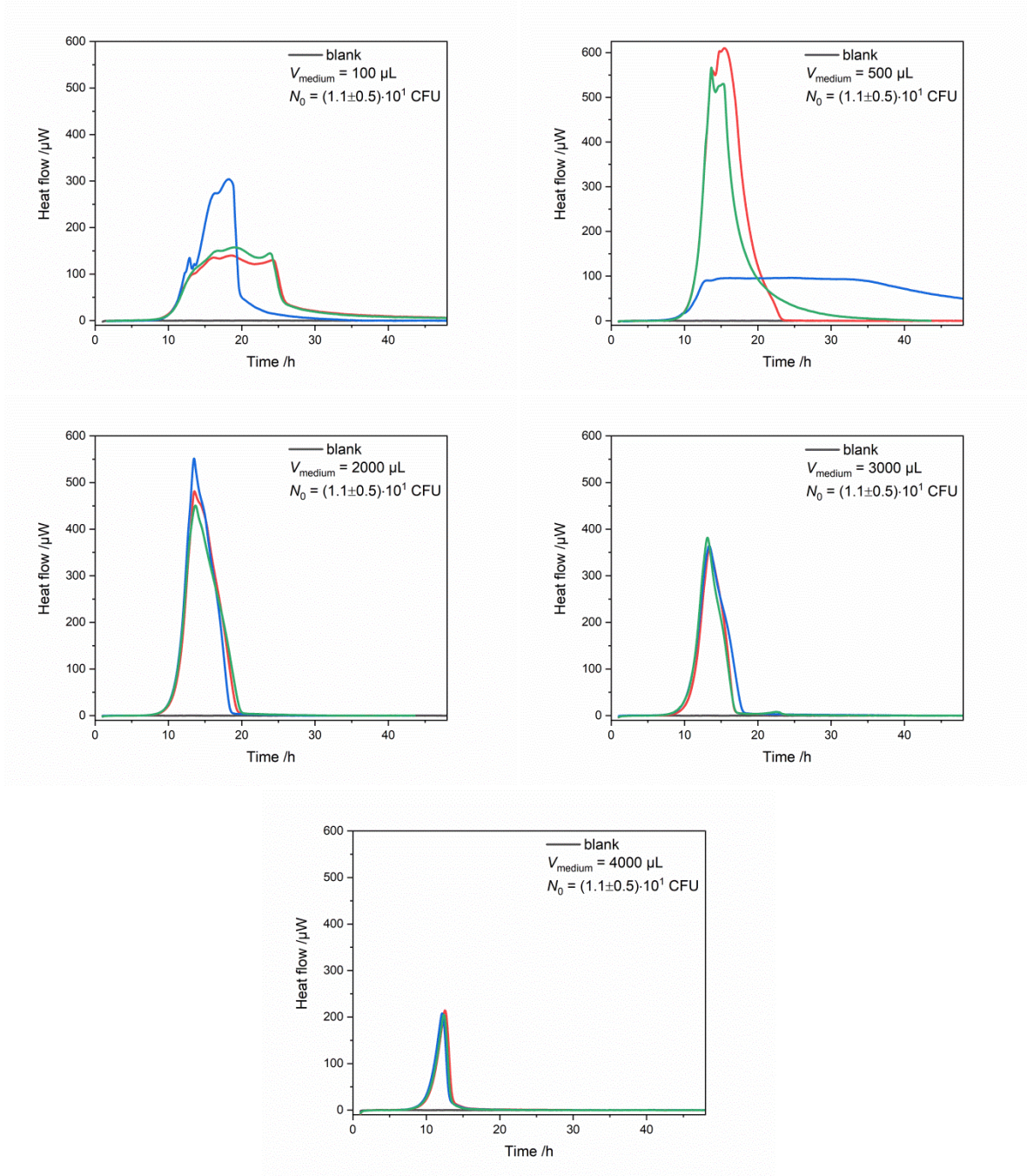


Figure S11: Influence of V_{medium} on the heat flow signals obtained from IMC experiments conducted on solid medium.

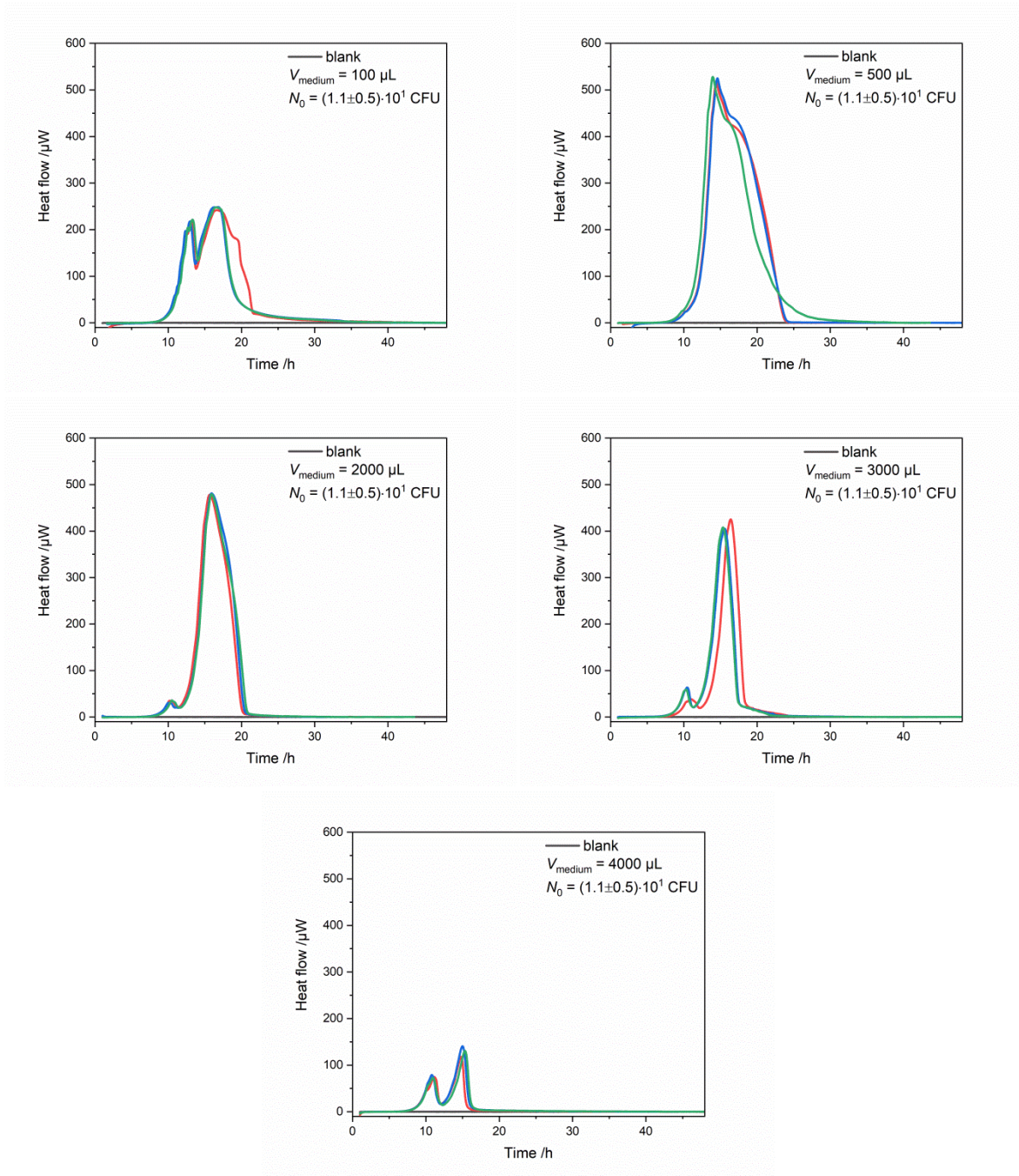


Figure S12: Influence of V_{medium} on the heat flow signals obtained from IMC experiments conducted in liquid medium.

S8 Threshold value of the calorimeter and dissolved oxygen in the medium

Early detection of bacterial contaminations is given if the threshold value determined by the applied calorimeter is below the solubility limit of oxygen c_{O_2} , because then the oxygen supply is not limited by diffusion. The heat Q_{theo} which corresponds to the concentration of dissolved oxygen in the medium c_{O_2} is given by the oxycaloric equivalent of $\Delta_k H_{O_2} = -455 \text{ kJ mol}^{-1}$ [3] eq. 9. The meaning of all the following symbols can be found in the main document.

$$Q_{\text{theo}} = c_{O_2} \cdot V_{\text{medium}} \cdot \Delta_k H_{O_2} \quad (9)$$

The detection of microbial contamination t_{dect} should be achieved before this oxygen is completely consumed (eq. 10).

$$Q_{\text{theo}} > \int_0^{t_{\text{dect}}} \Phi(t) dt \quad (10)$$

At the begin of microbial growth are all nutrients available in excess and exponential growth can be assumed (eq. 11).

$$\Phi(t) = N_0 \cdot \varphi_0 \cdot \exp(\mu \cdot t) \quad (11)$$

The solution of the integral equation 10 and 11 provides eq. 12.

$$Q_{\text{theo}} > \frac{N_0 \cdot \varphi_0}{\mu} \cdot (\exp(\mu \cdot t_{\text{dect}}) - 1) \quad (12)$$

t_{dect} is per definition the time if the heat production rate approaches to the detection threshold value of the applied calorimeter Φ_{dect} (eq. 13)

$$\Phi_{\text{dect}} = N_0 \cdot \varphi_0 \cdot \exp(\mu \cdot t_{\text{dect}}) \quad (13)$$

Combining eq. 9, 12 and 13 provides

$$\Phi_{\text{dect}} < \mu \cdot c_{O_2} \cdot V_{\text{medium}} \cdot \Delta_k H_{O_2} + N_0 \cdot \varphi_0 \quad (14)$$

Which means that if we like to prevent the influence of oxygen diffusion and thus to leave the area of exponential growth we have several options. We can i) choose calorimeter with a low Φ_{dect} , ii) enrich the medium with oxygen (e.g. by gassing with pure oxygen), iii) works with large sample volumes, iv) apply our method to slowly growing bacteria or v) start with a low initial number of contaminating bacteria (which is usually the case).

S9 Summary of the N_0 -dependent heat flow measurements performed in minimal medium

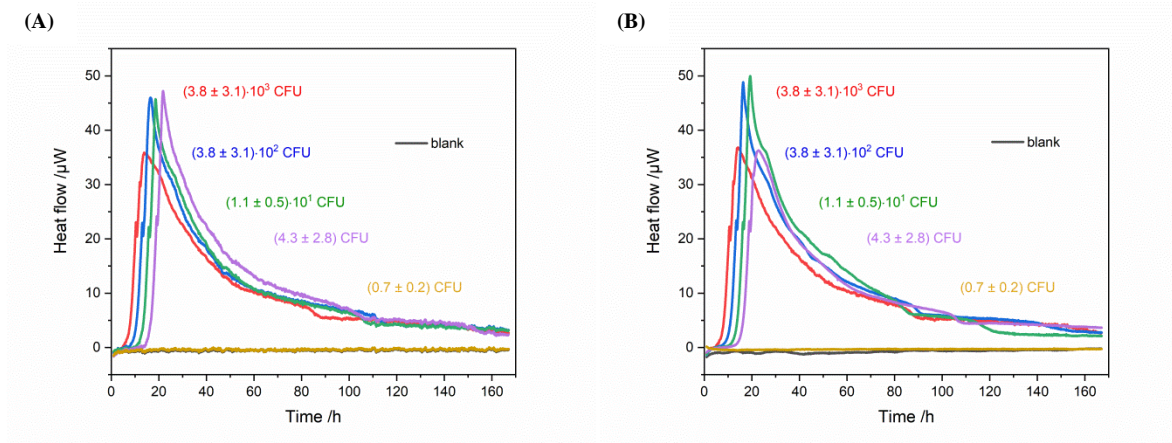


Figure S13: IMC experiments performed in LC using a minimal medium, MMKT2440 (A) and (B). The N_0 (mean \pm SD) in CFU are indicated next to the heat flow signals.

Reference

1. Benson, B.B. and D. Krause Jr., *The concentration and isotopic fractionation of oxygen dissolved in freshwater and seawater in equilibrium with the atmosphere I*. Limnology and Oceanography, 1984. **29**(3): p. 620-632.
2. Saha, K., *The earth's atmosphere - its physics and dynamics*. 1 ed. 2008, Berlin: Springer-Verlag Berlin Heidelberg. 367.
3. Gnaiger, E. and R.B. Kemp, *Anaerobic metabolism in aerobic mammalian cells: information from the ratio of calorimetric heat flux and respirometric oxygen flux*. Biochimica et Biophysica Acta (BBA) - Bioenergetics, 1990. **1016**(3): p. 328-332.

A3 Supplementary material for section 3.1.3 (published article 3)

Rapid culture-based detection of *Legionella pneumophila* using isothermal microcalorimetry with an improved evaluation method

Christian Fricke¹, Juan Xu², Feng-Lei Jiang², Yi Liu², Hauke Harms¹, Thomas Maskow^{1*}

¹Helmholtz-Centre for Environmental Research – UFZ, Department of Environmental Microbiology, Leipzig, Germany

²Key Laboratory of Analytical Chemistry for Biology and Medicine (Ministry of Education), College of Chemistry and Molecular Sciences, Wuhan University, Wuhan, 430072, China.

For correspondence:

*E-Mail: Thomas.Maskow@ufz.de, Tel. +49341 2351328

Contents

1. Thermal behavior of the calorimetric ampoule.....	1
2. Gompertz-Fit.....	2
3. Estimation of the total heat using the oxycaloric equivalent	3
Reference	4

1. Thermal behavior of the calorimetric ampoule

At the begin of the growth process, the metabolic heat evolution P_M can be described by **eq. (1)**.

$$P_M = P_0 \cdot e^{\mu \cdot t} \quad (1)$$

Here is P_0 the metabolic start activity (in W) which is proportional to the number of active cells and μ is the specific growth rate (in s^{-1}). The resulting heat is dissipated via a Peltier element with the area A (in m^2) and the heat conduction coefficient λ (in $W m^{-1} K^{-1}$) and measured as a voltage proportional to $(T - T_C)$.

$$P = A \cdot \lambda \cdot (T - T_C) \quad (2)$$

T , T_C stand for temperature in K and temperature of the calorimeter, respectively. The entire process is described by a heat balance equation (the calorimeter equation) **(3)**.

$$V_r \cdot \rho \cdot c_p \cdot \frac{dT}{dt} = P_0 \cdot e^{\mu \cdot t} - A \cdot \lambda \cdot (T - T_C) \quad (3)$$

V_r , ρ , c_p , t stand for the filling volume of the ampoule (in m^3), the density of the medium (in kg m^{-3}), the specific heat capacity (in $\text{J kg}^{-1} \text{K}^{-1}$) and the time (ins), respectively.

2. Gompertz-Fit

By integrating the received heat flow signals, the total heat of the growth can be obtained. The resulting heat curve showed classical sigmoidal behavior. Using logistic equations like the Gompertz function, parameters such as Q_{\max} , the saturation limit, μ_{\max} , the maximum slope of the curve and γ , refers to the shift along the time-axis can be obtained. The Gompertz fit and the heat integral are shown in **Fig. S1**.

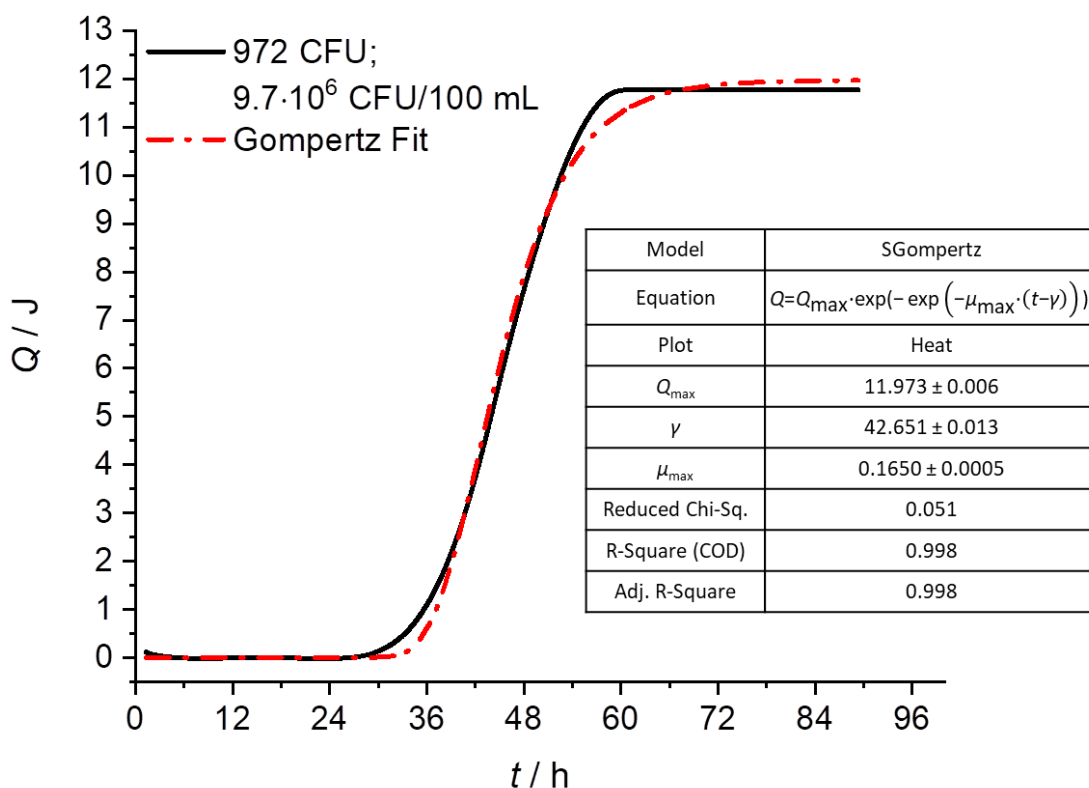


Figure S1: Heat over time diagram. The black line describes the integrated heat signal determined by metabolic activity. The red line shows the Gompertz fit.

The fit showed a high correlation ($R^2 = 0.998$) with the integrated heat signal. Microbiological quantities can be assigned to the individual parameters from the Gompertz Fit. The parameters obtained from the fit

are $Q_{\max} = (11.97 \pm 0.01) \text{ J}$, $\gamma = (42.65 \pm 0.01) \text{ h}$ and $\mu_{\max} = (0.1650 \pm 0.0005) \text{ h}^{-1}$. Q_{\max} represents the total heat. μ_{\max} the maximum growth rate of the respective bacteria and γ the lag time of bacterial growth.

3. Estimation of the total heat using the oxycaloric equivalent

The initial situation is illustrated in **Fig. S2**. The sample contained 1 mL substrate and 3 mL air in headspace.

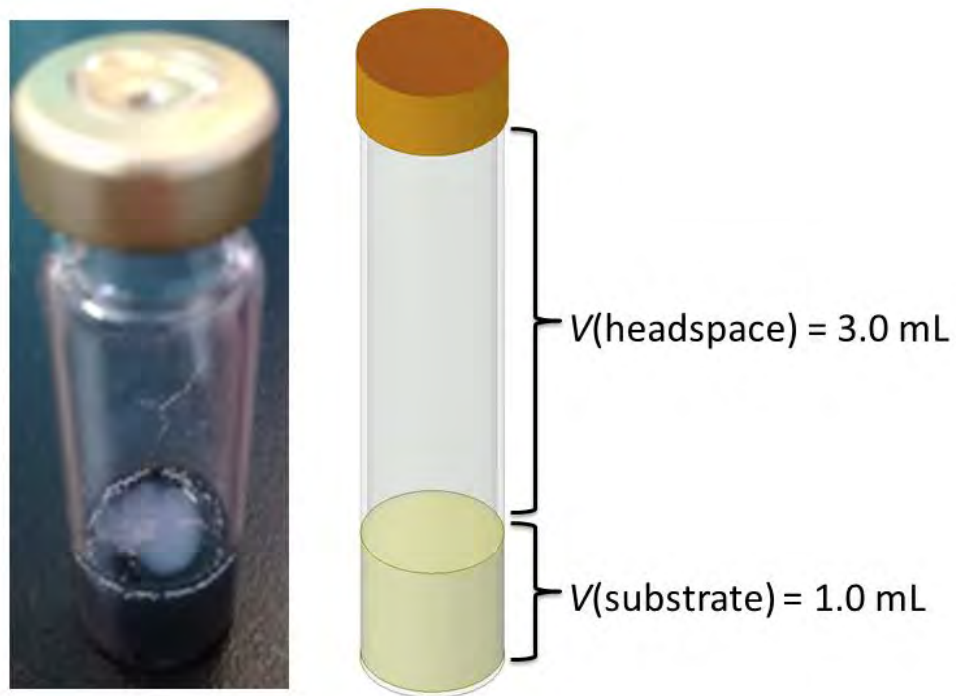


Figure S2: The schematic structure of the ampoules for monitoring *L. pneumophila* growth.

The following data are necessary for calculating the total heat production of *L. pneumophila* during aerobic growth.

Table 1: Summary of the physical quantities for calculating the total heat production

parameter	value	dimension	Reference
$V(\text{air})$	0.003	L	-
$\rho(\text{air})$	1.1381 ^a	kg·m ³	-
$w(\text{O}_2)$	23.14	%	(Saha, 2008)
$M(\text{O}_2)$	32	g·mol ⁻¹	-
$\Delta_k H_{\text{O}_2}$	(455 ± 25)	kJ·mol ⁻¹ O ₂	(Gnaiger and Kemp, 1990)

^a determined by the specific gas constant of dry air, $R_s = 287.058 \text{ J}\cdot\text{kg}^{-1}\cdot\text{K}^{-1}$ at 310.15 K

The mass of air and molecular oxygen can be calculated as follow:

$$m(\text{air}) = V(\text{air}) \cdot \rho(\text{air}) \quad (4)$$

$$m(\text{O}_2) = w(\text{O}_2) \cdot m(\text{air}) \quad (5)$$

The molar mass of molecular oxygen can be used to calculate the amount of molecular oxygen in the headspace.

$$n(\text{O}_2) = \frac{m(\text{O}_2)}{M(\text{O}_2)} \quad (6)$$

In the last step, the total heat released from the aerobic growth can be calculated using the oxycaloric equivalent $\Delta_k H_{\text{O}_2}$.

$$Q = n(\text{O}_2) \cdot \Delta_k H_{\text{O}_2} \quad (7)$$

The theoretical heat evolved during aerobic growth under the circumstances is $Q = (11.2 \pm 0.6) \text{ J}$.

Reference

- Gnaiger, E., and Kemp, R.B. (1990). Anaerobic metabolism in aerobic mammalian cells: information from the ratio of calorimetric heat flux and respirometric oxygen flux. *Biochimica et Biophysica Acta (BBA) - Bioenergetics* 1016, 328-332.
- Saha, K. (2008). *The earth's atmosphere - its physics and dynamics*. Berlin: Springer-Verlag Berlin Heidelberg.

A4 Supplementary material for section 3.2 (submitted manuscript)

Supplementary Material

Numerical heat flow and transport simulation as a development tool for the design of isothermal microcalorimeters

Christian Fricke¹, Toralf Klee², Sven Richter², Sven Paufler¹, Hauke Harms¹, Thomas Maskow¹

¹ Helmholtz Centre for Environmental Research – UFZ, Permoserstraße 15, 04318 Leipzig, Germany

² Loetec Elektronische Fertigungssysteme GmbH, Dresdener Straße 28, 06886 Lutherstadt Wittenberg

Table of content

S1 Evaluation of internal sensors	2
S2 Temperature profiles of external sensors	4
S3 Material assignment of the numerical model	6
S4 Boundary conditions for the heat transfer simulations on the heat sink	7
S5 Determining parameters for temperature control on the heat sink.....	9
S6 CFD simulation for determining the velocity magnitude at the interior fan.....	12
Reference.....	13

S1 Evaluation of internal sensors

For the evaluation of internal temperature sensors, $N = 41242$ data points were measured in the time interval from 6 to approx. 72 h and the statistical data (mean value, standard deviation and maximum and minimum) calculated thereof. The temperature profile and the obtained statistic data of the air in the outer zone are shown in Fig. S1.

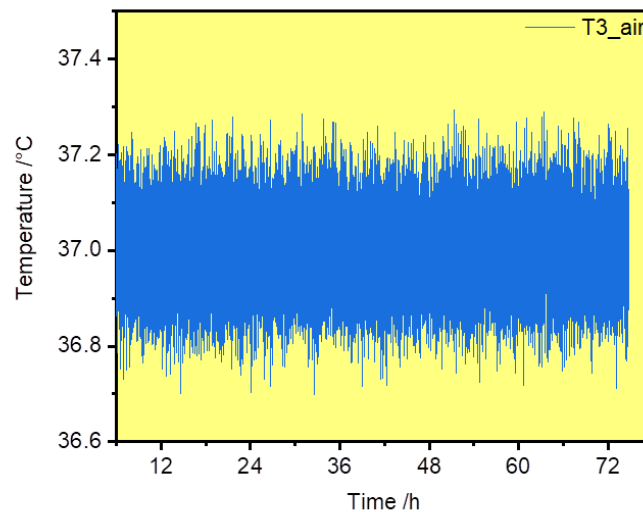


Figure S1: Temperature profile of the air in the outer zone. Statistic data were obtained: $T = (37 \pm 0.1) \text{ }^\circ\text{C}$, $T_{\min} = 36.7 \text{ }^\circ\text{C}$ and $T_{\max} = 37.3 \text{ }^\circ\text{C}$.

The temperature profiles and the obtained statistic data on the heat sink in the inner zone are shown in Fig. S2A, B.

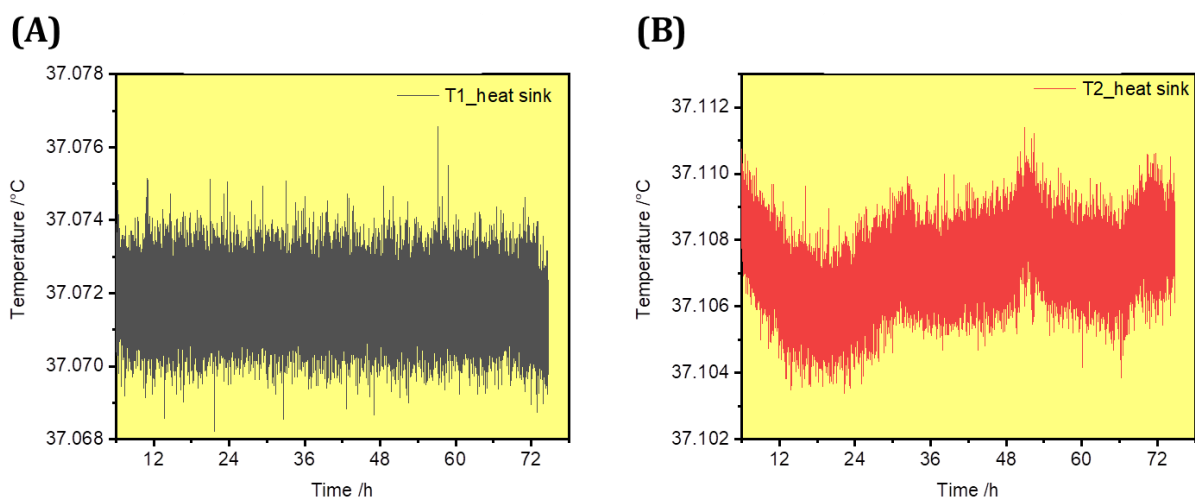


Figure S2: Temperature profiles on the heat sink in the inner zone. **A:** Measured temperature at the NTC sensor located under the reference channel, corresponding statistic data $T = (37.072 \pm 0.001) \text{ }^\circ\text{C}$, $T_{\min} = 37.068 \text{ }^\circ\text{C}$ and $T_{\max} = 37.077 \text{ }^\circ\text{C}$. **B:** Measured temperature at the NTC sensor located under channel 1, corresponding statistic data $T = (37.0107 \pm 0.001) \text{ }^\circ\text{C}$, $T_{\min} = 37.103 \text{ }^\circ\text{C}$ and $T_{\max} = 37.111 \text{ }^\circ\text{C}$.

The differential voltage ($\Delta U_{\text{HFS1,2}} = U_{\text{HFS1,2}} - U_{\text{HFS,reference}}$) profiles and the obtained statistic data on the heat flow sensor in channel 1 and 2 are given in Fig. S3A, B.

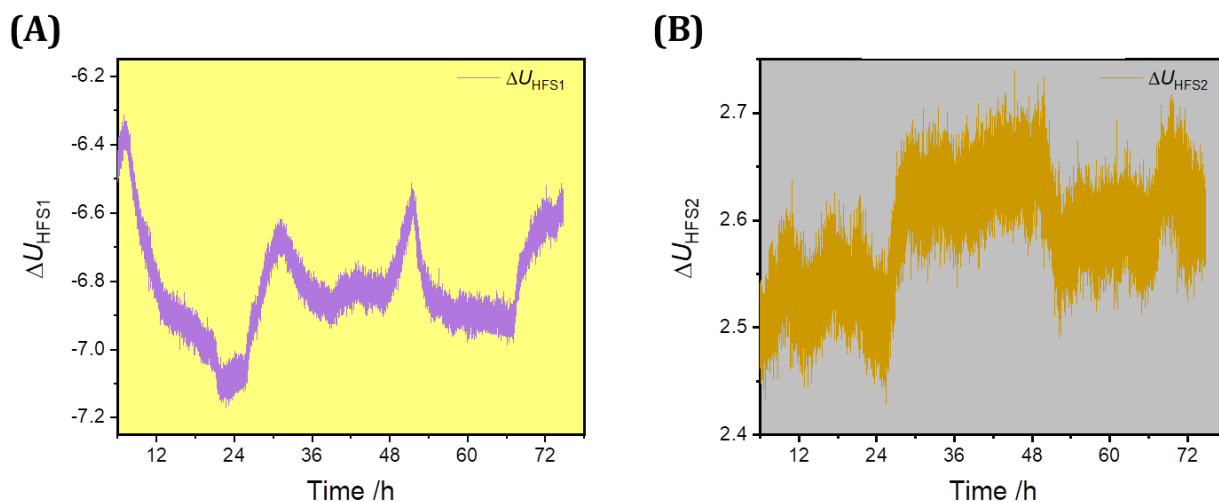


Figure S3: ΔU_{HFS} profiles of the heat flow sensors in channel 1 and 2. **A:** ΔU_{HFS1} signal in channel 1, corresponding statistic data $\Delta U_{\text{HFS1}} = (-6.82 \pm 0.15)$ mV, $\Delta U_{\text{HFS1,min}} = -7.17$ mV and $\Delta U_{\text{HFS1,max}} = -6.13$ mV. **B:** ΔU_{HFS2} signal in channel 2, corresponding statistic data $\Delta U_{\text{HFS2}} = (2.59 \pm 0.05)$ mV, $\Delta U_{\text{HFS2,min}} = 2.43$ mV and $\Delta U_{\text{HFS2,max}} = 2.74$ mV.

The time-dependent percentage power output of the heater foils is shown in Fig. S4. After reaching the setpoint temperature, the heater foils are turned off.

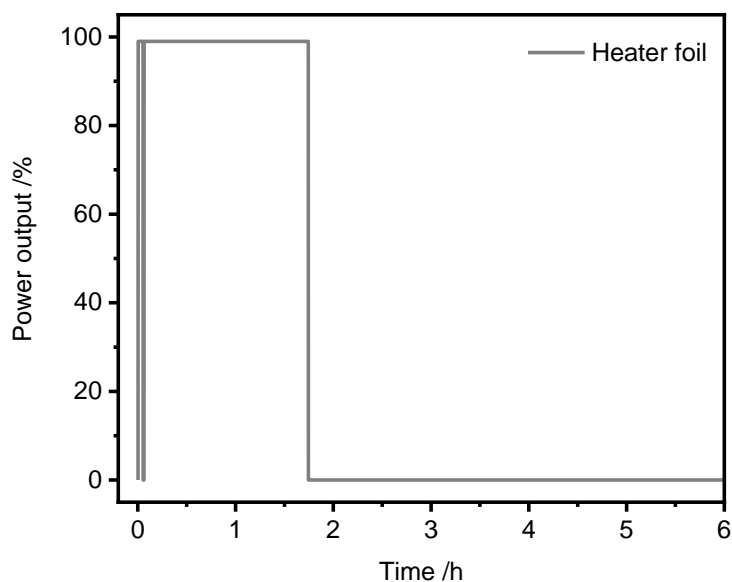


Figure S4: Percentage power output of the heater foils in the time interval from 0 to 6 h.

S2 Temperature profiles of external sensors

The steady-state temperature after approx. 360 min were determined and used for comparison with the numerical data. The actual position is given in Fig. 5 of the main article. Measurements were performed in triplicate. The temperature profile of the channels (Fig. S5), in the upper part (Fig. S6) and the lower part (Fig. S7) are given below.

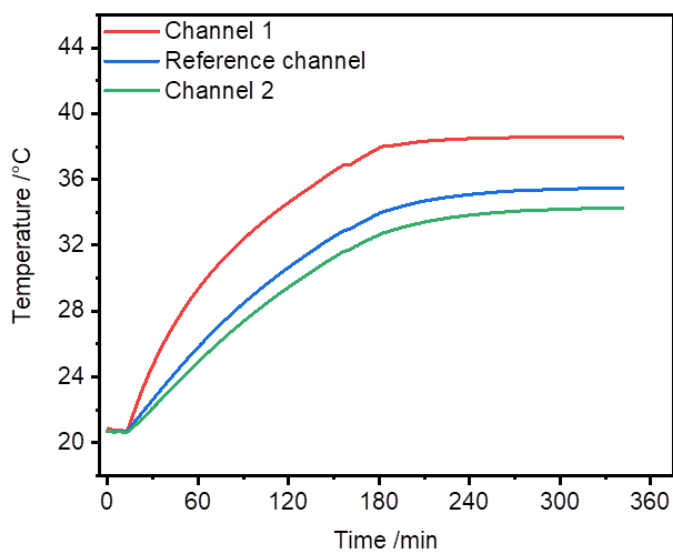


Figure S5: Temperature profiles of the channels. Average temperatures in steady-state are 38.5 °C (red curve, channel 1), 35.5 °C (blue curve, reference channel) and 34.3 °C (green curve, channel 2).

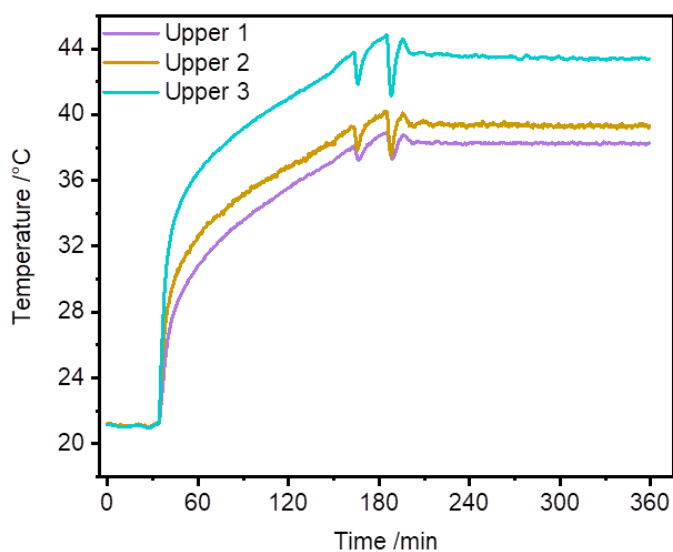


Figure S5: Temperature profiles at local points in the upper part. Average temperatures in steady-state are 38.2 °C (purple curve, upper 1), 39.4 °C (yellow curve, upper 2) and 43.5 °C (blue curve, upper 3).

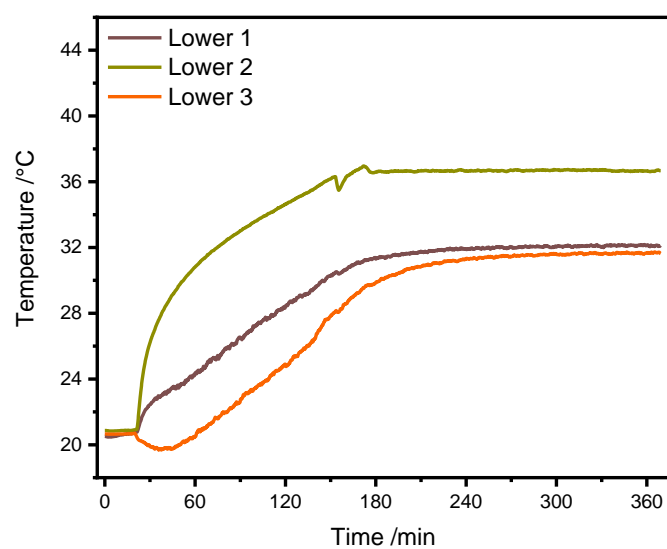


Figure S6: Temperature profiles at local points in the lower part. Average temperatures in steady-state are 32.1 °C (brown curve, lower 1), 36.8 °C (green curve, lower 2) and 31.7 °C (orange curve, lower 3).

S3 Material assignment of the numerical model

Tab. S1 summarizes the material assignment of all components. In some cases, a component is subdivided into several individual parts to which different materials are assigned.

Table S1: Summary of material assignments of all components.

material	Components	source of properties	Reference
aluminium	primary heat sink	$\rho = 2700 \text{ kg}\cdot\text{m}^{-3}$ $C_p = 900 \text{ J}\cdot\text{kg}^{-1}\cdot\text{K}^{-1}$ $k = 238 \text{ W}\cdot\text{m}^{-1}\cdot\text{K}^{-1}$	COMSOL library
	auxiliary heat sink		
	fan heater channel		
	fan heater element		
	thermal bridges		
	heat flow sensor		
	upper part channels		
air ^a	air domain outer zone	$\rho(pA, T), C_p(T)$ $k(T), \eta(T)$ $\gamma = 1.4^b$	COMSOL library
	air domain channel		
polyamide	spacer upper part	$\rho = 1150 \text{ kg}\cdot\text{m}^{-3}$ $C_p = 1700 \text{ J}\cdot\text{kg}^{-1}\cdot\text{K}^{-1}$ $k = 0.25 \text{ W}\cdot\text{m}^{-1}\cdot\text{K}^{-1}$	given by manufacturer
	sample holder		
	fan housing		
	lower part channels		
	spacer inner zone		
	heat flow sensor (insulation)		
	spacer lower part		
polyamide GF 30	carrier plates	$\rho = 1320 \text{ kg}\cdot\text{m}^{-3}$ $C_p = 1500 \text{ J}\cdot\text{kg}^{-1}\cdot\text{K}^{-1}$ $k = 0.24 \text{ W}\cdot\text{m}^{-1}\cdot\text{K}^{-1}$	given by manufacturer
acrylonitrile butadiene styrene	outer/inner insulation plates	$\rho = 1040 \text{ kg}\cdot\text{m}^{-3}$ $C_p = 1200 \text{ J}\cdot\text{kg}^{-1}\cdot\text{K}^{-1}$ $k = 0.144 \text{ W}\cdot\text{m}^{-1}\cdot\text{K}^{-1}$	given by manufacturer
aluminium oxide, 96 %	top/bottom Peltier modules	$\rho = 3800 \text{ kg}\cdot\text{m}^{-3}$ $C_p = 880 \text{ J}\cdot\text{kg}^{-1}\cdot\text{K}^{-1}$ $k = 25 \text{ W}\cdot\text{m}^{-1}\cdot\text{K}^{-1}$	given by manufacturer
steele	baffle	$\rho = 7850 \text{ kg}\cdot\text{m}^{-3}$ $C_p = 475 \text{ J}\cdot\text{kg}^{-1}\cdot\text{K}^{-1}$ $k = 44.5 \text{ W}\cdot\text{m}^{-1}\cdot\text{K}^{-1}$	COMSOL library
bismuth telluride	semi-conductor	$\rho = 7700 \text{ kg}\cdot\text{m}^{-3}$ $C_p = 154 \text{ J}\cdot\text{kg}^{-1}\cdot\text{K}^{-1}$ $k(T), S(T)^c, \sigma(T)^d$	COMSOL library
polyester	heating foil	$\rho = 1380 \text{ kg}\cdot\text{m}^{-3}$ $C_p = 1170 \text{ J}\cdot\text{kg}^{-1}\cdot\text{K}^{-1}$ $k = 0.154 \text{ W}\cdot\text{m}^{-1}\cdot\text{K}^{-1}$	given by manufacturer

^a properties are function of dependent variables

^b $\gamma = C_p/C_v$ (ratio of specific heats)

^c $S(T)$ = Seebeck voltage as a function of the temperature

^d $\sigma(T)$ = electrical conductivity as a function of the temperature

S4 Boundary conditions for the heat transfer simulations on the heat sink

For determining the PID controller parameters, a selected part of the test system was considered for numerical simulations. The selected compounds are illustrated in Fig. S7. To model the increase in temperature on the heat sink, appropriate heat flux boundary conditions have to be applied to the numerical model. Here, we assumed convective heat flux which can be described by eq. 3 (in the main article). Two parameters are responsible for the heat flux: (i) the external temperature T_{ex} in (K) and (ii) the heat transfer coefficient h (in $\text{W}\cdot\text{m}^{-2}\cdot\text{K}^{-1}$).

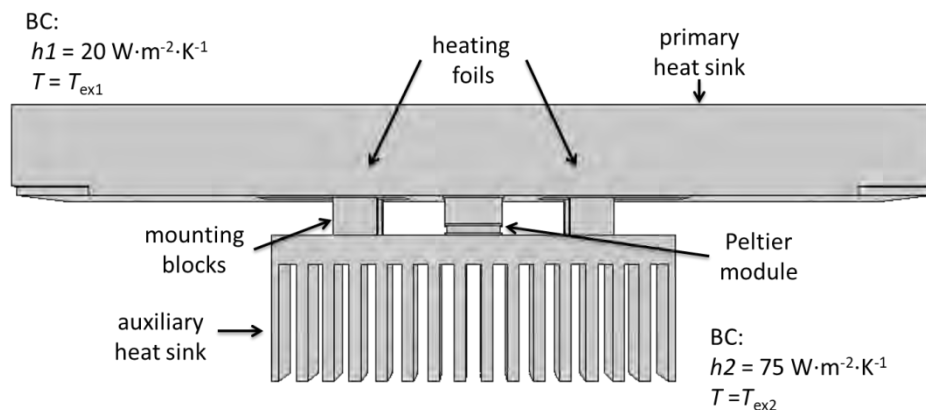


Figure S7: 3D numerical model of selected compounds to determined PID parameters for the temperature control on the primary heat sink (the two heating foils are placed on the bottom of the primary heat sink and therefore not visible).

The external temperature profiles on the primary and auxiliary heat sink are represented by the black curve and the red curve, respectively (see Fig. S8A). An appropriate heat transfer coefficient h was determined in a parametric sweep study, simulating the effect of h_1 on the increase in temperature (see Fig. S8B). The temperature was measured by a point located in the heat sink, which is served as a temperature probe. Both Peltier modules and heating foils were not regulated after reaching the desired set point temperature to simplify the simulations (this explains the linear increase in temperature beyond the 37 °C). We observed the best agreement applying $h_1 = 20 \text{ W}\cdot\text{m}^{-2}\cdot\text{K}^{-1}$. Here, experimental data is in strong correlation to numerical results. If h is too small ($< 20 \text{ W}\cdot\text{m}^{-2}\cdot\text{K}^{-1}$), the temperature increase is much faster than experimental results. If h is too large ($> 20 \text{ W}\cdot\text{m}^{-2}\cdot\text{K}^{-1}$), the opposite behaviour can be observed. The increase in temperature is too slow.

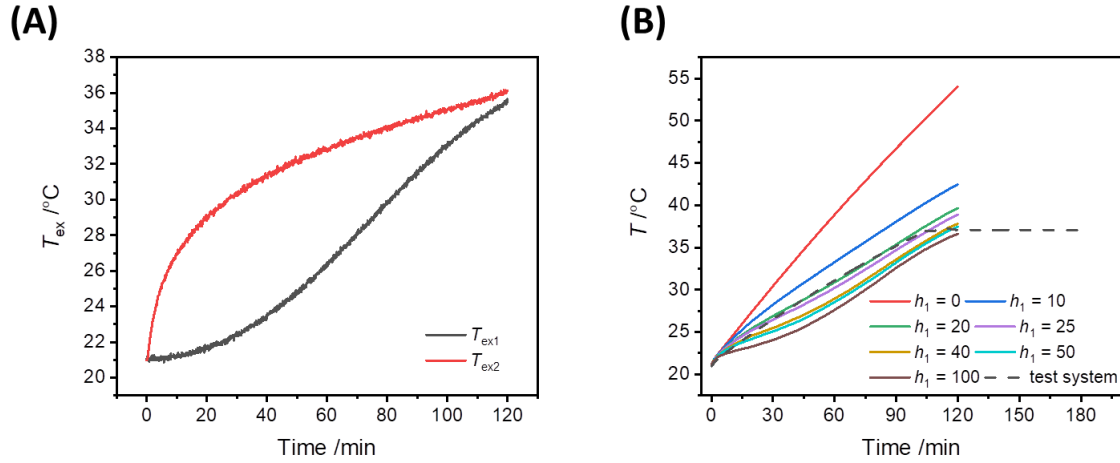


Figure S8: Temperature profile for determining heat flux boundaries for the simulations on the heat sink. **A:** Temperature profiles of the external temperatures. T_{ex1} represents the increase in temperature around the primary heat sink (black curve). T_{ex2} represents the increase in temperature around the auxiliary heat sink (red curve). **B:** Influence of the heat transfer coefficient on the increase of temperature on the heat sink. For comparison, the black dashed line showed experimental data of the test system under laboratory conditions.

The same approach was used to determine the heat transfer coefficient on the auxiliary heat sink h_2 . Here, the heat transfer is influenced by the fan's airflow because this heat sink is part of the outer zone of the test system. Therefore, we assumed a larger h_2 value and performed a parametric sweep study. The results are shown in Fig. S9 for $h_1 = 20 \text{ W}\cdot\text{m}^{-2}\cdot\text{K}^{-1}$. Since there is no strong variation in temperature increase between $h_2 = 25 \text{ W}\cdot\text{m}^{-2}\cdot\text{K}^{-1}$ and $h_2 = 200 \text{ W}\cdot\text{m}^{-2}\cdot\text{K}^{-1}$. We selected $h_2 = 75 \text{ W}\cdot\text{m}^{-2}\cdot\text{K}^{-1}$ for the PID control simulations on the heat sink.

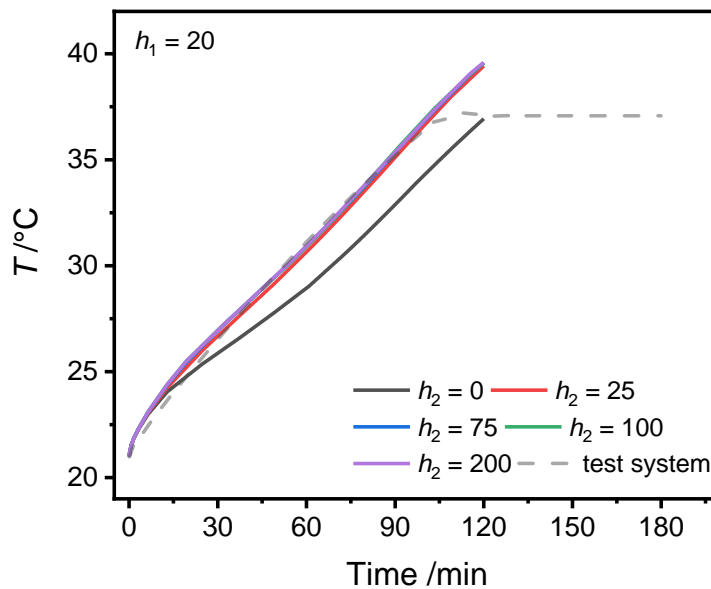


Figure S9: Influence of the heat transfer coefficient on the increase of temperature on the heat sink. For comparison, the black dashed line showed experimental data of the test system under laboratory conditions.

S5 Determining parameters for temperature control on the heat sink

Heat flux boundary conditions that enable heat exchange with the ambient air were determined in preliminary simulations. For these simulations, we only considered the primary heat sink, the two Peltier modules and heating foils as well as the auxiliary heat sink (see Fig. S7). Settings and results from these simulations are described in detail in S4.

In general, manually determining the control parameters of a control loop can be tedious and time-consuming. Numerical simulations offer an intelligent solution for this problem since an empirical approach can provide valuable information on the feedback system of the control loop. In the following time-dependent studies, we demonstrated how numerical simulations could be helpful to determine the control parameters during heating of the heat sink. We applied a PID controller for our simulations because the control loop of the IMC test system (shown in Fig. 2 of the main article) is too complex for integration in detail in our numerical simulations. The PID control loop is described in Fig. S10.

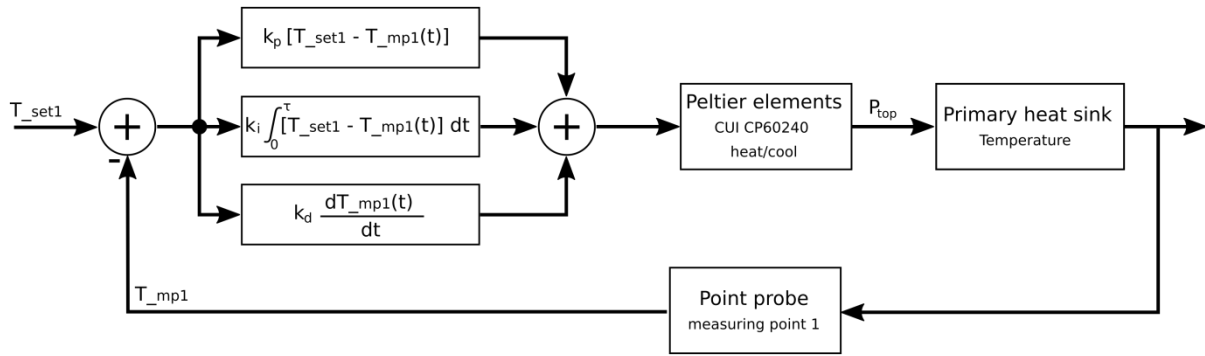


Figure S10: Signal flow diagram of the PID control loop used for the numerical simulations, which regulates the temperature on the primary heat sink by the two Peltier modules.

The underlying equation of the PID algorithm is as follow:

$$P(t) = P_{\text{bias}} + K_p(T_{\text{set}} - T(t)) + K_i \int_0^t (T_{\text{set}} - T(\tau)) d\tau - K_d \frac{d}{dt} T(t) \quad (1)$$

K_p , K_i , K_d are the proportional, integral and differential parameter, respectively. We started to investigate the influence of the proportional parameter K_p (in $\text{W} \cdot \text{K}^{-1}$) in a time-dependent parametric sweep study (from $1 \text{ W} \cdot \text{K}^{-1}$ to $400 \text{ W} \cdot \text{K}^{-1}$) until we observed an oscillation of the measured temperature. K_i and K_d were set to 0 (pure P-controller). This approach is based on the Ziegler-Nichols method for determining PID control parameters [1]. Fig. S11A, B displayed the behavior of the measured temperature depending on the applied K_p value.

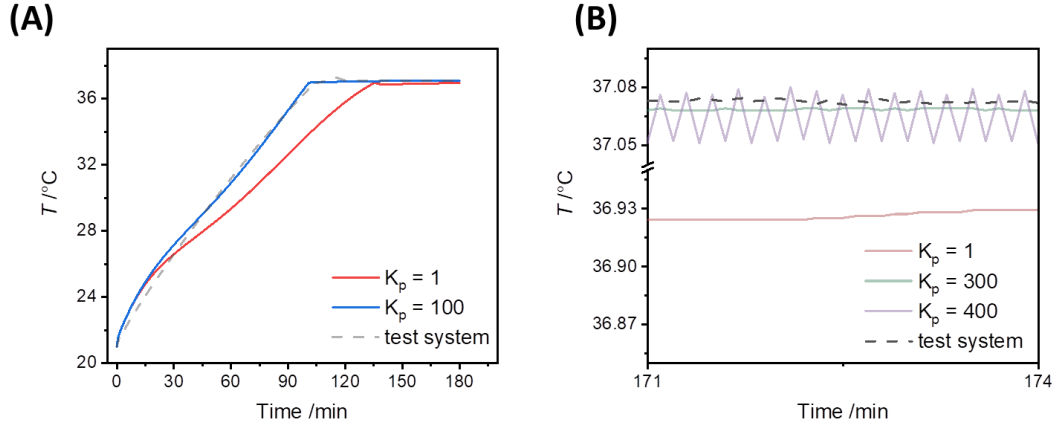


Figure S11: Simulated temperature profiles depending on different K_p values. For comparison, the dashed black line represents the measured temperature profile on the heat sink. **A:** Simulated temperature profile during the heat-up phase on the heat sink using $K_p = 1$ (red curve) and $K_p = 100$ (blue curve). **B:** Magnification of some simulated temperature profiles depending on the applied K_p value. $K_p = 1$ (red curve) and $K_p = 300$ (green curve) show a permanent residual setpoint error. Oscillation was observed for $K_p = 400$ (purple curve).

If the K_p value is too small ($K_p = 1$), we observed a creeping temperature increase. Higher K_p values such as $K_p = 100$ showed strong agreement with the experimental data (Fig S11A). In the beginning, there is a slight deviation, probably caused by the settings of the heat flux boundary conditions in this model (determined in preliminary simulations, see S5). The chosen boundary conditions cannot wholly represent the inertia of the ambient air of the heat sink (in the physical test system). Assuming complete isolation ($h = 0 \text{ W}\cdot\text{m}^{-2}\cdot\text{K}^{-1}$), the desired set temperature ($37 \text{ }^\circ\text{C}$) can be reached after 51.6 min (see Fig. S7A in the SI, here different h -values were simulated). This is in strong agreement with a simple estimation (time until the temperature of the primary heat sink is increased from 21 to $37 \text{ }^\circ\text{C}$ using the power of all heat sources ($37.6 \text{ J}\cdot\text{s}^{-1}$) and the total mass of the primary heat sink approx. 8.1 kg and the heat capacity of aluminium of $900 \text{ J kg}^{-1} \text{ K}^{-1}$) leading to 51.9 min.

As expected for a P-controller, a permanent residual setpoint error is observed for K_p values below a critical value (also known as ultimate gain, K_u) [2]. Above approx. $K_u = 360$, the temperature oscillates (Fig. S11B). Additionally, we determined from this oscillated response the period length $T_u = 10.8 \text{ s}$. According to the Ziegler-Nichols approach for a PI controller, the integral parameter is determined by eq. 2:

$$K_i = (0.54 \cdot K_u)/T_u \quad (2)$$

and the proportional parameter by eq. 14:

$$K_p = 0.45 \cdot K_u \quad (3)$$

In eq. 2 and 3, the parameters K_u and T_u were determined using a pure P-controller and are now used to achieve satisfactory control for the feedback loop using a PI controller. The obtained temperature profile is shown in Fig. S12. By applying a PI controller, the desired set point temperature can be

reached. However, we observed a great delay (280 min) in reaching the setpoint. The numerical simulation reveals the cause, an overshooting of the temperature with a magnitude of approx. 42.5 °C.

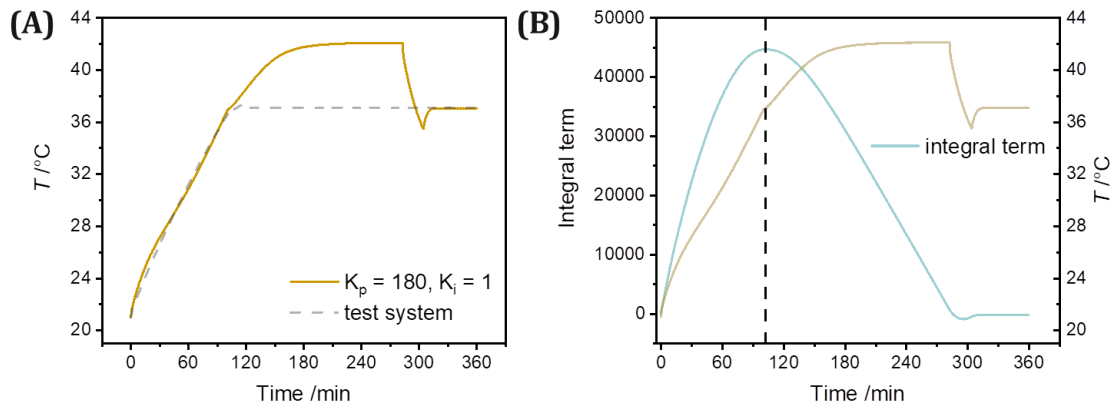


Figure S12: Simulated temperature profile and integral term of the heating up processes of the heat sink using a PI controller. **A:** Simulated temperature on the heat sink (yellow curve) and compared the measured temperature of the test system under laboratory conditions (black, dashed curve). **B:** The integral term (blue curve). The inflection point correlates with reaching the desired setpoint temperature of 37.07 °C. This is followed slowly by the elimination of the integral term.

The overshoot can be explained by the wind-up effect of a PI- or PID-controller [3]. Due to the significant difference between measured and setpoint temperature during the start-up phase, the integral term of the PI algorithm accumulates, becomes very large (see Fig. S12B), and reaches a turning point after reaching the setpoint. This affects the controlling behavior of the PI controller. Thus the power output of the Peltier modules is not regulated efficiently. After the turning point, the integral term slowly decays, allowing the output of the Peltier modules to be controlled appropriately to the desired setpoint temperature.

In order to avoid this wind-up effect, different anti-windup approaches are known, such as tracking back-calculation, conditional integration and limited integrator [4-6]. We applied a tracking time constant T_t [in s] to tackle this issue [7]. The obtained temperature profile is summarized in Fig. S13A, and the corresponding integral terms are shown in Fig. S13B. Applying the time constant, we were able to eliminate the integrator wind-up. Again, the temperature response of the numerical simulation is in strong agreement with experimental data of the test system under laboratory conditions. Due to the tracking time constant, an additional feedback loop is applied to the PI-controller. A second integral term with the opposite sign is generated to avoid a substantial overshoot (see Fig. S13B). Finally, the PI-controller achieved the desired setpoint temperature of 37.07 °C and properly regulated against disturbances on the heat sink.

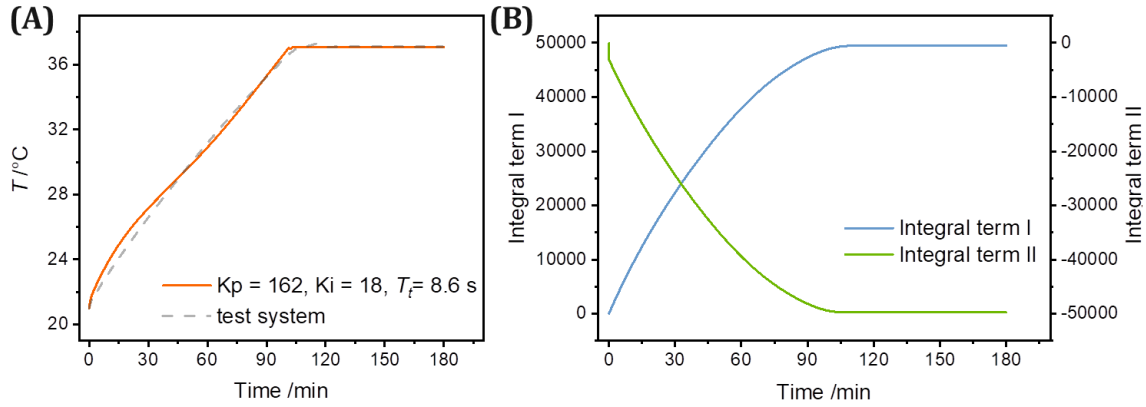


Figure 13: Simulated temperature profile and integral term of the heating up processes of the heat sink using a modified PI controller. **A:** Simulated temperature on the heat sink (orange curve) and for comparison the measured temperature of the test system under laboratory conditions (black, dashed curve). **B:** Courses of the integral term I (blue curve) and integral term II (green curve). The second integral term is obtained by applying the tracking time constant.

S6 CFD simulation for determining the velocity magnitude at the interior fan

In order to investigate the temperature distribution in the upper part in more detail, we determined in a stationary study the velocity magnitude v (in $\text{m}\cdot\text{s}^{-1}$) on the boundary condition that represents the interior fan in our numerical model. The corresponding 3D model is illustrated in Fig. S14A. The required data for describing the interior fan boundary condition (see eq. 7 in the main article) were taken from the technical datasheet of the fan (static pressure at no flow $p_{\text{nf}} = 0.05$ kPa and free delivery flow rate $V_{0,\text{fd}} = 0.0042$ $\text{m}^3\cdot\text{s}^{-1}$). Additionally, we performed a mesh refinement study to prove that the numerical solution is almost independent of the mesh density. The corresponding results are given in Tab. S2 and illustrated graphically in Fig. S14B. A less coarse mesh (increase in mesh elements) has little to no effect on the average velocity magnitude but would dramatically increase the computation time. However, no convergence was reached by refining the mesh even further, probably due to an exponential increase in computational resources required (see Fig. S14B).

Table S2: Results were obtained from the mesh refinement study to determine the velocity magnitude on the interior fan boundary.

Mesh	average velocity magnitude / $\text{m}\cdot\text{s}^{-1}$	number of mesh elements	computational time
extremely coarse	4.19	94236	2 min 54 s
extra coarse	4.19	139466	5 min 21 s
coarser	4.17	258984	6 min 57 s

The average velocity magnitude on the interior fan's boundary surface was determined to $4.2 \text{ m}\cdot\text{s}^{-1}$. This value is used as input for the numerical simulations on the temperature distribution of the upper part.

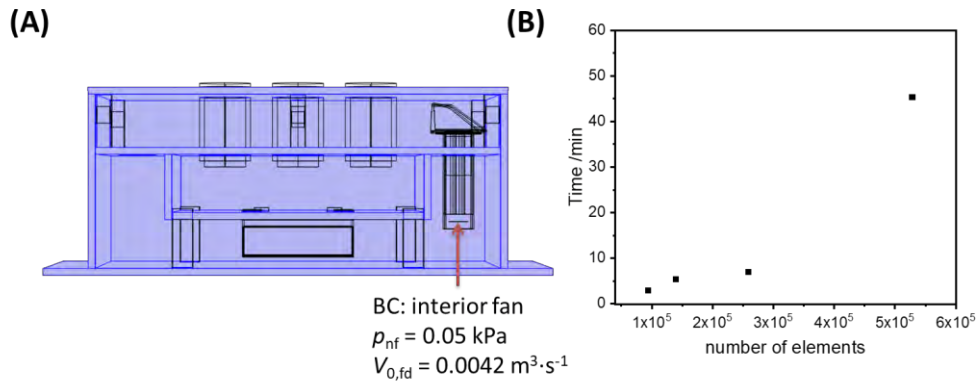


Figure S14: CFD simulations of the airflow caused by the interior fan. **A:** Reconstruction of the IMC test system in the simulation software. Parts of the inner zone were neglected to reduce computational time. Further, the fluid flow of the outer zone does not affect the fluid flow in the inner zone. **B:** Relationship between the number of mesh elements and computational time.

Reference

1. Ellis G. Chapter 6 - Four Types of Controllers. In: Ellis G, editor. Control System Design Guide (Fourth Edition). Boston: Butterworth-Heinemann; 2012. p. 97-119.
2. Bansal H, Sharma R, Ponpathirkootam S. PID Controller Tuning Techniques: A Review. 2012;2:168-76.
3. Kheirkhahan P, editor. Robust anti-windup control design for PID controllers. 2017 17th International Conference on Control, Automation and Systems (ICCAS); 2017 18-21 Oct. 2017.
4. Astrom KJ, Rundqwist L, editors. Integrator Windup and How to Avoid It. 1989 American Control Conference; 1989 21-23 June 1989.
5. Markaroglu H, Guzelkaya M, Eksin I, Yesil E. Tracking Time Adjustment In Back Calculation Anti-Windup Scheme. 2006.
6. Li X-I, Park J-G, Shin H-B. Comparison and Evaluation of Anti-Windup PI Controllers. *Journal of Power Electronics*. 2011;11(1):45-50. doi:10.6113/JPE.2011.11.1.045.
7. Ringh M. How to Simulate Control Systems Using the PID Controller Add-In. COMSOL Multiphysics; 2020.

A5 Author Contributions of Published Articles and Submitted Manuscript

Author contribution statement, Fricke Christian

Isothermal Micro(bio-)calorimetry - Method Optimization and Instrument Development for a Rapid and Reliable Detection of Bacteria

Author contribution statement:

Title: Rapid Calorimetric Detection of Bacterial Contamination: Influence of the Cultivation Technique

Journal: Frontiers in Microbiology

Authors: Fricke Christian, Harms Hauke, Maskow Thomas

Christian Fricke (first author):

- designed the experimental setup
- performed the laboratory work
- analyzed the data
- edited the manuscript

Hauke Harms (author 2):

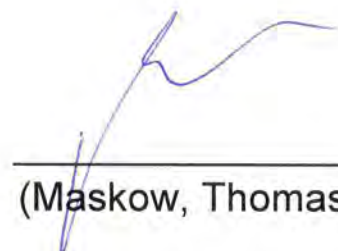
- provided consultation for the work
- contributed significantly to the preparation of the manuscript

Thomas Maskow (senior author):

- developed the project idea and concept
- provided consultation for the work
- contributed significantly to the preparation of the manuscript



(Fricke, Christian)



(Maskow, Thomas)

Author contribution statement, Fricke Christian

Isothermal Micro(bio-)calorimetry - Method Optimization and Instrument Development for a Rapid and Reliable Detection of Bacteria

Author contribution statement:

Title: How to speed up the detection of aerobic microbial contaminations by using isothermal microcalorimetry

Journal: Journal of Thermal Analysis and Calorimetry

Authors: Fricke Christian, Harms Hauke, Maskow Thomas

Christian Fricke (first author):

- designed the experimental setup
- performed the laboratory work
- analyzed the data
- edited the manuscript

Hauke Harms (author 2):

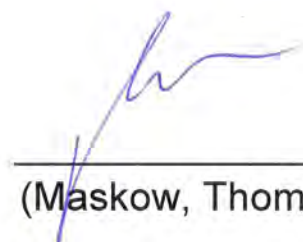
- provided consultation for the work
- contributed significantly to the preparation of the manuscript

Thomas Maskow (senior author):

- developed the project idea and the concept
- provided consultation for the work
- contributed significantly to the preparation of the manuscript



(Fricke, Christian)



(Maskow, Thomas)

Author contribution statement, Fricke Christian

Isothermal Micro(bio-)calorimetry - Method Optimization and Instrument Development for a Rapid and Reliable Detection of Bacteria

Title: Rapid culture-based detection of *Legionella pneumophila* using isothermal microcalorimetry with an improved evaluation method

Journal: Microbial Biotechnology

Authors: Fricke, Christian, Xu Juan, Jiang Feng-Lei, Liu Yi, Harms Hauke, Maskow Thomas

Christian Fricke (first author):

- designed the experimental setup
- performed the laboratory work
- analyzed the data
- edited the manuscript

Juan Xu (author 2):

- initial operated the microcalorimeter

Feng-Lei Jiang, Yi Liu (author 3,4):

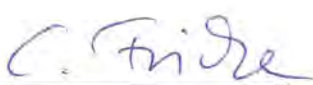
- provided consultation for the work
- contributed to the preparation of the manuscript

Hauke Harms (author 5):

- provided consultation for the work
- contributed significantly to the preparation of the manuscript

Thomas Maskow (senior author):

- developed the project idea
- analyzed the data
- provided consultation for the work
- contributed significantly to the preparation of the manuscript



(Fricke, Christian)



(Maskow, Thomas)

Author contribution statement, Fricke Christian

Isothermal Micro(bio-)calorimetry - Method Optimization and Instrument Development for a Rapid and Reliable Detection of Bacteria

Title: Numerical heat flow and transport simulation as a development tool for the design of isothermal microcalorimeters

Journal: Thermochimica Acta (submitted)

Authors: Fricke Christian, Klee Toralf, Richter Sven, Paufler Sven, Harms Hauke, Maskow Thomas

Christian Fricke (first author):

- developed the numerical model and concept of the test system
- performed the laboratory work
- evaluated the numerical model and analyzed the data
- edited the manuscript

Toralf Klee, Sven Richter (author 2,3):

- developed the concept of the test system
- manufactured the electronic system of the test system
- designed and implemented the software
- contributed to the preparation of the manuscript

Sven Paufler (author 4):

- developed the concept of the test system
- provided consultation for the work
- designed figures for the manuscript
- contributed significantly to the preparation of the manuscript

Hauke Harms (author 5):

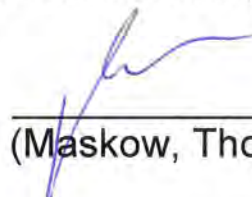
- contributed to the preparation of the manuscript

Thomas Maskow (senior author):

- developed the project idea and concept of the test system
- provided consultation for the work
- contributed significantly to the preparation of the manuscript



(Fricke, Christian)



(Maskow, Thomas)